Development of a medical imaging-based technology for cancer treatment

By

Chris Lobstein-Adams

SUBMITTED FOR THE DEGREE OF DOCTOR OF PHILOSOPHY

AT THE UNIVERSITY OF SUSSEX

School of Engineering and Informatics

University of Sussex

Brighton

October 2015

UNIVERSITY OF SUSSEX

Chris Lobstein-Adams

SUBMITTED FOR THE DEGREE OF DOCTOR OF PHILOSOPHY

"Development of a medical imaging-based technology for cancer treatment"

SUMMARY

The Electrical Impedance Mammography (EIM) device is an imaging system developed at the University of Sussex for the detection of breast lesions *in vivo* using quadrature detection of impedance.

The work describes a novel technique to integrate Ultrasound-guided Focused Ultrasound Surgery (USgFUS) with the existing EIM system. The benefits that such a system could provide include the possibility of non-invasive detection, diagnosis and treatment of breast cancer all within a single device and involving no radiation. Furthermore the timescales involved would allow the process to be considered an outpatient procedure such that a patient can be diagnosed and treated on the same day using the same device.

Various geometries of transducer were investigated for physical compatibility as well as the ability to target the entire specified volume, based on the dimensions of the existing system. Simulations were performed using a custom written code based on Huygen's principle, allowing minimum surface area and power requirements to be determined and feasibility of designs to be evaluated.

The use of phase differences in the excitation signals applied to individual elements was also investigated, thus the effect of steering the simulated focus could be observed, an important factor to consider when attempting to incorporate a transducer into a device with restricted dimensions.

Resulting simulated pressure fields were used to obtain acoustic intensity fields, which could then be used as inputs in the Pennes Bio-Heat Transfer Equation (BHTE) allowing temperature distributions to be observed.

Preliminary studies proved the feasibility of using the suggested transducer design in conjunction with the existing EIM system. Pressure fields and heating patterns were all within acceptable limits, confirming the ability of the device to effectively ablate cancerous tissue. Additionally the capability to steer the resultant focal point was validated, and a thermal dose model was implemented allowing different heating patterns to be quantitatively compared.

Declaration

I Chris Lobstein-Adams hereby declare the contents of this thesis have not and will not be distributed in part or in full to another University or Institution towards an award of any other degree.

Signature

Chris Lobstein-Adams

Dated: 9th October 2015

Acknowledgements

I would like to thank the Engineering Department of the University of Sussex for continuing support through not only this, but all projects I have had the pleasure of undertaking over the last seven years I have spent studying at the University. The Biomedical Engineering team has had particular influence on the work presented, and it has been my pleasure to work alongside each and every member.

Particularly I would like to acknowledge Dr. Wei Wang for the original objective of the project undertaken and for his encouragement along the way. I would like to thank Dr. Rupert Young for his role in my development at the University, initially as my personal tutor and finally as a secondary supervisor to my DPhil studies. Furthermore and perhaps most importantly I would like to express my gratitude to Prof. Chris Chatwin, who has always made himself available when problems have been encountered, offering advice, guiding my work and agreeing to supervise my degree when external pressures were encountered.

Where information from external sources has been used appropriate references will appear in the text of this thesis.

Chris Lobstein-Adams

University of Sussex

October 2015

List of Abbreviations

AC	–	Alternating Current
BEM	–	Boundary Element Method
BHTE	–	Bio-Heat Transfer Equation
CE	–	Conformité Européenne
CT	–	Computed Tomography
CW	–	Constant Wave
DP	–	Discrete Particle
EIM	–	Electrical Impedance Mammography
EIT	–	Electrical Impedance Tomography
FDA	–	Food and Drug Administration
FE	–	Finite Element
FEA	–	Finite Element Analysis
FUS	–	Focused Ultrasound Surgery
GUI	–	Graphical User Interface
HIFU	–	High Intensity Focused Ultrasound
HIFUS	–	High Intensity Focused Ultrasound Surgery
HVT	–	Half Value Thickness
IMCPA	–	Integrated Multi-functional Confocal Phased Array
LUV	–	Large Unilamellar Vesicles
MLV	–	Multilamellar Vesicles
MRI	–	Magnetic Resonance Imaging
MR(I)gFUS	–	Magnetic Resonance (Image) Guided Focused Ultrasound Surgery

MWA	–	Microwave Ablation
PC	–	Personal Computer
PHIFU	–	Pulsed High Intensity Focused Ultrasound
PRF	–	Pulse Repetition Frequency
PW	–	Pulsed Wave
PZT	–	Lead Zirconate Titanate
RAM	–	Random Access Memory
RF	–	Radio Frequency
RFA	–	Radio Frequency Ablation
RTI	–	Reflex Transmission Imaging
SPECT	–	Single Photon Emission Computed Tomography
SUV	–	Small Unilamellar Vesicles
TAP	–	Total Acoustical Power
TD	–	Thermal Dose
UCA	–	Ultrasound Contrast Agent
USgFUS	–	Ultrasound Guided Focused Ultrasound Surgery

List of Symbols & Units

º	–	Degrees (angular)
°C	–	Degrees Celsius (temperature)
µm	–	Micrometre (distance)
Ω	–	Ohms (impedance/resistance)
cm	–	Centimetres (distance)
dB	–	Decibels
Hz	–	Hertz (frequency)
hr(s)	–	Hour(s) (time)
J	–	Joules (heat/energy)
kg	–	Kilogram (mass)
L	–	Litre(s) (volume)
m	–	Metre (distance)
min(s)	–	Minute(s) (time)
mm	–	Millimetres (distance)
Np	–	Nepers (logarithmic gain/loss)
ns	–	Nanoseconds (time)
Pa	–	Pascal (pressure)
Rayl	–	Rayleigh (acoustic impedance)
s	–	Second(s) (time)
W	–	Watts (power)

α	–	Attenuation coefficient (dB/cm MHz)
α_R	–	Reflection coefficient
θ_i	–	Angle of incidence (°)
θ_c	–	Critical angle (°)
θ_r	–	Angle of refraction (°)
λ	–	Wavelength (m)
ρ	–	Density (kg/m^2)
ϕ_i	–	Phase of element ‘i`
A	–	Area of transducer (m^2)
a	–	Cross-sectional area (m^2)
C_b	–	Specific heat, blood (J/kg °C)
C_t	–	Specific heat, tissue (J/kg °C)
c	–	Local speed of sound (m/s)
c_i	–	Incident region speed of sound (m/s)
c_r	–	Refracted region speed of sound (m/s)
d	–	Diameter (m)
d_{cf}	–	Distance from centre of array to focal point (m)
d_i	–	Distance from centre of element ‘i’ to field point (m)
d_{if}	–	Distance from centre of element ‘i’ to focal point (m)
f	–	Frequency (Hz)
f	–	Focal length (m) {3.11 & 4.2}
I	–	Intensity (W/m^2)

I_0	–	Reference intensity (W/m^2)
k	–	Thermal Conductivity (W/m °C)
P	–	Total acoustic Power (W)
p	–	Pressure (Pa)
p_0	–	Reference pressure (Pa)
p_m	–	Pressure maximum (Pa)
$p(x,y,z)$	–	Pressure at field point (x,y,z) (Pa)
q	–	Heat (J)
q_{met}	–	Metabolic heat (J)
r	–	Radius (m)
R	–	Constant in thermal dose equation
S	–	Element area (m^2)
T	–	Temperature (°C)
T_a	–	Arterial temperature (°C)
t	–	Time (s)
t_0	–	Initial time (mins)
t_{43}	–	'Equivalent minutes' (mins, thermal dose)
t_f	–	Final time (mins)
w	–	Blood perfusion rate (kg/m^3 s)
x	–	Distance to focus (m) {5.1}
Z	–	Acoustic Impedance (Rayl or kg/m^2 s)

Table of Contents

List of Figures

List of Tables

List of Publications

1. C Lobstein-Adams, N Beqo and W Wang. *Electrical Impedance assisted Ultrasound guided Focused Ultrasound Surgery*. In *EIT conference, Bath 2011. Proceedings. Pg. 69.*

2. N Beqo, B Lingham, C Lobstein-Adams, G Sze and W Wang. *Dual scans with Combined Ultrasound and Electrical Impedance Mamography*. In *EIT conference, Bath 2011. Proceedings. Pg. 65.*

3. C Lobstein-Adams, C Chatwin. *HIFU and acoustic surgery, an modern alternative to the scalpel*. (Planned article).

Chapter 1:

Introduction & Background

1.1: Chapter Introduction

This chapter provides an introduction and general background to the investigation undertaken for this thesis. Numerous ablative cancer treatments will be discussed and High Intensity Focused Ultrasound (HIFU) will be introduced, with a focus on the application of these methods for the ablation of cancerous tissue. A brief history of HIFU will also be presented along with examples of HIFU devices that are currently on the market for the surgical treatment of various cancer types. Additionally, following the conclusion an outline of each chapter is provided for reference.

1.2: Thesis Introduction

In the chapters that follow relevant background information on acoustics and specifically on HIFU will be given, including a comprehensive review of relevant literature. In addition a brief account of the underlying theory of transducer design will be given and numerous types of transducer will be presented, with examples, along with a summary of the attributes of each. The problem at hand will then be defined, and the design specification(s) will be listed. From this a suitability study of transducer designs will be given, and decisions made will be presented as to which transducer(s) will be the most practical for the intended application. The design parameters for the intended application will subsequently be investigated and selected, followed by a report of simulations performed to optimise a number of these parameters using a custom code written in MATLAB [1] thus providing a feasibility and optimisation study simultaneously. The pressure fields from these (simulated) transducers will be used to calculate acoustic intensity fields which will subsequently be set as inputs in the Pennes Bio-Heat Transfer Equation (BHTE) [2] allowing the resulting temperature rise in a simulated target tissue (modelled using varying attenuation coefficients) to be calculated using the COMSOL Multiphysics software package [3]. This will additionally include results of a custom model, designed to allow different transducers to be quantitatively compared using a measure called the 'equivalent thermal dose' [4]. Following this the outcome of the simulations will be summarised thus allowing the results to be presented in a concise form. Finally the transducer manufacture, including additional equipment to facilitate operation (such as driving circuitry) will be briefly outlined. For reference there will also be appendices included at the end of the thesis. These contain the original project proposal & a sample of the MATLAB code written for the simulation of the various acoustic intensity fields.

To summarise the results of this thesis it has been shown that the incorporation of a surgical HIFU device into the existing EIM system developed at the University of Sussex is both possible and practical. The design of such a device has been outlined up to the point of plausible manufacture.

Once completed this single device system potentially offers detection, diagnosis and treatment of breast cancer all within the timescale of an out-patient procedure, with the possibility of expanding the system to treat cancers other than that of the breast.

1.3: Cancer Treatment via Ablation: The Options

Advances in medical technologies over the last number of decades have allowed for the development and growth of new and exciting treatment methodologies. Included in this list are a number of treatments capable of destroying tissue via ablation, some of which require direct access to the target tissues, while others can be performed non-invasively.

Radiofrequency ablation (RFA) makes use of an electric current applied directly to the target tissue via contact electrodes. The electric current causes resistive heating within the tissue, and generally devices of this type have integral sensors installed in the treatment 'tip' to allow temperature rises to be monitored and controlled [5]. Commonly used for suppression of atrial fibrillation, this treatment methodology has recently found an increased use for the treatment of cancers, using small diameter probes from which retractable electrodes can be used to make contact with the malignant target tissue. Treatments of this kind generally last for up to 25 mins [6]. Patient comfort during the procedure is questionable due to the need for electrodes to make direct contact with the tissue for effective treatment. For this reason anaesthesia is generally recommended during treatments of this nature.

Laser ablation is a feasible treatment capable of destroying pathogenic tissue although this too requires the penetration of the skin to effectively reach the target tissue area(s). This is generally achieved using very small needles containing thin fibres capable of transmitting suitable frequencies of light, generally in the near-infrared end of the spectrum. The mechanism of tissue destruction utilised here can be referred to as photocoagulation [7] and generally takes a few minutes of exposure to effectively destroy the target tissue.

Microwave ablation (MWA) can be utilised as a percutaneous and as an open-surgical procedure. In general, a thin microwave antenna is inserted directly into the target tissue and electromagnetic microwaves are used to agitate the tissue to frequencies as high as 2.45 GHz [6]. This causes agitation of the water molecules present which causes the production of heat leading to cell death via coagulative necrosis [8].

Although research into MWA continues, advantages can be readily seen in the ability to ablate larger tumour masses within comparatively short treatment durations compared with those of alternative thermal ablation methods. Having said this MWA does require contact with the tissue to be treated and so cannot be called a non-invasive procedure as some other treatment methodologies claim.

Cryoablation generally uses argon gas or liquid nitrogen delivered through a small probe directly into the target tissue. The tissue is subsequently frozen, thawed and frozen again a number of times until cell death occurs [9]. As with many of the treatment methodologies mentioned so far, cryoablation can be guided using diagnostic ultrasound to facilitate the accurate placement of the probe, laparoscopically or percutaneously and therefore can be referred to as a 'minimally-invasive' treatment procedure.

Numerous therapies based on radiation have also been researched and used in practice as early as the 1960s. These include brachytherapy, involving the insertion of a radioactive source into the tumour site, hadron therapy, involving the use of a beam of 'heavy protons' to deliver energy to the target tissue and the 'Gamma Knife' which utilises a bowl-shaped array of gamma ray sources causing a natural focus at the geometric centre of the sphere, of which the bowl forms a section of, delivering sufficient energy to destroy unwanted tissue. For more information on these technologies the reader is directed toward the review paper [6].

High Intensity Focused Ultrasound Surgery (HIFUS) or Focused Ultrasound Surgery (FUS) offers a truly non-invasive surgical option. The following sections describe the theory and application of HIFU as a surgical tool.

1.4: Introduction to HIFU

High-Intensity focused ultrasound surgery otherwise referred to as FUS or HIFUS uses a focused ultrasound machine to destroy pathogenic tissue, such as that of a cancerous tumour. This is achieved by the coherent focusing of ultrasonic waves leading to precise heating of a localized area to a temperature of above 56°C (for one second) thus destroying the target cells by thermal ablation [10]. This process of heating and destruction can be compared to the focusing of sunlight using a magnifying glass (see Figure 1).

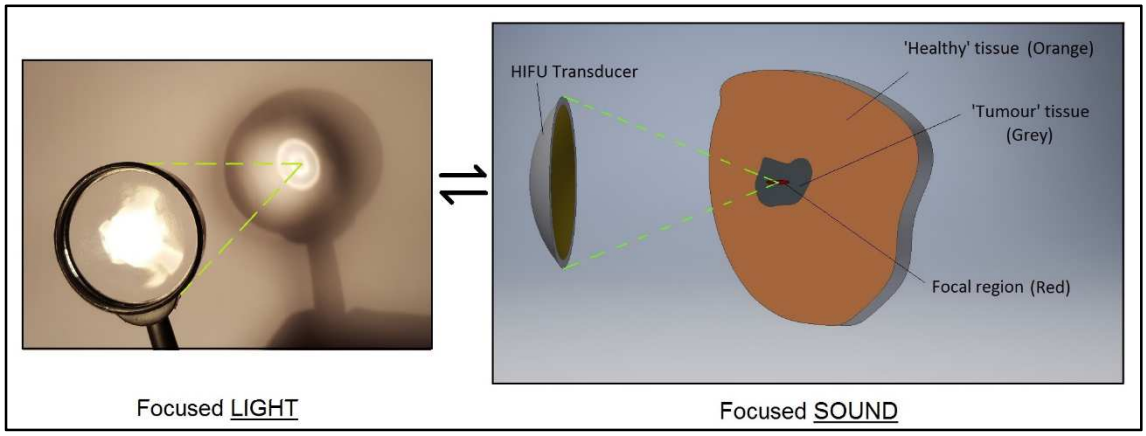

Figure 1 - ***HIFU analogous to focusing sunlight using a magnifying glass***

HIFU has been widely used to treat prostate cancer with promising results and is an approved therapy in many parts of the world, including Australia, Canada, China, South Korea and some parts of Europe. At present investigations are under way to determine the feasibility of HIFU treatments for other types of cancers such as those that affect the brain, breast, liver, pancreas, rectum, kidney, testes and bones.

1.5: HIFU, A Brief History

Investigations into the use of HIFU for non-invasive tissue ablation have been carried out as early as the 1940s. In the 1950s and 1960s Francis and William Fry, amongst others, performed work that led to treatments of neurological disorders using the combination of ultrasound and a high precision milling machine to accurately destroy tumours of the brain [11]. This type of clinical trial however has until recently been difficult to perform due to the problems and complexity associated with the targeting of the ultrasound beams. As both ultrasound technology and general medical imaging have advanced the use of HIFU for the treatment of tumours has once again become an area of interest.

In 1994 the first CE (mandatory conformity marking for products sold in Europe) approved commercial HIFU machine was launched by Focus Surgery of America. In depth studies at the time showed that the machine developed, the Sonablate 200 [12] was able to destroy prostate tissue without long term side effects and with no bleeding or blood loss. Later a French company EDAP-Technomed, developed a similar technology called Ablatherm [13] of which a 2006 study showed that non-recurring survival rates were in the region of 50 % and 70 % for intermediate and low risk patients respectively**.**

Magnetic resonance imaging (MRI) guided procedures using HIFU (MRgFUS or MRIgFUS) were first developed in the early 1990s and were patented in the US in 1992. In 2000 the technology was further developed by an Israeli company, Insightec, who went on to produce the ExAblate 2000 [14] the first MRI guided HIFU system to obtain market approval from the Food and Drug Administration (FDA) and to sell commercially in the U.S. The company Chongqing Haifu of China developed a similar system in 2001, using ultrasound in place of magnetic resonance to guide the HIFU ablation and the process was certified for use on benign and malignant tumours.

Sumo Corporation developed a treatment called HIFU-2001 [15] which is capable of treating tumours related to many internal organs such as the liver and kidneys. This treatment is well known, perhaps mostly for the fact that the procedure does not

require any use of anaesthetics, although these could be recommended in certain cases.

This concludes the brief history of the organisations that appear as the major players in the development of HIFU for surgery. It is worth noting here that although the above companies have made significant progress in the field of HIFU development there are also many other highly influential groups working on various HIFU applications, and the list of organisations discussed should not be taken as absolute. In the next chapter a number of the publications produced by these other groups will be reviewed, alongside the groups mentioned specifically above.

1.6: Research Aims, Objectives & Achievements

1.6.1: Aims

The research project described is the integration of a therapeutic High Intensity Focused Ultrasound (HIFU) transducer array into an existing Electrical Impedance Mammography (EIM) non-invasive medical imaging device. The resulting system therefore would allow dual modalities of diagnosis and treatment to be available using a single device. The aim of this research is to show that this integration is feasible, and to develop the design of a suitably compatible therapeutic device.

1.6.2: Objectives

The objectives of this project are to answer the following questions.

- Can EIM be used in conjunction with HIFU to provide both diagnosis and targeted treatment?
- How can a HIFU transducer be integrated into the existing EIM system designed by the Biomedical Engineering (BMEng) group at the University of Sussex?
- What factors must be considered when designing and manufacturing a HIFU transducer? (Including, but not limited to the phasing of array elements and electronic steering)

Given satisfactory answers to these questions the design of a suitable device will be progressed to a stage at which manufacturing is plausible.

1.6.3: Achievements

To summarise, the research work performed has shown that the incorporation of a surgical HIFU device into the existing EIM system developed at the University of Sussex is indeed feasible. It has been proven that modification of the existing electrode plate would allow sufficient space to position a suitably powerful HIFU transducer, capable of targeted tissue ablation within a known volume, namely that of human breast tissue. The proposed design allows for steering a surgical focal point within the target volume while avoiding permanent tissue damage to non-targeted areas.

1.7: Chapter Conclusion

In this chapter a brief introduction has been presented and several ablation techniques have been discussed with a focus on the advantages and disadvantages they provide in comparison to HIFU, as a surgical instrument. This overview suggests that, at least for the current undertaking, HIFU presents the most practical choice.

A brief history on HIFU has also been given, along with some examples of surgical HIFU devices that have gained approval from the respective legislative bodies in countries around the world. HIFU and HIFU transducers will be discussed in detail later in this thesis (see Chapter 3).

1.8: Thesis Structure

For reference the contents of each of the subsequent chapters will be summarised.

1.8.1: Chapter 2

This chapter presents a comprehensive literature review of relevant publications. Available at the time of writing. To facilitate relevance to the reader a short chronological review is given to set the scene. An in-depth review follows, with sections dedicated to transducer design and theory as well as medical trials and accounts to allow for project perspective.

1.8.2: Chapter 3

Here principles of acoustics and interaction with matter are laid out. HIFU is introduced in more detail, with examples of currently available devices given. Types of transducer are presented with various geometries and methods of focusing being described

1.8.3: Chapter 4

In this chapter the 'problem' is defined. A design specification is created based on transducer and acoustics theory with many of the necessary properties and construction restrictions being introduced, explained and chosen.

1.8.4: Chapter 5

The first sets of simulations are presented here. Initially the theory will be explained and parameters used will be listed, followed by the results and findings from the simulations performed. The work presented includes calibration of the parameters used to allow accurate and obtainable results. All the results relate to the computed acoustic pressure and intensity fields, with simulated focal intensities of the proposed HIFU transducer presented.

1.8.5: Chapter 6

In this chapter theory relevant to the time-dependent tissue temperature rise, resulting from the acoustic intensities presented in the previous chapter will be described. A thermal dose model will also be introduced.

1.8.6: Chapter 7

Here project conclusions will be discussed. In later sections proposals for future work to further the goals of this project will be laid out. It is hoped that one or more of these directions will be taken up by another research project at some point, following the submission of this thesis.

Chapter 2:

Literature Review

2.1: Chapter Introduction

Presented in this chapter is a comprehensive literature review split into numerous sections. The first section provides a short chronological review of the larger groups working on similar areas in HIFU devices and research since 2003. Following this an in-depth review of over thirty published papers will be presented. This in-depth review will be further divided between reports on medical trials and those focusing on transducer design and acoustic field simulation.

Much of the inspiration for the transducer design described in later chapters came from the publications included in this section. Where appropriate, references to these papers will be made in the subsequent chapters of this thesis.

For reference & prior to the literature review, please refer to the image below (see Figure 2, [15]) showing a typical, simplified HIFU arrangement for surgery.

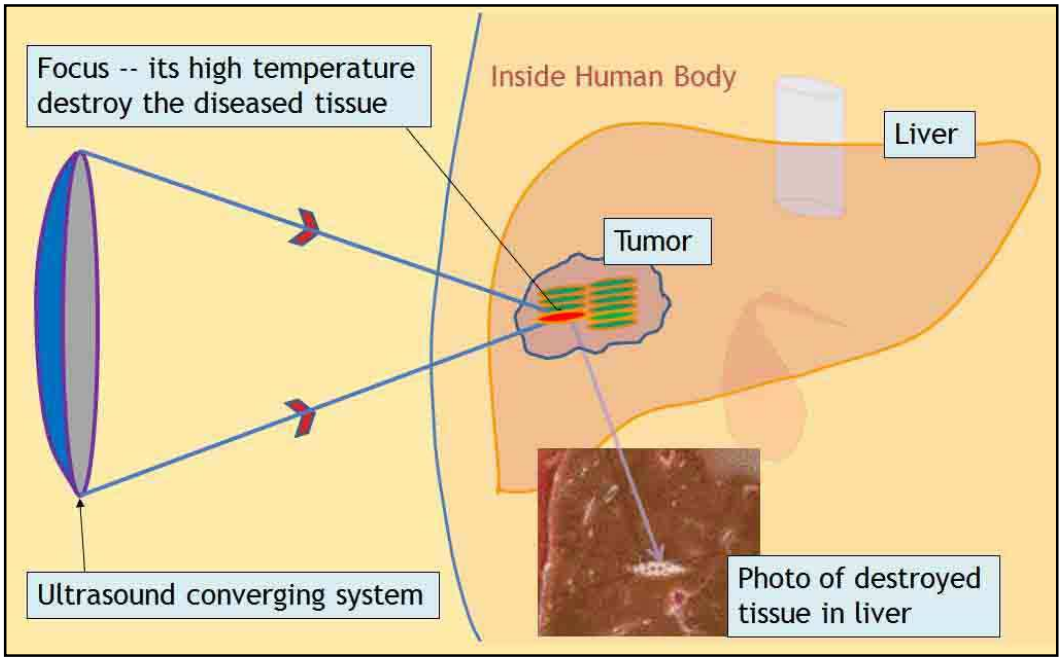

Figure 2 - ***Simplified HIFU process applied to a liver tumour***

2.2: Brief Chronological Review of Recent Literature

The brief history already presented (see Section 1.5) is an overview of the work performed by large commercial groups, who can be described as leaders in the field of using HIFU for ablation of tumours. These groups have published many scientific papers on the subject of HIFU, as have other, non-commercial groups from around the world. This section will briefly summarize these more recent findings in chronological order beginning from 2003, and where applicable summarise the results of experiments and trials that have been performed. More detailed reviews of the technology and its medical application follows later in this thesis (see Section 2.3).

From the available literature the Chongqing Haifu (HIFU) Technology Company of China appear to have the greatest experience with ultrasound guided HIFU treatments (USgFUS) of all the groups researched. In 2003, 28 women with biopsy proven breast cancer were randomized into a HIFU treatment group and a control group [16]. All patients had a single tumour, no larger than 6 cm in diameter, at a location at least 0.5 cm away from skin and lung tissue and 2 cm away from the nipple. Twenty-five patients in the control group underwent modified radical mastectomy, while the remaining twenty-three received HIFU treatment 1-2 weeks prior to modified radical mastectomy. The HIFU treatment encompassed the tumour volume and a portion of healthy tissue, measuring 1.5-2 cm around the tumour. Following HIFU treatment 14 of the 23 patients experienced mild local pain, and one experienced minimal skin burn, but these patients had entirely recovered after 10 days following the treatment. Pathological examination showed the tumours in the HIFU group patients underwent complete coagulative necrosis in the defined tumour volume, showing HIFU as a promising surgical tool, given a suitably located tumour. One after-effect of the treatment that some patients found distressing was the presence of a firm, palpable lump in the area of ablation. This lump was predicted to reduce in size over time, but it is suggested that the lump(s) may take a number years to disappear completely, in the case where HIFU treatment is not followed by conventional surgery. Although cosmetic this may cause some patients to reconsider whether HIFU treatment is the

most suitable treatment methodology for their own particular case. This decision would most probably vary from patient to patient.

In 2004 The Haifu group of Chongqing treated a further 24 patients with breast cancer [17]. These patients underwent HIFU treatment 1-2 weeks before receiving modified radical mastectomy, with no patients undergoing any discomfort throughout the procedure. Following treatment patients experienced slight oedema around the area of treatment but this rapidly faded. Pathological examination showed a very clear boundary between ablated and healthy tissue and also the complete necrosis of the target volume, including the predefined boundary of healthy tissue.

Also in 2004, the HAIFU group produced an overview of the work carried out to date [18]. This report described many treatments for different types of cancer and will now be briefly summarized. A total of 474 patients with liver cancer and tumour size from 4 to 14 cm received HIFU treatment. The survival rates after 6 months and one year were 82.6 % and 53.4 % respectively. 106 patients with biopsy proven breast cancer underwent HIFU treatment along with adjuvant therapy. After a mean follow-up time of 22 months all the patients were alive, with one patient experiencing local recurrence that was subsequently treated by modified radical mastectomy. Some 153 patients diagnosed with osteosarcoma were treated using HIFU. These patients had tumours ranging from 5 to 46 cm in size. After a mean follow-up time of 23 months survival rate was reported as 85 %. Additionally 77 patients with soft tissue sarcoma were treated, and after a mean follow-up time of 21 months, survival rate was 90 %. In addition to the cases mentioned above patients with renal cancer were treated successfully. Interestingly 10 patients with pancreatic cancer were also successfully treated, with an unexpected effect that HIFU treatment alleviated pain immediately following treatment.

In 2005 and 2007, 22 and 23 patients with breast cancer were treated respectively. In both cases treatment was successful with no severe complications. Both papers conclude that HIFU is a safe, effective and feasible treatment for patients with breast cancer, although large scale clinical trials are suggested to confirm the future role of HIFU treatment [19], [20].

In 2008 work was carried out to determine the feasibility of using a split beam transducer, modified from a Sonablate 500 machine [12] to create multiple focal points simultaneously [21] thus reducing treatment time. This transducer was compared to another, single focus transducer, operating at an identical frequency. The transducers were concave and spherical in shape with a diameter of 5 cm, utilizing 1 MHz frequency ultrasound for therapeutic purposes and a 10 MHz diagnostic transducer for imaging. To split the focus adjacent sections were driven 180 degrees out of phase, creating four focal points simultaneously without significant changes in intensity in front and behind the focal area. Although the application of these transducers was limited to that of hyperthermia, involving heating tissue to only a few degrees above body temperature for an extended period of time, the results did show that a split focus transducer has the benefit of reducing treatment time and producing similar effects, given a suitable (power) correction factor. Scanning of this split focus, in terms of HIFU transducers may be more complex depending on the target volume and shape, but nevertheless a reduction in treatment time benefits both patients and those administering the treatment. For this reason a split focus transducer seems beneficial, although more development work may be needed before clinical trials are undertaken using such a device.

In 2009 a study was performed to determine the effective use of HIFU for the ablation of deep tumours (10 to 20 cm from the skin surface) [22]. This group, working from Shanghai Jiao Tong University in China developed a large scale spherical array, using 90 circular elements with unequal spacing. The array had an effective diameter of 21 cm and a radius of curvature of 18 cm. This allowed the array to focus within a volume of 2 cm x 2 cm x 3 cm at a distance of 15 to 18 cm from the back of the transducer without grating lobe intensity reaching the predefined unacceptable level of 15 % of the main lobe intensity. Outside of this volume grating lobe levels were unacceptable. Porcine muscle tissue was used to demonstrate the capability of the transducer successfully. The group also showed that two focal points could be generated simultaneously. In conclusion, the thermal ablation of deep tumours is theoretically possible using the transducer designed in this study, although it would seem more experimental work would be beneficial before clinical trials commence.

2.3: In-depth Literature Review

As the technology for accurate and efficient use of HIFU has only become readily available within the last decade or so the majority of papers reviewed here were published in the period from 2000 to 2010. Nevertheless, there still remain papers published prior to 2000 that contain much relevant information and indeed some that date back to the early 1940s when the potential applications of HIFU were first considered. To give an overall view of the works reviewed to date an attempt will be made to order these publications chronologically, although in some cases work carried out by certain groups may span a number of years, such as in the case of on-going medical trials. In these cases relevant publications will be presented together to preserve the continuity of the review. Additionally the literature reviewed will be divided between papers relating to transducer design and acoustic field simulation and those relating to medical (and animal) trials. In total thirty-three separately published papers will be reviewed.

2.3.1: Transducer Design & Acoustic Field Simulation

In 1989 the Institute of Cancer Research UK, led by Gail ter Haar, published a paper focusing on the use of HIFU for the treatment of liver tumours [23]. In this study *in vitro* tests using excised porcine liver were carried out. The equipment used was of particular interest as an acoustic (Perspex) lens system was utilised, alongside a 10 cm diameter piezoelectric (PZT4) disc transducer, to create lesions at a focal distance of 14 cm with all equipment (and experimental material) being mounted within a degassed water bath. The focal region was ellipsoid in shape and measured approximately 1.5 cm (length) and 1.5 mm (centre diameter) and could be said to be similar in size to a grain of rice. Focal region shape and placement were the objects of this study, and it was found that more energy is required to create a lesion of comparable size at deeper target depths. This energy can be obtained by either increasing exposure time or by increasing the intensity of the incident ultrasound. When exposure time is increased with intensity held constant the resulting lesion becomes larger. This continues until the lesion increases to a size at which additional exposure time does not create a larger legion, seen as a plateau in the graph of exposure time against lesion volume.

Increasing the ultrasonic intensity (by altering the applied voltage to the transducer) also increases the lesion size observed and additionally causes the lesion to be formed nearer to the surface of the tissue, closer to the transducer. This is thought to be caused by non-linear distortion of the ultrasound, causing part of the high frequency components to be absorbed prior to the focal plane being reached. Also worth noting here is the use of ultrasonic imaging to follow the lesion formation in real-time, as lesion tissue shows up as a highly echogenic area on ultrasound images although it is acknowledged that more detailed studies are required to correlate these areas with realized tissue damage, which would hence allow for more accurate treatment and treatment planning.

In 1993 a paper produced by INSERM, France and authored by J.Y. Chapelon was published in the IEEE Ultrasonics Symposium [24]. This publication describes the demonstration of an annular array type transducer using electronic focusing, a significant improvement over using fixed focus transducers. The spherically curved annular array was truncated by two parallel planes to facilitate use via the rectal cavity, for the treatment of prostate cancer. Simulations were performed and acoustic pressure fields were calculated to allow relevant design criteria to be determined. An ultrasound guided prototype was constructed, and the piezoelectric surface was divided into 7 rings operating at a frequency of 2 MHz. This was chosen to minimize the total number of elements and hence reduce the complexity of the driving electronics. Simulation was performed using the impulse response method [25], using a modified impulse response evaluated for a curved strip transducer in a separate paper [26]. Following simulation the array design parameters were decided. The frequency was chosen by considering desired focal area, target depth and optimal heat deposition. In this case frequency was maximised to allow increased heat deposition and better control over ablation (as attenuation increases with frequency [27]) and to avoid the effects of cavitation which occurs above a threshold acoustic pressure [4]. The aperture size was selected according to the power density tolerated by the system (approximately 25 W/cm^2) and as this device was designed for transrectal application, the annular transducer was truncated by two parallel planes to reduce size in one dimension thus decreasing patient discomfort. The geometric focal length is

determined by the radius of curvature of the shell and is defined somewhere in the mid-range between the minimum and maximum focal lengths of the array when using electronic focusing. The number of elements and the element arrangement were chosen to maximise element area, thus reducing element crosstalk, minimising the number of elements and hence reducing the number of inter-element gaps, which in turn allows for an increased sensitivity of the array while keeping grating lobes at an acceptable level. Also noted is that, in line with basic ultrasound theory, grating lobes can be avoided (for any focal range) if individual elements are less than a wavelength wide. Consequently, two probes were fabricated (Imasonic, France), both air-backed with a quarter wave matching plate. The final dimensions were a diameter of 50 mm, truncated at 31 mm (outer four elements) with inter-element gaps of 0.3 mm. The power was provided by an eight channel amplifier with variable power from 5 to 50 W, used in conjunction with a 6-bit delay line module with a resolution of 50 ns. The driving electronics were controlled using a 486 personal computer (PC). Once manufactured, the transducer was tested using a hydrophone. These tests showed a very close correlation between simulated and practically obtained results, with small discrepancies thought to be caused by non-linear effects, which were not accounted for in the simulation. Additionally the transducer was shown to produce lesions in bovine liver after 25 exposures of four seconds each, at an intensity of 1000 W/cm^2.

Also published in the 1993 IEEE Ultrasonics Symposium was a paper from the Intec Research Company/Focus Surgery based in California (USA). In this paper quantitative Schlieren imaging [28] was used to non-destructively test the acoustic field produced in a water bath by a transducer [29]. The resulting image was combined with an attenuation function to give an approximation of the beam profile in 3D. The dose rate of therapy is defined (power deposited per unit mass) by assuming linear behaviour and a non-temperature dependent dose rate. Several factors, useful when comparing therapeutic transducers are also given. These include the peak-to-skin dose ratio (ratio of dose at focus to elsewhere in tissue, especially important at the skin interface) the total acoustic power (TAP) at focus (fraction of power at focus compared to that delivered by the transducer, at the transducer surface) and various axial profiles (acoustic intensity along the beam path). Although numerous assumptions and

emissions have been made in order to simulate the acoustic fields, the work presented in 1993 is still largely relevant and accurate. In addition a number of equations are derived concerning the expected focal spot size (related to the transducer size and frequency used) and the optimum frequency to give a maximum net acoustic gain. In summary, although dated, this paper contains valuable information on basic transducer characterisation, useful when approximations are necessary.

One year later, the Intec Research Company/Focus Surgery (CA, US) published another paper in the 1994 IEEEE Ultrasonics Symposium. In this publication the design of an annular phased array for therapeutic treatment of deep tissue targets, in the range 6 to 10 cm, is described [27]. The annular array was designed with a natural focus (radius of curvature of the array) of 10 cm, operating at 1.25 MHz. This frequency was chosen using the method presented in a separate publication [29]. The 'f-number' or ratio of aperture to focal length [31] of the array was set to unity to allow a large focus to skin dose ratio. Instead of using the 'equal area element' approach, commonly used in the design of annular arrays, here the smallest number of elements (advantageous due to reducing the complexity of driving electronics) required for the defined focal range is given when their 'weighted mean radii correspond to equal phase shifts'. It so happens that in this case the resulting elements are very close to being equal in area, although this is only true due to the specific dimensions of transducer, and this may not hold for non-identical arrays. This design resulted in ten elements that differ from their neighbours at most by 90^{o} (a quarter wavelength). To simulate the designed array a Rayleigh-Sommerfeld integration was performed. The results of this simulation were eventually compared to Schlieren images of the manufactured transducer, which showed actual focal distances to be within 2 mm of those simulated, although cross-talk between elements remained - indicating an area that could be improved on.

Moving forward a few years to 1999 INSERM (France) published a paper on the use of 1.5D phased arrays for HIFU applications in the 1999 IEEE Ultrasonics Symposium. The array was designed with the treatment of prostate cancer in mind and as such has the ability to electronically focus the produced ultrasound beam in a 2 by 2 cm area centred at the natural focus of the spherically curved transducer [32]. The feature that

sets this transducer apart from similar arrays is that annular elements were not used. Instead use was made of lateral (parallel) strips each containing a number of elements. From simulation the number of strips (‘n’) and the number of elements on each strip (‘m’) were decided. This lead to n=5 and m=42 being used with the central strip having width 11 mm and lateral strips 5.5 mm, the latter being connected in pairs about the central strip to simplify driving electronics. This resulted in a total of 126 separately driven elements, designed such that all have a common, equal area. The array was built to be compatible with existing apparatus (Ablatherm - EDAP Technomed, France) for transrectal use and as such had a 54 mm diameter shell, truncated at 36 mm with a focal length of 40 mm. The material used was 1-3 piezocomposite (Imasonic, France [33]) driven at 2.5 MHz, with a quarter-wavelength matching layer and air backing. The efficiency of the produced array was found to be approximately 40 % when using a bandwidth of 1 MHz (2 – 3 MHz), a reduction from the 75 % obtained using the same material in a single element transducer. By comparing simulated to realized results, it was shown that a phase resolution inferior to one tenth of the signal period causes the beam focusing to deteriorate significantly. Phase resolutions more accurate than one tenth signal period were found to give no improvement and so a phase resolution of one tenth was chosen as the most practical. One final point worth noting here is that, as the developed transducer had a large bandwidth, it is possible that it could be used in a dual-mode application, providing imaging and treatment modalities using the same device. This is an interesting characteristic that has the potential benefit of a single device capable of performing the function of two separate machines: diagnostic and therapeutic.

Finite Element Analysis (FEA) is a commonly used tool to simulate acoustic fields caused by piezoelectric sources. One such study, published in the 2000 IEEE Ultrasonics, Ferroelectrics and Frequency control conference proceedings, used FEA (Boundary Element Method, BEM) on a 1D linear phased (diagnostic) transducer to investigate (numerically) inter-element crosstalk, effects of sub-dicing elements and directivity patterns [34]. The latter it was found heavily depends on transducer size and interestingly on the materials used to ‘fill’ the kerf (spaces between elements) while sub-dicing can reduce lateral modes which are detrimental to the transducer’s

operation. Using a ‘lossy’ (soft material with high mechanical damping) kerf filler can also reduce lateral modes and sub-dicing can be used to ‘artificially’ alter the ratio of element height to width (aspect ratio) to a value of two or more, causing unwanted (lateral) modes to be pushed to higher frequencies. Reducing element crosstalk is especially important for phased arrays as it will adversely affect the directivity pattern *and* the sensitivity of the array. The software package ANSYS [35] was used, and care was taken to ensure at least 8 (finite) elements per wavelength were present in the mesh used (reduced error to less than 1 %). A linear phased array was simulated with a steering angle of 54^{o}, operating at 2.5 MHz. The kerf between elements was 0.1 mm, with element width of 0.3 mm (approximately equal to half a wavelength in water, hence no grating lobes [36]). The results were checked using an analytical solution of the Helmholtz integral for two simple cases, which showed a good correlation to the FEA simulations. It was shown that to reduce crosstalk and lateral modes of vibration all matching layers (and to some extent the backing layers) should be sub-diced. Sub-dicing of the elements alone is not sufficient to achieve acoustic isolation and as a rule, crosstalk between neighbouring elements should be less than -30 dB to avoid artefacts in acquired images. Also shown in this paper is the effect of element diameter on the directivity pattern. It is shown graphically that the directivity of a 0.5 mm diameter (less than one wavelength) element is much broader than that from a 5 mm diameter element (more than one wavelength) when both are operating at 1.25 MHz (wavelength 1.2 mm) although the latter case shows small side lobes around the main lobe (the 0.5 mm directivity pattern is almost semi-circular, comprising only a single lobe).

Focus Surgery (Indianapolis, US) in conjunction with Kitasato University (Japan) and the Hitachi Ltd. Central Research Laboratory (Japan) produced a publication in 2001 regarding the use of split-beam transducers for the transrectal treatment of prostate cancer. Six transducers were compared using simulation with the goal of increasing the volume of tissue treated at one time. The objective was to reduce the overall treatment time and hence reduce costs and decrease patient discomfort [37]. Final lesion volume, focal and rectal wall temperatures, sonication time and TAP were used as the criteria for comparison. The Sonablate 500 (Focus Surgery) transrectal probe

was used to mount and control the different transducer configurations, which were subsequently tested on turkey breast tissue held within a degassed water bath. The majority of the configurations involved dividing the transducer surface into four quadrants, with controllable phase (90^{o} resolution) for each. Results showed that overall treatment times could be reduced by a factor of 1.85, compared to the control, a single element transducer with similar dimensions. Although encouraging results were achieved in this study, in the case of breast cancer treatment only a relatively small volume of tissue is sought to be ablated, whereas the entire prostate gland is commonly ablated in prostate cancer treatments. In the case of breast cancer a larger focal volume, as produced by the split-beam transducers, is not necessarily advantageous, as a smaller focal volume would allow more accurate ablation control. For this reason it may be assumed that split-beam transducers, although very useful in other applications, are not particularly suitable for the treatment of breast cancer, at least in early diagnosed cases (involving smaller tumour volumes).

Also in 2001 a series of papers and articles were published by the Department of Physics (Royal Marsden Hospital/Institute of Cancer Research, UK) authored by Gail ter Haar. One such article presents a history of HIFU and an in depth description of the effect on tissue and relevant parameters to consider when designing and using a HIFU system [4]. Of particular interest here were two equations; one to estimate tissue heating due to attenuation and the other to quantify the 'thermal dose' so as to compare different treatment regimes. The latter outputs a time (in seconds) equivalent to the case that the tissue was held at 43 ^{o}C (for example 56 ^{o}C for 1 to 2 s is equivalent to 43 ^{o}C for 240 mins). The trials described show the ability of HIFU to seal blood or occlude blood vessels, which could potentially lead to tumour shrinkage without ablating the entire volume. This could be used as a standalone procedure or indeed as a pre-treatment to tumour ablation, thus reducing treatment times and therefore increasing the viability of HIFU as a cancer therapy. Also of interest is the suggestion that Reflex Transmission Imaging (RTI) or Elastography could be used to locate ablated volumes, thus improving treatment accuracy over (USgFUS) which encounters problems when visualising ablated tissue. Although this technology (Elastography) would be greatly beneficial when producing a lower cost FUS system (as

compared to an MRgFUS system) its widespread use has not yet been accepted, and it remains an interesting developing technology. In another publication it is stated that lesion size is dependent on frequency used, with smaller lesions being created using higher frequencies [38]. For example a 10 cm transducer with a focal length of 14 cm driven at 1.7 MHz will produce a lesion approximately 1.5 mm in diameter and 15 mm in length (ellipsoid). Also suggested is that the effect of heat removal by blood perfusion during FUS can be largely ignored if exposures with durations of less than three seconds are used [39]. Another interesting point made was that (assuming a tissue attenuation of 0.7 dB/cm/MHz) the optimum frequency for HIFU treatments is one that gives a total attenuation through the tissue (skin surface to focal point) of 10 dB [40]. In a further publication by members of the same group, an in-depth look into the histological appearance of tissue damage caused by HIFU treatment is presented [41]. Also included is a description of the applications of HIFU in terms of which tissues can be treated, along with a brief history of HIFU clinical trials up to the point of publication and a comparison with other thermal ablation techniques. Although relevant and useful, this information will not be presented here and readers are advised to refer to the relevant publication [41] if further details are sought.

Although not directly related to HIFU a paper on the design of a novel '2D' phased array for hyperthermia cancer therapy was published (2001). In contrast to HIFU applications, hyperthermia involves prolonged, moderate heating typically for durations of an hour or more, and transducers for hyperthermia generally utilise lower frequencies and are not necessarily focused. This study involves the computer simulation of three transducer configurations, one utilising square elements and the other two circular elements of differing geometries. The resulting pressure fields from the arrays were simulated using the pseudo-inverse method [42] with the equations used and a simplified process of derivation being presented. The results of these simulation studies showed arrays with circular elements to be superior to those with square elements. Indeed if an equal intensity distribution pattern is input, the simulation shows that the necessary number of circular elements is smaller and the intensity gain greater (by 1 dB) than that obtained using square elements, in addition to much smaller grating lobes being generated (30 dB reduction). Although the

information presented in this publication pertains to hyperthermia cancer treatment, much of the transducer array design work is relevant to HIFU transducer design, especially when attempting to reduce grating lobes which can cause undesirable heating effects if present in FUS applications.

Imasonic (France) published a paper on piezocomposite materials developed for high performance transducers in 2002 [33]. These materials offer several advantages over standard piezoelectric materials. The generation of high power densities and high efficiencies of the composites allow transducer size to be minimized. The composites consist of rod shaped piezoceramics embedded in a matrix of polymer material, commonly epoxy. This allows the effect of lateral modes, and indeed of element cross talk to be greatly reduced, the former allowing an increased flexibility of the aspect ratio (element thickness to width) which has typically to be kept above two. In addition reducing element crosstalk allows more accurate beam control and hence a higher quality transducer. The use of a piezocomposite material also allows for a more mechanically robust transducer, less affected by small shocks than purely piezoceramic transducers. Two piezocomposites are described, named 'HI-1' and 'HI-2'. The former has efficiency between 60 % and 70 %, can operate at frequencies up to 10 MHz, is air backed and can produce a maximum acoustic power output of 10 W/cm^2. 'HI-2' has a slightly lower efficiency (40 % to 60 %), can operate up to 5 MHz, has solid backing and, most importantly, has a maximum acoustic power output of 30 W/cm^2. This latter material has a very high acoustic power output compared to that of piezoceramic transducers, thus can allow smaller sized arrays equally capable of therapy as their larger, non-composite counterparts. The wide bandwidth, especially of 'HI-1' opens the path to the fabrication of dual-mode transducers and has been previously investigated [43] allowing images to be obtained from an array primarily designed for therapy. In conclusion the piezocomposites described here provide a much more attractive option than generic piezoceramics. Modern transducers utilise these advantages and use piezocomposites in their construction. It is recommended that Imasonic 'HI-2' be used where space is a concern, such as in the case of the HIFU/EIM project for the present research. This will be covered in more detail in the relevant following chapters.

An interesting paper was published in 2003, at the Third International Symposium on Therapeutic Ultrasound. This paper documents the design and characterization of four transrectal phased array transducers for HIFU treatment of the prostate [44]. Three of the transducers were spherically sectioned annular arrays, truncated by two parallel planes as is commonly used for transrectal devices. All were based on the Sonablate 500 (Focus Surgery, US). These three arrays vary in size, operating frequency and piezoelectric materials used and were designed to ablate at a focal depth range of 25 mm to 45 mm. The arrays were fabricated and tested, all giving satisfactory results. A fourth array is also described in this paper. This array, although not fabricated, suggests an advantage over the other three due to the proposed ability to focus not only in the depth direction, but also in the longitudinal direction. Use of an array such as this would eliminate the need for the linear displacement of a transrectal transducer, replacing physical displacement with an electronic focal range of -20 to +20 mm (longitude) and 25 mm to 45 mm (depth). This 'concept' array measures 80 mm by 22 mm, operates at 4 MHz and has a cylindrical section (curvilinear) type shape. Six element rows are present, each with a large number of small elements, allowing electronic focusing in the depth direction. Use of sub-apertures allows steering in the longitudinal direction. A further feature of interest concerning this transducer is that it is capable of performing imaging as well as therapy, thus is another example of a 'dual-mode' transducer. This is achieved by using the centre two rows of the array to acquire 1D radio frequency (RF)-lines, via electronically scanning a small sub-aperture. These 1D lines are then combined to give a 2D image. In conclusion this type of array offers a large advantage over other transrectal transducers, and the ability to use imaging in addition to therapy makes the design an attractive option for limited space applications. It is yet to be seen however if the images obtained from the transducer are of sufficient quality to be feasibly used to guide surgery, as the work was limited to simulation. Regardless, it is this author's opinion that the described array represents a vast improvement over similar transducers, with the ability to act in both imaging and therapeutic modalities, likely representing the 'next generation' of HIFU arrays for focused ultrasound surgery.

In 2004 a paper was published by the Pennsylvania State University in the International Journal of Hyperthermia. This paper describes the design, simulation and *ex vivo* testing of a two-dimensional MRI compatible phased array for the ablation of benign prostatic hyperplasia [45]. The array was fabricated using 1.79 mm thick piezo-material PZT-8 (high power) with a 14^{o} steering angle (transverse and longitudinal) and natural focus at 40 mm from the transducer when operating at 1.2 MHz. To simulate, the array was modelled as a 64 element (8 by 8) rectangle measuring 20 mm by 20 mm. Initially the elements measured 2.5 mm by 2.5 mm (diced 70 % through material, with kerf 96 µm) but this design was found to produce -3.47 dB grating lobes. This was reduced to -8.24 dB by using tapered elements to remove periodicity [46] the central elements being largest and tapering towards all edges (2 mm, 2.33 mm, 2.66 mm, 3 mm, 3 mm, 2.66 mm, 2.33 mm, 2 mm). A conductive matching layer was used to allow maximum power transfer and had acoustic impedance equal to the geometric mean of that of PZT-8 and tissue. For simulation purposes the phase of each element was determined by measuring the path between each element and the focus, and comparing this distance against the path between the centre of the array and the focus. The calculated phase of each element was then used to calculate the pressure at each point (x,y,z) in the field using Huygen's principle (see [45] for equation(s) used). Using the pressure field the acoustic intensity at all points was calculated. The intensity was then used to calculate the power deposited at each point, and this power was used as the heat input term in the BHTE to approximate the expected temperature rise in tissue caused by the incident ultrasound. For comparison the resultant pressure field from the constructed transducer was measured using a hydrophone. To test the ablation ability of the transducer *ex vivo* tests were performed on porcine liver held in a water bath. For these tests each element was driven at an average electrical power of 8 W, for sonications lasting 10 s, 12 s, and 20 s, at distances between 30 mm and 40 mm from the transducer. These sonications resulted in lesions 2 mm, 2.9 mm and 4 mm (diameter) respectively. Interestingly the array was able to produce a single large lesion by phasing elements to create four individual foci that are close enough to each other such that a single, larger lesion is formed. Sonication was set to 25 s to allow for the additional power required, and the focal depth was set to 30 mm. The resultant lesion was approximately 4 mm in diameter. Additionally the phasing of elements

could generate a heating regime that could reduce inter-sonication cooling time by sonicating non-neighbouring elements in a predetermined pattern. One final point worth noting here is that the use of piezocomposites could address the low width to thickness ratio used in this study. This would improve results as the effect of lateral modes on the ultrasound propagation would be reduced, hence the overall efficiency of the array would be improved.

In 2006 a novel HIFU transducer was modelled and fabricated, allowing 'rib-sparing' by switching off certain elements of the transducer. The design of this device was described in a paper published in the 5th International Symposium on Therapeutic Ultrasound (2006). The transducer itself was built in collaboration with Imasonic (France) and consisted of a spherical (11 cm diameter, 15 cm radius of curvature) shell transducer with 10 lateral strip elements operating at 1.7 MHz [47]. This is unusual as spherical section arrays commonly have ring-shaped electrodes as opposed to the strip shapes used here. It was shown that by phasing the excitation of these elements the focus could be displaced +/- 4 mm from the beam axis. Larger displacements however caused secondary peaks to become too large, thus causing an undesirable heating pattern. The focus could also be shifted by up to 10 mm axially, but both this, and the radial focusing caused the focal area to widen. Above 5 mm and 10 mm (radial and axial steering) respectively caused the focal peak intensity to be reduced by 50 % or more. Beam broadening was achieved by focusing each side (5 elements) to the opposing side, thus allowing a larger focal spot to be created. This would therefore allow treatments to be completed more rapidly while covering the same target volume, but does however increase the power required by at least 50 %, which may not be possible with smaller transducers where overall size limits the maximum producible acoustic power.

Also in 2006 a paper was published describing the development of an annular phased array for the ablation of uterine fibroids with a focal range from 30 to 60 mm [48]. Sonications at depths of 30 mm (acoustic intensity 4100 W/cm^2) and 60 mm (acoustic intensity 6100 W/cm^2) lasted 15 s, the latter (deeper) focus producing lesions at least 63 % larger than the former (more shallow) focus. Also sonications with focal spots

that began further from the transducer produce longer lesions than those that were targeted nearer to the transducer. The transducer array operated at 3 MHz and comprised 11 elements all made from 1-3 piezocomposite (Imasonic, France [33]) with a natural focus at 50 mm. The element areas were all equal to 105 mm^2 with a gap of 0.3 mm between neighbouring elements. The overall transducer shape was that of a typical transrectal device (spherical section truncated by two parallel planes) and measured approximately 75 mm by 35 mm. A clamp held an imaging probe to the therapeutic probe and a polyurethane 'pillow' was used, with a pump, to circulate water around the HIFU transducer to ensure the temperature remained below 40 ^{o}C. Using a computer controlled driving system the phase of signals applied to all elements were calculated, with the total electrical power delivered to the device being varied between 0 and 165 W. Using this system the sonication time could be controlled by entering values on the computer screen user interface. Interestingly a novel imaging algorithm was used to allow improved visualisation during the HIFU process. This involved sampling the ultrasound images and interleaving this sampling with the sonication periods. The resultant ultrasound images (during HIFU treatment) were interference free. To test the effectiveness of the device lesions were created in excised porcine liver, following characterisation using a hydrophone. The results of these experiments showed that larger lesions form when higher electrical power was applied to the transducer, and this effect increased with increasing focal depth. Also the lesion position shifted slightly from the expected location when target depth was greater than 35 mm, with these shifts increasing in magnitude when higher powers were used. This summarises the main findings of the paper. As this paper includes a novel idea and also much in depth results data it is recommended that the interested reader refer to the original publication [48] for more details.

Presented in another paper published in 2006 was a modified method for simulating the pressure field produced by a 2D square phased array. The aim of this study was to analyse the feasibility of using a square (NxN) phased HIFU array for neurosurgery applications. Although different methods exist, Huygen's principle is used here taking into account ultrasonic propagation through two homogenous media (water and brain tissue). This method is presented for a 2D and 3D geometry and an expression

including the transmission coefficient is derived, thus allowing the effect of attenuation to be included in the model. The final simulation used the following parameters. There were 25 (5 by 5) square elements, each having area 4 mm x 4 mm with a 0.5 mm gap between neighbouring elements. The transducer was driven at 1.6 MHz at a total acoustic power of 120 W. The density and sound velocity of water and brain were taken to be 1000 kg/m^3, 1480 m/s and 1030 kg/m^3, 1541 m/s respectively. The corresponding attenuation coefficients were (water) 0.023 Np/m MHz and (brain) 5 Np/m MHz. Using these parameters the operation of the transducer was simulated. The result was a maximum intensity of 1.5 MW/m^2, and the resulting plots, focused at (0, 0, 50 mm) showed large grating lobes. The model was then modified to include more elements (10 by 10) of a smaller size (approximately 1 - 1.5 mm^2). When focusing at exactly the same point there were almost no grating lobes present, although the maximum intensity was reduced by a factor of approximately three, which is to be expected as the overall dimensions, and therefore surface area (and maximum applied electrical power) were less than in the previous model. In conclusion it was shown that it is possible to obtain focused beams by utilising phasing of elements in an N by N square array.

One year later, in 2007, a paper describing a novel transducer for the ablation of larger volumes was published. The transducer was designed to reduce treatment times by increasing the focal zone size [49]. This is achieved using a toric transducer shape comprising eight (segmented) elements. In operation, each sector performs a 5 s sonication, followed by the next sector. This resulted in a conic focal zone, approximately 9 cm^3 (average diameter 2 cm) in volume after a total of 40 s treatment time (8 sectors activated for 5 s each). The transducer operated at 3 MHz with a focus at 70 mm and a 7.5 MHz imaging probe was located in the central aperture of the array, coaxial to the HIFU beam path. When used during surgery, a polyurethane envelope surrounds the transducer, through which 0.3 L/min of degassed water at 15 ^{o}C is passed for cooling purposes. To assess the transducer operation *in vivo* experiments were performed on healthy porcine liver following a laparotomy (abdominal incision). The subjects were anesthetised and exposures were performed using an acoustic power of 60 W with the HIFU transducer being held by hand. Four

days post treatment the subjects were euthanized, and the liver was sliced to allow inspection of lesions and a histological analysis to be performed. In conclusion, different to other transducers the transducer described in this paper allows the typical waiting times between sonications (to allow cooling) to be removed completely. Instead once one sector has completed sonication (5 s) the next sector is activated immediately. It has therefore been shown that a large reduction in treatment time (one of the potential drawbacks of widespread use of FUS) has been achieved, although this will be mostly beneficial to applications in which large volumes are to ablated, such as the prostate, and less so to those requiring very precise control of the focal spot size and position.

In the same year another paper containing much useful information on transducer design, was published in the 6th International Symposium on Therapeutic Ultrasound [50]. The transducer was designed to be capable of 'rib-sparing' by switching off certain elements when sonicating close to or around the ribs. Called the 'Teleson II' the transducer design was based on the 'Teleson I' produced by the same group, except in the earlier model the user had to switch between imaging and therapeutic arrays during treatment. In the Teleson II the power amplifier has the ability to perform rapid switching and can successfully interleave the HIFU and the imaging wave propagation. Also included in the Teleson II are some new features, including controlled cavitation and radiation force elastography. The latter utilises a pulse of HIFU to displace the tissue a very small amount such that a 'tissue stiffness' image can be produced allowing accurate visualisation of the lesion location which, using typical ultrasound imaging, is rather difficult. Control software was developed to allow control via a graphical user interface (GUI). This software was capable of automated beam plotting, automated temperature mapping and HIFU delivery control, which all control a motorised gantry allowing movement in three dimensions. The HIFU delivery control can be adjusted to create single lesions, arrays of lesions, straight line tracks, arrays of tracks and even non-linear tracks such as circles and 3D spirals. It was shown that using a 2D spiral pattern the same amount of lesion volume could be created in under three minutes compared to the 30 minutes or more it would take if using single lesions.

Cavitation, due to the propagation of ultrasound through tissue, is a phenomenon that has the potential to greatly increase the efficiency of HIFU treatments, and indeed cavitation typically precedes thermal effects (with results appearing within one acoustic cycle [51]) although its effects can be largely unpredictable. In a paper published in 2008, experiments were performed to evaluate the use of cavitation for predictable thermal ablation [52]. This had been achieved in the past by using pulsed HIFU (PHIFU), high focal intensities and short duty cycles (one cycle being a short sonication followed by a long pause) [53], [54]. Using these previous studies as guidelines, a successful preliminary study showed non-thermal ablation using PHIFU exposures of frequency 0.87 MHz, a pulse repetition frequency (PRF) of 100 Hz, a duty cycle of 15 % and a peak (spatial) intensity of 5900 W/cm^2 [55]. Previous studies also found that ultrasound contrast agent (UCA) can enhance the effects of cavitation and so for the main experiments the same parameters were used (at a focal length of 150 mm) with the addition of UCA. The test subjects were 20 rabbits, divided into a control (10) and a PHIFU group (10) who had been inoculated with VX2 tumour cells 2-3 weeks prior to PHIFU treatment. Twenty-four hours following surgery the subjects were sacrificed and an immunohistochemical examination was performed showing that PHIFU with UCA can inhibit tumour cell proliferation and cause cell apoptosis. Interestingly it is stated that “non-thermal effects (mechanical and cavitational) will occur” if focal intensity is greater than 1500 W/cm^2. Although the exact boundary is dependent on other factors as well, this is an interesting guideline figure to consider when designing a transducer for thermal ablation however should not be considered an absolute value.

One type of transducer that does not appear in many papers is the cylindrical array type transducer. In a paper published, again, in 2008 a 1.5D cylindrical phased array was developed and tested. Following a study concerning dimension optimisation, the aperture of the array was chosen and measured 150 mm (azimuth) by 120 mm (elevation) with a radius of curvature (and natural focus) of 150 mm. The transducer was fabricated from PZT-4 1-3 composites comprising 512 (64 in azimuth direction by 8 in elevation direction) elements operating at 0.9 MHz [56]. The design was then simulated using the Field II software [57] and demonstrated the ability to focus from

145 mm to 175 mm and -15 mm to +15 mm in the depth and azimuth directions respectively. As a precaution a surface acoustic intensity of 12.6 W/cm^2 was applied to a sample piece of PZT-4 (22 elements) which showed no appreciable temperature rise within a period of 50 minutes, indicating the feasibility of using such an intensity for long treatments. Interestingly it was found that using a water bag could extend the dynamic focusing range by 2 cm, in the depth direction.

Constant wave (CW) HIFU procedures, given suitable parameters, essentially 'fix' tissue *in situ.* PHIFU exposures however, as has previously been stated, are more likely to give rise to cavitation when propagated through tissue. This can be utilised for more efficient tissue destruction and is also thought to be useful in the enhancement of drug delivery via altering tissue permeability, although accurate control is required for both these applications. One concern of using PHIFU is the possibility that it may inadvertently increase the metastatic burden by facilitating dissemination of tumour cells. This was investigated in a 2008 paper in which lung cancer in a murine model was used to evaluate the extent, if any, of the exacerbation of metastases cause by PHIFU exposures [58]. The exposures were performed using a modified Sonablate 500 (Focus Surgery, US) with a 5 cm diameter, 4cm focal length concave spherical transducer operating at 1 MHz. The parameter used for exposures were a TAP of 40 W, an intensity (spatial average) of 2685 W/cm^2, a PRF of 1 Hz and duty cycle of 5 % with 100 pulses at each point. The average treatment time was 15 minutes. Mice were split into a control and a PHIFU group, the control group given 'sham' exposures of 0 W, but otherwise treated identically to the PHIFU group. Twenty four hours following treatment subjects were sacrificed and a histological examination was performed. Samples were analysed using a custom built MATLAB image processing code to quantify the extent of metastases in each case by calculating the metastatic area fraction of the lung in question. In conclusion the results showed that although PHIFU can increase metastases, the results between the control and PHIFU group were 'not statistically different' using a paired student t-test. It is for this reason, along with the unpredictable nature of its action that until further evidence is presented cavitation should be avoided, at least in this author's opinion.

One particular area of interest in the development of HIFU for surgical use is the case of the 'dual-mode' transducer. As previously mentioned this type of transducer uses the same array for therapy and imaging, the imaging elements generally being located centrally and coaxially to the therapeutic elements, thus allowing the same acoustic path to be followed. A paper published in 2009 describes an investigation into using such an array for the simultaneous diagnosis and therapy of prostate cancer, in real time [59]. Typically dual mode transducers operate in pulsed wave (PW) operation, thus allowing signal timing to be utilised to interleave imaging with HIFU exposures, hence avoiding unwanted interference. In contrast the transducer described has been designed to additionally allow real-time imaging during CW operation. This was achieved using a Barker code implementation with various cycles-per-bit settings for the coded excitation of the imaging elements, thus when the returning signal (coded excitation plus interference from HIFU) was received the coded signal could be extracted (for more details please see [59]). The integrated multi-functional confocal phased array (IMCPA) had a cylindrical section shape and comprised three rows of phased elements, the centre (6 MHz, with a -6 dB fractional bandwidth of 50 %) for imaging and the outer two (4 MHz, with a -6 dB fractional bandwidth of 30 %) for therapy. The imaging array had 128 elements with a 0.73 wavelength (188 µm) pitch, 25 µm inter-element spacing (kerf), 8 mm height and was fabricated from PZT-5H piezocomposite. The therapeutic arrays had 0.5 wavelength pitch (also 188 µm), 25 µm kerf and 15 mm height, were fabricated from PZT-4/PZT-8 piezocomposite, had a natural focus at 40 mm and were capable of generating a focal intensity of 2000 W/cm^2. In addition the overall size of the transducer was 24mm by 28 mm, thus facilitating use via the rectal canal. The transducer was simulated using the Field II program [57]. In conclusion imaging was made possible due to the use of coded excitation, although the images received were not completely interference free. It is suggested that the additional use of a notch filter could improve this, but until there is a broader understanding on how to implement these filters, this type of transducer may overcomplicate applications for which a simpler, single-mode transducer is more suitable.

The surgical resection of tumours deep within a tissue is only feasible in a low percentage of cases, as access to the tumour maybe restricted due to overlying tissues and in some cases organs. FUS offers a practical alternative to open surgery for the treatment of these types of tumours, and one such transducer was designed and described in a paper published in 2009. In this study the designed transducer was of spherical section (bowl shape) with diameter 21 cm and radius of curvature of 18 cm. The transducer comprised 90 circular PZT-8 elements, each with diameter 1.4 cm and thickness 0.2 cm, arranged into six rings, with all elements being driven at a frequency of 1 MHz. All elements were mounted onto the shell at tangents to the element centres. The transducer was designed to be able to electronically focus with a 3D volume (2 cm by 2 cm by 3 cm), thus is termed a 2.5D transducer. Previous arrays similar to that described were designed with large numbers of elements, typically over 200 [60]. As element size is inversely proportional to frequency, small elements used in conjunction with high frequencies would make the required target depth very difficult to achieve. Therefore, provided that the target depth can be achieved, the element number should be minimized, and the elements themselves must not be excessively small. With this in mind the element number was kept below 100. The f-number (ratio of focal length to aperture) was set to unity to minimize unwanted heating in the near field (pre-focal volume). As has been previously stated, the ratio of inter-element spacing to the wavelength should be kept as low as possible to avoid the presence of grating lobes. In contrast however the aperture of the array should be maximised to increase the focal steering range. Eventually it was decided to use a large array with unequal element spacing to reduce grating lobes [61] and as such the elements were arranged in rings, with the first elements in each ring at a different angle (to the x-axis) meaning varying distances between elements in every two neighbouring rings. The vertical distance between elements in neighbouring rings was also varied. The electric power provided to the transducer (for simulation) was approximately 840 W, with a (TAP) output of 540 W, or 6 W per element. The operation of the transducer was simulated using the inverse method [61] to calculate element phase and amplitude of signals, and the point source method [62] was used to simulate the resultant pressure field. To verify the simulated results *ex vivo* experiments were performed on porcine muscle, cut into cubes. Using a TAP of 300 W, these experiments showed the ability to

focus within the defined volume and also that the array could produce two separate lesions by generating multiple foci simultaneously, with lesions created being between 5 and 6 mm in diameter after a 50 s heating period. Other lesions generated were between 2 and 6 mm in diameter (17 s heating period) depending on how far away from the natural focus they were targeted (further away gave larger lesions). The array described in this paper is of particular interest due to the ability to steer in a (pre-defined) 3D volume. Although this transducer was large and intended for deep tissue ablation, a similar approach could be taken with smaller transducers designed for reduced focal depths. This will be investigated in further works, as it offers a major advantage in situations where motorised gantries are not suitable.

A final paper that will be reviewed in this section describes a novel method of creating focused sound waves, without the use of a traditional transducer. Instead a tuneable non-linear acoustic lens, in the form of ordered arrays of granular chains is used [63]. The amplitude, size and location of the resulting focal 'sound bullet' (a single wave front, as opposed to comparable, linear lenses that produce oscillations) can be controlled by varying the pre-compression of the chains, a method that has not been reported previously. A 'conformal striker' is used to create an impact on the acoustic lens, which is coupled to an (elastic) interface at which spherical wavelets are emitted into the medium, following the pattern of the displaced 'power law' spheres which is in turn controlled by the pre-compression of the chains of spheres (pre-compressed using bottles containing varying volumes of water). If a striker of mass equal to 21 spheres (in the lens) has a velocity of 1 m/s it was shown that a 38 dB pressure gain (or 79 Pa relative to a reference pressure of 1 Pa) can be achieved. Due to the non-linearity of the lens the pressure gain can be increased arbitrarily by increasing the speed of the strikers' impact, and indeed at a velocity of 4 m/s a pressure gain of 57 dB (674 Pa) can be obtained. In addition to small 'bullets' the acoustic lens apparatus was capable of producing planar wavelengths, by approximating a focal point at infinity. Although not designed particularly for FUS procedures, the system could potentially be used for HIFU treatments as the focal points ('bullets') are very well defined and come into focus in a similar manner to a typical curved HIFU transducer, although the pressures involved would have to be increased by more than one order of magnitude.

Interestingly this method of producing focused sound waves can be performed using air as the propagation medium. The system was simulated using the assumption of many radiating circular wave fronts, the actual modelling being performed using a finite elements (FE) model coupled to a discrete-particle (DP) model.

2.3.2: Medical Trials: A Brief Review of Literature

In the 1999 IEEE Ultrasonics Symposium a paper concerning the feasibility of MRI monitored HIFU therapy was published by the University of Heidelberg Medical School, Department of Radiotherapy (Germany). In the study 15 target volumes of sheep breast were treated by applying 30 to 128 pulses of ultrasound at a frequency of 1.7 MHz (25-75 W per pulse giving acoustic powers of 16-47W) using a specially designed MRI-compatible transducer system [64]. The transducer was mounted on a positioning system that allowed linear translation in addition to tilt angles up to 20^{o} and was covered with a Mylar film window. The transducer was capable of producing a focal ellipsoid of 8.7 mm length and 1.1 mm diameter (-3dB zone). Using this setup eight female sheep were treated, each receiving two treatments with a four week interval. Treatment was performed using 9 s sonications followed by a 20-50 s pause to prevent accumulation of energy (heat) in the tissue. Following treatment the test subjects were sacrificed and a histological examination was performed, revealing a very good correlation between MRI monitored results and actual, realized results. This showed MRI was capable of measuring temperature rise in the treated tissue (thermometry). In conclusion, following successful treatment of sheep breast tissue it is suggested that human trials are feasible and would be possible using a slightly modified setup.

Following on from the above study a further paper was published by the same group in 2001, again on the use of MRIgFUS. In this study a clinical trial was carried out on a human patient for the treatment of breast cancer, the first such report of MRIgFUS used to treat a malignant tumour in humans [65]. HIFU treatment was given as an adjuvant therapy so as not to compromise other treatment modalities, and the treatment was followed by surgical removal of the tumour 5 days post HIFU surgery, in turn followed by other (commonly used) adjuvant therapies. The patient was a 56-year-old menopausal female deemed a typical candidate for breast conserving surgery,

with a well circumscribed tumour mass of 2.2 x 2 x 1.4 cm^3. The treatment plan utilised 80 ultrasound pulses of 9 seconds each at an acoustic power of 30 – 50 W. A 13 s cooling period between sonications was also implemented to prevent unwanted temperature rise in the surrounding, healthy tissues. During the treatment the patient experienced no pain despite being given no anaesthesia, with only a mild sensation of pressure being experienced during the sonications. Histological examination of the resected tumour showed a very good correlation between the location and boundaries of the ablated volume and that observed during treatment using MRI, showing MRIgFUS to be a useful and effective procedure for the treatment of breast cancer. In addition it is suggested that FUS could be used to facilitate gene transfer and targeted drug deployment, although this topic is beyond the scope of the described work.

In the period 2003 to 2007 the Chongqing University of Medical Sciences published a series of papers detailing the outcome of HIFU treated clinical trial patients. The Chongqing group have, to this authors knowledge, treated the highest number of human patients using HIFU, with 1038 patients with solid tumours treated in the period from December 1997 to October 2001 alone [18]. In a report published in 2003 an account is given of the treatment of 48 women with biopsy proven breast cancer (clinical trial phase II) [16]. All patients had a single palpable tumour no more than 6 cm in diameter and located 0.5 cm and 2 cm (minimum) from the ribcage and nipple respectively. The women were randomised into a control group (25) and a HIFU treated group (23) with all patients undergoing breast conserving surgery and adjuvant treatment (radiation/chemo/hormone therapy) with the HIFU group receiving a FUS procedure 1-2 weeks prior to open surgery. During the surgery the entire tumour volume was ablated, including a 1.5 to 2 cm margin of healthy tissue as is regularly performed during traditional breast conserving surgery. In total the HIFU treatment lasted from 45 mins to 2.5 hrs, with median treatment time of 1.3 hrs. Following exposure to HIFU some of the treated patients experienced oedema in the tissue surrounding the treated area, although this disappeared in all patients after 7-10 days post treatment. Fourteen patients in the HIFU group experienced mild skin burns, but in all cases this had recovered fully 10 days post HIFU. Immediately prior to HIFU treatment all patients were given intravenous sedation (4) or general anaesthesia (18).

Following open surgery the ablated specimens were examined histologically and lesions created by HIFU were measured. No bleeding was observed in any of the patients, indicating the safety of the procedure. There was however a palpable lump and an observable 'rim' of cells surrounding the ablated zone representing an inflammatory response to the treatment. The device used for treatment was a 12 cm PZT-4 transducer with a focal length of 90 mm operating at 1.6 MHz. The transducer had a fixed focus, which was displaced using six-direction movement controlled via PC. The peak focal intensities ranged from 5 to 15 kW/cm^2 and produced focal zone ellipsoids approximately 3.3 mm in length and 1.1 mm in diameter. The procedure was guided using a 3.5 – 5 MHz imaging transducer situated at the centre of the HIFU transducer, coaxial to the therapeutic beam. In a similar study published the following year 24 patients with pathologically confirmed breast cancer were treated, aged 23-65 years. Here the HIFU apparatus remained unchanged as that described previously, except the transducer (Haifu Model-JC) was driven at 0.8 MHz, with an average exposure time of 3500 s [19]. The patients selected had tumour masses ranging from 2 to 4.7 cm in diameter (mean 3.2 cm) and the majority of patients (19) were at clinical stage IIb. Following HIFU treatment patients underwent modified radical mastectomy and ablated tumour masses were removed and subsequently examined. Three of the patients underwent MRI and Single Photon Emission Computed Tomography (SPECT) examination before and after treatment, and the changes in tumour properties were observed.

A further paper was published by the above group (Chongqing, China) in 2004, providing an account of the 1038 patients with solid carcinomas treated in China from 1997 to 2001, 313 of whom were treated at the Chongqing University of Medical Sciences [19]. All patients were treated with the same device (described previously) operating at 0.8 MHz or 1.6 MHz depending on the application, and the procedure was similar for all those treated. A total of 106 patients with biopsy-proven breast cancer were successfully treated, with at least half of patients exhibiting total reabsorption of ablated tissue within 1 to 2 years. After a mean of 22 months a 100 % survival rate was observed, with all but one patient disease-free. Some 153 patients with primary and metastatic malignant neoplasms (osteosarcoma) in various locations (including bone

and lungs) were treated, with tumours of up to 46 cm in some cases. In a follow-up to the treatment (mean time 23 months) 85 % of patients were still alive, with five undergoing limb amputation due to local recurrence. Of the 77 patients treated for soft tissue sarcoma 18 were treated at the Chongqing Centre. Of these 18, 90 % (16) survived, after a mean follow-up time of 21 months 10 % (2) died of metastasis post HIFU treatment, and three of the survivors had to undergo a second HIFU treatment. Of the nine patients treated at the Chongqing Centre seven were alive at the follow-up time (mean 9 months) and showed stable lung metastases. Two patients died, one and three months postoperatively, due to cachexia and dyspnoea caused by severe lung infection. For the ten patients with unresectable pancreatic cancer, treatment with HIFU was a success. An interesting phenomenon was observed in these and other advanced stage cancer patients. In these patients, that suffered from severe cancer related pain HIFU was observed to effectively reduce this pain, thus improving patients quality of life both physically and psychologically. Overall complications with HIFU treatment were very low. Between 5 and 10 % patients suffered from mild fevers up to 38.5 ^{o}C for up to seven days following treatment, and it was observed that fever severity was proportional to the volume of the ablated tissue with several patients treated for very large tumours exhibiting fevers of up to 39.5^{o}C for two to three weeks. In total 10-20 % of patients experienced mild skin burns, however this was reduced to just 5 % through experience in evaluating skin damage as seen in real-time diagnostic images (during treatment). A sizable portion of treated patients (20-30 %) experienced mild local pain within the week following HIFU treatment, although only 5-10 % were given analgesics (oral) to combat this effect.

In a further study twenty two patients were selected (non-randomized) with disease stages I to IV. These patients' results were followed up at intervals, with the mean total follow-up time being 54.8 months [19]. The trial used the same equipment as previously described and the cosmetic result was judged to be 'excellent' in 94 % of treated patients. Disease free survival (and recurrence free survival) rates were 100 % (100 %), 100 % (89 %), 100 % (89 %), 95 % (89 %) and 95 % (89 %) at one, two, three, four and five years respectively. An interesting point made in this paper is the fact that compared to the West, in China women tend to be examined less regularly, hence

once discovered tumours are commonly above 2 cm, a size for which breast conserving surgery is not recommended in the West. Instead a radical mastectomy is commonly performed, and this becomes a more attractive option with increasing tumour size as treatment with HIFU will result in a palpable lump remaining, which although benign, will adversely affect some patients psychologically. Providing more information to patients may reduce this somewhat but as FUS is a non-invasive procedure there is no easy method of removing ablated tissue, apart from leaving the body to remove the cell debris by natural phagocytosis.

In a subsequent paper the histological and microscopic cellular changes of the patients treated in a previous study were quantified and analysed. As this does not relate directly to the project at hand a summary of these results will not be presented here. For more information please see [20]. One interesting equation given in this paper is that for calculating the volume of a (focal) ellipsoid, expressed as:

$$\frac{4}{3}\pi \times \frac{1}{2}length \times \frac{1}{2}width \times \frac{1}{2}thickness \qquad \{2.1\}$$

In 2006 a report in the European Oncological Disease Briefing (Issue 1) detailed the HIFU treatment of 118 patients who experienced local recurrence following radiotherapy for prostate cancer treatment from 1995 to 2002 [66]. All patients showed an absence of metastases on bone scan, computed tomography (CT) and MRI. In all cases patients were treated using the ABLATHERM transducer device manufactured by EDAP-TMS (France). Of the 118, 56 patients required hormonal treatment due to positive follow-up biopsies. Overall the survival rate was 71 % at 60 months post-operatively, with negative biopsies in 84 % of patients. Progression free survival rates were dependent on patients' initial risk and were 78 %, 49.5 % and 14 % for low, medium and high risk patients respectively. A number of patients experienced side effects due to the necrosed tissue 'migrating' into the urethra. These included some cases of urethrorectal fistula, but this was prevented by modifying the treatment parameters for later patients (post 2002). Using these modified parameters also reduced the more common narrowing (stenosis) of the urethra and bladder neck from 35 % to 6 %.

2.4: Chapter Conclusion

In this second chapter a literature review of a number of relevant publications has been given, describing the work of various groups focusing on HIFU techniques and devices, along with a number of accounts and results from relevant medical trials and other topics relevant to the narrative of the work described in this research. Revolving around the development of HIFU as a surgical technique, much of the information presented will be referenced in the following chapters and as such serve as both background and introduction to the main body of work presented henceforth.

In addition to general information and inspiration gathered from these reviewed publications, particular note should be given to the paper published in 2001 and authored by Gail ter Haar. In this article [4] a 'thermal dose' model was introduced, describing a method of quantitatively comparing the effect different heating regimes has on the necrosis of tissue. Using this model allows different temperature and exposure times to be compared. To such an end this technique will be utilised in a later section of this thesis when the results of simulations are being analysed.

Chapter 3:

Acoustics Theory & HIFU

3.1: Chapter Introduction

In this third chapter theory relevant to the interaction of acoustics and matter will be presented, with a focus on interaction with biological tissue. Background information involving HIFU and HIFU devices briefly described in the preceding chapter will be expanded on with examples of currently available HIFU devices being given.

Ultrasound transducers will be described and characterised beginning with simple single-element transducers. Transducer arrays and methods of beam focusing will be also be explained. Finally a comparison of various transducer geometries will be presented and considered, with an emphasis on the ability to focus and steer the propagated ultrasound within a three dimensional space, or volume.

3.2: Physics of Sound Waves & Interaction with Matter

Sound is by definition a mechanical energy that propagates through a medium via compression and rarefaction of the particles present in the medium [27]. This motion can be described as a longitudinal wave and is analogous to the motion of an elastic spring attached to a piston. The pressure variations, due to the compression and rarefaction caused by the sound wave, vary sinusoidally with time, with the compression corresponding to the peaks and the rarefactions to the troughs of the sine wave.

Ultrasound is defined as sound at a frequency of above 20 kHz (the human hearing threshold) with diagnostic ultrasound using frequencies of up to 30 MHz [31]. As ultrasound passes through a medium it transports energy. The rate of this energy transport is termed 'power', but as in most cases the ultrasound beam is focused into a small area (on a defined two dimensional plane) it is more prudent to refer to ultrasound in terms of 'intensity', or power per unit area. The intensity *(I)* of an ultrasound wave is related to the maximum pressure in the medium and is given by the following equation [31]

$$I = p_m^2 / 2\rho c \qquad \{3.1\}$$

Where 'P_m' is the maximum pressure, 'ρ' is the density of the medium and 'c' is the local speed of sound [31].

The velocity of ultrasound propagation is dependent on the medium it is propagating through. For example the speed of sound in air is approximately 330 m/s whereas through soft tissue and lead zirconate titanate (PZT, a common material used for transducer elements) sound velocities are approximately 1540 m/s and 4000 m/s respectively [27].

As ultrasound propagates through a medium energy is lost. This is due to scattering, absorption and reflection. The cumulative effect of these mechanisms is generally referred to as 'attenuation' and is important as the majority of energy lost (due to absorption) is irreversibly converted to heat (in soft tissue absorption accounts for 60 – 90 % of the attenuation, and scatter accounts for the remainder [31]).

The resulting behaviour when a sound wave encounters an object depends greatly upon the size of the object in comparison to the wavelength of the sound wave. As the frequency *(f)* of the wave is in general controllably fixed, the wavelength *(λ)* then depends on the local speed of sound in the medium.

$$\boldsymbol{\lambda = c/f} \qquad \textbf{\{3.2\}}$$

Thus the wavelength of sound in air and soft tissue are approximately 0.33 mm and 1.54 mm respectively, at a frequency of 1 MHz. If an encountered object is much larger than the wavelength and is relatively smooth [31] then part of the beam will be reflected and part will be transmitted, with an expected loss of intensity. This is termed 'specular reflection'. If the obstacle is small in comparison to the wavelength (surfaces become more 'rough' as wavelength decreases) then the wave energy will 'scatter' in numerous directions and little, if any, energy is transmitted in the original direction of the beam. This effect can be referred to as 'non-specular' reflection and is analogous to a mirror surface that has been 'steamed up' with the water droplets acting as non-specular reflectors, scattering the incident light thus reducing visibility [31]. Scattering can also occur due to small particles reflecting the beam within a medium. It is this mechanism that gives rise to characterized organ images that can be identified when using diagnostic ultrasound. Areas with high scatter amplitude are termed 'hyperechoic' and those with a lower scatter amplitude 'hypoechoic' [27]. Generally acoustic scatter from non-specular reflectors (scatterers) increases with increasing frequency, while non-specular scatter is generally frequency independent.

Following the encounter of a boundary or interface between two mediums, the remaining energy in the ultrasonic beam will drop exponentially. It is therefore beneficial to describe this loss in decibels *(dB)* using the following established formula

$$\boldsymbol{dB = 10log\ (I/I_0)} \qquad \textbf{\{3.3\}}$$

Where 'I_0' is the reference intensity, which is in this case the intensity of the beam immediately prior to encountering the boundary.

[NB: When dealing with pressure changes the above formula is altered to dB = 20log(p/p_0), where 'p' is pressure and 'p_0' is the reference pressure]

This can be calculated if the attenuation coefficient 'α' is known. For soft tissues 'α' can be approximated as 0.5 dB per cm per MHz [27]. Some attenuation coefficients are given below (see Table 1, [27]) for reference.

Table 1 - ***Examples of attenuation coefficients in human tissues***

Substance	**Attenuation coefficient for 1 MHz beam (dB/cm/MHz)**
Water	0
Blood	0.18
Soft tissues	0.3 - 0.8
Fat	0.5 - 1.8
Muscle	0.2 - 0.6
Bone	13 - 26

For example if a 1 MHz ultrasound beam propagates through 2 cm of fat, then 3 cm muscle the total energy loss would be as follows.

(0.6 dB/cm)*(2 cm) + (1,2 dB/cm)*(3 cm)

= 4.8 dB

This 4.8 dB loss equates to an approximate loss of 66 % of the original beam energy.

The ultrasound 'half-value thickness' (HVT) corresponds to the thickness of tissue that causes a 50 % (-3dB) decrease in intensity and is a useful measure when dealing with diagnostic ultrasound problems.

Reflection of ultrasound at an interface is dependent on the 'acoustic impedance' *(Z)* of the medium involved. This value is equal to the product of the density in the medium and the local speed of sound.

$$\boldsymbol{Z = \rho c} \qquad \textbf{\{3.4\}}$$

The magnitude of energy reflected at a boundary can be calculated using the acoustic impedance values of both media, giving a 'reflection coefficient' *(α_R)* as follows [31].

$$\boldsymbol{\alpha_R = [(Z_2 - Z_1)/(Z_2 + Z_1)]^2} \qquad \textbf{\{3.5\}}$$

The amount of energy reflected varies greatly when dealing with different pairs of media. For example 99.95 % of energy is reflected at an air-liver interface, whilst only 1.5 % is reflected from the interface between muscle and liver, due to the differences in acoustic impedance. The differences of acoustic impedance in tissues allows diagnostic ultrasound scanning to visualize internal bodily structures, although if the angle of incidence is more than three degrees it is unlikely that the reflected portion of the beam will return to the transducer, as the angle of incidence and of reflection are equal. This obviously depends on the transducer's size and of the depth of the reflector.

Another important interaction of ultrasound at a boundary is that of refraction. In this case the angle of the transmitted beam is altered due to the difference in local speed of sound on either side of the boundary as follows [31]

$$\boldsymbol{sin\theta_i/sin\theta_r = c_i/c_r} \qquad \textbf{\{3.6\}}$$

Here θ denotes the angle and 'i' and 'r' refer to the incident and refractive regions respectively. Also if $c_r > c_i$ then the angle will become steeper as it passes over the boundary. If the magnitude of the incident angle is great enough no ultrasound is transmitted. The angle at which this occurs is termed the 'critical' angle and is obtained by setting the refractive angle to 90 °, therefore θ_i becomes θ_c, the critical angle.

3.3: HIFU Background Theory

3.3.1: Summary

HIFU makes use of a focused ultrasound device to precisely and effectively destroy target tissues by thermal ablation (see Figure 2, [15]).

This process can be guided by computerized MRI or by ultrasound, which is more commonly referred to as ultrasonography when used in this type of application. These two systems are generally referred in their abbreviated forms, MRgFUS (or MRIgFUS) and USgFUS respectively. Currently only MRgFUS is able to accurately measure the heating effect produced by HIFU in real-time. Additionally MRI can operate from any angle and also has an increased tissue contrast than that of ultrasound. The drawback when using MRgFUS is that it cannot provide a continual feed of data due to the nature of its operation, instead images have to be captured at discrete intervals using computer equipment. Regardless of this MRgFUS is generally accepted to be the superior of the two processes, although future developments in both procedures may alter this balance.

As previously mentioned, the HIFU procedure operates on the principle that when an acoustic wave travels through tissue some of the energy of the wave is absorbed and converted to heat. Using focused beams this effect can be exploited deep within tissues, using a very small focus point to localize heating such that surrounding tissues are unaffected [11]. This occurs due to the energy in the individual waves being of small enough magnitude to not adversely affect the overlying or surrounding tissues. When focused correctly the areas of high pressure are superimposed (at the focal point) meaning energy deposition is much higher in the focal region than in the surrounding tissue. The focus is very well defined such that a target tissue (such as a cancerous tumour) can be rapidly heated and subsequently necrosed (given 1-2 s at a temperature of 56 °C or an equivalent dose[4]) without any permanent damage to the surrounding cells. By focusing consecutively at more than one location, or indeed scanning the beam a larger portion of tissue can be ablated.

Focusing and scanning of the beam can be achieved in a number of different ways. The beam can be focused geometrically using a curved transducer, or with an adjustable (acoustic) lens system. If the focal length is fixed, then an external positioning system with sufficient degrees of freedom can be used to adjust the position and depth of the focus by physically displacing the transducer and therefore the fixed focal point. Alternatively a phased array of transducer elements can be used to electronically focus and direct the ultrasound beams [27]. This is accomplished by dynamically adjusting the phase of the signals applied to the array elements, effectively steering the beam to the desired location(s). These differing transducer types will be discussed in detail in a subsequent section of this thesis (see Section 3.4).

Once the ultrasound beams are focused for a sufficient period, the target tissue undergoes coagulative necrosis and the oxygen supply to the cell is halted due to the destruction of the surrounding blood vessels [68]. The architecture of the tissue remains intact with the affected cells appearing grey and faded under microscopic analysis, which at least one author has described as having an ‘island and moat’ structure [27]. As this procedure involves precise ablation of the target tissue without the need to physically reach the tissue it is referred to as a *non-invasive* surgical process and can also be combined with more conventional methods of treatment such as radiotherapy and chemotherapy to achieve a desirable systematic effect.

A further point worth noting is the effect of 'cavitation' in the propagation of ultrasound. If gas bubbles are present in a medium then the compressions and rarefactions of the sound wave will cause the bubbles to shrink and expand, which can give rise to increased scatter. This is referred to as 'stable cavitation' [68]. If the ultrasound beam is intense enough the disturbance caused can be of such magnitude that extremely small bubbles are produced in the medium, generally in zones of rarefaction. These bubbles grow in size until the next compression, in which they will shrink and will eventually collapse creating shock waves and extremely high temperatures at the cellular level. This effect is generally termed as ‘unstable’ or 'dynamic cavitation' and is currently being researched as an additional method to destroy pathogenic tissue in HIFU treatments [69].

3.3.2: Uses of HIFU

As already stated guided HIFU procedures have been successfully used to destroy cancerous tumours in various bodily organs. However, the widespread use of this technique has not yet been approved by most major health organizations, and more research work is called for before HIFU treatments become common practice. Nonetheless there are other interesting areas in which HIFU has been used to successfully treat patients.

One of these areas is the combined use of HIFU to directly treat cancer at the same time of facilitating a localized release of anti-cancer drugs. This can be achieved by encasing the drugs in temperature sensitive bubbles (often referred to as vesicles) artificially created from a similar material to that found in cell membranes [21]. The structure of these 'liposomes' is such that one ‘end’, the 'head' of the vesicle is hydrophilic while the 'tail' is hydrophobic, which causes the liposomes to orientate themselves such that they are similarly lined when up in the presence of water. The ‘bilayer’ formed prevents the encapsulated drugs from escaping the liposome until some trigger causes the drug to be released. This can be achieved when the bilayer interacts with a particular cell membrane, or in the case of their use with HIFU, when a temperature above that which is found in the body is used to breakdown the bilayer, thus releasing the 'packet' of drugs to the area within which this high temperature occurs. The high temperature region may be created by using HIFU technology, or more commonly using a hyperthermia device, that heats a larger portion of tissue (than HIFU generally does) to a lower temperature, of around 45 °C. Using liposomes for targeted drug release allows concentrations of drugs 10 times higher than those used in traditional methods to be released, hence allowing for more effective drug use with greatly reduced side effects as the drugs are not released system wide. There are presently three main types or categories of these liposomes: multilamellar vesicles (MLV) small unilamellar vesicles (SUV) and large unilamellar vesicle (LUV) all of which are generally used to deliver different types of drug [21].

Uterine fibroids can also be treated using HIFU. This procedure was approved by the FDA in 2004 and is widely accepted as a plausible method of treatment. The treatment

of atrial fibrillation, a common form of heart arrhythmia can also be achieved using HIFU. In this procedure defective heart tissue is ablated, allowing treatment without the need for largely invasive conventional surgery. The use of HIFU in this application has been approved throughout Europe and is undergoing approval by the FDA for use in America.

3.3.3: Advantages of HIFU

By far the largest advantage of HIFU procedures is the non-invasive nature of treatment. The capacity to precisely target areas deep within tissue using external equipment while simultaneously avoiding damage to the surround tissues is largely unique within the medical procedures of today. In effect HIFU can be used as a surgical tool, performing operations inside the body without the need for open surgery. While radiation and chemotherapy are accepted methods of treatment in the area of cancer, HIFU can be used to non-systematically target the affected zone. This is possible due to the nature of the passage of ultrasound through biological tissue, which only has a destructive effect when precisely focused, in this case on the tumour or other diseased tissue. It is this characteristic that makes the use of HIFU such an attractive, non-invasive option. Additionally blood vessels surrounding the ablated volume are effectively cauterized, preventing repair of the ablated tissue and also bleeding into the surrounding tissues(s).

3.3.4: Other Groups' Work & Example Devices

Fully guided HIFU systems are already available commercially. One company that offers these systems is Chongqing Haifu Technology of China which was briefly mentioned earlier in this thesis. Chongqing offer Magnetic Resonance guided systems, and an example of the kind of specification that they offer is given for reference below (see Table 2 [70]).

Table 2 - ***Example specification of typical Chongqing surgical HIFU device***

Focal region for treatment:	1.1mm × 3.3mm—1.4mm × 5.6 mm
Range of acoustic intensity within focal field:	5000 W/cm^2—25000 W/cm^2
Therapeutic frequency:	0.8 MHz—2.4 MHz
Accumulative error of the linear movement:	± 1 mm
System noise:	≤65 dB(A)

Blatek Ultrasound Transducers is a company that offers MRI compatible HIFU transducers to a worldwide market. They will design and fabricate transducers to meet customer specific requirements or applications. An example of a typical set of parameters that can be specified by the customer is given below (see Table 3 [71]).

Table 3 - ***Example specification of typical Blatek Ultrasound Transducers surgical HIFU device***

Material availability	1-3 piezocomposites, PZTs
Power handling	Up to 30 W/cm^2
Efficiency	50 % to 75 %
Frequency range	0.2 MHz to 6.0 MHz
Shaping capability	Spherical and Cylindrical (F Number 1)
Size range / spherical	Up to 6 ” Diameter
Size range / cylindrical	Unlimited
Bandwidth	30 % to 70 %
Impedance	50Ω ± 5Ω
Phase angle	0º ± 5º
Array capability	Yes
MRI compatibility	Yes

Piezo Technologies is another company that specialises in HIFU products, in particular custom, semi-custom and modular transducer products. Also Precision Acoustics is a company that design and fabricates HIFU transducers, as is Sonic Concepts, which offers a wide range of HIFU transducers for different applications and also provide data sheets for all their products on their website.

3.4: Characterisation of Different Transducer Types

Ultrasound transducers convert electrical energy into mechanical energy and, in the case of imaging (diagnostic) transducers, mechanical to electrical energy. This is made possible by the use of piezoelectric materials that deform when a voltage is applied to either side. Similarly a mechanical deformation causes a voltage to be developed across the material [31] (see Figure 3, [27]).

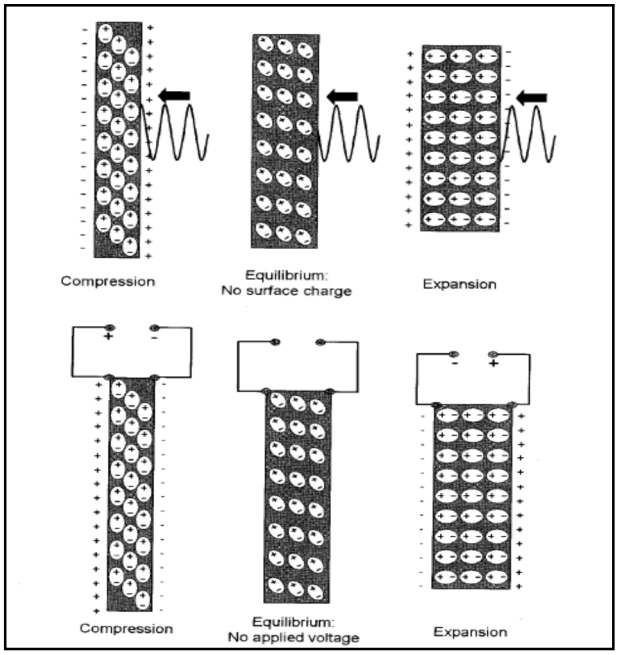

Figure 3 - *Piezoelectric principle*

Many natural crystal structures exhibit piezoelectric characteristics (such as quartz) but this is generally at low temperatures. Synthetic piezoelectric crystals are most often used in ultrasound transducers. One such material is PZT (a piezoelectric ceramic) which has no piezoelectric properties at room temperature. To prepare PZT for use the material is heated to above its 'Curie' temperature (approximately 340 °C for PZT) and a voltage is applied to align the dipoles in the crystal structure [27]. The material is then cooled whilst the voltage remains applied. The resulting material shows piezoelectric properties at room temperature.

The deformation of the piezoelectric material due to a voltage being applied causes a pressure wave to be emitted from the surface of the transducer. If an alternating current (AC) source is used a series of sinusoidal pressure waves will be produced. In

focused ultrasonic transducers this effect is exploited, and many pressure waves can become superimposed at the focal point, thus resulting in an elevated acoustic intensity. This is the principle on which FUS operates.

3.4.1: Ultrasound Transducers

3.4.1.1: Single Element Transducers

In resonance transducers a voltage 'spike' is applied, causing the material to resonate at its natural frequency, which is determined by the material thickness. When the material undergoes contraction-expansion-contraction (one cycle) compression waves move toward the centre of the crystal, from the front and back faces. If the crystal element thickness is equal to one wavelength (in the crystal) then the compression waves would arrive at the edges just as the next contraction begins, thus the second signal would be dampened, meaning a large reduction in efficiency. If the element thickness is equal to half of the local wavelength then the compression wave reaches the transducer edge just as expansion begins, meaning they constructively combine. This case is true for all transducer element thicknesses with an odd multiple of half wavelengths [31] although increased thickness adds to attenuation and therefore decreases efficiency. In general the element thickness should be equal to half the wavelength of ultrasound in the material such that each compression wave adds constructively to the subsequent expansion (see Figure 4, created using [3]) and that extra attenuation is not added by excessive thickness of the material (for example three or even five half wavelength thicknesses). Resonant transducers generally transmit (and receive) at a 'centre frequency' [27].

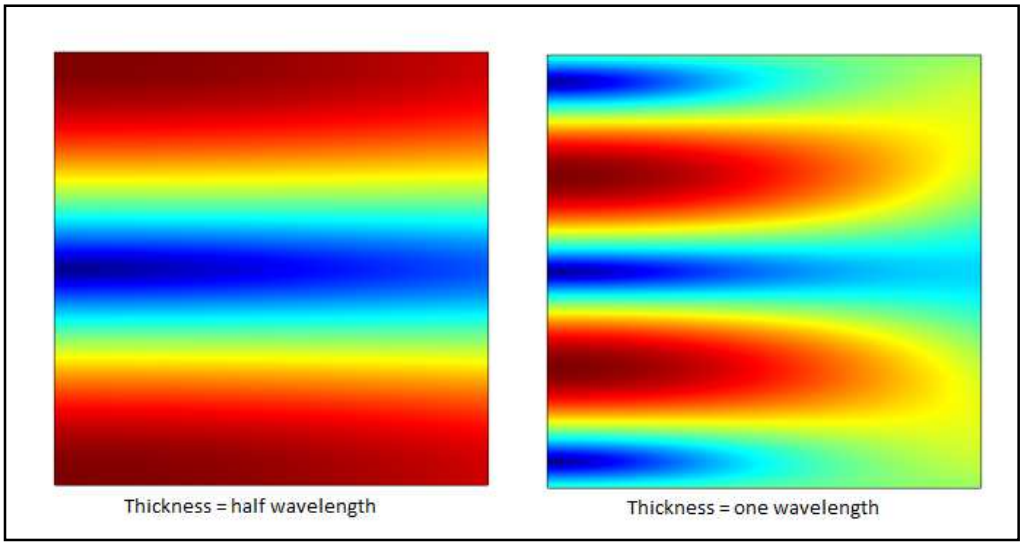

Figure 4 - ***Pressure field showing effect of piezoelectric material thickness on preferential wave emission: Red (compression), Blue (rarefaction)***

In general transducer assemblies have certain common features, including an insulating case, a shield, an acoustic absorber, a backing block, the piezoelectric element and a matching layer as shown in the diagram below (see Figure 5, [27]).

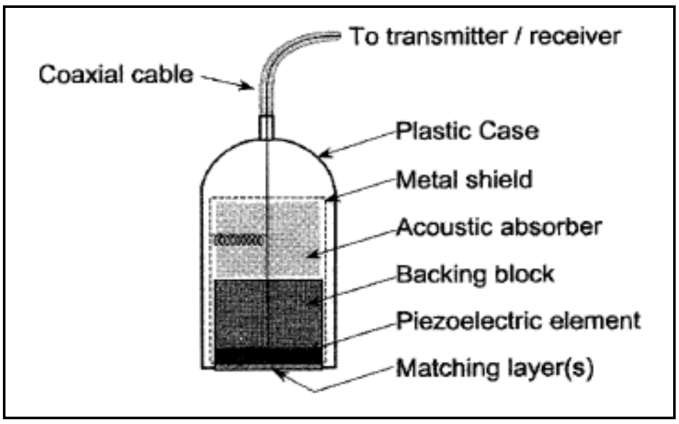

Figure 5 - ***Single element transducer***

The backing (or damping) block, if present, is located behind the piezoelectric element. This block absorbs the backwards propagated ultrasonic waves caused by the vibration of the element. It also absorbs stray signals from the housing, but its main function is to dampen the forwards propagated ultrasound to create a pulse, rather than a continuous wave. In diagnostic applications short pulses allow detail along the main beam axis to be enhanced, although it also introduces a broader band of frequencies around the resonant frequency. This effect is generally termed 'ring-down' and is quantified using a measure named the 'Q-factor' *(Q)* [27].

$$\boldsymbol{Q = center\ (resonant)\ frequency/Bandwidth} \qquad \textbf{\{3.7\}}$$

A high Q-factor value indicates a narrow bandwidth and long (spatial) pulse length given rise to by a small amount of damping, while a low Q means shorter pulses and a wider bandwidth, the effect of heavier damping (see Figure 6, [27]). When designing a HIFU transducer it is preferable to have a high Q-factor. One exception to this is in the case of a dual mode transducer where the same array is used for both imaging and therapy, such as that suggested in a previous study [72]. Here there will be a compromise between wide bandwidth (for more comprehensive imaging) and narrow bandwidth (for efficient therapy).

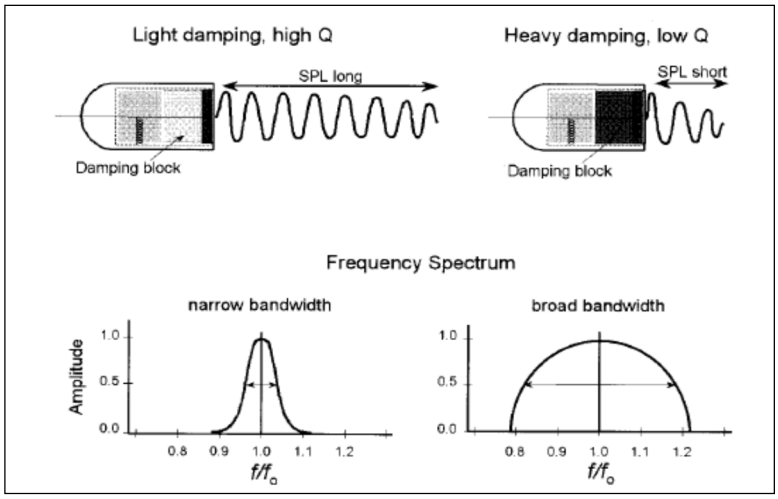

Figure 6 - ***Relationship between damping, pulse length and Q-factor***

The matching layer (see Figure 5) exists to minimize the loss caused by the difference in acoustic impedance between the transducer and the propagation medium and as stated is designed to have a thickness equal to one-quarter of the ultrasound wavelength in the piezoelectric material used. This layer should have acoustic impedance equal to the geometric mean of the piezoelectric material and the tissue, in line with the formula below [31].

$$\boldsymbol{Z_{matching\ layer} = \sqrt{(Z_{transducer}\ x\ Z_{medium})}} \qquad \textbf{\{3.8\}}$$

Where, as previously stated

$$\boldsymbol{Z = \rho c} \qquad \textbf{\{3.4\}}$$

There can in fact be more than one matching layer, and in this case the layers are chosen such that they have acoustic impedance that are intermediate to those of the transducer and the tissue being diagnosed or treated, although as already noted if more than one layer is present, the total layers must be an odd multiple of the one-quarter wavelength measure, for example three layers each with a one-quarter wavelength thickness. From the above, an increased number of matching layers may appear to improve efficiency, but the increase in material thickness leads to increased attenuation. For this reason only one matching layer, of one-quarter wavelength thickness is typically used.

Non-resonant transducers can be adjusted to alter their centre frequency, and for this reason they are sometimes referred to as 'multi-frequency' transducers, with bandwidths exceeding 80 % of the centre frequency [31]. These transducers are commonly fabricated using rod like elements mounted to a plate, with epoxy used to create a smooth face and are generally referred to as piezocomposites. An advantage of this type of transducer is that acoustic properties are closer to that of tissue, therefore matching layers are not as important and the efficiency of transmission is increased [27]. These transducers are excited using a square wave 'burst' allowing the centre frequency to be chosen within the limits of the transducers bandwidth.

3.4.1.2: Transducer Arrays

Up to this point only single element transducers have been discussed. It is much more common for transducers to employ multiple piezoelectric elements arranged into arrays, typically containing 128 to 512 individual elements of rectangular shape [27] although circular and other shaped elements can be used. These arrays can be activated in a linear, or in a phased sequence.

Linear arrays typically have more elements and as such are generally larger assemblies. Each operation involves the activation of a number of adjacent elements, which in effect produces a 'synthetic aperture', the width of which is determined by the number of elements activated and the element spacing. Linear arrays can also utilise phasing of elements to direct and control the ultrasound propagation (linear phased array).

Phased arrays generally comprise less than 128 elements and are physically smaller than their (non-phased) linear counterparts [27]. In this kind of array all elements are used, with small time delays between element excitation signals that allow the beam to be steered and focused without physically moving the transducer (see Figure 7, [73]). This presents a major benefit over linear arrays, which generally require a very precise mechanical positioning system for accurate steering and focusing.

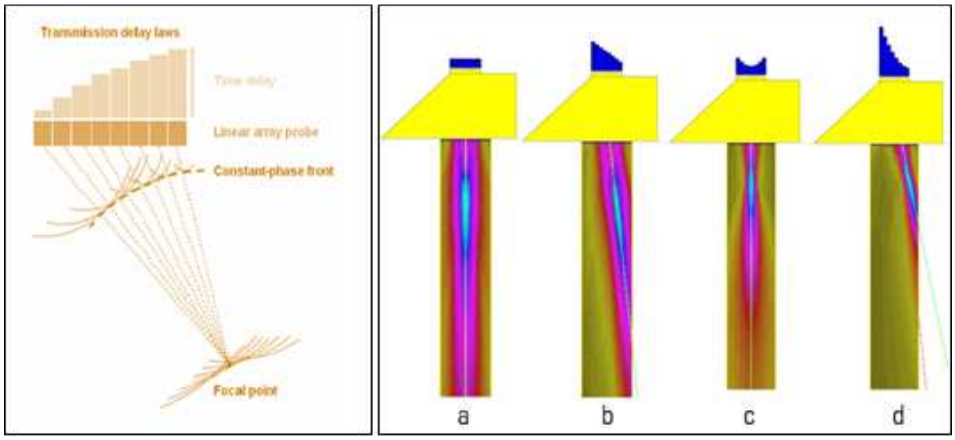

Figure 7 - ***Steering and focusing using a phased array***

3.4.1.3: Beam Properties

As previously stated an ultrasound beam propagates as a longitudinal wave from the transducer into the medium. The beam pattern created consists of two sections. In the 'near field' the beam converges progressively towards the focal point. After reaching this point the beam diverges (the 'far field').

In a simple, single-element transducer the near field length is proportional to the transducer diamete. In multiple element transducers the 'transducer diameter' is taken as the diameter of the group elements that are excited at one time (synthetic aperture).

The near field or Fresnel zone [27] convergence occurs due to the constructive and destructive interaction of waves emitted from the transducers surface. This can be

modelled as a large, or infinite, number of small (point) sources, each of which emitting ultrasound radially (see Figure 8 [27]).

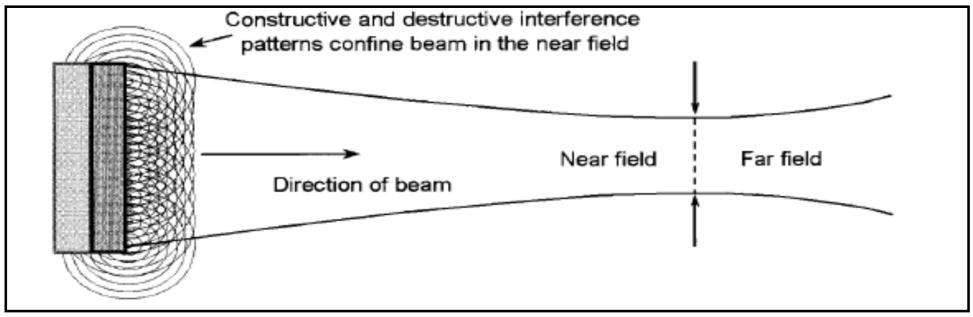

Figure 8 - ***Huygen's principle – showing radial propagation from point sources***

The length of the near field is dependent on transducer diameter (or radius *(r)* as below) and frequency, and it can be calculated, for flat faced transducers, as follows [31].

$$\boldsymbol{Near\ field\ length\ =\ r^2/\lambda} \qquad \textbf{\{3.9\}}$$

This shows how a transducer with a higher frequency and a larger diameter leads to a longer near field length and therefore will have a greater range before intensity begins to decrease.

It is worth noting here that pressure distributions in the near field are complicated due to the interactions of the wavelets created. Only once the far region is reached do the pressure variations decrease in a continuous fashion [27].

The far field or Fraunhofer zone is defined as the point at which beam divergence begins. The divergence angle can be given by [31]

$$\boldsymbol{sin\theta\ =\ 0.6(\lambda/r)} \qquad \textbf{\{3.10\}}$$

These estimations of Fresnel zone length and beam divergence apply mainly to linear diagnostic transducers, although they can be used to provide indications in HIFU transducer design. In medical imaging applications transducers with long near field lengths are preferred. This leads to higher frequencies being used and employing larger diameters when designing transducers for this type of use.

3.4.1.4: Focusing

Single element transducers can be focused by using a curved element, or by using a focusing lens. In both cases the focal point is generally fixed, and movement is achieved through mechanical devices. In a phased array transducer the constructive and destructive interferences between waves are used to steer and focus the beam. For example a shallow focus is achieved by activating the outer elements first and the centre elements last (see Figure 7). In both cases a focal point is produced. The intensity at the focal point can be 100 or more times the intensity produced at the surface of the transducer [31].

For example, in the case of 'cupped' transducers the focal length is approximately equal to the radius of curvature of the transducer. Furthermore the focal zone *length* can be approximated using the formula below [31].

$$\boldsymbol{Focal\ zone\ length\ =\ 10\lambda\left(\frac{f}{d}\right)^2} \qquad \textbf{\{3.11\}}$$

Where $(\frac{f}{d})$ is referred to as the 'f-number' of the transducer. This then shows the focal zone length, for a transducer with f-number equal to one (common for HIFU transducers) will be approximately 10 times the local wavelength of the propagated ultrasound (approximately 15 mm at a frequency of 1 MHz in soft tissue, similar to that observed in a previous study [4]).

The degree of focusing of a transducer can be quantified by the ratio of near field length to focal length. If this value is lower than six, the focusing is considered weak, if it is equal to 20 or more then the transducer can be said to have a strong degree of focus [31].

Note: As previously stated, the term '$\left(\frac{f}{d}\right)$' or the ratio of focal length to diameter of the transducer, is generally referred to as the 'f-number', and it is widely used to concisely describe transducer geometry.

3.4.2: Transducer Geometries

As the geometry of a particular transducer depends heavily on the application it is designed for there exists a multitude of differing geometries to choose from. In the following section transducer geometries that can be effectively utilised for HIFU use will be described here.

3.4.2.1: Planar + Lens

This type of transducer setup generally involves a planar, single element transducer used in conjunction with a suitable acoustic lens, commonly fabricated from acrylic resin (see Figure 9, created using [74]). One example of this apparatus is used in a previous study [23] where a 10 cm diameter PZT-4 disc transducer (single element) is focused using a Perspex lens with radius of curvature 6.3 cm, resulting in a total focal length of 14 cm. A similar transducer arrangement is used in the Haifu model JC [70]. Here a 12 cm diameter PZT-4 disc transducer again constructed as a single element, is used in conjunction with an acoustic lens resulting in a total focal length of 90 mm, although in this case the transducer/lens assembly can be displaced using a highly accurate mechanical positioning system, allowing adaptable treatment planning. This type of arrangement can be said to be analogous to the focusing of the incident sunlight using a magnifying glass, which given the right conditions, can cause the temperature at the focus to become elevated to the point that combustion occurs.

The drawback of using this kind of transducer arrangement is that energy is lost as the ultrasound propagates through the lens. This results in a lower overall efficiency. In addition the focal spot can only be shifted by physically moving the apparatus, or changing the lens used.

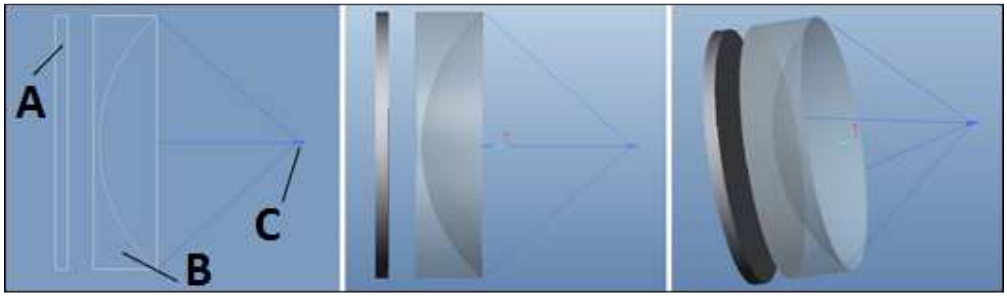

Figure 9 - ***Diagram showing planar transducer (A) focused to a point (C) using an acoustic lens (B)***

3.4.2.2: Linear & Linear Phased Arrays

Linear arrays comprise a number of elements, generally in just one direction (one row) although this is not always the case. The elements in liner phased arrays can be used to alter the position of the focus by altering the phase (or timing) of the input signal to each element. This allows not only transverse steering but also dynamic depth focusing, as can be seen in the diagram below (see Figure 10, [75]). This type of transducer is commonly used in diagnostic ultrasound devices, where the focusing is weak and is utilised to obtain a higher quality image, rather than focusing to create high peak intensity at the focus, as is performed when using HIFU in surgical applications. In HIFU applications there is a need to focus in the elevation direction, as well as in the transverse. This generally requires a different type of transducer geometry.

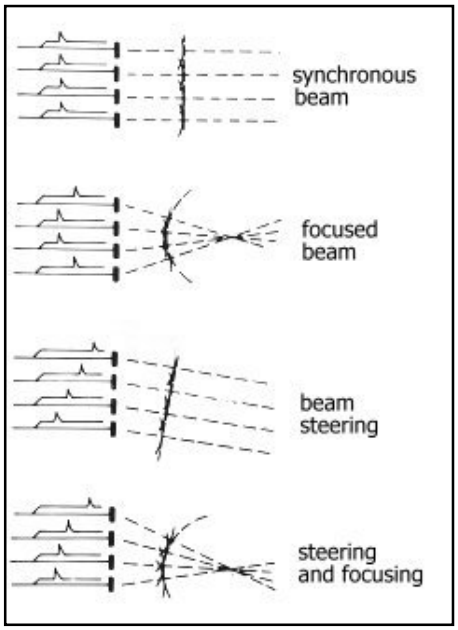

Figure 10 - ***Using phased excitation signals to steer and focus a linear array***

3.4.2.3: Linear Phased Array with Lens

Similarly to phased cylindrical-section arrays this kind of transducer assembly allows pre-focusing in the elevation direction while utilising phased signals to focus in the azimuth direction (see Figure 11, [75]). Using this type of arrangement does not seem to carry any major advantage over using a cylindrical-section phased array, which utilises curved elements in place of a curved acoustic lens, to allow pre-focusing in the

elevation direction. One advantage that this type of transducer arrangement may provide is a lower initial cost, as the manufacturing process to create a cylindrical-section linear array is more complicated and therefore generally more expensive. Although this is true, the higher running caused by using a lens due to decreased efficiency will eventually overshadow the lower initial cost of fabrication. It is for these reasons that the arrangement described cannot be recommended. If this general type of assembly is sought it is this author's opinion that a curved linear phased array, with radius of curvature equal to the equivalent lens radius of curvature should be used thus allowing focusing in two planes with no 'extra' losses in the lens apparatus. It should be noted here that using this type of arrangement, controlling focal depth is made difficult by the fixed curvature of the lens, while focal position in the azimuth direction can be controlled using phased excitation signals to the individual elements in the array.

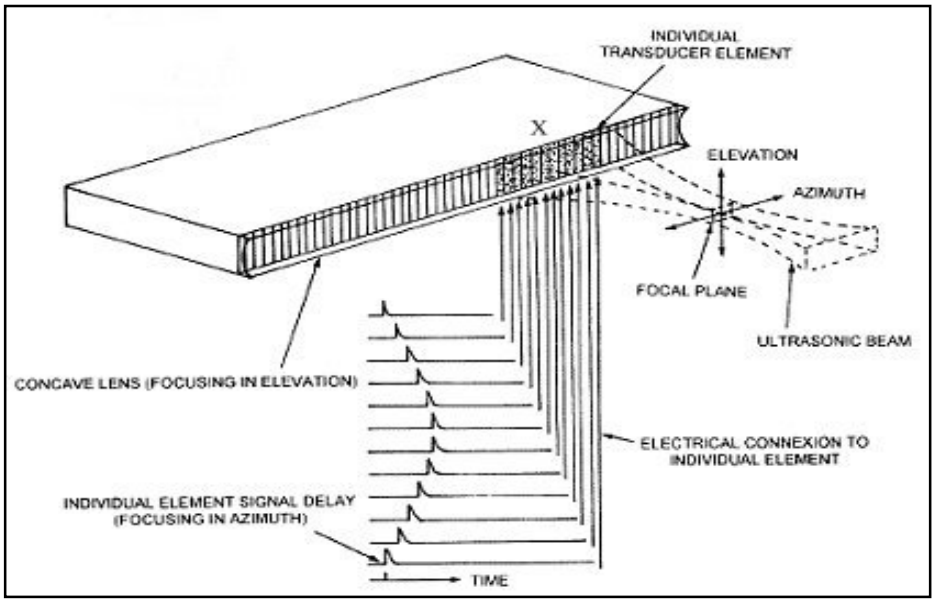

Figure 11 - ***Diagram of a phased linear array, pre-focused in the short axis dimension using an acoustic lens***

3.4.2.4: Spherical-section / Annular Phased

Spherical-section transducers generally resemble the shape of a bowl and have a natural focus equal in length to the radius of the transducer (see Figure 2 for an example). It is common when using annular transducers to also use a motorised gantry to allow the transducer to be accurately positioned for use.

Spherical section phased transducers generally make use of annular or 'ring' electrodes, which can be used to control the focal depth by manipulating the phase difference of the excitation signals provided to each element. An important design note for this type of ring arrangement is that grating lobes (for example side lobes around the main, focal lobe) can be avoided if the pitch of the ring elements (measured between element centres) is less than a wavelength wide in the transducer material used [24].

3.4.2.5: Annular Truncated (Transrectal/Transvaginal)

This type of transducer is a modified version of the above. Here two parallel planes are used to truncate the originally bowl shaped transducer. This results in a 'spoon' or 'scoop' shape, the primary advantage of which is the facilitated entry of the transducer into the rectal or vaginal cavities.

As with their non-truncated counterparts, these transducers can also make use of ring elements and phasing of excitation signals, the difference here is that only the centremost elements are full rings, while the outer elements form partial rings due to the truncation of the two parallel sides (see Figure 12, [76]).

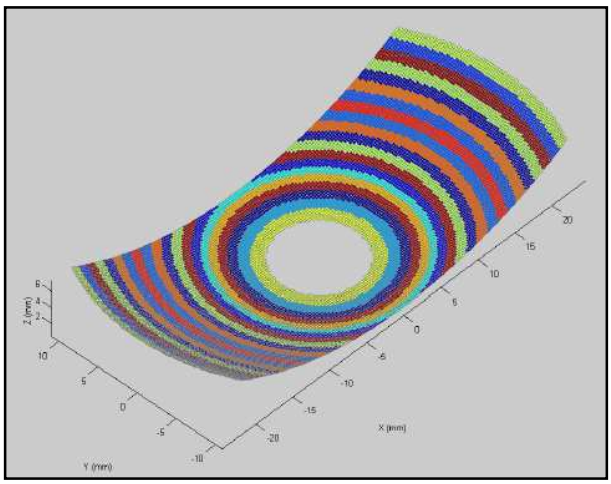

Figure 12 - ***Diagrammatic representation of a truncated annular phased array – coloured bands represent neighbouring ring elements***

3.4.2.6: Cylindrical-section / Linear-concave

As previously mentioned this type of transducer array utilises geometry to pre-focus in the elevation direction. Just as the spherical-section type transducers have a natural

focus at a distance equal to the radius of the 'bowl', annular arrays are pre-focused at a distance equal to the radius of curvature of the cylindrical section used in construction. Compared to their annular counterparts the cylindrical focusing will be weaker because they are naturally focused in only one direction (the elevation direction) not two (azimuth and elevation) as in annular transducers. In effect these transducers focus 'along a line' rather than to a predetermined central point.

3.4.2.6.1: Cylindrical-section / Linear-concave - Phasing Techniques

Using differently phased signals applied to the elements of an array in this type of transducer allows more than one method of dynamic focusing. As the 'beam' produced is already focused in the elevation direction (as described above) using multiple elements in the azimuth direction therefore allows the beam to be steered along the 'line' of focus (in the 'x-direction' shown in Figure 13, left [77]). This is an effective method of use in terms of FUS provided there is sufficient intensity at the desired focal point. It is worth noting here that the resultant focal zone (when focusing off-centre using phasing) and hence the lesion produced would be at an angle to the cylindrical z-axis, therefore a more complex treatment plan would be required to compensate for this effect to allow optimal coverage of the target volume.

Another option is to use synthetic apertures. This involves exciting only some of the elements in the (hypothetical) cylindrical array. If for example the array had sufficient power output using only half the available elements then a focus could be achieved anywhere within the centre two-quarters (of the array (see Figure 13, right). The focus formed in this case would not be at angle as the beam has not been steered.

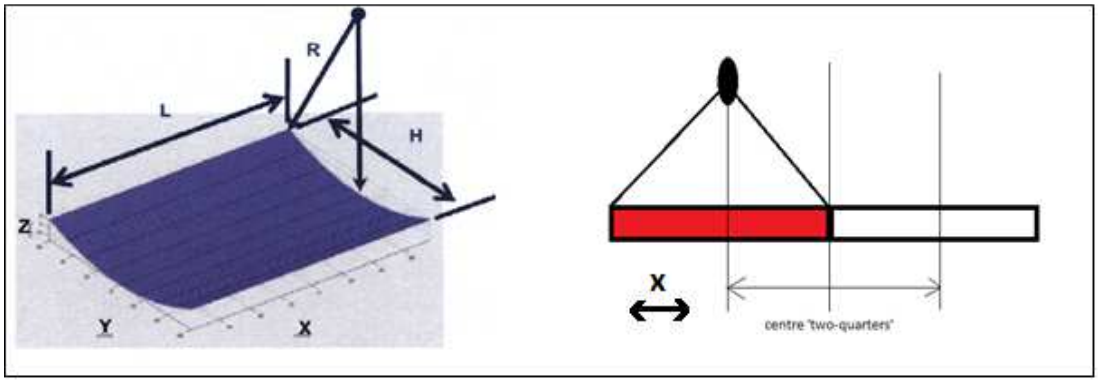

Figure 13 - ***(Left) Diagram of a cylindrical phased array transducer - (Right) Half of transducer elements activated, giving a focus at one quarter along transducers length***

3.5: Chapter Conclusion

In conclusion this chapter has introduced theory relevant to acoustics and sound wave propagation and its interaction with matter. The concept of acoustic intensity has been introduced, as well as an expanded description of attenuation coefficients with examples of typical values for the attenuation of acoustic waves within some common tissues being given. Acoustic impedance has also been introduced which will be an important physical property to consider during HIFU transducer design.

A further explanation of HIFU has been given, with information on ultrasound and magnetic resonance imaging as methods of guiding surgical HIFU treatments.

Furthermore an explanation of the basic construction of devices capable of producing ultrasound has been presented along with factors that affect the properties of the acoustic fields, produced by these transducers. The concept of a focal ‘f-number’ has been briefly introduced. Information on various methods of beam focusing and steering has also been presented, which is an important factor when considering the design of a surgical device capable of tissue ablation within a volume, as is the main focus of this research. A number of ultrasound transducer geometries have been described and characterised, forming a basis for the suitability study presented in the following chapter (see Section 4.3).

Chapter 4:

Integration of HIFU & EIM

4.1: Chapter Introduction

In this chapter the problem at hand, to integrate a HIFU device into an existing Electrical Impedance Mammography (EIM) imaging system, will be fully defined. From this definition a suitability study of the transducer geometries described in the previous chapter will be given, with a focus on integration with the EIM system. A suitable transducer geometry will then be selected and following this a design specification will be created. Various properties of the proposed transducer will be decided in this section, specifically those that will affect the resultant acoustic field of the resultant HIFU device and thus the effectiveness of the device as a surgical tool.

4.2: Problem Definition

As stated in the introduction to this thesis, the main objective of this study is to integrate a HIFU transducer into the existing EIM scanning apparatus. In addition the field of view of the HIFU transducer, and therefore the treatable zone, should be as close as possible to the entire volume scanned by the EIM system. This must be considered when defining suitable transducer designs. It is therefore now pertinent to define the restrictions imposed by this existing imaging device.

The existing device is designed to diagnose and locate cancerous tissue within the human breast and to this effect has been designed to have a patient interface in the form of a cylindrical tank, with a diameter of approximately 18 cm. Within this cylinder, or 'scanner head' (see Figure 14, created using [74]) an 'electrode plate' (see Figure 15, created using [74]) is installed, fixed within which are a number of equally spaced electrodes covering the plate, that form the active part of the apparatus when performing an EIM scan (note in Figure 14 all but the central electrode hole have been removed due to intellectual property issues). The electrode plate can be translated vertically using a stepper motor (located below the scanner head) via a leadscrew arrangement. The plate can also be rotated using a second steeper motor.

The electrodes are a vital part of the EIM system, to which modifications should be minimised. Having said that, in previous projects involving modifications and additions to this plate removal of a small number of these electrodes has been permitted. Without going into great detail this removal leaves an available space of approximately 7 cm by 2.5 cm, therefore this is the *maximum* available space for addition of a HIFU transducer, assuming it were to be installed into the plate. This space would therefore allow a physical footprint of 17.5 cm^2, a figure that must be considered when determining the acoustic power produced, and therefore the maximum focal intensity possible, as the power produced is directly proportional to the active surface area of the transducer. It should be noted here that different piezoelectric materials will have differing maximum acoustical powers, therefore with a limited available space a material with a high acoustic power output should be selected. Appropriate material selection will be covered later in this thesis.

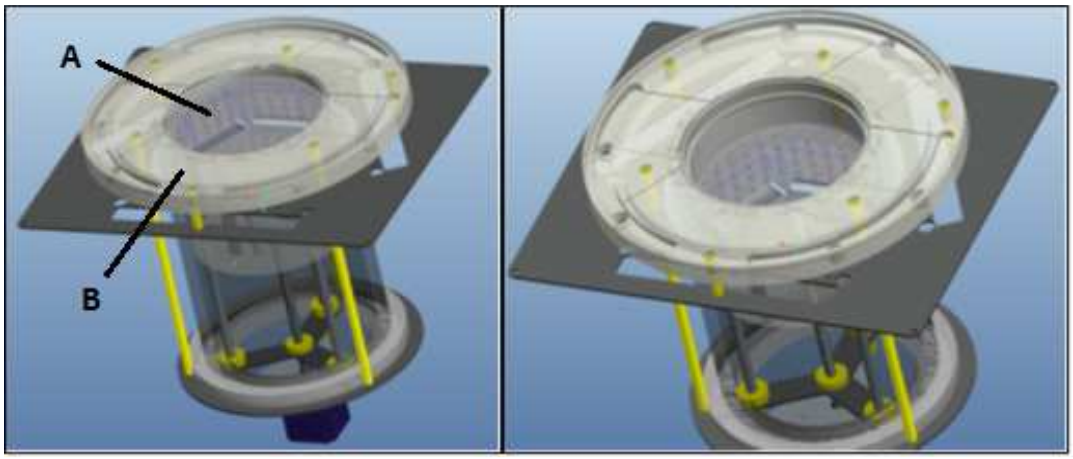

Figure 14 - ***EIM system 'scanner head'; (A) 'Electrode plate', (B) 'Top surface of scanner head' (flush with system bed cushioning prior to patient being positioned)***

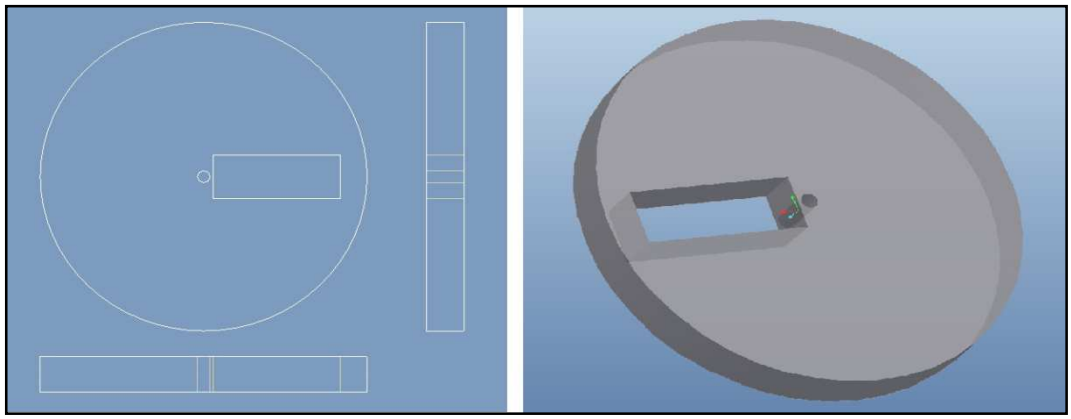

Figure 15 - ***Plan view (left) and 3D view (right) showing simplified 'electrode plate' showing centre EIM electrode hole and rectangular section removed for hypothetical installation of HIFU transducer***

One of the challenges that must be overcome if the HIFU transducer is to be installed into the electrode plate is the centre electrode (see Figure 15). This electrode is vital in the operation of the EIM system, thus cannot be removed. This means that the centre 'column' above this electrode would not easily be covered by the field of view of the HIFU transducer, if the transducer was to be placed in the gap shown. Although this is a potential drawback to the operation and effectuality of the FUS treatment it has been decided that at this prototyping stage it is more important to achieve a working 'proof of concept' design that confirms the feasibility of HIFU transducer incorporation and that the problem of this centre electrode will be addressed at a later date once the prototype has been proven successful. One possible solution to this problem is to focus *outside* the length of the array by using phased excitation signals. The feasibility of this 'extreme' focus will be explored using simulations, the results of which will be presented later in this thesis (see Chapters 5 & 6).

At present the patient is required to lie face down on the system 'bed' and insert one breast into the scanner head (located in a cut-out in the bed cushioning) after which the electrode plate is lifted using a motor to a distance of less than 1 cm away from the skin of the prone breast. The breast itself may be compressed using a second plate giving a maximum tissue 'height' of 4 cm. During an EIM scan the scanner head is filled with a weak saline solution at temperature of approximately 37 °C. Therefore the total distance from the plate to the chest wall of the patient is 5 cm, 1 cm saline solution (maximum) and 4 cm breast tissue. A further challenge to HIFU transducer incorporation is that there must be no interval between the EIM scanning of the patient and the HIFU treatment, as movement of the patient, be it purposeful or not, would adversely affect the treatment plan and could result in ablation of healthy tissue or failure to ablate the target tumourous tissue. The compression of the breast itself will assist in preventing movement but the main consideration here is that the HIFU transducer must be in place *before* the EIM scan commences to ensure minimum movement between scanning (EIM) and treatment (HIFU). Therefore it is not possible to 'swap' the electrode plate for a 'HIFU' plate and as such, the HIFU transducer must be incorporated into the existing plate, or must be situated outside of the scanner head itself. Situating the HIFU transducer outside the scanner head has some drawbacks. Firstly, the scanner head is housed in a bed or 'trolley' that contains the various subsystems allowing EIM scans to take place. At present the space within the trolley and around the scanner is limited by design. This allows the physical footprint of the complete system to be minimised (to be of similar size as that of a standard hospital bed) but also means that the available space is limited. Secondly the scanner head cylinder itself is constructed from thick Perspex, so the ultrasound waves would be attenuated somewhat. This means the transducer would have to be able to provide enough 'extra' acoustical power output to compensate for this. Given the limited space around the scanner head this may become a problem, as the acoustical power output is dependent on the active surface area of the transducer. Furthermore, to avoid this problem an acoustic 'window' would have to incorporated into the scanner head design, and as the scanner head must be watertight, this would mean a significant if not total redesign of the apparatus would be needed. In this author's

opinion this should be avoided unless absolutely necessary, at least at this ‘proof of concept’ design stage.

4.3: Suitability Study

Now the problem at hand as been defined and a brief description of relevant transducer types has been given (see Section 3.4) it is relevant to shortlist the transducer types that are most compatible with the existing apparatus. The possible configurations therefore will be briefly described and following this the most appropriate design will be selected.

One possible configuration is to use a spherical-section array from underneath the cylinder. Using annular elements would allow 'depth' of the focus to be controlled, such that a focal point could be created anywhere along the 'central axis' of the transducer. Although this would allow a focus along the central axis of the cylinder from where the transducer is mounted, steering side-to-side would be difficult to accomplish. Tilting the transducer to achieve this would mean the coupling to the cylinder would be made difficult. Also to allow this tilting there would have to be an auxiliary movement system in addition to those already present in the existing apparatus. Alternatively this movement system would have to be capable of translating the transducer around the base of the cylinder such that the whole volume, and therefore the whole of the breast, could be treated. All these methods would involve not only an additional motorised movement system, but also a suitable coupling or acoustic window. As described previously this would be difficult to achieve due to the cylinder having to remain watertight at all times. For this and all the previous reasons mentioned it is suggested that this design not be used, unless a complete redesign of the existing scanner head is to be carried out.

A cylindrical-section transducer mounted to the side wall of the scanner head cylinder is another option. In this case, with a transducer of sufficient length, a focus could be generated anywhere along the length of the transducers focal plane within the cylinder volume. The problem here then would be achieving a variable focal depth ('into' the cylinder) which is difficult even when using a phased cylindrical-section array due to pre-focusing in the perpendicular direction. Also coupling to the cylinder would remain a problem, as with the case of a spherical-section array, which is a major concern if the present design is to main unchanged.

A further possibility would be to use a number of cylindrical-section or spherical-section arrays with differing radii of curvature. This would allow focusing at a number of depths. The drawback here is that to cover the entire range of possible focal regions many transducers would have to be incorporated. This means higher costs, additional space requirements and very precise placement would be necessary. Also the issue of coupling and an acoustic window would remain. Therefore this may not be the most efficient or effective solution, given the existing setup and geometryof the system.

Given the above arguments it seems logical *not* to mount the HIFU transducer(s) to the side of the cylinder (although it should be noted this does not mean this will necessarily be the case in future designs). Another option, discussed in passing earlier in this thesis is to position a transducer *underneath* the target volume. The easiest way to implement this would be to integrate a transducer into the existing electrode plate, such that the active surface is in direct contact with the liquid in the scanner head (which is in turn in direct contact with the patient). This would minimise losses due to attenuation that would be present if the ultrasound had to propagate though the thick Perspex scanner head cylinder, as in the previous suggested designs. In addition the existing electrode plate has not one but two motors, one controlling the height of the plate, and the second the rotation, both present already for EIM scanning. Given that in the existing design the plate can both rotate and move vertically it seems that the optimum solution, at least with the present EIM system, would be to mount a transducer into the plate, thus removing the need for an additional movement system and keeping the costs of implementation to a minimum. Given the volume of the prone breast, a HIFU transducer situated in the gap in the plate (see Figure 16) could, when combined with the existing movement system, potentially cover the entire volume of the scanner head cylinder, minus the central ‘column’ above the centre electrode as previously explained. At present this seems to be a most effective and efficient solution for the integration of a HIFU device into the existing EIM apparatus.

As described earlier two transducer types seem suitable for use if placement is to be *below* the target volume. The first would be to use spherical truncated type transducer (see Figure 12) typically used in transrectal treatment, such as that of the prostate. The

parallel truncated planes would allow the transducer to fit into the gap in the electrode plate, and using annular elements, would allow control of focal depth. A disadvantage however would be that a motor system would still be needed to translate the device from one end of the gap to the other, thus allowing the full volume to be targeted. This could be achieved also by tilting the transducer, but would also require an additional motor to be added to the system. Furthermore the advantage of controlling focal depth is somewhat negated by the fact the plate already has a motorised mechanism allowing vertical movement, therefore it is suggested that this arrangement is not the optimum solution.

Finally the configuration that seems most effective is that of using a linear concave (cylindrical-section) transducer mounted in the gap in the electrode plate (see Figure 16, created using [74]).

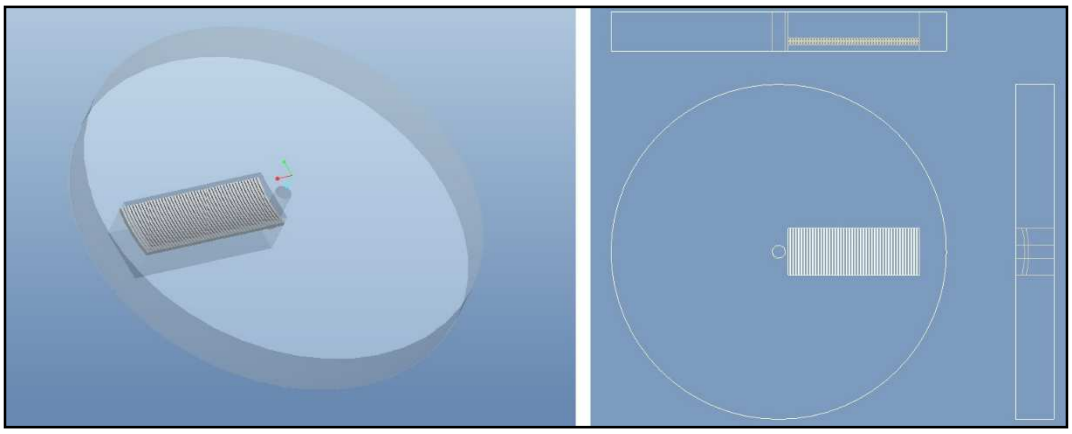

Figure 16 - ***Linear concave HIFU transducer array situated within gap in electrode plate.***

As described earlier in this thesis this type of transducer naturally focuses ‘along a line’ at a distance from the transducer equal to the radius of curvature of the section. This line can be ‘concentrated’ into a single focal point by making use of phase differences between the excitation signals sent to each element. Furthermore this point can be steered anywhere along the line by altering the phase difference between elements, thus allowing a focal point to be generated anywhere along the line of natural focus (the transducer lateral axis). Adding to the usability of this type of transducer is that use can be made of ‘synthetic apertures’ in that not all elements have to be excited at once. This provides a double advantage as it would allow perpendicular focal points and therefore lesions (when focused within tissue) to be created rather than those at

an angle which would be produced when steering the beam using phasing of elements, so allowing for a less complex treatment plan to cover the area to be ablated. In addition unwanted grating lobes could be avoided by selecting only certain elements and avoiding those which destructively interfere with the treatment plan. This second advantage would require a fair amount of planning and simulation to perfect, but would be a great help when targeting unhealthy tissue close to bone, such as the ribcage [50] and thus would facilitate treatment of patients with smaller breast sizes. An example model of a transducer of this type is shown below (see Figure 17, created using [78]).

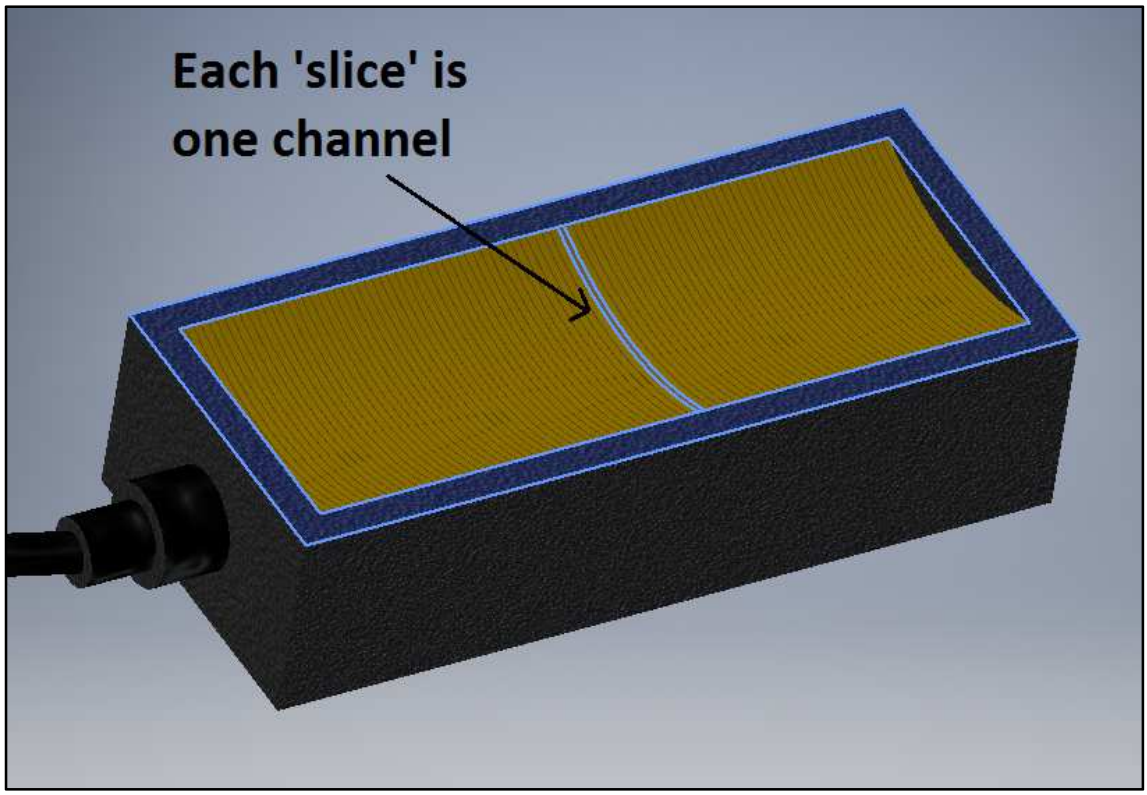

Figure 17 - ***Example geometry of an extracorporeal linear curved phased array transducer***

Finally the issue of targeting above the centre of the centre electrode of the electrode plate may be circumvented by using phased signals to focus *outside* the length of the HIFU array. This will be verified by simulation to check the feasibility of such a focus. Thus targets within the centre two-quarters of the length of the array could be treated using *half* the total number of elements, centred on the target volume, while focal targets outside the centre two quarters of the array could be treated by using *all*

elements, with phase difference being employed to focus, even at points *outside* of the transducer's length (an 'extreme' focus).

4.4: Design Specification

Now that the geometry of the transducer has been described it is relevant to begin to detail the exact parameters that would be best suited to the application at hand. All transducers have particular common features, most of which interrelate to each other in some way or another. These features will now be listed and then detailed according to the geometry selected in the previous section of this thesis. It should be noted however that certain parameters will only be known once manufacturers have been consulted, as not all information, for example concerning the piezoelectric material used, is freely available and manufacturers often have their own proprietary materials of which details are not released to the public.

The features common to all transducers are:

- Piezoelectric material
- Operating frequency
- Array dimensions
- Element dimensions (thickness, width and length)
- Inter-element spacing (kerf)
- Matching layer
- Backing/damping materials
- Housing and Insulation
- F-number
- Driving electronics and circuitry (see Section 7.3.2)
- Control system

In addition to being inter-related to one another, the above factors will affect the resulting:

  - Q-factor
  - Electrical efficiency
  - Total acoustical power (TAP) output
  - Intensity at focus

And therefore the:

- Resulting heat deposition or 'thermal dose' in the tissue being treated

4.4.1: Piezoelectric Material

As space is strictly limited by the dimensions of the available gap in the electrode plate the piezoelectric material must be selected carefully. To successfully ablate tissue it is advantageous to have as high a focal intensity as possible (within reason) and therefore the material used in this case must be capable of producing a high peak focal intensity. Due to space restrictions this means a high TAP which will vary depending on the material used. Below (see Table 4) is a comparison of a number of materials commonly used in transducer construction [33], [79], [80].

Table 4 - ***Comparison of common piezoelectric materials used in transducer manufacture***

Material name	Comparative description	Commonly used in
PZT-4	Low dielectric losses, commonly used in electrical power generating systems	Medium to high power applications
PZT-5H	Very high sensitivity and permittivity, best suited to receiving/measuring applications	Diagnosis/Imaging (eg. Hydrophones)
PZT-8	Similar to PZT-4 with even lower mechanical losses, used in application requiring high power output	High power applications
IMASONIC HI-1	Proprietary piezocomposite offering high efficiency (60-70 %), mechanically robust and flexible in shape and size (when used in construction of arrays) up to 10 W/cm^2 acoustical output	Medium power applications
IMASONIC HI-2	Proprietary piezocomposite with lower efficiency than HI-1, but offering a high acoustical output of up to 30 W/cm^2	High power applications (eg. Therapy)

As the limited space available is a major concern, both PZT-8 and Imasonic HI-2 seem to offer potential benefits. Imasonic have been pre-selected as the manufacturers for the designed transducer and so it seems that their proprietary material HI-2 would be the most logical choice. Given that the properties of HI-2 are not publically available PZT-8 properties will be used for any estimations in later sections of this thesis. It should be noted that this will lead to an underestimation of produced powers which could later be improved once more information on HI-2 is obtained.

4.4.2: Operating Frequency

When using a HIFU transducer for tissue ablation certain parameters have to be decided upon. These parameters include dimensions, geometry, materials used in construction, required output power and also the frequency at which the transducer will be driven. This last parameter, the frequency, should be chosen to match the required depth of focus, with lower frequencies being used to ablate deeper targets and vice-versa. As this parameter effects other design decisions it is pertinent to define it before continuing on.

It has been shown that a suitable frequency is such that the transmitted signal undergoes 10 dB attenuation when propagating through the tissue overlying the target zone [38], [56], [26]. At present, the maximum volume of breast tissue that can be scanned in the existing EIM device gives a maximum breast 'height' of 4 cm, so if we assume a tissue attenuation coefficient *(α)* of 0.7 dB/cm/MHz [38], [56] we can then approximate the optimum frequency to be used, given the transducer being mounted *below* the target volume (for example incorporated into the electrode plate, see Figure 16 & Figure 19, created using [74], also see Figure 18).

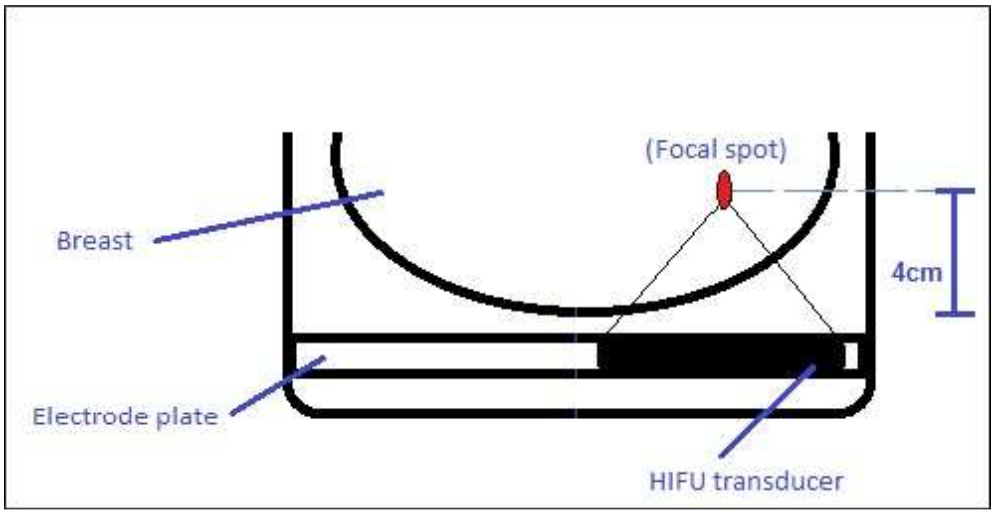

Figure 18 - Diagram showing possible arrangement of HIFU transducer in existing EIM system (vertical)

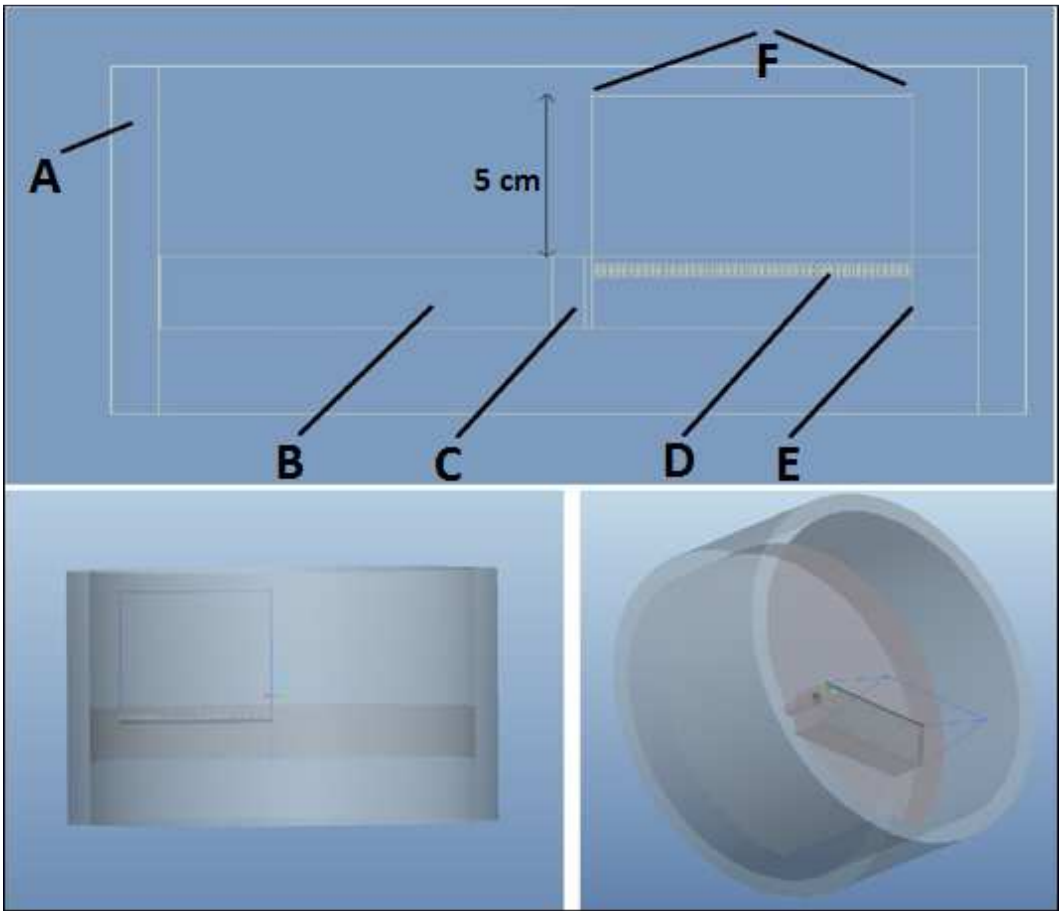

Figure 19 - ***Diagram showing possible arrangement of HIFU transducer in existing EIM system); (A) 'Scanner head cylinder', (B) 'Electrode plate', (C) 'Central EIM electrode', (D) 'Transducer element array', (E) 'Edge of transducer', (F) ''Possible focus points (anywhere along length of line)'***

-Given 4 cm tissue depth, attenuation will be: 2.8 dB/MHz

It is worth noting here that a 1 cm water 'stand-off' will also be used, giving an actual focal distance of 5 cm, but as the attenuation coefficient of water is approximately 0.0022 dB/cm/MHz [81] compared to 0.7 dB/cm/MHz of breast tissue the 1 cm of water will attenuate the sound waves far less and therefore can be fairly omitted from estimations made at this stage.

Given optimum frequency is when total attenuation in tissue is equal to 10 dB

-Optimum frequency will be: 3.57 MHz

It can also be shown that optimum frequency can be estimated using the following formula [41]

$$\boldsymbol{F = \left(\frac{20}{ln10}\right) * \left(\frac{1}{x\alpha}\right)} \qquad \textbf{\{4.1\}}$$

Using this formula, with focal height $\boldsymbol{(x)}$ equal to 4 cm and $\boldsymbol{\alpha}$ equal to 0.7 dB/cm/MHz, gives an optimum frequency of 3.1 MHz.

Another point here worthy of note is that the attenuation coefficient for breast tissue (α) is very difficult to calculate or quantify as each individual will have a different composition of tissues making up the breast. For general 'soft tissue' however, an attenuation coefficient in the range 0.3 to 0.8 is widely accepted [27] with 0.5 to 0.7 being values that have been used in previous, similar estimations, 0.7 being used most commonly.

Cavitation can be caused by low frequencies of ultrasound [22] and therefore it is recommended that the higher of the above two frequencies should be used to avoid the unnecessary effects and unpredictability that cavitation may cause. To simplify further calculations 3.57 MHz will be rounded down to 3.5 MHz.

This frequency is similar to those used in transrectal type devices (35 mm focal length/5 MHz [82], 50 mm focal length/3 MHz [48]). Although these devices are

relatively small they can still produce focal intensities (spatial average) of above 6000 W/cm^2 [48] well within the range needed for HIFU ablation (100 – 10 000 W/cm^2 [83] and typically around 1500 W/cm^2).

In the case that the transducer is mounted to the *side* of the EIM system cylinder, a similar estimation to that just performed can be carried out. In this case the maximum focal depth will be greater, so the optimum frequency will be lower. Here the maximum focal depth into the tissue is approximately 8 cm.

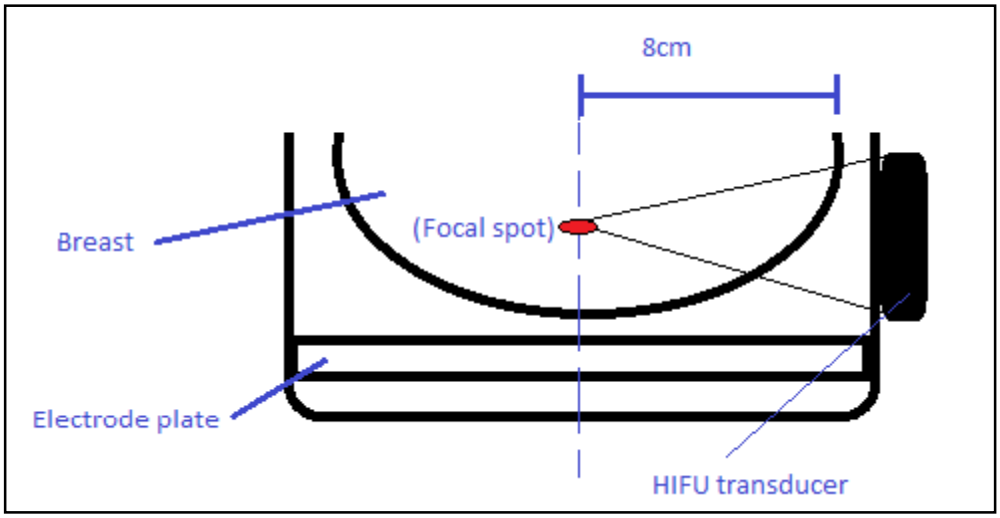

Figure 20 - ***Diagram showing possible arrangement of HIFU transducer in EIM system (horizontal)***

Using 8 cm focal depth and assuming an attenuation coefficient (α) of 0.7 MHz/dB/ cm [38], [56] as previously, we can see that

-Given 8 cm tissue depth, attenuation will be: 5.6 dB/MHz

Given optimum frequency is when total attenuation in tissue is equal to 10 dB

-Optimum frequency will be: 1.79 MHz

As previously stated it can also be shown that optimum frequency can be calculated using the following formula [41]

$$\boldsymbol{F = \left(\frac{20}{ln10}\right) * \left(\frac{1}{x\alpha}\right)} \qquad \textbf{\{4.1\}}$$

With 'x' set equal to 8 cm and 'α' equal to 0.7 MHz/dB/cm, this formula yields an optimum frequency of 1.55 MHz. Again, for the reasons described previously, the higher of these two frequencies should be chosen, and to simplify further calculations this will be taken to be 1.8 MHz.

This frequency is similar to those used in larger, extracorporeal devices such as the 1.25 MHz annular array with a focal length of 10cm, as described in [30].

4.4.3: Intensity at Focus: Transducer Power Requirements

As stated in the preceding section the minimum focal intensity produced by the designed transducer must be greater than 1000 W/cm^2 and preferably more than 1500 W/cm^2. Using this as a benchmark figure the required acoustic power output from the transducer can be estimated. This is an important step as it will determine the necessary transducer surface area, for a given transducer material with a set maximum (material) power density.

As the cross section of the focal region (ellipsoid) can only be determined by simulation or indeed physical measurement there will be a certain amount of error involved in this estimation, as such the power estimation here should not be taken as exact. Nevertheless, using an estimation of this kind allows an idea of the order of magnitude of power necessary to ablate tissue to be obtained and therefore the minimum required transducer surface area which will determine the feasibility of use in space-restricted applications. Using the formula below [41] and assuming an annular transducer with focal length 4 cm and aperture of 3 cm, operating at 3.5 MHz in water (sound velocity 1526 m/s at 40 °C [84]) the focal ellipsoid cross sectional area is approximately

$$a = \frac{\lambda^2 f^2}{A} \qquad \{4.2\}$$

Here 'a' is the cross sectional area of the focal ellipsoid, 'λ' is the wavelength of ultrasound (0.43 mm at 3.5 MHz) in water, 'f' is the focal length (50 mm) and 'A' is

the area of the transducer (1750 mm^2). This approximation yields a focal area of 0.27 mm^2.

This is obviously only an estimation as the actual, realized focal ellipsoid cross-section can only be calculated by precise simulation or physical measurement given the material properties of soft tissue (breast tissue) are not exactly the same as that of water, although they are similar. However this value is comparable to those obtained experimentally, with one such paper reporting cross sections of 0.4 to 1.5 mm^2 for focal depths of 30 to 60 mm, with a transducer operating at 3 MHz [48]. Also smaller focal zones are generally associated with higher frequencies, so it can be assumed that this value is within the order of the expected focal cross-section, once it is (physically) measured.

Using this focal area the required power output of the transducer can be approximated by working backwards, starting with a set required intensity at the focus. If we assume that the required focal intensity is set at 2000 W/cm^2 (overestimated) we can then calculate the corresponding focal power by multiplying by the area of the focal ellipsoid. This calculation yields a focal power of 5.4W. In calculating the optimum frequency earlier we defined the attenuation in tissue to be 10 dB. This then allows the power, incident at the tissue boundary, to be calculated as 54 W. Between the transducer and the tissue boundary there is a small gap that, when in operation, would be weak saline solution (effectively water). If this standoff is taken to be 1 cm, then the attenuation in this area can be calculated using the attenuation coefficient of water (0.0022 dB/MHz/cm [31]). Working through similar steps as for the attenuation in tissue it can be shown that the attenuation in 1 cm of water (at 3.5 MHz) will be 0.0077 dB, which equates to an approximate power loss of 0.1 W. This means the total acoustic power output from the transducer must be at least 54.1 W to achieve a reasonable intensity at the focus, given a transducer with dimensions as described above. Assuming a transducer efficiency of 50 % (material IMASONIC ‘HI-2’ [33]) this means an approximate electrical power of 108.2 W should be applied to the transducer.

Given the available space in the EIM system electrode plate (as previously described) this power will be applied to a transducer with a *maximum* surface area of 17.5 cm^2 (7 cm x 2.5 cm). As the maximum acoustical output from HI-2 is 30 W/cm^2 [33] the required power should be relatively easy to achieve, although the maximum output may be dependent on other factors that will not become apparent until discussions with Imasonic themselves commence. Ignoring this for the time being, and assuming a maximum *achievable* output power of 25 W/cm^2 coupled with the available space, it can be shown that an acoustical power output of 437.5 W is theoretically achievable.

For the transducer shown previously (see Figure 20, 1.8 MHz, focal length 8 cm, aperture 6 cm) working through the same steps, yields an approximate focal area of 1.66 mm^2 and an acoustic power output of 333 W with a corresponding electrical power input of 666 W.

4.4.4: Array Dimensions, Element Dimensions & f-number

The maximum physical 'footprint' of the completed array has already been defined as the size of the space in the EIM electrode plate (7 cm x 2.5 cm). The dimensions of the piezoelectric material used in the construction of an ultrasound transducer are of vital importance. This must be taken into account when designing the array and, more importantly, when deciding the dimensions of each element in the array. The dimensions used will be dependent on the operating frequency. The thickness of the material for example, as mentioned previously, must be equal to half the wavelength of sound (in the piezoelectric material) for preferential emission [31], [27].

Given a frequency of 3.5MHz and the sound velocity in the piezoelectric material used, the wavelength is known and therefore the optimum element thickness can be chosen. PZT-8 (as example, although Imasonic HI-2 will eventually be used) has a sound velocity of 4600 m/s [84] therefore the wavelength of sound (in PZT-8) equals 1.314 mm, while the wavelength in water (at 40 °C [84]) equals 0.43 mm and the wavelength in tissue equals 0.44 mm. Therefore the optimum thickness of PZT-8 used in transducer construction would be (1.314/2 mm) or 0.657 mm.

Although the thickness of the piezo material used is quite easily defined, determining suitable width and length of each element in the array is more difficult. If we assume a cylindrical-section array is to be used we can, at least for the time being, estimate the dimensions from those used in a previous study [56]. Here element width was varied between one and three wavelengths (in water) with one wavelength being the most effective in terms of preventing the creation of unwanted, non-focal lobes. If we take the element width to be one wavelength in water, this gives a width of 0.43 mm, which doesn't agree with the 'rule' that the aspect ratio (thickness to width) of each element must be equal or greater than two to avoid unwanted lateral modes of vibration [34]. It should be noted however that simulations, of which results will be presented later, will be used to determine if these dimensions are valid, and these values will not be finalised until confirmation is obtained from the results of these simulations.

The 'length' of each element is dependent on the radius of curvature of the cylindrical-section, which will be equal to 5 cm. As the available space in the EIM electrode plate is 2.5 cm this is the maximum aperture in the 'height' direction, although the measure itself will be equal to the cord length of the arc section (see Figure 21).

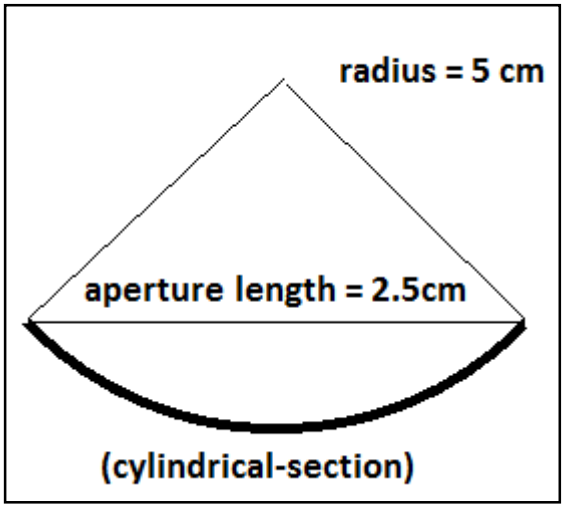

Figure 21 - ***Diagram showing cross-section of cylindrical transducer with radius of curvature and aperture length***

Finally the inter-element spacing or 'kerf' needs to be defined. This parameter will also be varied in simulations to find the optimum value or range but as space is limited it follows the kerf should be minimised to allow the active transducer surface to have maximum surface area, hence maximum power output given the space and power

restrictions described previously. As a guide, at least one group have reported good results using a kerf with a size of half a wavelength (in water) [56]. It should also be noted that the minimum sized kerf will depend in part on the limits of the manufacturing techniques involved in the manufacture of the transducer, a limit that will only become known once discussions with the manufacturers commence.

As the transducer will have a 2.5 cm aperture and a focal length of 5 cm, the transducer can be said to have an 'f-number' of 0.5. This measure may not be as useful for characterising cylindrical transducers as compared to their annular counterparts, but it has been included to facilitate comparison between this and other transducers.

4.4.5: Transducer Construction

4.4.5.1: Matching Layer

As mentioned in a previous section of this thesis a matching layer is generally present between the piezoelectric material and the propagation medium. This allows losses caused by differences in acoustic impedance (at the boundaries) to be minimised, thus increasing the overall efficiency of the transducer. The matching layer is designed to have thickness equal to one-quarter of the wavelength in the piezoelectric material used and, again as previously mentioned, should have an acoustic impedance given by the formula below [31].

$$Z_{matching\ layer} = \sqrt{(Z_{transducer}\ x\ Z_{medium})} \qquad \{3.8\}$$

Where, as before

$$Z = \rho c \qquad \{3.4\}$$

More than one matching layer can be used, but as this would increase the attenuation of the ultrasound it is generally recommended to use just one matching layer. As the density and sound velocity of the material most likely to be used (Imasonic HI-2) is presently unknown, values for PZT-8 will be used instead. Assuming a density and sound velocity of 992.2 kg/m^3, 1526 m/s and 7600 kg/m^3 , 4600 m/s for water (at 40 °C [84]) and PZT-8 [85] respectively, we can calculate the corresponding acoustic

impedances as 1.514 MRayl and 34.96 MRayl. This gives an optimum matching layer acoustic impedance of 7.275 MRayl, if PZT-8 wereto be used in the transducer construction.

Although the density and sound velocity of Imasonic HI-1 and HI-2 technologies are unknown, the range of acoustic impedance has been presented [33] and is in the range 8 to 12 MRayl. This gives an optimum matching layer impedance in the range 3.48 to 4.26 MRayl

4.4.5.1: Backing & Damping, Q Factor

As described previously the backing (or damping) block is located behind the piezoelectric element (see Figure 5) and absorbs backwards propagated and stray ultrasonic waves produced by the piezoelectric elements. The main function of the damping block is to dampen the forward propagated ultrasound to create a pulse, rather than a continuous wave. Increased damping introduces a broader band of frequencies around the resonant frequency. The extent to which the damping causes this effect is quantified using a measure named the 'Q-factor'.

$$\boldsymbol{Q = center\ (resonant)\ frequency/Bandwidth} \qquad \textbf{\{3.7\}}$$

Here, as previously mentioned, a high Q-factor value indicates a narrow bandwidth around the resonant frequency (long pulses) caused by a small amount of damping, while a low Q-factor indicates a wider bandwidth (short pulses) given rise to by heavier damping.

Generally, excluding certain special cases, it is preferable to have a high Q-factor for HIFU applications, such that a narrow bandwidth is achieved. This allows the effects of attenuation to be more easily predicted as attenuation is directly proportional to the frequency of the ultrasound propagating through the medium of interest, thus the energy deposited, or thermal dose can be more accurately planned for. This is an important feature of HIFU transducers designed for precise thermal ablation of target tissues.

The backing material that will be used for the transducer design outlined in this thesis will not be known until the manufacturers are consulted. Having said this there will be some solid backing present going on the available description of the HI-2 material technology manufactured by Imasonic. This backing is present to allow more efficient cooling and to provide increased resilience to mechanical and thermal shocks [33].

4.4.5.1: Housing & Insulation

The housing and insulation of a typical, single element transducer has been presented diagrammatically earlier in this thesis (see Figure 5 - 'plastic casing'). The shape, dimensions and material used will be defined with the aid of the manufacturers and will be influenced by the available space in the EIM electrode plate, described earlier. It is important that both the housing and the transducer's active surface are all watertight and submersible as the transducer will be sealed into the plate to prevent liquid reaching the sensitive electronics mounted below. Again, the details of this will become more apparent once discussions with the manufacturers begin.

4.5: Chapter Conclusion

To conclude, in this chapter a full problem definition has been given, describing various factors that must be taken into consideration for the successful design of a HIFU transducer capable of integration with the existing EIM system. A suitability study has shown that for this integration a cylindrical-section / linear concave geometry will be effective, using a phasing technique to steer the focused beam along one axis while using the stepper motor controlled movement of the EIM electrode plate to control movement in the remaining two axes. This will theoretically allow targeting of a focal point within the majority of the cylindrical 3D volume within the scanner head of the EIM system.

Numerous properties of the proposed transducer have also been defined. The piezoelectric material selected was a proprietary material manufactured by transducer specialists Imasonic (France) allowing a high output from a small active surface area. An optimum frequency of 3.5 MHz was chosen and array dimensions were decided based on the available space between electrodes mounted in the EIM electrode plate. It has also been shown that a suitable focal intensity is theoretically achievable using the approximate design parameters selected. Finally a matching layer, backing, damping and housing were also discussed, although final decisions will be effected by the manufacturer's preferred fabrication techniques.

The properties selected in this section will be used, where appropriate, in the simulations presented in the following chapter. It should be noted here that these properties may be subject to change as simulation results illuminate factors that were not yet considered at this point in the research.

Chapter 5:

Pressure Field Simulations

5.1: Chapter Introduction

In this chapter the theory and model used in the simulations will be described and referenced. The results of these simulations will then be presented. These results will be divided between those used to calculate the acoustic field intensity created by the selected transducer geometry (performed in MATLAB) and those used to calculate the resulting temperature distribution in the simulated target tissue volume (performed in COMSOL Multiphysics). The results of the latter simulations will be presented in the following chapter (see Chapter 6).

A brief account of why certain parameters had to be modified prior to manufacture will also be given, including the reasoning behind the optimisation of relevant parameters.

Care has been taken to omit research and information *not* directly related to the numerical analysis involved. For more information on why this type of transducer has been chosen, and for a comprehensive background of HIFU applications, transducer design and theory please refer to the previous chapters of this thesis.

5.2: Simulation Theory

The simulations presented here were performed primarily using a custom-written MATLAB code (see Appendix A) to solve the Rayleigh integral based on Huygen's principle (see formula below) [86] [45], thus allowing the resultant pressure field produced by the transducer in question to be calculated.

$$p(x,y,z) = \sum_{i=1}^{n} \sqrt{\frac{2P\rho}{cA}} \left(\frac{fS}{d_i}\right) \exp\left[j\left(\phi_i - \frac{2\pi d_i}{\lambda}\right) - d_i\alpha\right] \qquad \textbf{\{5.1\}}$$

Where '$p(x,y,z)$' is the pressure at field point (x,y,z), 'P' is the total acoustic power, 'S' is the element area, 'd_i' represents the distance from the centre of each element to the field point (x,y,z), 'ϕ_i ' is the phase of each element and all other symbols are as previously stated.

The phase of each element 'ϕ_i ' can be calculated using an inverse method, outlined in the formula below.

$$\phi_i = \frac{2\pi}{\lambda}\,(d_{if} - d_{cf}) \qquad \textbf{\{5.2\}}$$

Where 'd_{if}' is the distance from the centre of element 'i' to the focal point and 'd_{cf}' is the distance from the centre of the array to the focal point (see Figure 22, created using [78]).

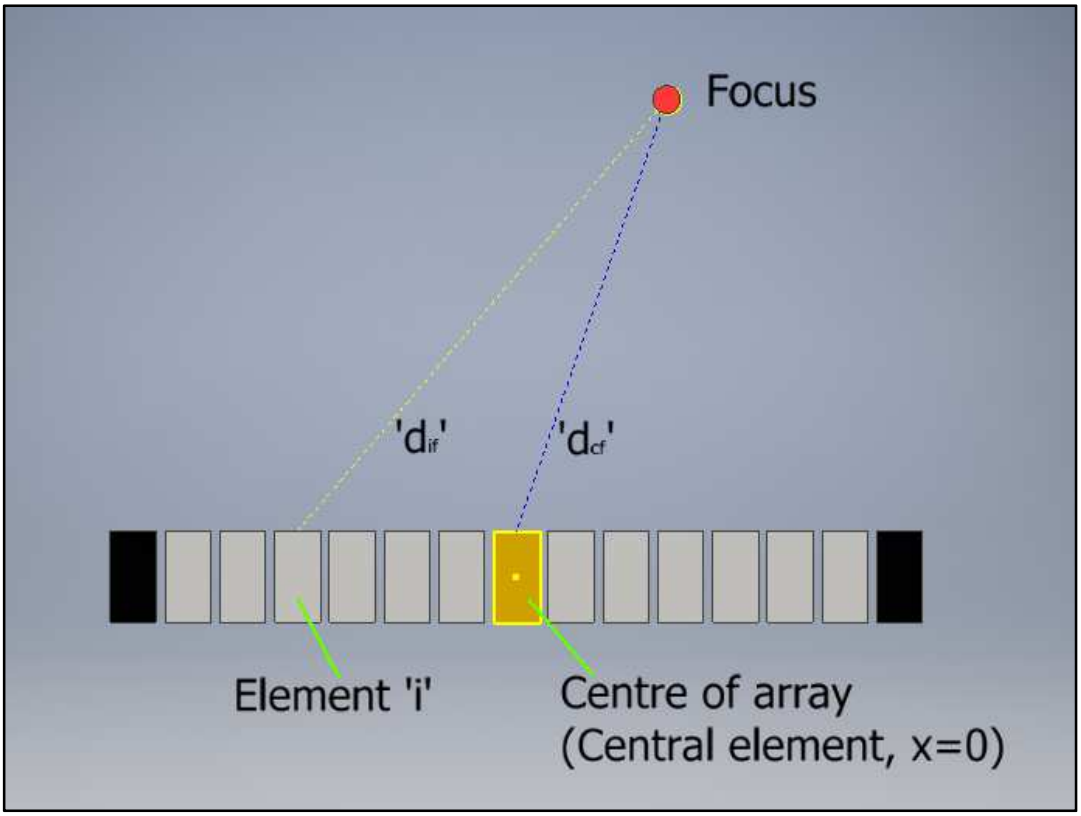

Figure 22 – Diagram showing the inverse method used for calculating 'ϕ_i '

Using this method simulations involved choosing an arbitrary focal point and using the inverse principle to calculate the necessary phase difference for each element in the array. Thus the desired focal point is produced by the superposition of waves (produced from all the excited elements) at the pre-determined focus.

Once pressure fields had been obtained, the corresponding acoustic intensity field could be calculated using the formula presented below.

$$I(x,y,z) = \frac{|p(x,y,z)|^2}{2\rho c} \qquad \{5.3\}$$

The acoustic intensity field is a useful indicator of how the transducer will perform, with almost every HIFU transducer on the market being able to produce an acoustic intensity in excess of 1 kW/cm^2 (at the focus) and commonly in excess of 1.5 kW/cm^2.

5.3: Simulation Details

The parameters and variables used in all simulations are tabulated here, for reference (see Table 5).

Table 5 - ***List of parameters used in simulations***

Parameter	Description	Value	Unit	Used in
P	Total acoustical power (TAP)	20	W cm^{-2}	Rayleigh integral
ρ	Density	1000	Kg m^{-3}	Rayleigh integral & BHTE
c	Acoustic velocity	1500	m s^{-1}	Rayleigh integral & BHTE
A	Total active transducer area	(Dependent on element dimensions)	m^2	Rayleigh integral
f	Frequency	3.5	MHz	Rayleigh integral
S	Element area	(Dependent on element dimensions)	m^2	Rayleigh integral
λ	Wavelength	4.29×10^{-4}	m	Rayleigh integral
α(*)	Attenuation	Various: (5 / 7.5 / 10)	Np cm^{-1} MHz^{-1}	Rayleigh integral
d_i	Distance from element 'i' to field point	Variable	m	Rayleigh integral
φ_i	Phase difference of element 'i' to centre element	Variable	m	Rayleigh integral

C_t	Specific heat (Tissue)	3550	J kg^{-1} $°C^{-1}$	BHTE
K	Thermal conductivity	0.5	W m^{-1} $°C^{-1}$	BHTE
w	Blood perfusion rate	0.5	Kg m^{-3} s^{-1}	BHTE
C_b	Specific heat (Blood)	3550	J kg^{-1} $°C^{-1}$	BHTE
T_a	Arterial temperature	37	°C	BHTE
T	Field temperature	Variable	°C	BHTE

(*) Note that the attenuation can only be estimated, with different authors generally using different attenuation coefficients. The range of values quoted as used by other researchers was 5 to 10 Np m^{-1} MHz^{-1}, thus it was decided to use 7.5 Np m^{-1} MHz^{-1} for most simulations. Additionally, 5 and 10 Np m^{-1} MHz^{-1} were also used as in a number of simulations to investigate the effect this had on the resultant pressure, intensity and heating patterns.

In a previous section of this thesis the decision process for the choice of transducer geometry and positioning in the existing apparatus is described in detail. To briefly summarise the transducer geometry is of the linear concave or curvilinear type, allowing pre-focusing in the short axis dimension. The transducer will be of such a size to fit into an electrode plate similar to those used in the current EIM system. This allows rotation and vertical translation of the transducer using the existing movement mechanisms and control system. Using a design such as this will allow focal points virtually anywhere within the scanner head main cylinder, for ablation at tissue depths up to 5 cm (see Figure 16 & Figure 19, created using [74]).

As the design specification of the transducer requires the ability to focus a small distance outside the length of the array (as can be seen in Figure 19) in the space above the central electrode and between the outer end of the array and the scanner head wall) simulations were designed to observe the level of unwanted grating lobes given

this condition. This was investigated for the case of *half* elements and for the case of *all* elements being excited in the simulations performed. As the total possible length of the array was fixed at 70 mm, this meant that only 35 mm of array was simulated at any one time for the case of *half* elements being activated. Therefore the experimental distance outside the arrays length related to a field co-ordinate of 0, 25 mm, assuming that the centre of the *half* array elements was positioned at 0, 0 mm. This experimental focus at 0, 25 mm equated to a focus at a distance of 7.5 mm outside the length of the array for the case of *half* elements. Similarly for the case of *all* elements being activated, the centre of the array is again positioned at 0, 0 mm, with an experimental focus at 0, 45 mm, or 10 mm outside the array length. Both of these targeting regimes, if successful, would allow the total volume of the scanner head cylinder to potentially be ablated.

To avoid confusion, the results presented focus on the plane shown below (see Figure 23, created using [78]).

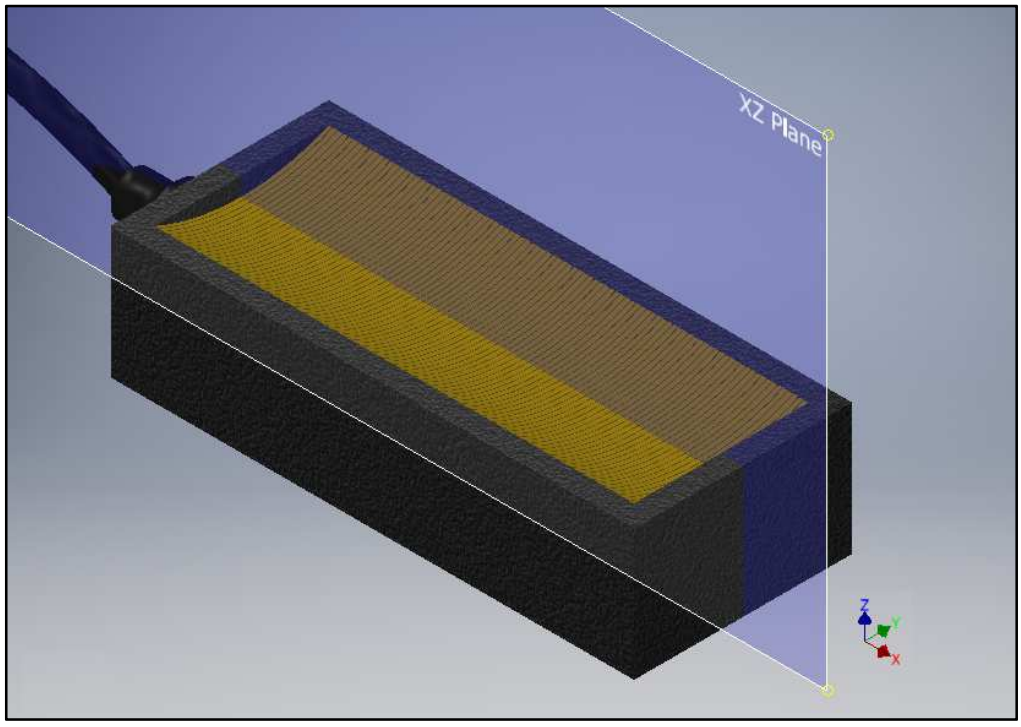

Figure 23 - Model showing simulation plane (XZ) & axes

5.3.1: MATLAB Simulation Results

Initially tests were carried out to determine the parameters that would give a suitably accurate answer in a reasonable time frame. A summary of these results is presented herein.

5.3.1.1: Sub-element Spacing Test Results

From these results (see Table 6) it can be seen that the 'most efficient' sub-element spacing was **λ/6**, which was within approximately 0.2 % of **λ/10**, showing an acceptable degree of accuracy whilst allowing simulations to be performed more rapidly and not using up all the PCs resources such that supporting research work could continue in parallel. The tests were performed using an operating frequency of 1 MHz, with a grid (or mesh) size of **λ/5**, a high enough value to be sure that a 'fair' result could be observed, without taking more than 24 hours to run.

Table 6 - ***Results of initial sub-element spacing suitability tests***

Sub-element spacing ('λ')	No. sub-elements	Max pressure (Pa)	Change from previous (%)	'Efficiency rating' (% change X no. sub-elements)
1	17	5026.32	-	-
1/2	34	4789.15	4.7186	160.4319
1/3	51	4756.41	0.6837	34.8702
1/4	68	4743.83	0.2644	17.9784
1/5	85	4736.31	0.1586	13.4830
1/6	102	4731.41	0.1034	10.5420
1/8	135	4725.40	0.1270	17.1427
1/10	169	4721.65	0.0793	13.4126
1/15	253	4716.84	0.1020	25.8023

5.3.1.2: Mesh/Grid Size Test Results

The following table shows the results of the grid/mesh size tests (see Table 7). These tests had to be cut short due to the PC on which simulations were performed encountering problems due to lack of available memory (RAM). For this reason the mesh size of **λ/5** was chosen, which coincides with the generally accepted minimum value for the measuring of a periodic (for example sine) wave.

Table 7 - ***Results of initial mesh/grid size suitability tests***

Mesh/grid size ('λ')	Max pressure (Pa)	Change from previous (%)	PC RAM used (%)
1	3786.21	-	20
1/2	3787.40	0.0313	25
1/3	3787.44	0.0012	25 to 30
1/4	3787.40	0.0011	70
1/5	3787.48	0.0020	85
1/6	-	-	(PC Crash)

5.3.1.3: Pressure Field Simulation Characterisation

The following were performed using the parameters listed at the beginning of this section. Any other relevant parameters will be listed, along with the results as they are presented. As there are many different test results, presenting all the associated plots would be wasteful. Instead only those directly relevant to that which is being described will be included, although references to plots not presented may be made at times.

All simulations here were performed by simulating only half the total number of elements in the array, thus allowing steering and focal strength to be more rapidly evaluated. Therefore the total length of the simulated array comprising half the elements was 35 mm. This 'half' array is centred around x=0 mm, therefore a focus at x=25 mm represents focusing beyond the end of the array by 7.5 mm ((25 - (35/2)) mm). The table below (see Table 8) shows the attenuation coefficients and focal point distances used in simulations performed at this early stage in the design process.

Table 8 - ***List of attenuation coefficients & focal points used in simulations 1 to 16***

Simulation no.	Attenuation coefficient used (Np m^{-1} MHz^{-1})	Distance from centre of array to focus (mm)
1	5	0
2	5	10
3	5	20
4	5	25
5	5	40
6	5	0
7	5	10
8	7.5	0
9	7.5	10
10	7.5	20
11	7.5	25
12	7.5	0
13	10	0
14	10	10
15	10	20
16	10	25

[*NB. The simulations underlined in* Table 8 *are those that are presented graphically below (see* Figure 25 to Figure 30)]

The results of the above simulations will now be presented, graphically. Please note all plots in this chapter use the axes format shown below (see Figure 24) with the co-ordinate system as shown previously (see Figure 13 (left)).

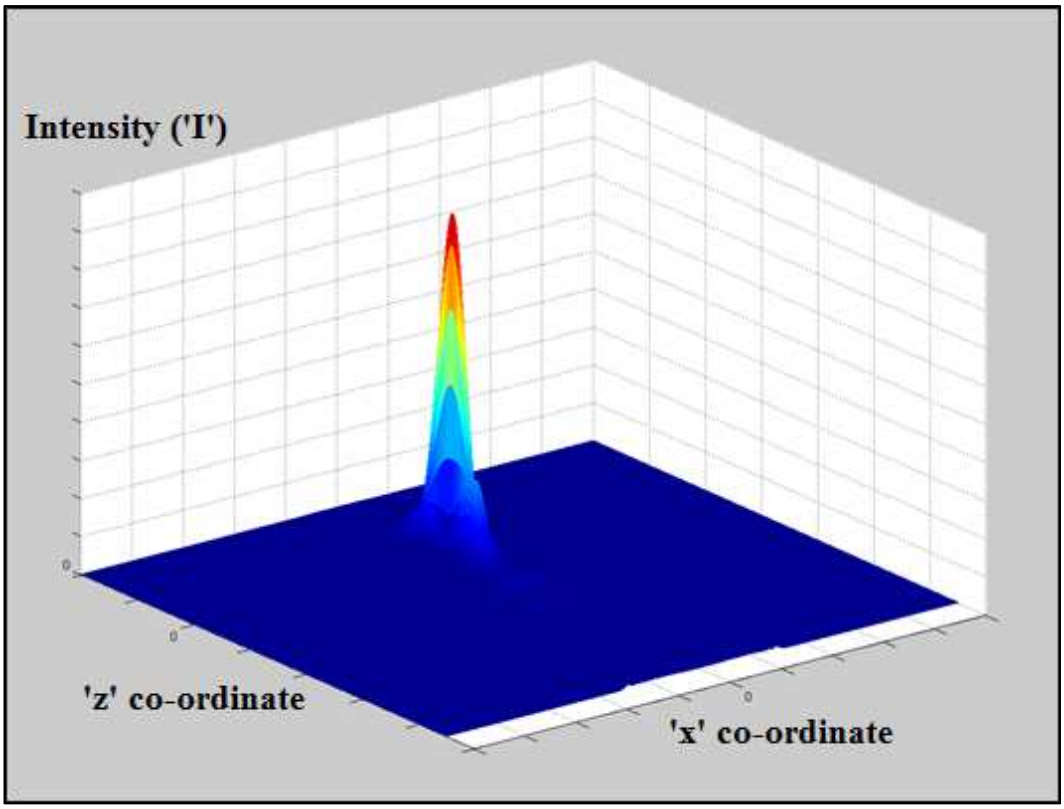

Figure 24 - Representative Intensity plot showing axis labels

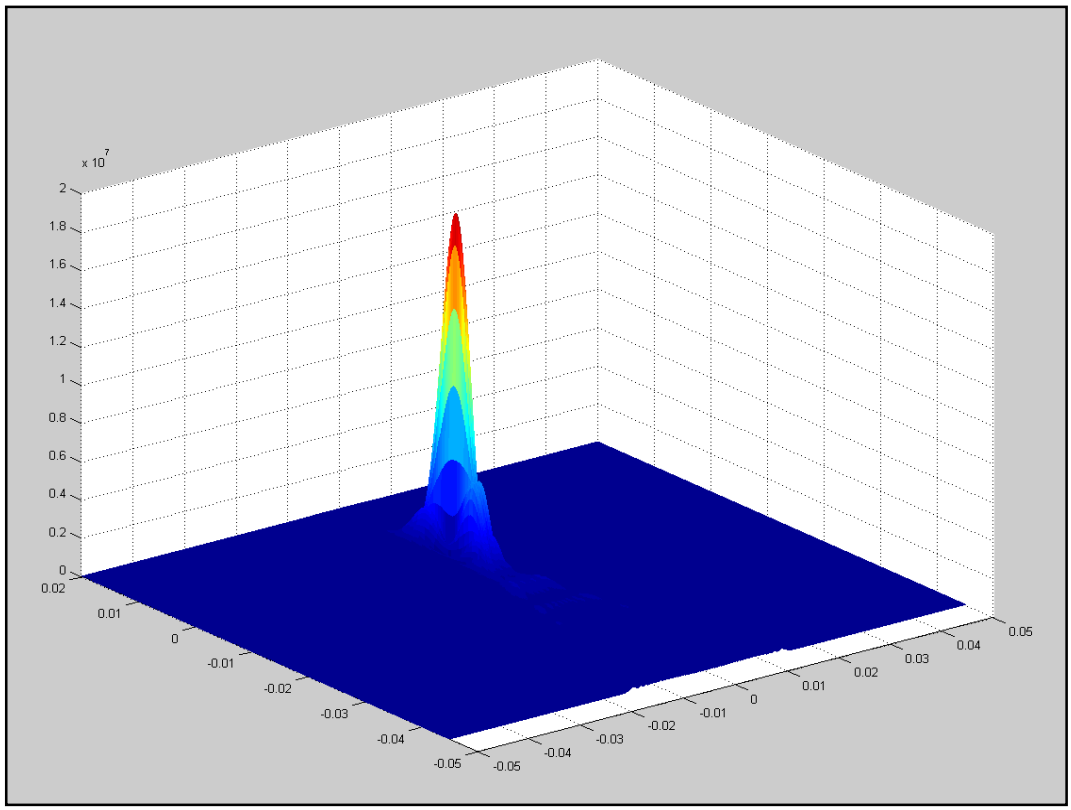

Figure 25 - ***Acoustic Intensity (W m^{-2}), Focus at x=0, α = 7.5 Np m^{-1} MHz^{-1} (Sim No.8)***

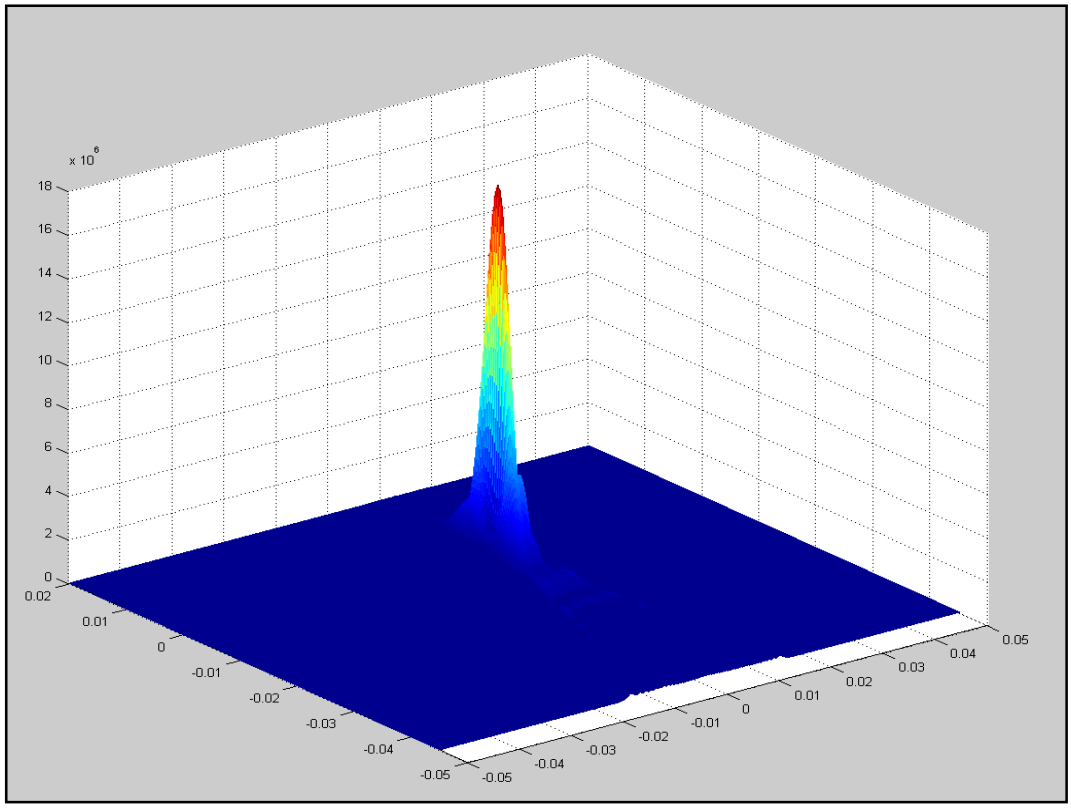

Figure 26 - ***Acoustic Intensity (W m^{-2}), Focus at x=-10, α = 7.5 Np m^{-1} MHz^{-1}(Sim No.9)***

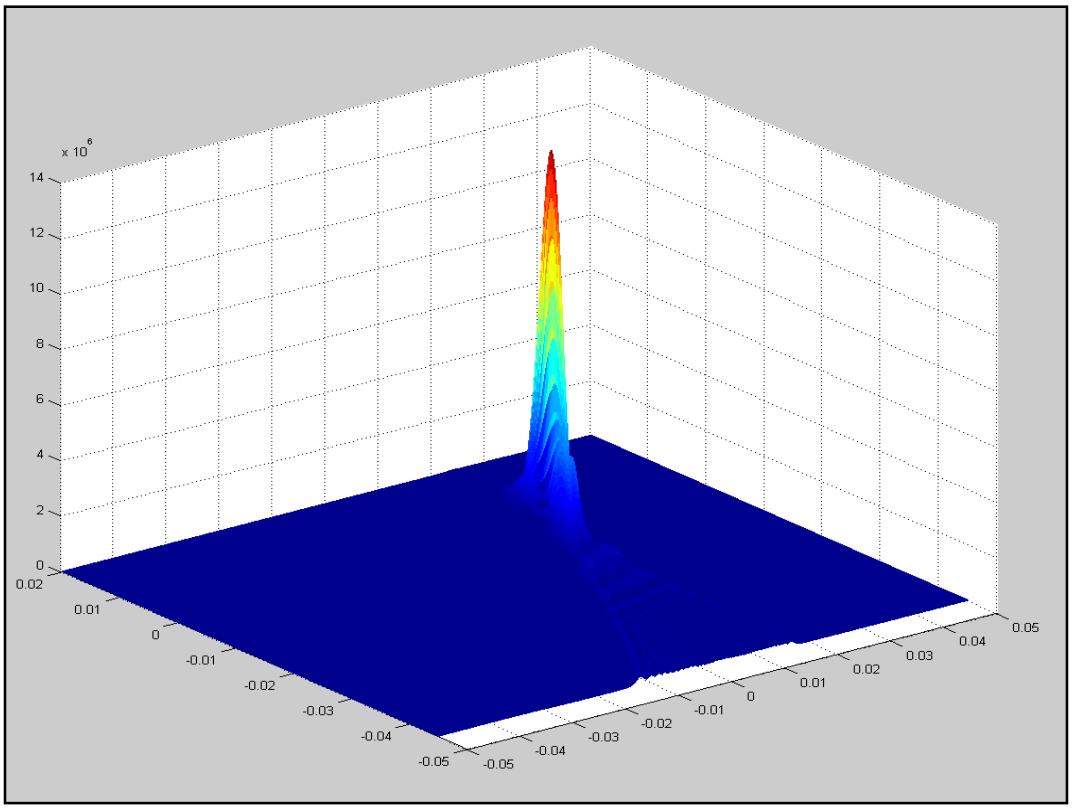

Figure 27 - ***Acoustic Intensity (W m^{-2}), Focus at x=20, α = 7.5 Np m^{-1} MHz^{-1}(Sim No.10)***

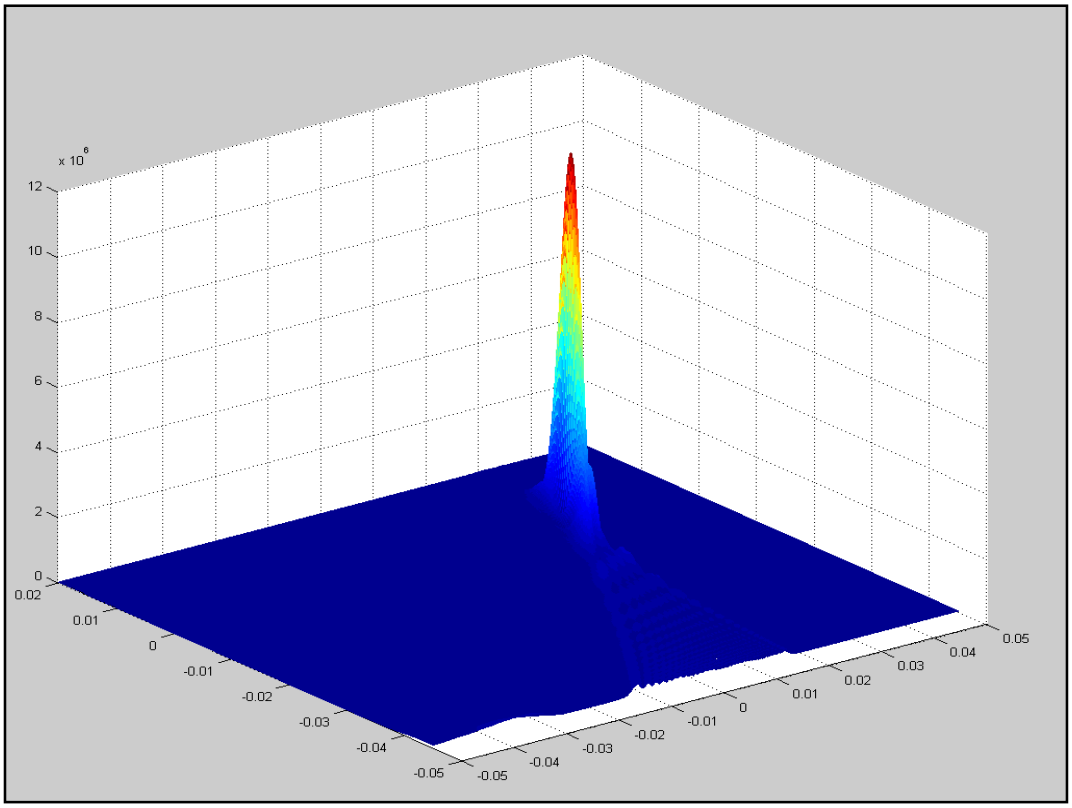

Figure 28 - ***Acoustic Intensity (W m^{-2}), Focus at x=25, α = 7.5 Np m^{-1} MHz^{-1}(Sim No.11)***

From the above four intensity plots it can be seen that *zero* grating lobes are present. All four plots were obtained using an attenuation coefficient of 7.5 Np m^{-1} MHz^{-1}. For reference the following two plots (see Figure 29 & Figure 30) show the results of two further simulations, showing the effect of modifying the attenuation coefficient to 5 Np m^{-1} MHz^{-1} and 10 Np m^{-1} MHz^{-1}. Both of these simulations were performed assuming an extreme focus which in this case is x=25 mm (as in Figure 28).

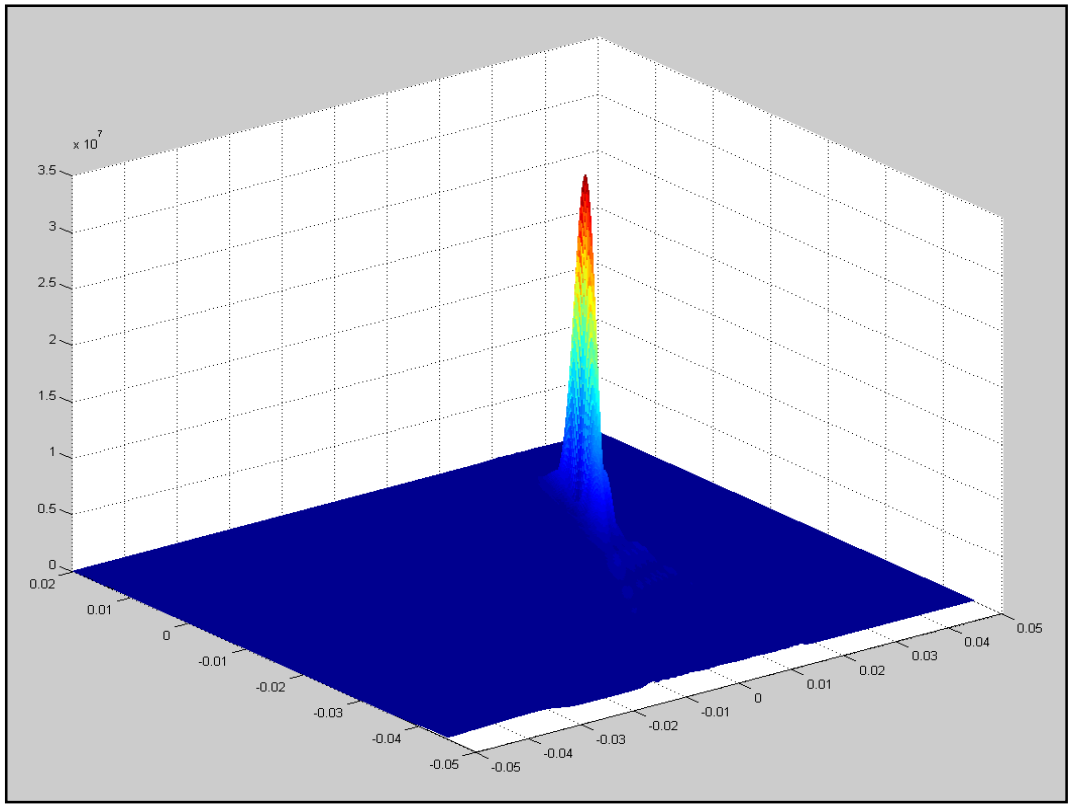

Figure 29 - ***Acoustic Intensity (W m^{-2}), Focus at x=25, α = 5 Np m^{-1} MHz^{-1}(Sim No.4)***

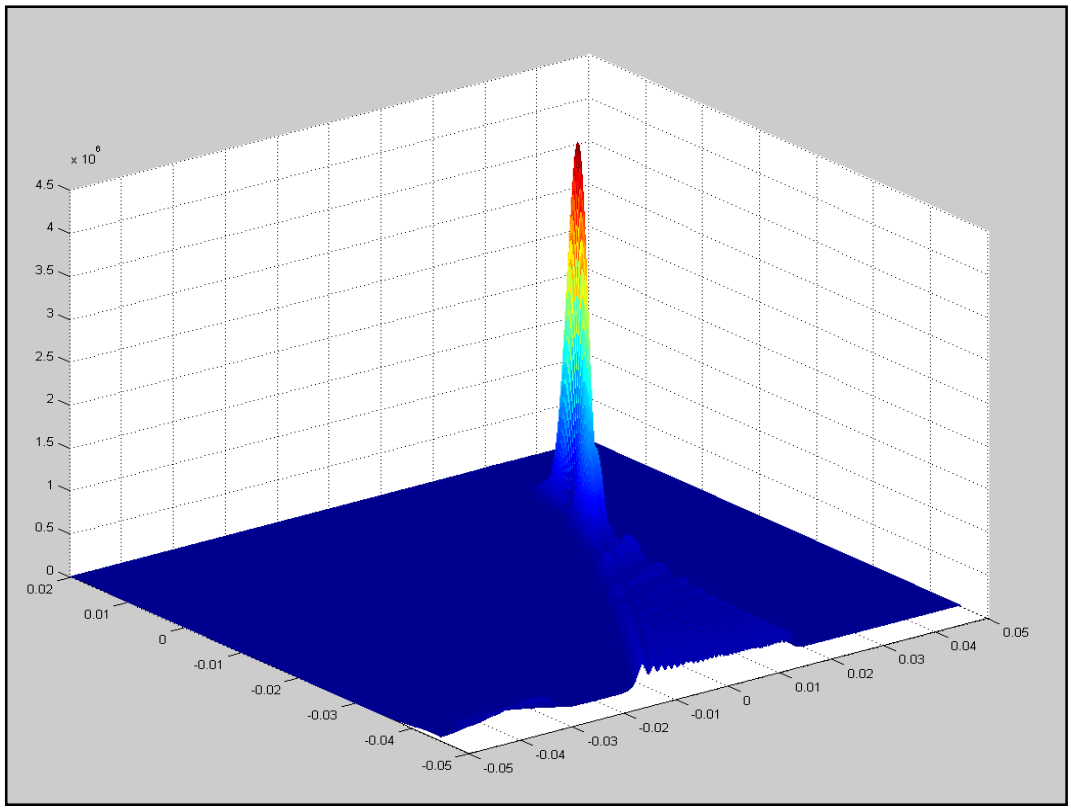

Figure 30 - ***Acoustic Intensity (W m^{-2}), Focus at x=25, α = 10 Np m^{-1} MHz^{-1}(Sim No.16)***

5.3.1.4: Initial Optimisation Tests - Pre-manufacturing Discussions:

As talks with the manufacturers had not begun before the first simulations began the manufacturing limitations were unknown. After some testing and troubleshooting of the simulation code the first set of simulations were performed. In these tests an element width of 0.22 mm and an inter-element spacing (or 'kerf') of 0.05 mm were used. These equated to approximately half a wavelength and an eighth of a wavelength (in water) respectively, thus adhering to the rule of thumb that grating lobes can be avoided for extended focal ranges if the element width is kept to half a wavelength in the propagation medium, or less. Given that the maximum allowable physical footprint of the array is 70 mm (by 25 mm) this meant that using the element dimensions stated, the total array would comprise 259 elements. In these simulations half the array elements were used, rounding down to 129 elements so as to keep an odd number (as the centre element is located at the origin) and therefore an evenly balanced contribution from elements both 'sides' of the centre element.

From the previous two plots (see Figure 29 & Figure 30) we can see observe the expected change in intensity due to a different attenuation coefficient being used. At an extreme focus of x=25 mm using 7.5 Np m^{-1} MHz^{-1} gave an approximate focal intensity of 1000 W cm^{-2}. In contrast reducing the attenuation coefficient to 5 Np m^{-1} MHz^{-1} gave rise to a focal intensity of close to 3000 W cm^{-2}, triple that obtained at 7.5 Np m^{-1} MHz^{-1}. At 10 Np m^{-1} MHz^{-1}, a focal intensity of approximately 400 W cm^2 was observed, equal to approximately half the value obtained at 7.5 Np m^{-1} MHz^{-1}.

For all the following simulations an attenuation coefficient value of 7.5 Np m^{-1} MHz^{-1} will be used. Generally values of 5 to 7 Np m^{-1} MHz^{-1} are used for simulations of this type, however using 7.5 Np m^{-1} MHz^{-1} allows us to therefore underestimate slightly the focal intensity achieved and so will ensure that the designed transducer will be able to ablate tissue in a reasonable timeframe even if the active surface area of the transducer is further reduced, to fit in and be compatible with the existing system.

5.3.1.5: Initial Optimisation Tests - Post-manufacturing Discussions:

Prior to beginning discussions with the chosen manufacturers of the transducer all simulations were performed to find the optimum design parameters that would allow firstly a satisfactory acoustic intensity at the focus (given the dimensional restrictions) and secondly would not produce any grating lobes that would cause undesirable heating in non-targeted tissue areas. From the simulation results presented previously this was achieved for a range of focuses as shown in the intensity plots (see Figure 25 to Figure 30).

Unfortunately, following initial discussions with manufacturers the element dimensions were found to be unrealistic due to manufacturing limitations and the predicted difficulty of designing electronics for the driving of the array. To overcome this problem it was obvious the element dimensions and spacing would have to be modified such that manufacture and driving of the array would be feasible. Therefore another set of simulations were performed, using a range of element sizes, from 0.32 mm to 1.0 mm, with inter-element spacing of 0.05 mm (as in previous simulations), 0.1 mm and in some cases 0.2 mm. The following table (see Table 9) shows a summary of the variables used in the simulations carried out.

<u>Note:</u> As in the previous section only the results directly related to the narrative of the thesis will be presented so as to avoid including meaningless results and to facilitate focus on those that have more of a bearing on the design of the transducer to be manufactured. In this case a range of element widths will be simulated each with inter-element spacing of 0.05 mm and 0.1 mm, all focused at the 'extreme' focal point of x=25 mm.

Table 9 - ***List of variables used in simulations 17 to 41***

Simulation no.	Element width (mm)	Inter-element spacing / kerf (mm)	Distance from centre of array to focus (mm)	No. of elements simulated
17	0.32	0.05	15	95
18	0.32	0.05	25	95
19	0.32	0.1	25	83
20	0.35	0.05	15	87
21	0.35	0.05	25	87
22	0.35	0.1	15	77
23	0.35	0.1	25	77
24	0.35	0.2	25	63
25	0.4	0.05	0	77
26	0.4	0.05	15	77
27	0.4	0.05	25	77
28	0.4	0.1	25	71
29	0.4	0.2	25	59
30	0.43	0.05	15	73
31	0.43	0.05	25	73
32	0.43	0.1	25	68
33	0.5	0.05	15	63
34	0.5	0.05	25	63
35	0.5	0.1	25	59
36	0.6	0.05	25	53
37	0.6	0.1	25	51
38	0.64	0.05	15	51
39	1	0.05	15	33
40	1	0.05	25	33
41	1	0.1	25	31

[*NB. The simulations underlined in* Table 9 *are those that are presented graphically in* Figure 31 to Figure 44]

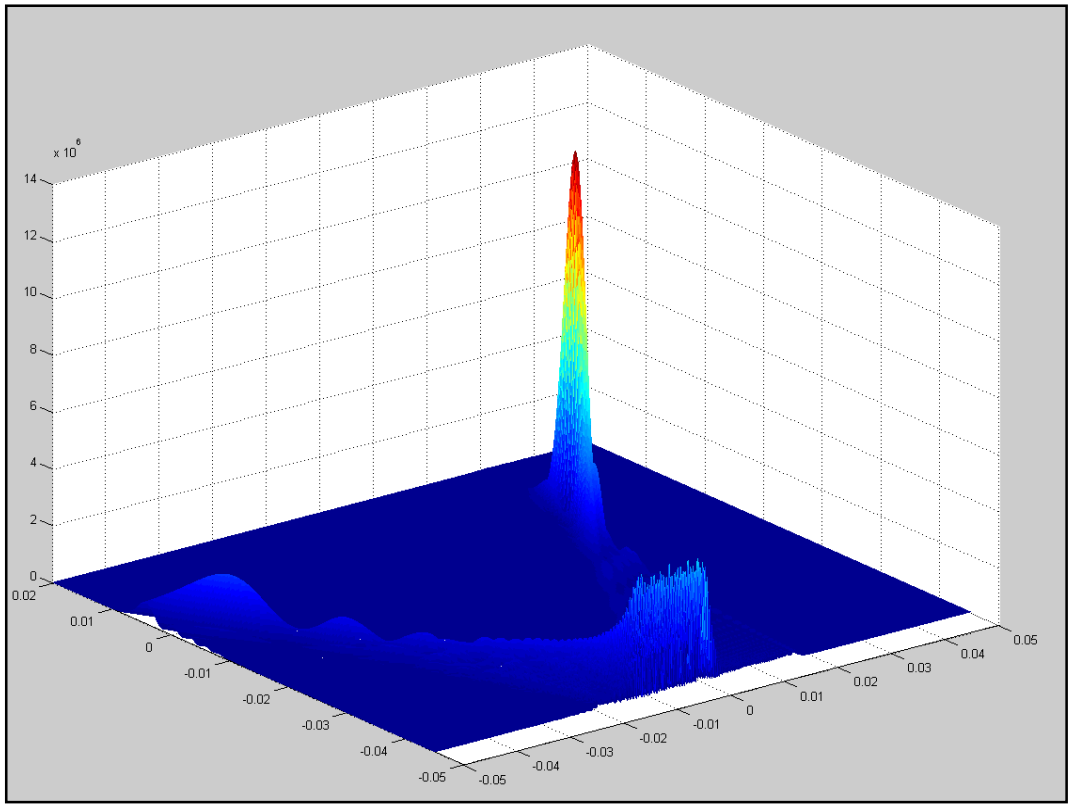

Figure 31 - ***Acoustic Intensity (W m^{-2}), element width 0.32 mm, Focus at x=25, kerf = 0.05 mm (Sim No.18)***

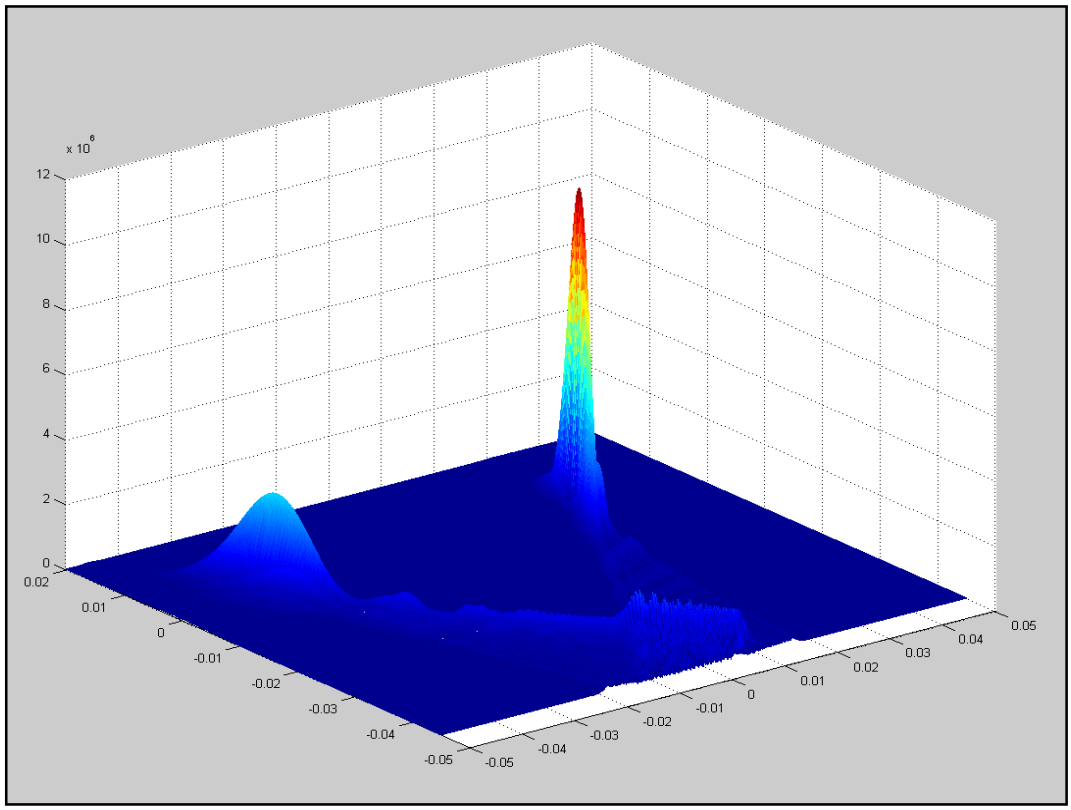

Figure 32 - ***Acoustic Intensity (W m^{-2}), element width 0.32 mm, Focus at x=25, kerf = 0.1 mm (Sim No.19)***

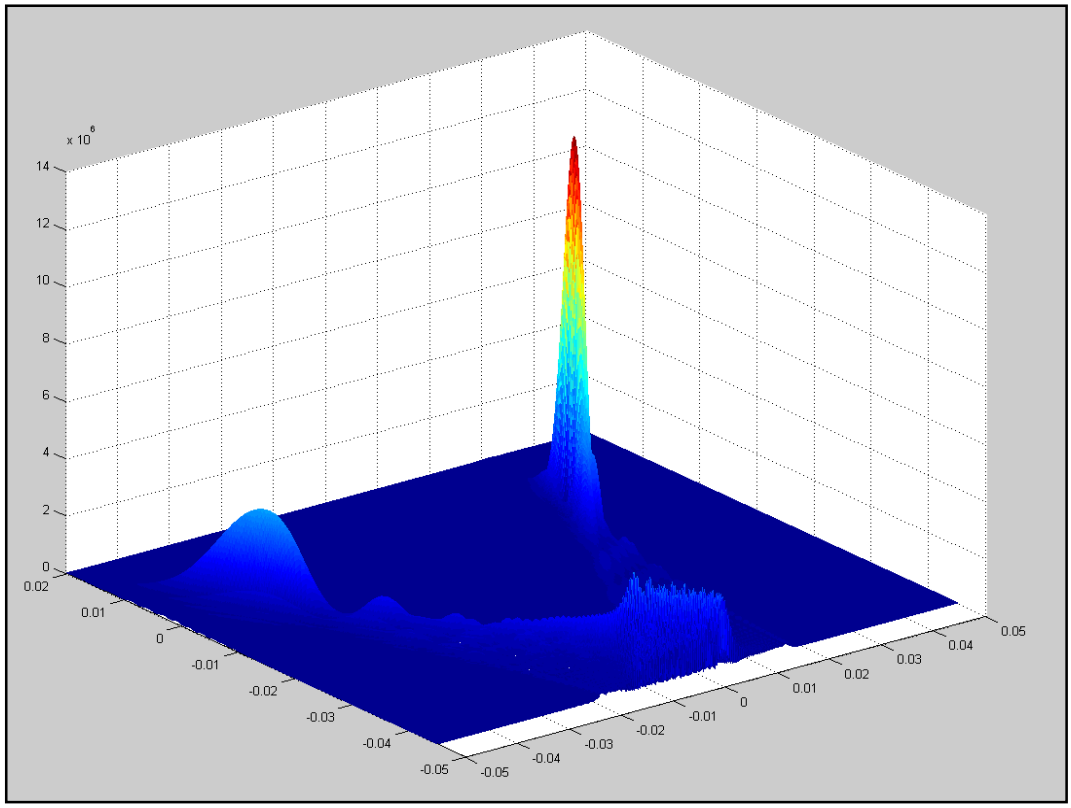

Figure 33 - ***Acoustic Intensity (W m^{-2}), element width 0.35 mm, Focus at x=25, kerf = 0.05 mm (Sim No.21)***

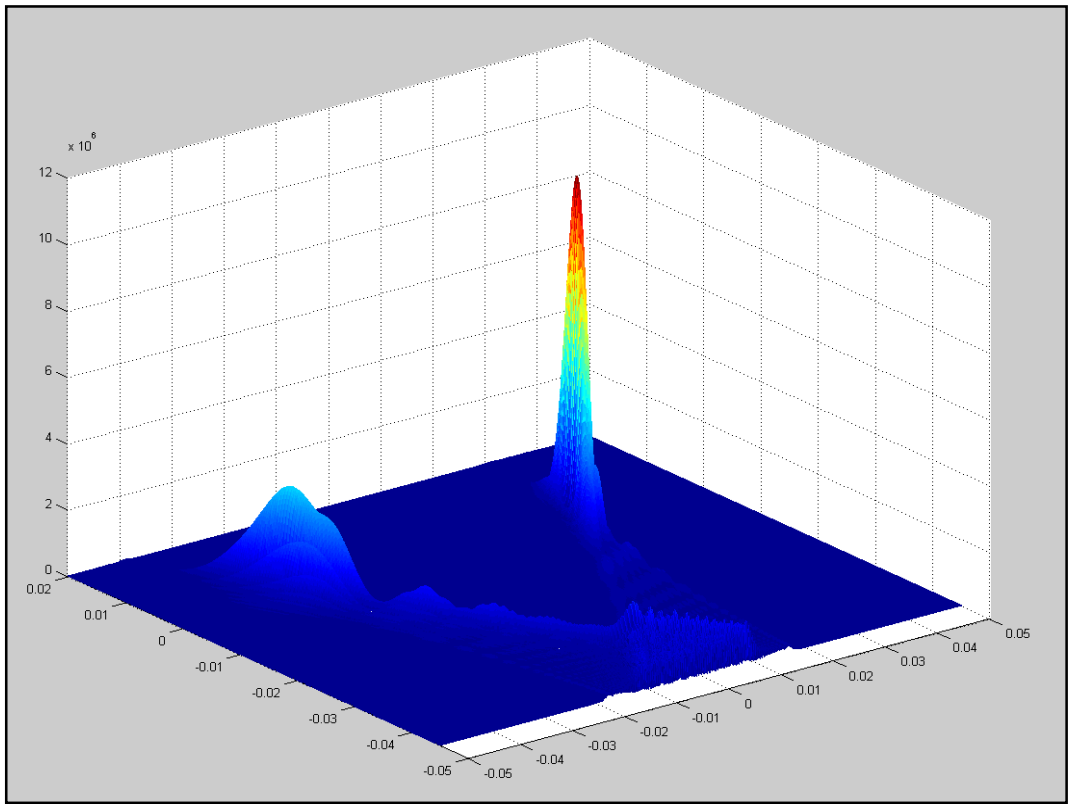

Figure 34 - ***Acoustic Intensity (W m^{-2}), element width 0.35 mm, Focus at x=25, kerf = 0.1 mm (Sim No.23)***

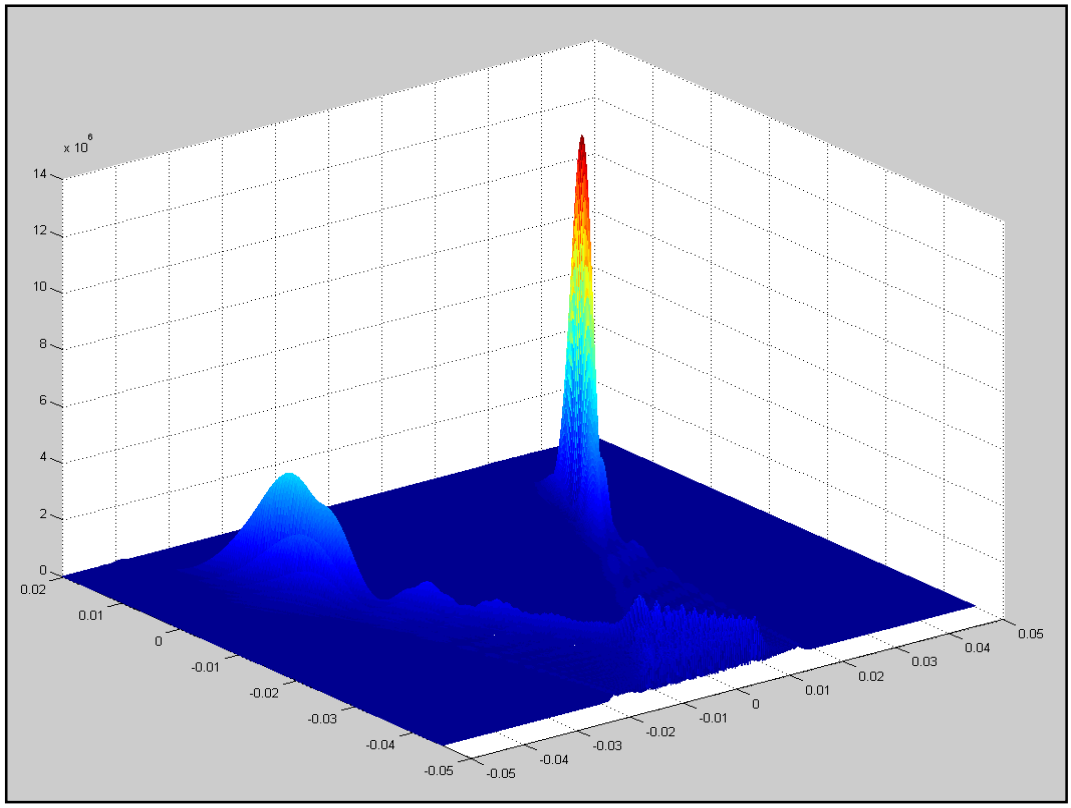

Figure 35 - ***Acoustic Intensity (W m^{-2}), element width 0.40 mm, Focus at x=25, kerf = 0.05 mm (Sim No.27)***

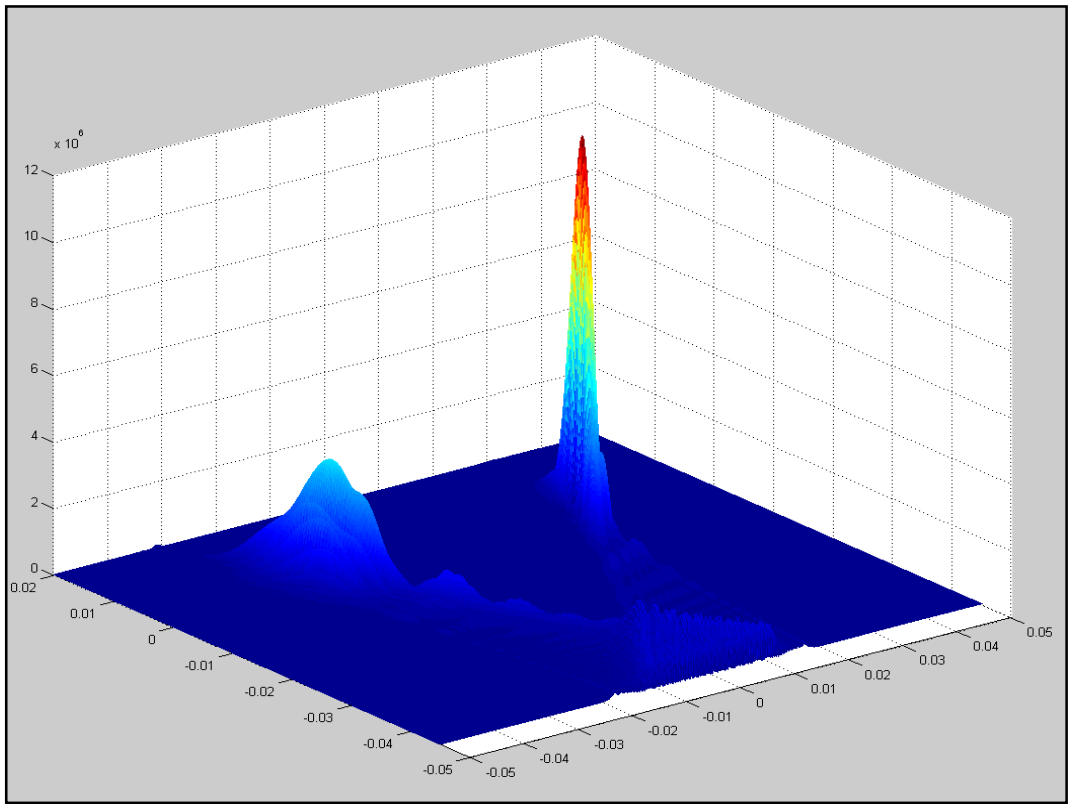

Figure 36 - ***Acoustic Intensity (W m^{-2}), element width 0.40 mm, Focus at x=25, kerf = 0.1 mm (Sim No.28)***

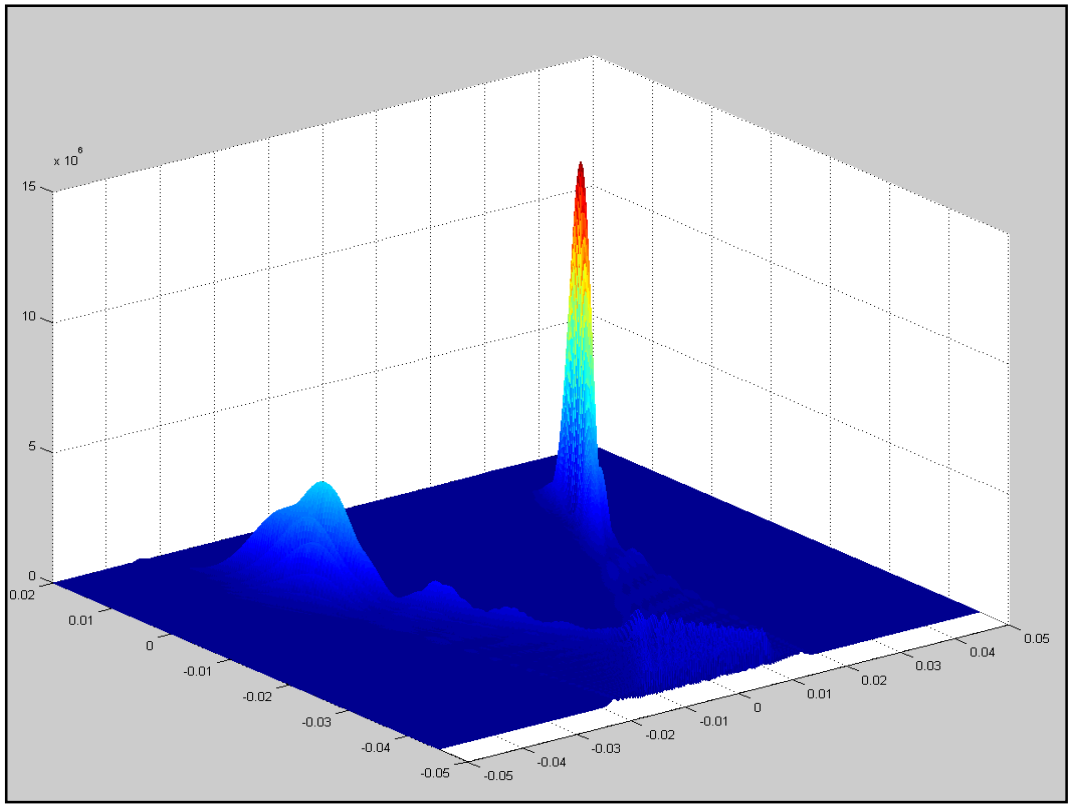

Figure 37 - ***Acoustic Intensity (W m^{-2}), element width 0.43 mm, Focus at x=25, kerf = 0.05 mm (Sim No.31)***

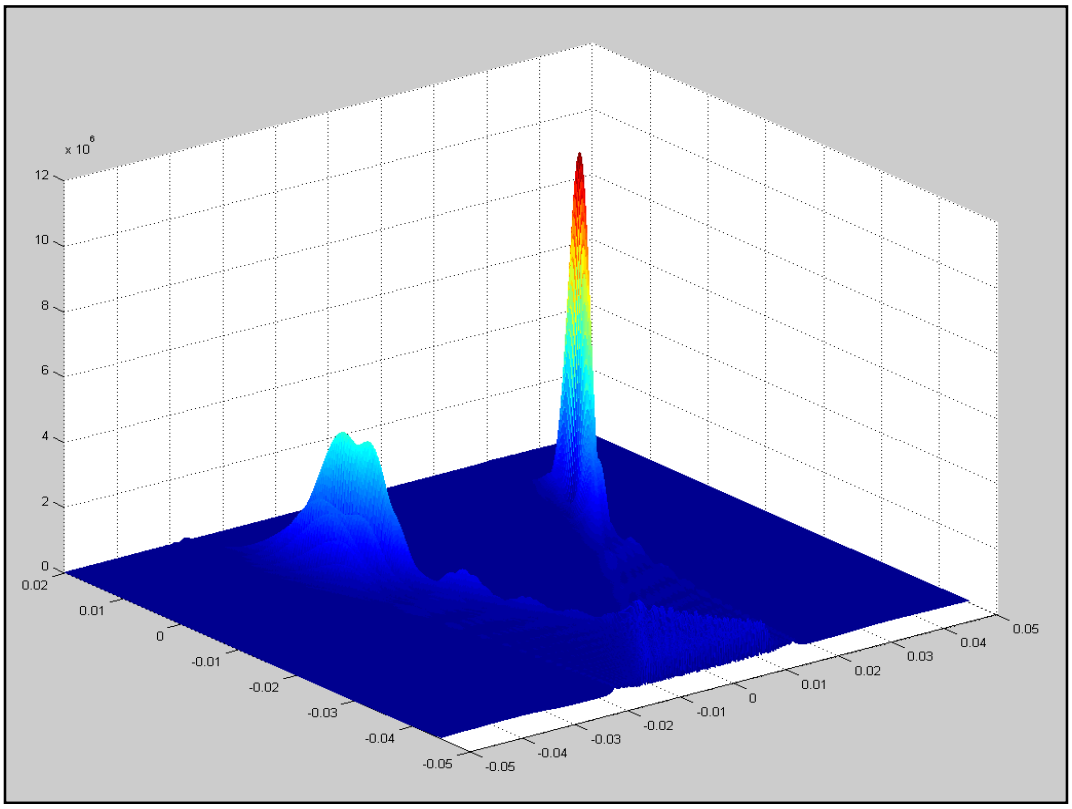

Figure 38 - ***Acoustic Intensity (W m^{-2}), element width 0.43 mm, Focus at x=25, kerf = 0.1 mm (Sim No.32)***

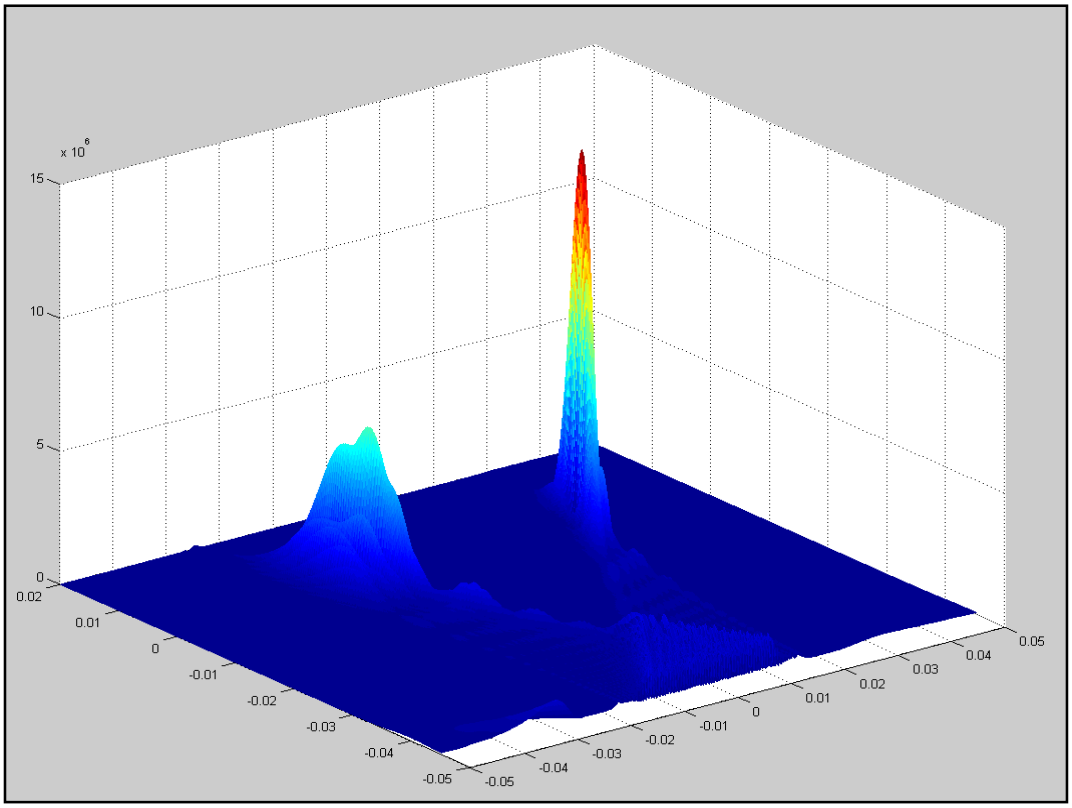

Figure 39 - ***Acoustic Intensity (W m^{-2}), element width 0.50 mm, Focus at x=25, kerf = 0.05 mm (Sim No.34)***

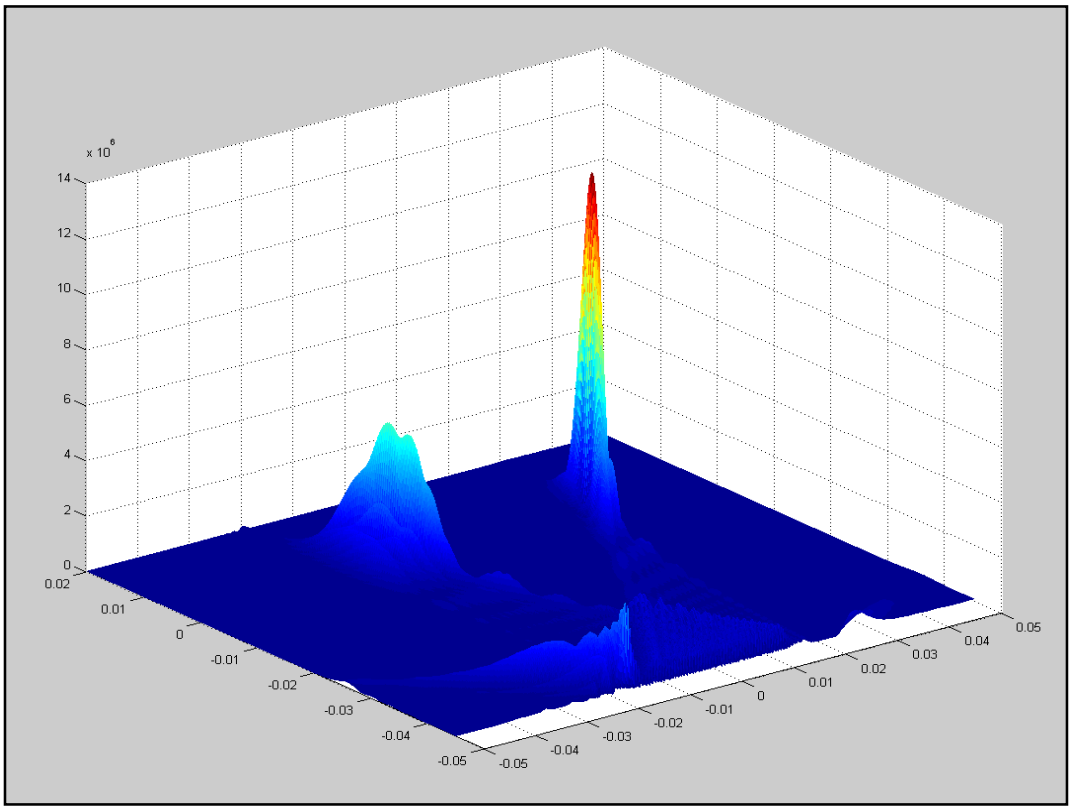

Figure 40 - ***Acoustic Intensity (W m^{-2}), element width 0.50 mm, Focus at x=25, kerf = 0.1 mm (Sim No.35)***

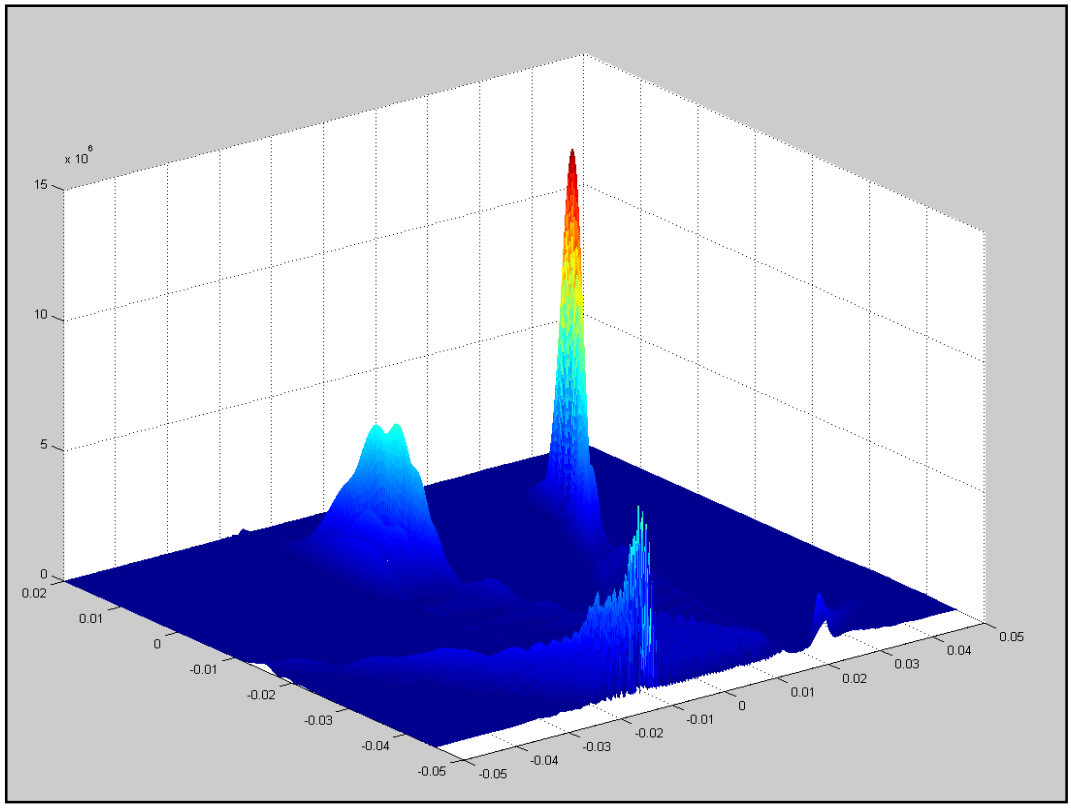

Figure 41 - ***Acoustic Intensity (W m^{-2}), element width 0.60 mm, Focus at x=25, kerf = 0.05 mm (Sim No.36)***

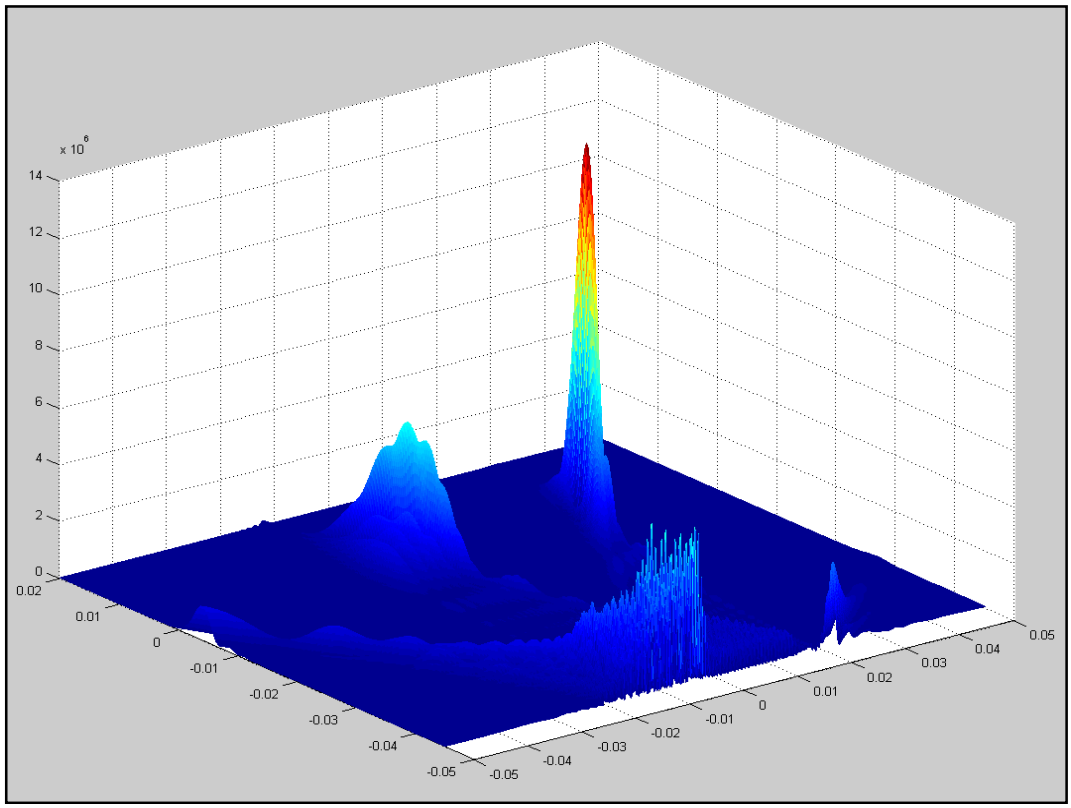

Figure 42 - ***Acoustic Intensity (W m^{-2}), element width 0.60 mm, Focus at x=25, kerf = 0.1 mm (Sim No.37)***

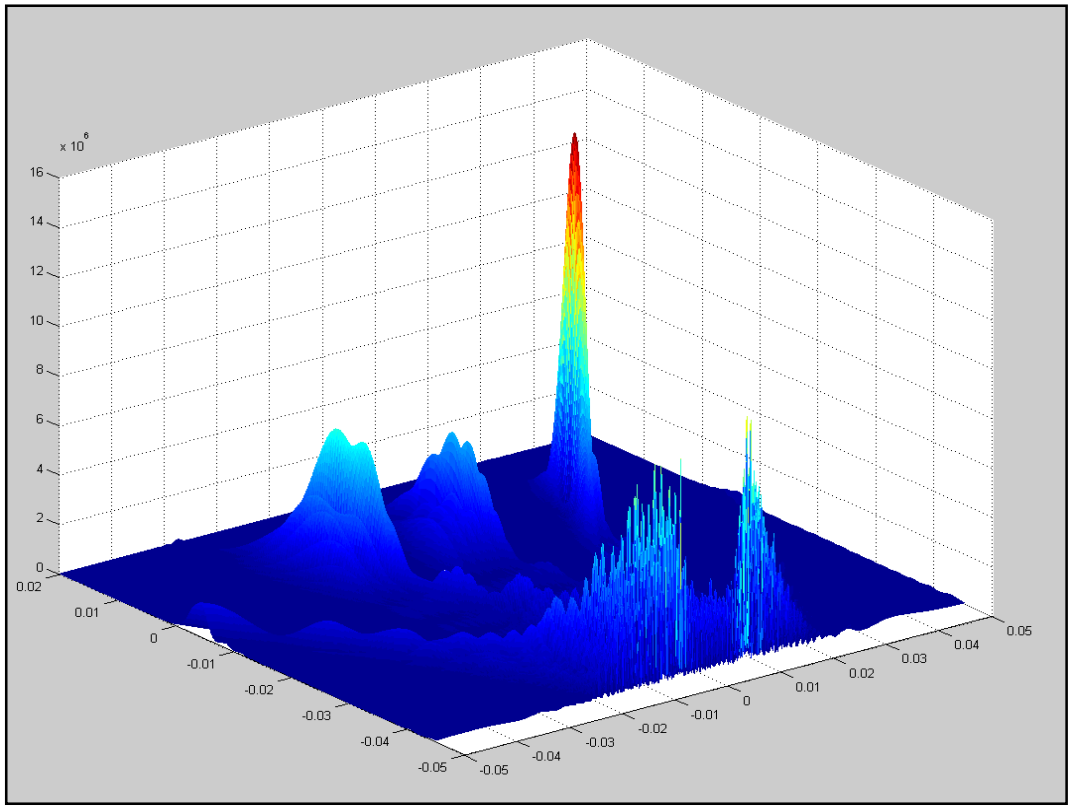

Figure 43 - ***Acoustic Intensity (W m^{-2}), element width 1.0 mm, Focus at x=25, kerf = 0.05 mm (Sim No.40)***

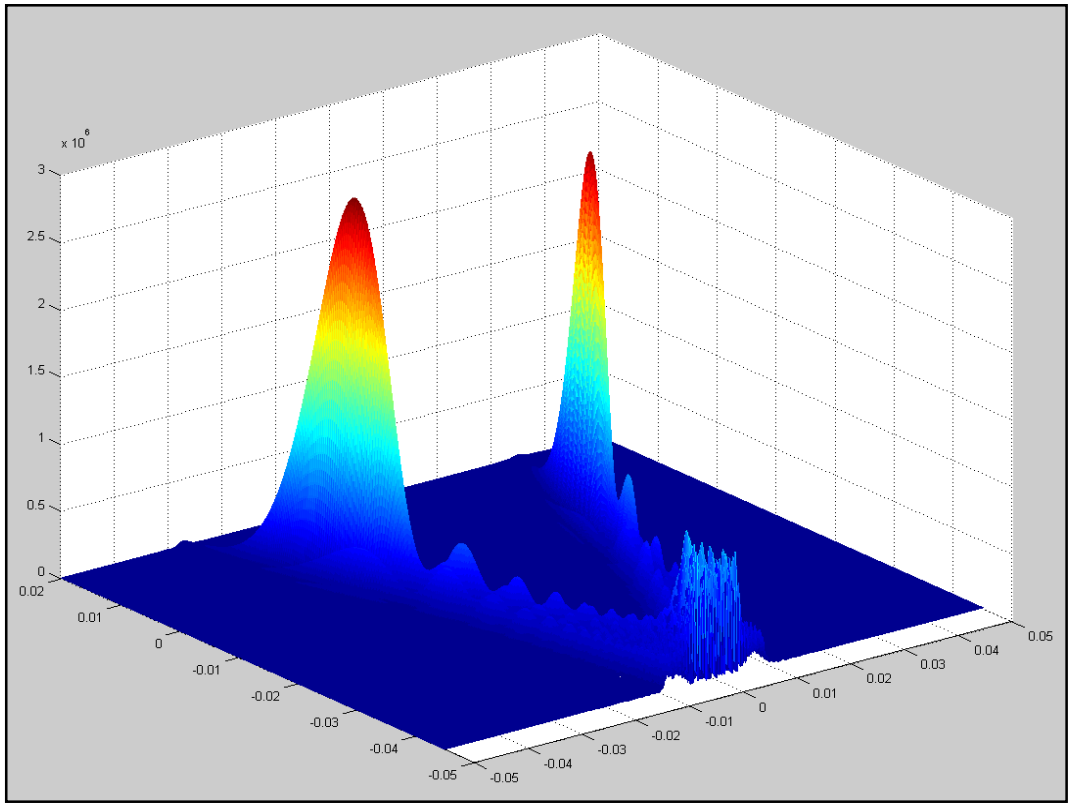

Figure 44 - ***Acoustic Intensity (W m^{-2}), element width 1.0 mm, Focus at x=25, kerf = 0.1 mm (Sim No.41)***

In summary, the optimum element width and spacing values from this set of simulations were found to be 0.35 mm and 0.05 mm respectively. This can be seen from the plots (see Figure 31 to Figure 44) and from the collated results data, presented in the table below (see Table 10).

Table 10 - ***Results of initial optimisation tests post-manufacturer discussions*** **(Figure 31 to Figure 44)**

Sim. No.	Elem width (mm)	Kerf (mm)	No. of elements simulated	Max. Focal Int. (W m^{-2})	Max. Front lobe Int (W m^{-2})	Max. Side lobe Int. (W m^{-2})	Max. lobe / Max. Focal Int. (%))
18	0.32	0.05	95	1300	400	200	30.8
19	0.32	0.1	83	1040	190	350	33.7
21	0.35	0.05	87	1350	300	380	28.2
23	0.35	0.1	77	1050	180	350	33.3
27	0.4	0.05	77	1390	180	450	32.3
28	0.4	0.1	71	1180	150	380	32.2
31	0.43	0.05	73	1400	125	490	35.0
32	0.43	0.1	65	1100	100	400	36.3
34	0.5	0.05	63	1400	120	550	39.3
35	0.5	0.1	59	1250	300	500	40.0
36	0.6	0.05	53	1480	700	600	47.3
37	0.6	0.1	51	1350	550	500	40.7
40	1	0.05	33	1580	750	600	47.5
41	1	0.1	31	270	100	280	103.7

Although the above plots show the existence of grating lobes, the previous set of plots (see Figure 25 to Figure 30) were produced using parameters that *cannot* be used for manufacture, performed prior to discussions with manufacturers. Selecting suitable element dimensions now comes down to a compromise between manufacturing and electronic driving difficulties, and the reduction of unwanted lobes. From the above plots it appears that using an element width of up to 0.43 mm seems to give acceptable levels of grating lobes, compared to larger element widths, even at the

extreme focus (x=25 mm). Also reducing the element width to 0.32 mm (approximately ¾ of a wavelength, in water) does not seem to be of great benefit compared to an element width of 0.35 mm, which still remains under one wavelength in magnitude (approximately 0.43 mm) and so should give satisfactory results according to other studies [56].

Considering all the above tabulated results it seems as though using an element width of 0.35 mm and spacing of 0.05 mm gives the optimum results, in terms of both maximum focal intensity *and* ratio of grating lobes to main lobes (28.15 %, see Table 10). Hence, if the manufacture and driving of an array with these dimensions is feasible, then these are the values that will be used. If these values are still too small for manufacture then it is possible that the element width could be increased to 0.43 mm and the spacing to 0.1 mm (as necessary). Although this would not be desirable as such, if it would allow for manufacture to proceed where other, smaller dimensions do not, then it would be the next most suitable choice.

It should be noted at this point that the simulations presented in this section were performed using a 'one-media code', assuming the entire field comprises of homogenous breast tissue, with an attenuation coefficient of 7.5 Np m^{-1} MHz^{-1}. Work to expand the code to include the case of two-media, namely breast tissue and water, as would be the case when the array is in normal operation would be necessary for accurate treatment planning. Using the one-media code will therefore underestimate the focal intensity (as the attenuation coefficient of breast tissue (approximately 5 to 7.5 Np m^{-1} MHz^{-1}) is much larger than that of water (approximately 0.025 Np m^{-1} MHz^{-1}) the attenuation would be *lessened* using the two-media code and the focal intensity would be increased) and so the intensities at focus obtained from the previous set of simulations can be said to be the *minimum* possible values that may be obtained when targeting at the *maximum* possible tissue depth. Furthermore the attenuation coefficient value used was larger than that generally used by other researchers, so as the focal intensity would be further *underestimated*, thus ensuring a desirably high value of intensity at the focus when the transducer itself is manufactured and tested.

5.3.1.6: IMASONIC Design Suggestions & Modifications

At this point in the design process transducer manufacturer Imasonic specified a minimum element width and inter-element spacing of 0.43 mm and 0.1 mm. This is not ideal but is close to that suggested previously, and so these values will be used, at least for the initial 'proof of concept' transducer.

The use of IMASONIC HI-1 piezocomposite was also suggested for this particular application as the dimensions and geometry involved makes using HI-2 piezocomposite much more difficult. A solid backing is generally not used with HI-1. Instead an air backing is used. Reported transducer efficiency will be in the region of 40 %, according to manufacturer Imasonic.

Additionally Imasonic have suggested an acoustical power output of 1 to 10 W cm^{-2}. This is very low compared to the 20 W cm^{-2} used in the above simulations. To check the feasibility of such a low power a new set of simulations was performed (see Figure 45 to Figure 50). In these simulations acoustical powers of 1 W, 5 W and 10 W were used, with each being simulated using attenuation coefficients of 5 Np m^{-1} MHz^{-1} and 7.5 Np m^{-1} MHz^{-1} (six simulations in total). Additionally, to compensate for the reduced acoustical power *all* elements are active in creating a single focus, and the 'extreme focus' will therefore be at x=45 mm (half the total array length + 10 mm to allow the focus to reach the central column of the scanner head) with the transducer centre being located at x=0.

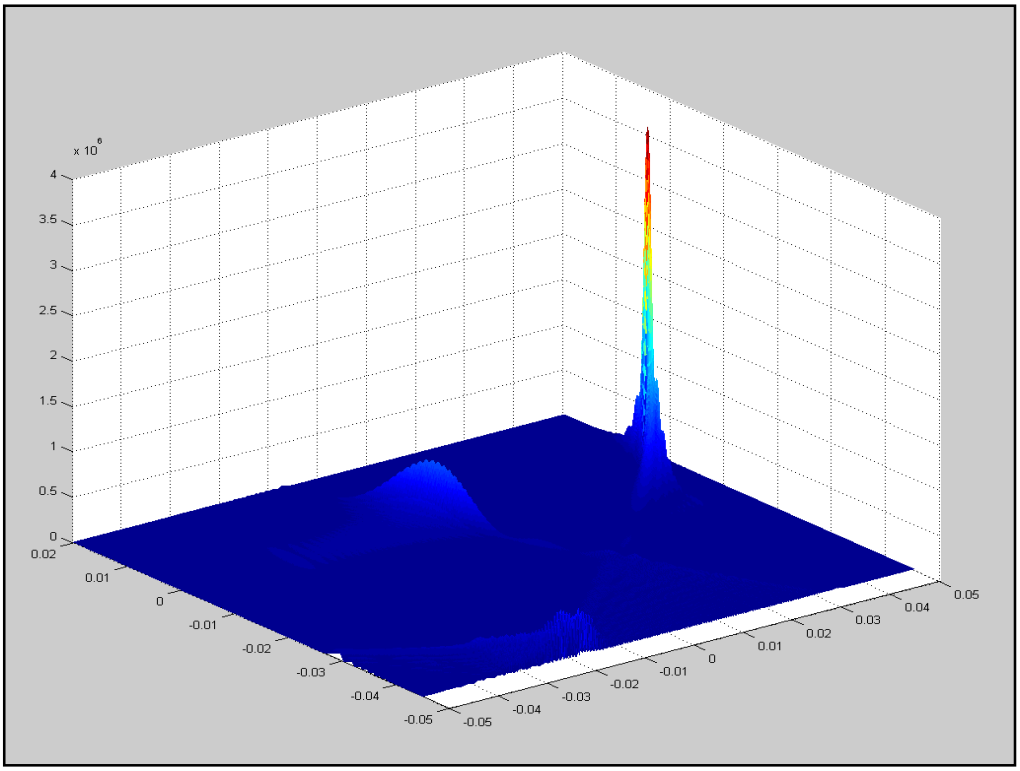

Figure 45 - ***Acoustic Intensity (W m^{-2}), element width 0.43 mm, Focus at x=45, kerf = 0.1 mm, α = 5 Np m^{-1} MHz^{-1} TAP = 1 W cm^{-2} (Sim No.42)***

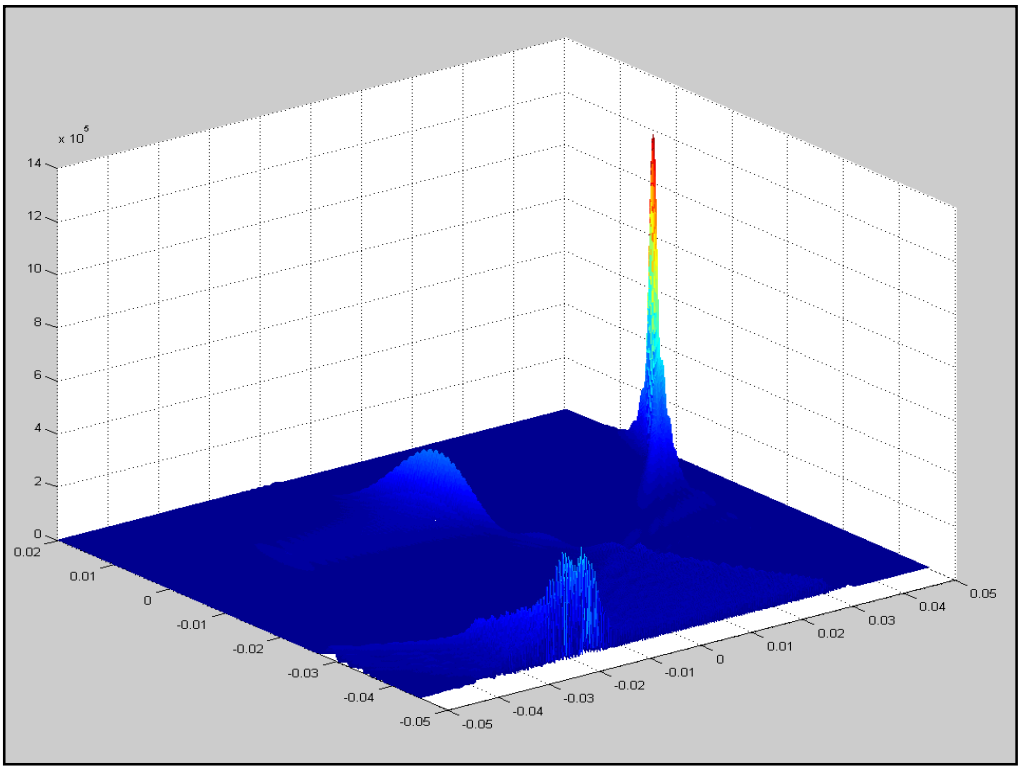

Figure 46 - ***Acoustic Intensity (W m^{-2}), element width 0.43 mm, Focus at x=45, kerf = 0.1 mm, α = 7.5 Np m^{-1} MHz^{-1} TAP = 1 W cm^{-2} (Sim No.43)***

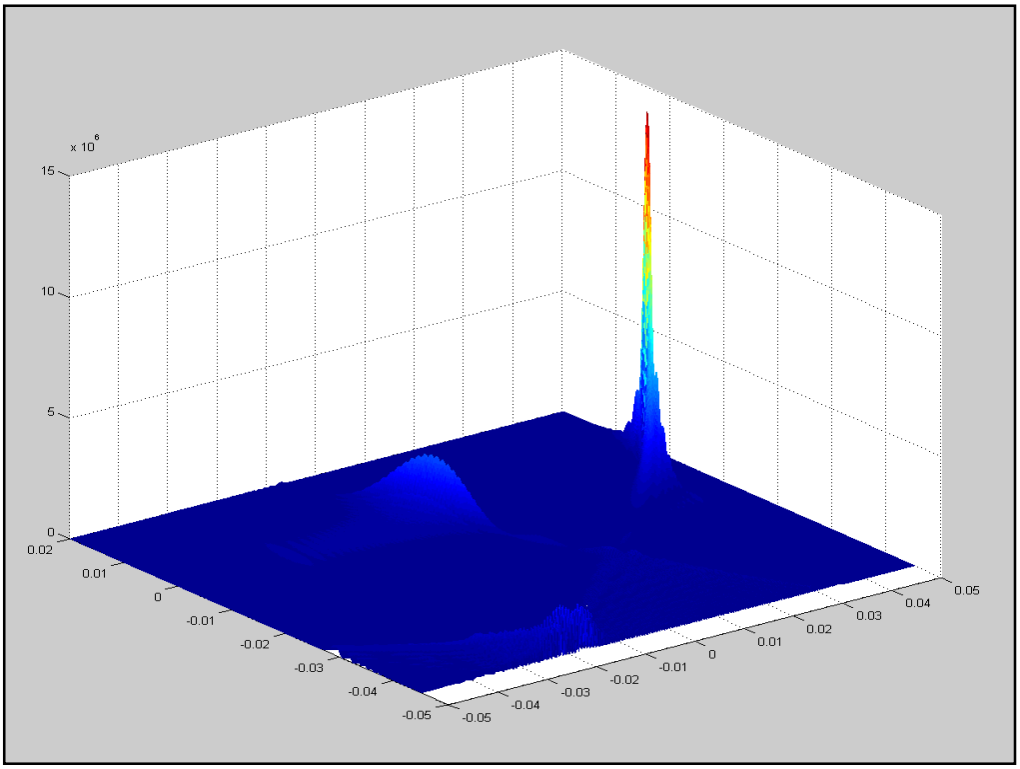

Figure 47 - ***Acoustic Intensity (W m^{-2}), element width 0.43 mm, Focus at x=45, kerf = 0.1 mm, α = 5 Np m^{-1} MHz^{-1} TAP = 5 W cm^{-2} (Sim No.44)***

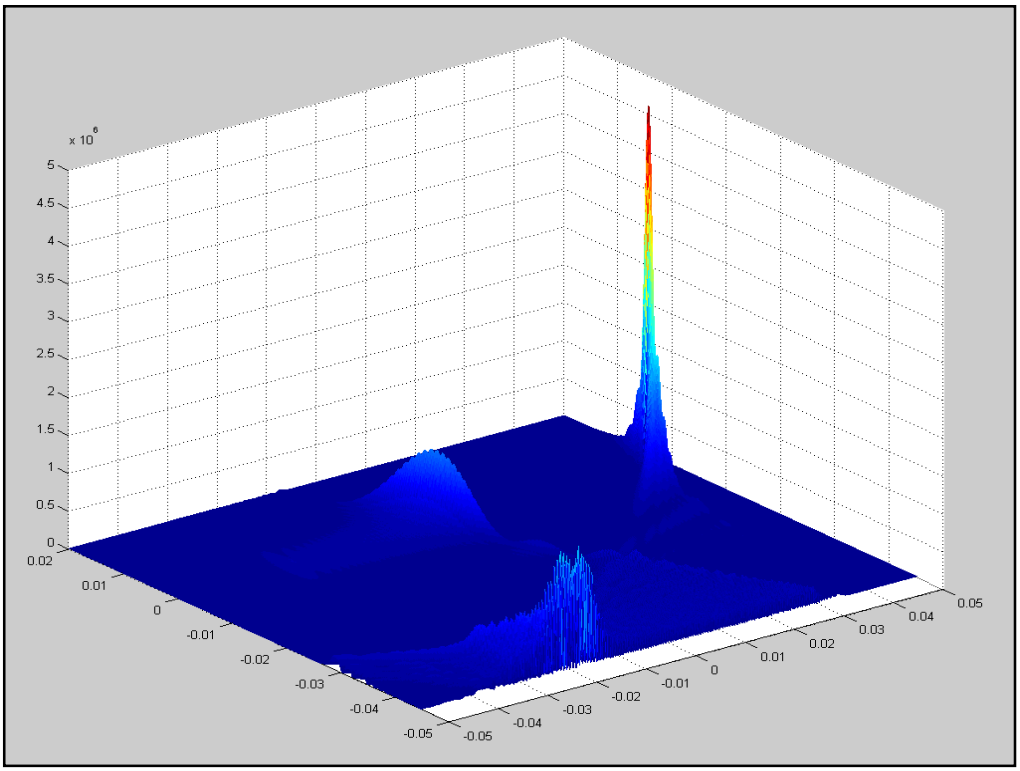

Figure 48 - ***Acoustic Intensity (W m^{-2}), element width 0.43 mm, Focus at x=45, kerf = 0.1 mm, α = 7.5 Np m^{-1} MHz^{-1} TAP = 5 W cm^{-2} (Sim No.45)***

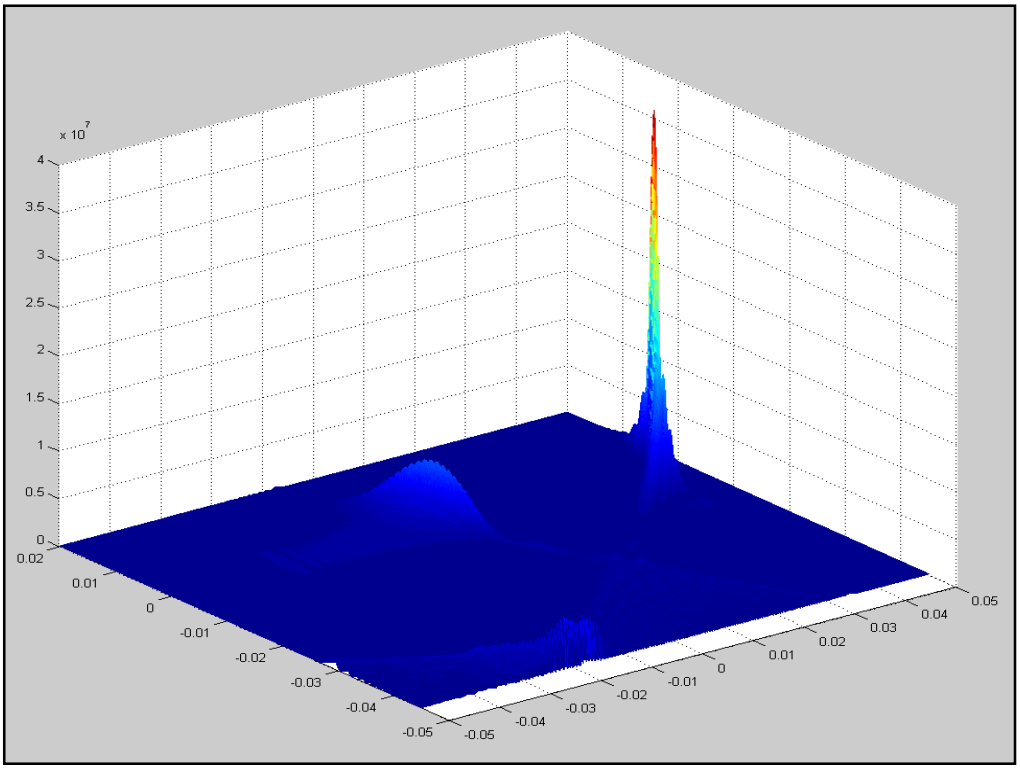

Figure 49 - ***Acoustic Intensity (W m^{-2}), element width 0.43 mm, Focus at x=45, kerf = 0.1 mm, α = 5 Np m^{-1} MHz^{-1} TAP =10 W cm^{-2} (Sim No.46)***

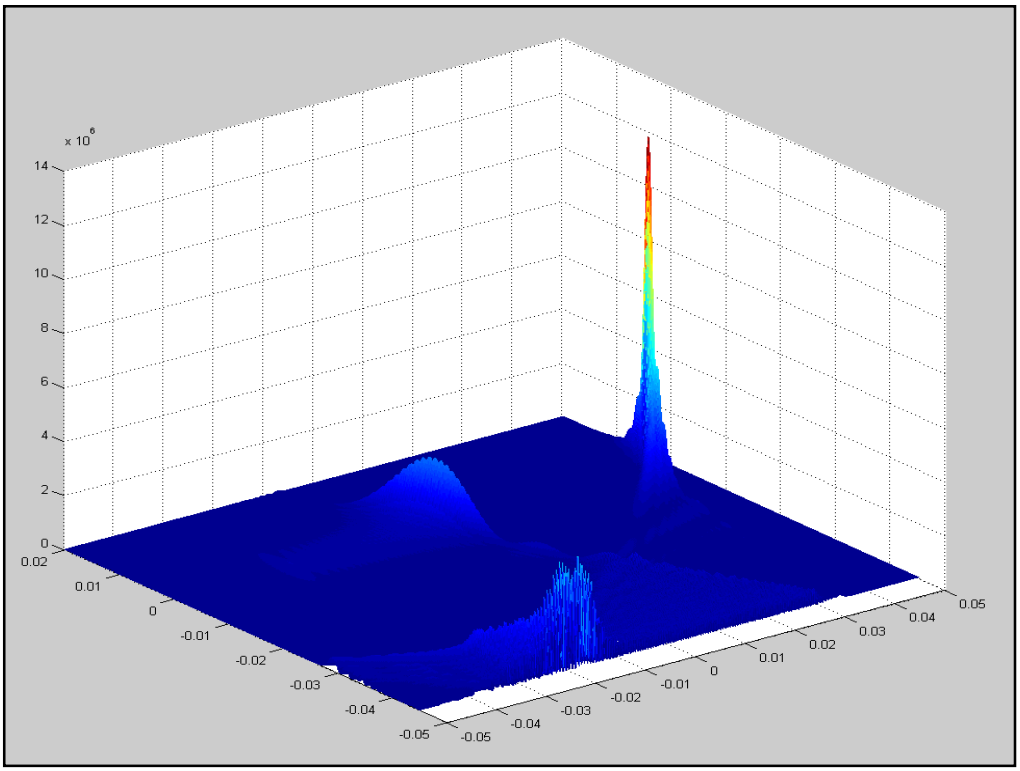

Figure 50 - ***Acoustic Intensity (W m^{-2}), element width 0.43 mm, Focus at x=45, kerf = 0.1 mm, α = 7.5 Np m^{-1} MHz^{-1} TAP =10 W cm^{-2} (Sim No.47)***

As can be seen in the above intensity mesh plots the use of the lower attenuation coefficient (5 Np m^{-1} MHz^{-1}) has the effect of reducing unwanted areas of higher intensity near to the face of the transducer. Additionally using a lower attenuation coefficient gives a much higher focal intensity, as presented in the table below (see Table 11).

Table 11 - *Results of the effects of TAP on focal & lobe intensities* (see Figure 45 to Figure 50)

Sim. no.	TAP (W cm^{-2})	Attenuation coefficient (Np m^{-1} MHz^{-1})	Max. focal Int. (W cm^{-2})	Max. front lobe Int. (W m^{-2})	Max. side lobe Int. (W m^{-2})	Max. lobe / Max Focal Int. (%)
42	1	5	375	50	75	20.00
43	1	7.5	125	40	25	32.00
44	5	5	1450	200	270	18.62
45	5	7.5	485	150	110	30.93
46	10	5	3750	400	700	18.67
47	10	7.5	1240	400	280	32.25

To ablate tissue a higher focal intensity is advantageous. From the above results (see Table 11) it seems that using a TAP of 1 W cm^{-1} may not achieve a desirable level of intensity at the focus, thus may not be able to rapidly heat the target volume to a temperature at which thermal ablation would occur. Furthermore using an attenuation coefficient of 7.5 Np m^{-1} MHz^{-1} in combination with a TAP of 5 W cm^{-2} yields a focal intensity of less than 500 W cm^{-2}, which is significantly less than the recommended focal intensity of 1000 W cm^{-2} recommended for tissue ablation earlier in this thesis. This is however not to say that this particular combination cannot be used, but ablating using such a low intensity may result in unwanted tissue heating and will also increase the necessary exposure (and therefore treatment) times involved. This will become more apparent in a subsequent section of this chapter in which the COMSOL simulations are presented, showing the actual heating effect caused by the intensity fields similar to those presented above. The reader is advised to refer the section

entitled ‘COMSOL Simulations’ (see Section 6.3) to observe these effects on tissue heating.

As the attenuation of each individual breast will vary it seems relevant to take the higher of the two values used in the previous six simulations. For this reason an attenuation coefficient of 7.5 Np m^{-1} MHz^{-1} will be used in all subsequent simulations. Again, this will allow powers and heating regimes to be underestimated and therefore ensures that the power produced by the transducer is not *below* the simulated values, but *above* or equal to them, in reality.

5.3.1.7: Phase Range & Resolution Simulations

To facilitate the design of the driving electronics circuitry it is pertinent to define the range and the resolution of the time delay (ns) necessary to achieve adequate focal intensities while minimising unwanted grating lobes. Higher resolution will lead to more of a defined focus, as waves will superimpose more accurately, while low resolution could lead to unplanned superimposing, leading to unexpected areas of high acoustic intensity, which could adversely affect the treatment planned. On the other hand, as the complexity of the time delay circuitry will increase with increasing (more defined) resolution, the resolution should be minimised, while retaining as high a degree of accuracy as possible.

To allow the effect of time delay resolution to be investigated a number of simulations were carried out. These were performed for two cases, *all* elements being activated and *half* elements being activated. The tables below (see Table 12 & Table 13) show the results of these simulations and compares results, in terms of grating lobe level, max pressure and max intensity levels against those obtained with no rounding.

Table 12 - ***Phase resolution test results, all elements focused at the extreme focus of x=45 mm***

Phase Res. (rads)	Time delay res. (ns)	Grating lobe value (W m^{-2})	Change in lobe value (%)	Max Pressure 'P' (kPa)	Change in 'P' (%)	Max Int. (W cm^{-2})	Change in Int. (%)
no rounding	(n/a)	440220	-	3358.5	-	484.24	-
0.01	0.455	440202	0.0041	3358.4	0.0030	484.22	0.0041
0.05	2.276	440287	0.0152	3358.8	0.0089	484.32	0.0165
0.1	4.552	439806	0.0939	3356.9	0.0476	483.79	0.0929
0.2	9.104	438973	0.2833	3353.7	0.1429	482.87	0.2829
0.5	22.760	432437	1.7678	3328.7	0.8873	475.68	1.7677
1	45.520	407449	7.4442	3231.1	3.7934	448.19	7.4447

Table 13 - ***Phase resolution test results, half elements focused at the extreme focus of x=25 mm***

Phase Res. (rads)	Time delay res. (ns)	Grating lobe value (W m^{-2})	Change in lobe value (%)	Max Pressure 'P' (kPa)	Change in 'P' (%)	Max Int. (W cm^{-2})	Change in Int. (%)
no roundin g	(n/a)	506631	-	2547.7	-	278.65	-
0.01	0.455	506660	0.0056	2547.7	0	278.66	0.0036
0.05	2.276	506646	0.0029	2547.7	0	278.66	0.0036
0.1	4.552	505404	0.2422	2544.6	0.1217	277.97	0.2440
0.2	9.104	504042	0.5110	2541.2	0.2551	277.22	0.5132
0.5	22.760	499585	1.3910	2529.9	0.6987	274.77	1.3924
1	45.520	460646	9.0766	2429.3	4.6470	253.36	9.0759

Furthermore, in previous studies a digital time delay circuit has been used to produce a time delay of 2 ns [44]. With an operating frequency equal to 3.5 MHz this approximately equates to a phase resolution of 0.044 rads. To confirm the feasibility of

using a 2 ns resolution two more simulations were performed, one for the case of *all* elements and one for *half* the elements being excited (see Table 14). As before, the extreme foci of x=45 (all elements) and x=25 (half elements) were used.

Table 14 - ***Effect of time delay resolution on simulation results***

No. Elem's	Phase Res. (rads)	Equiv. Time delay res. (ns)	Grating lobe value (kW m^{-3})	Change in lobe value (%)	Max P (kPa)	Change in P (%)	Max Int. (W cm^{-2})	Change in Int. (%)
All (128)]	None	(n/a)	440.2	-	3359	-	484.24	-
All (128)	0.044	2	440.2	0.0038	3359	0.0030	484.26	0.0041
Half (64)	None	(n/a)	506.6	-	2548	-	278.65	-
Half (64)	0.044	2	506.5	0.0172	2547	0.0118	278.6	0.0179

Looking at the above tabulated simulation results (see Table 12 to Table 14) it can be seen that for the case in which only *half* the elements are excited that there is no change when increasing the resolution to 0.01 rads from 0.05 rads, both of which are less than 0.006 % different to the reference in terms of grating lobe level, maximum pressure and maximum acoustic intensity levels. Using 2 ns resolution (approximately 0.044 rads) still allows error, in terms of intensity and grating lobe level, to be kept below 0.02 %. To facilitate the design of the driving electronics 2 ns appears as an acceptable delay resolution, with increasing resolution having little effect. Also as 2 ns has been used previously [44] this seems to offer the best compromise between electronic circuit complexity and realistic accuracy approximations.

For the case in which *all* elements are excited using a phase resolution of 0.05 rads gives a deviation of less than 0.02 % from the reference simulation. Using 0.044 rads (approximately 2 ns) gives an error of less than 0.005 %, which is deemed to be acceptable.

In fact there seems to be little change between resolution values up to the point that resolution exceeds 0.2 rads. Between 0.2 rads and 0.5 rads the difference to the reference simulation becomes greater than 1 %. At this point however it will be assumed that a resolution of 2 ns will be used as this will ensure accuracy while avoiding overly complex driving electronic circuitry.

5.3.1.8: Expected Focal Intensities of Suggested Design

This set of simulations was designed to allow the effect of TAP on focal intensity to be observed. As stated in a previous section the attenuation coefficient will be taken to be 7.5 Np m^{-1} MHz^{-1}. The element width and spacing (kerf) will be equal to 0.43 mm and 0.1 mm respectively for the reasons described previously (Imasonic manufacture limitations) and TAP at the transducer will be taken to be 3 W cm^{-2} (representing a comparatively *low* TAP which would allow the transducer to produce longer exposures with less probability of damage, a concern when using higher TAP values) with simulations to be repeated if this TAP appears to give too high or too low a focal intensity. The focal spot will be steered from x=0, to x=20, x=35, x=37.5 and x=45 mm (a*ll* elements being activated, x=37.5 mm being vertically above the far end of the transducer array length) to additionally allow the effect of steering (on focal intensity) to be observed. Furthermore, as discussed in the previous section, a phase resolution of 2 ns (or 0.044 rads) will be used in this next set of simulations, which will allow more realistic results to be obtained. Following these simulations involving *all* the elements of the array (see Figure 51 to Figure 55 & Table 15) another set will be performed in which only *half* the elements will be activated, with adjusted focal points at x=0, x=15, x=17.5, x=20 and x=25 mm (see Figure 56 to Figure 60 & Table 16).

5.3.1.8.1: All Elements

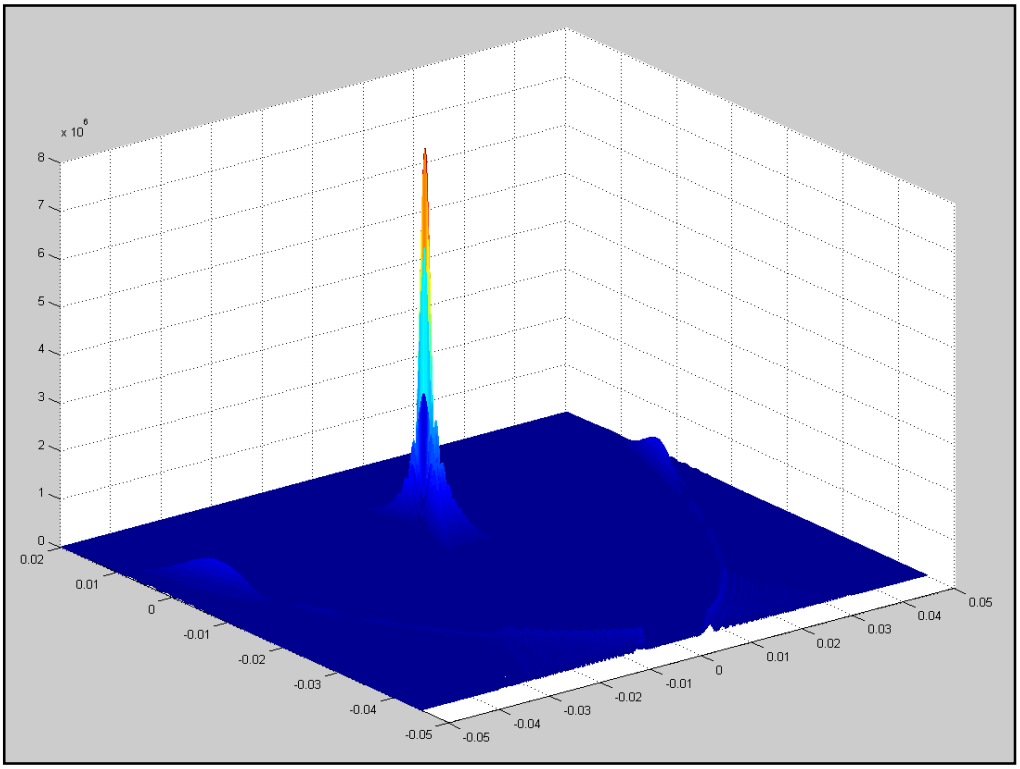

Figure 51 - ***Acoustic Intensity (W m^{-2}), element width 0.43 mm, Focus at x=0, kerf = 0.1 mm, α = 7.5 Np m^{-1} MHz^{-1} TAP =3 W cm^{-2}, ALL elements activated (Sim No.48)***

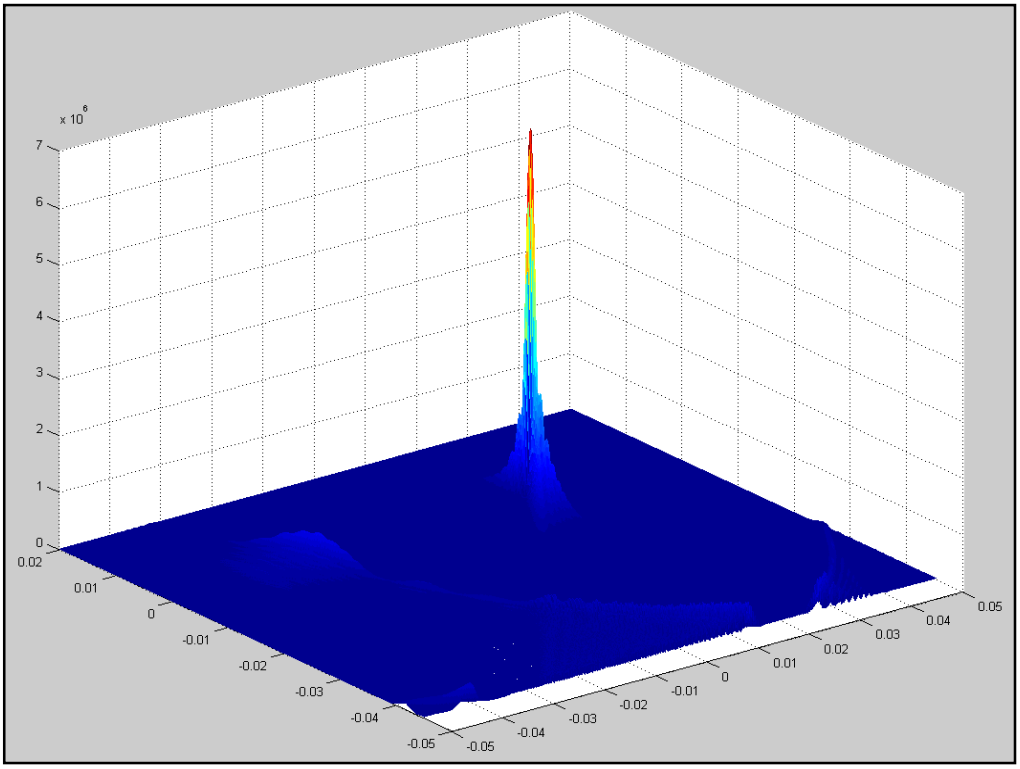

Figure 52 - ***Acoustic Intensity (W m^{-2}), element width 0.43 mm, Focus at x=20, kerf = 0.1 mm, α = 7.5 Np m^{-1} MHz^{-1} TAP =3 W cm^{-2}, ALL elements activated (Sim No.49)***

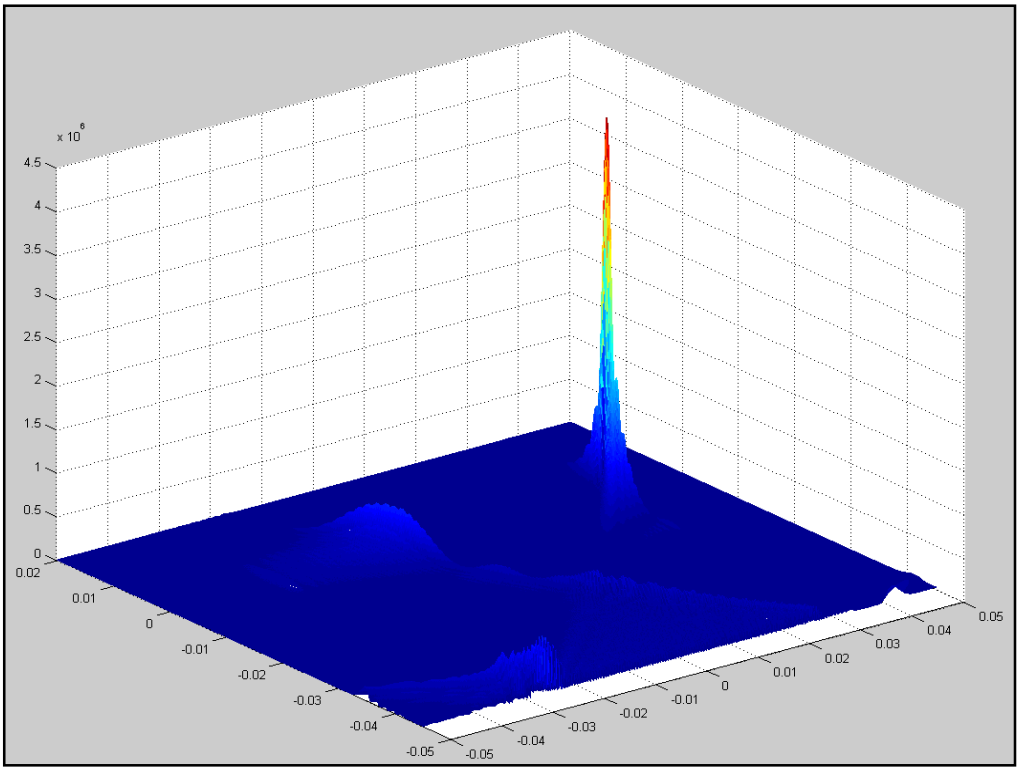

Figure 53 - ***Acoustic Intensity (W m^{-2}), element width 0.43 mm, Focus at x=35, kerf = 0.1 mm, α = 7.5 Np m^{-1} MHz^{-1} TAP =3 W cm^{-2}, ALL elements activated (Sim No.50)***

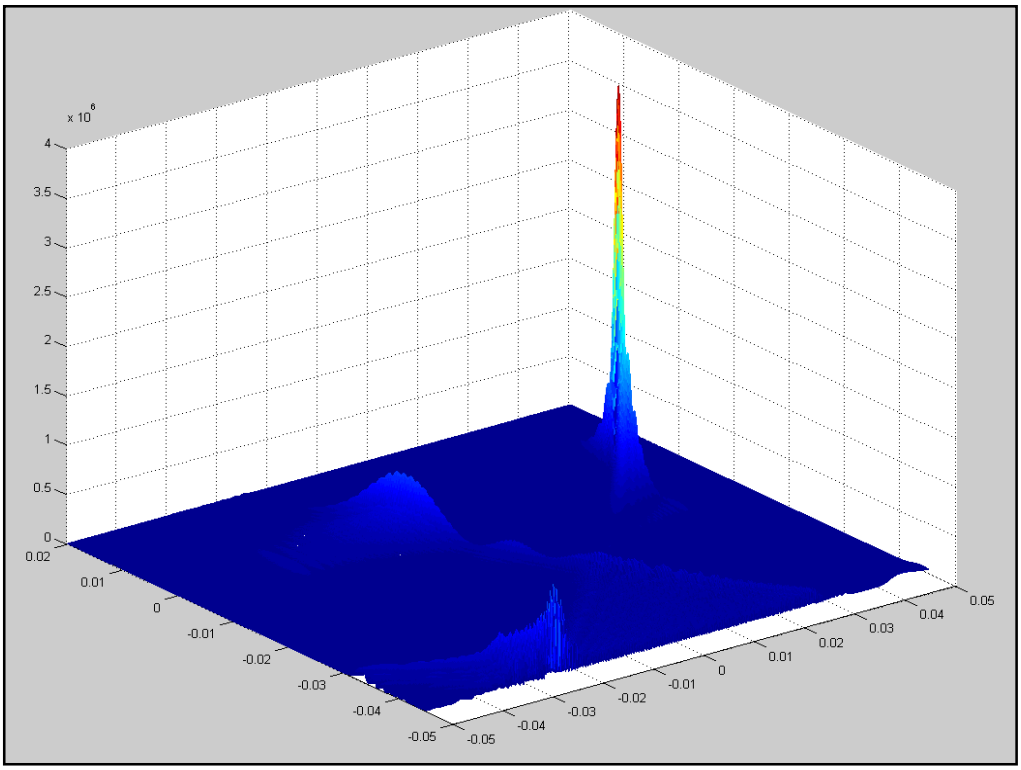

Figure 54 - ***Acoustic Intensity (W m^{-2}), element width 0.43 mm, Focus at x=37.5, kerf = 0.1 mm, α = 7.5 Np m^{1} MHz^{-1} TAP =3 W cm^{-2}, ALL elements activated (Sim No.51)***

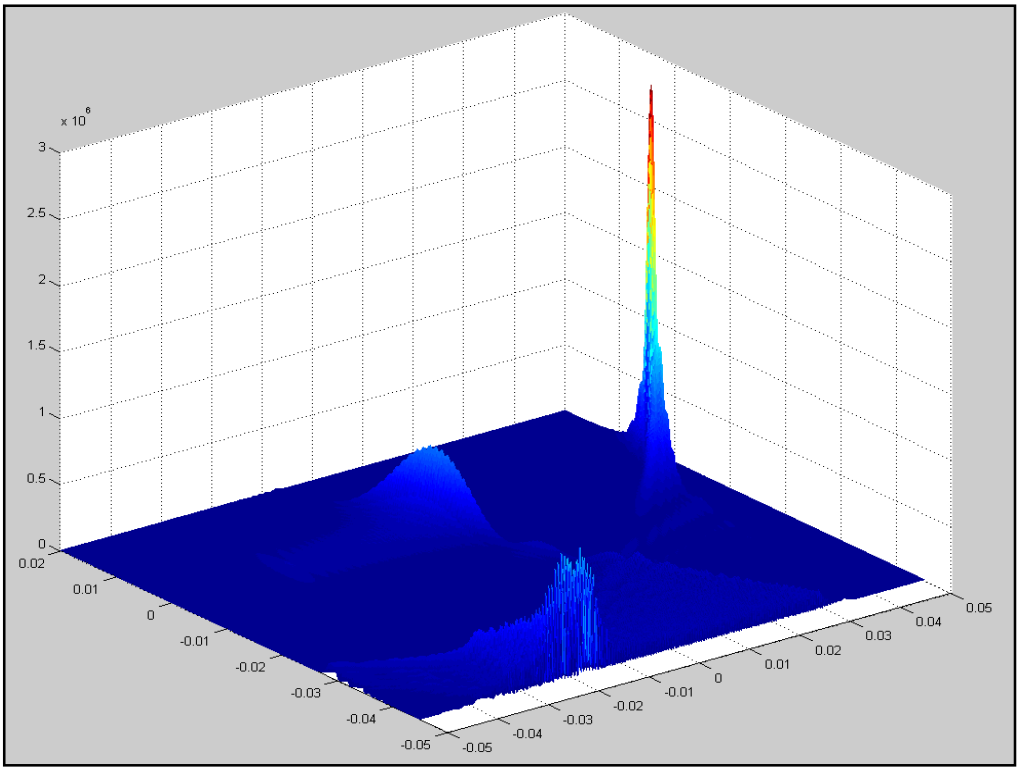

Figure 55 - ***Acoustic Intensity (W m^{-2}), element width 0.43 mm, Focus at x=45, kerf = 0.1 mm, α = 7.5 Np m^{-1} MHz^{-1} TAP =3 W cm^{-2}, ALL elements activated (Sim No.52)***

The numerical results from the plots presented above are tabulated below (see Table 15). It can be observed that grating lobes are generally acceptable up to the point at which the focus is steered out of the transducer array length. This will be discussed further following the next set of simulations, which involve activating only *half* the total number of elements in the array (64 elements centred on the geometric centre of the transducer).

Table 15 - ***Expected focal intensities with ALL elements activated*** **(Figure 51 to Figure 55)** ***(TAP 3 W cm^{-2}, element width 0.43 mm, kerf 0.1 mm, phase resolution 0.044 rads)***

Distance of focus from array centre (mm)	Focal intensity (W cm^{-2})	Max grating lobe (W/cm^{-2})	Grating lobe as a fraction of Focal Intensity (%)
0	795.4	74.69	9.39
20	659.3	65.03	9.86
35	432.1	59.32	13.73
37.5	392.6	67.55	17.21
45	290.3	64.75	22.30

5.3.1.8.2: Half Elements

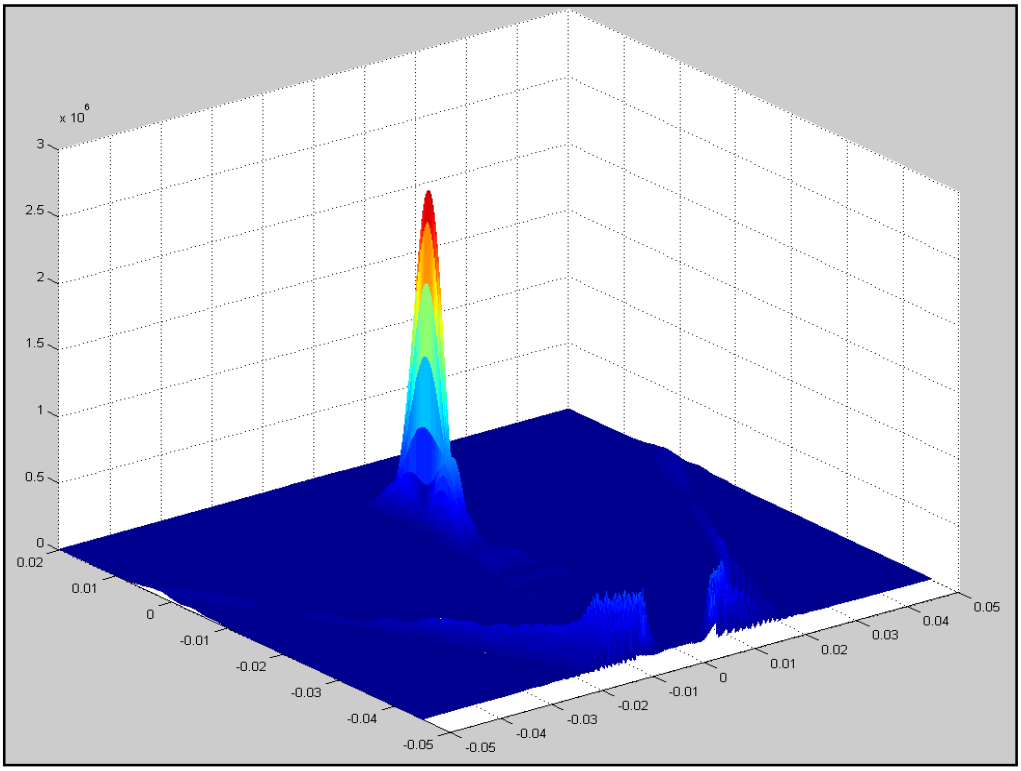

Figure 56 - ***Acoustic Intensity (W m^{-2}), element width 0.43 mm, Focus at x=0, kerf = 0.1 mm, α = 7.5 Np m^{-1} MHz^{-1} TAP =3 W cm^{-2}, HALF elements activated (Sim No.53)***

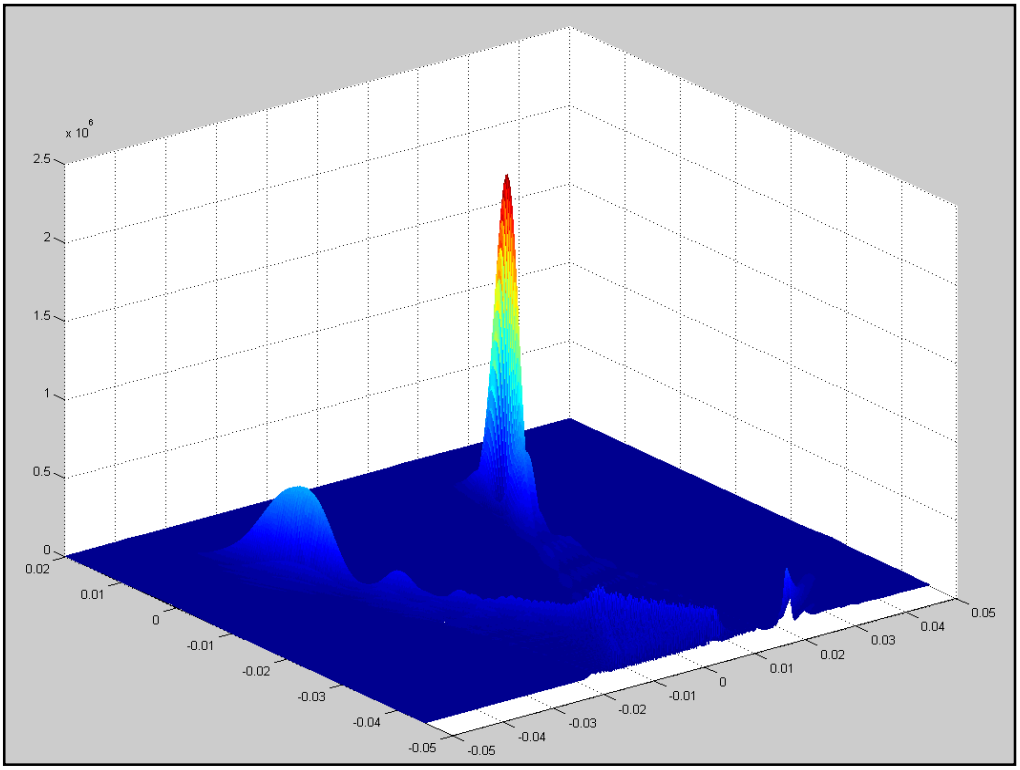

Figure 57 - ***Acoustic Intensity (W m^{-2}), element width 0.43 mm, Focus at x=15, kerf = 0.1 mm, α = 7.5 Np m^{-1}MHz^{-1} TAP =3 W cm^{-2}, HALF elements activated (Sim No.59)***

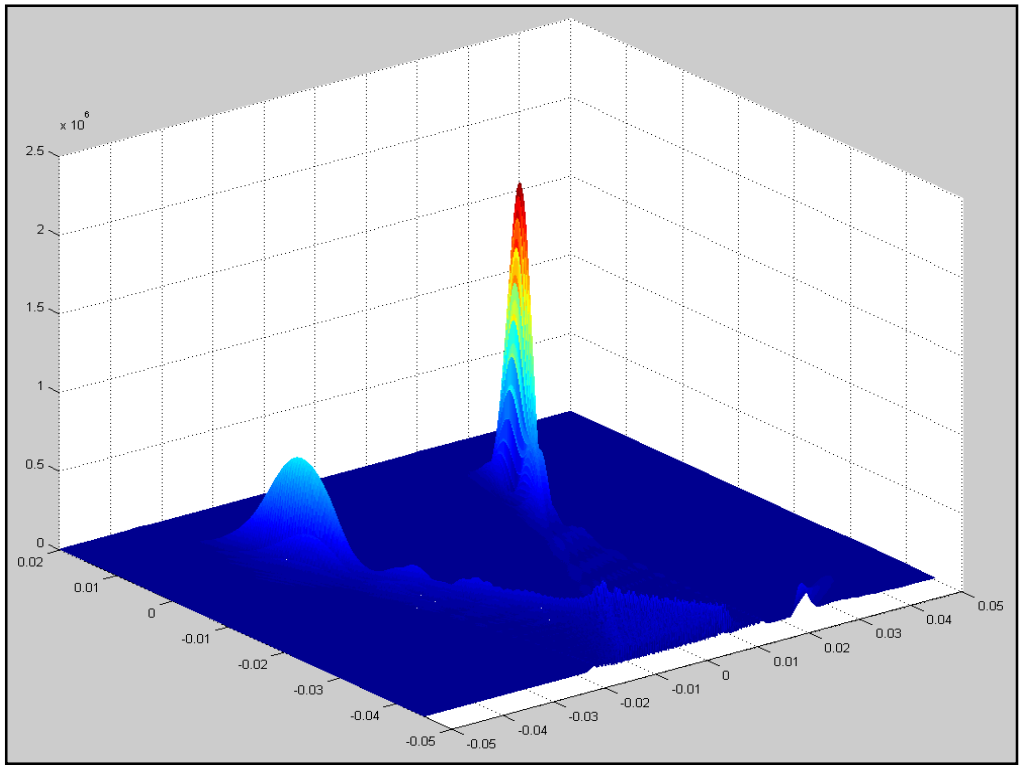

Figure 58 - ***Acoustic Intensity (W m^{-2}), element width 0.43 mm, Focus at x=17.5, kerf = 0.1 mm, α = 7.5 Np m^{-1} MHz^{-1} TAP =3 W cm^{-2}, HALF elements activated (Sim No.60)***

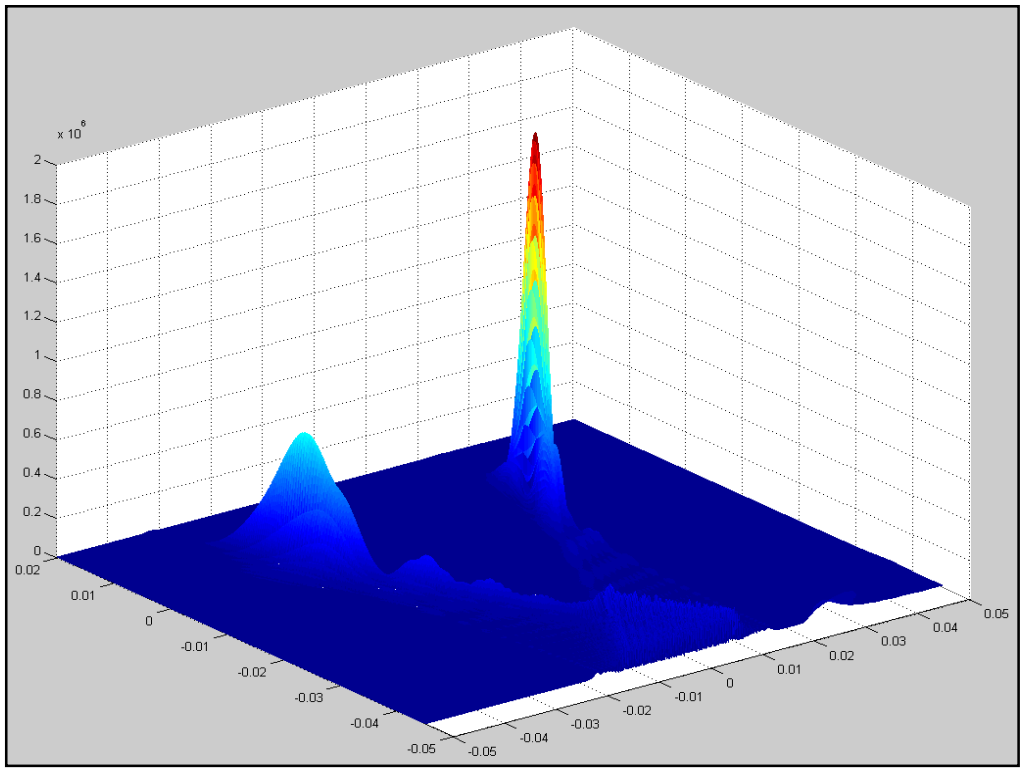

Figure 59 - ***Acoustic Intensity (W m^{-2}), element width 0.43 mm, Focus at x=20, kerf = 0.1 mm, α = 7.5 Np m^{-1} MHz^{-1} TAP =3 W cm^{-2}, HALF elements activated (Sim No.61)***

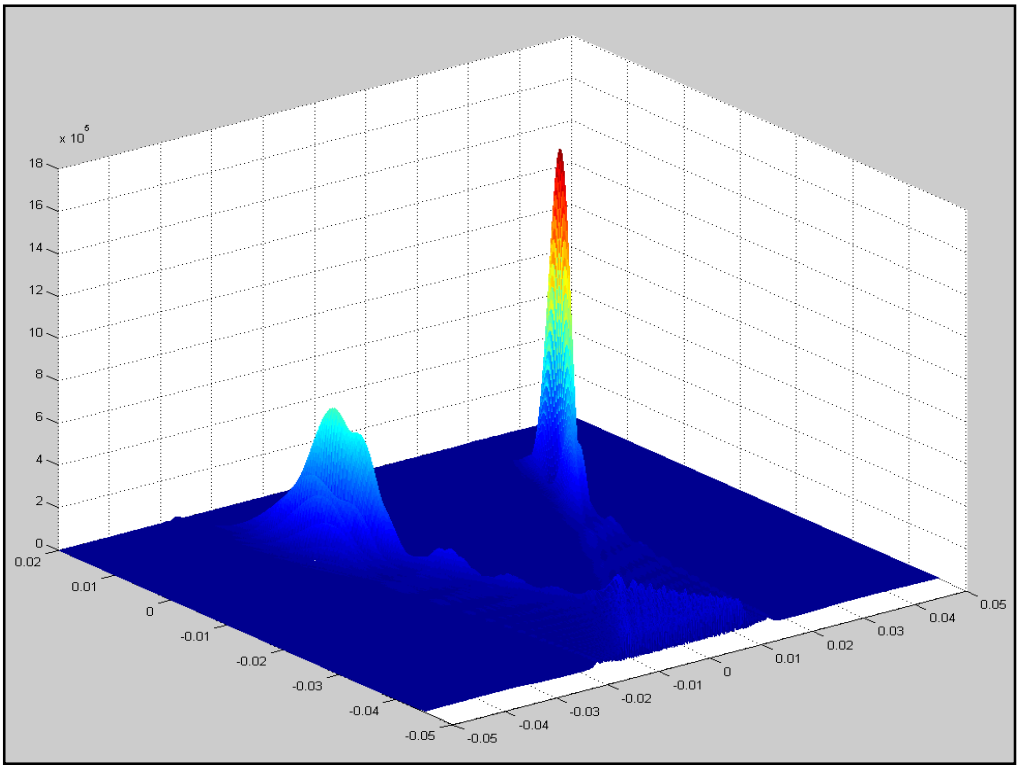

Figure 60 - ***Acoustic Intensity (W m^{-2}), element width 0.43 mm, Focus at x=25, kerf = 0.1 mm, α = 7.5 Np m^{-1} MHz^{-1} TAP =3 W cm^{-2}, HALF elements activated (Sim No.62)***

Table 16 - ***Expected focal intensities with HALF elements activated (*Figure 56 to Figure 60) *(TAP 3 W cm^{-2}, element width 0.43 mm, kerf 0.1 mm, phase resolution 0.044 rads)***

Distance of focus from array centre (mm)	Focal Intensity (W cm^{-2})	Max grating lobe (W cm^{-2})	Grating lobe as fraction of focal intensity (%)
0	256.9	6.495	2.53
15	219.2	62.85	28.67
17.5	207.8	71.95	34.62
20	194.8	72.66	37.30
25	166.8	71.13	42.64

From the above two sets of results (see Table 15 & Table 16) it can be seen that the more the focus is steered away from the geometric centre of the transducer the greater the grating lobes become. Interestingly, it can also be seen here that the ratios of these grating lobes to the main (focal) lobe are actually less for the case in which *all* the elements are activated, with focal points *outside* the length of the (active) transducer (the 'extreme' foci) compared to the greater ratios of grating to main lobes

when only *half* the elements are activated, even with focal points *within* the length of the (active) transducer. For this reason, and especially when steering to the ‘extreme‘ focal points at and beyond the length of the transducer, it is recommended that all elements are activated. When focal point are required in the central ‘two-quarters’ of the transducer however it would be advantageous to use dynamic apertures (focused on the centre of the aperture) instead of steering the focus such as to allow *vertical* lesions to be created (perpendicular to the transducer) rather than those created at an angle which would result from using phased excitation signals to steer the focus if more elements were used. These vertical lesions would facilitate the targeting and treatment planning as the volume covered would be easier to estimate compared to creating a comprehensive treatment plan using only angled lesions.

The heating patterns resulting from the above intensity fields are investigated in the ‘steering simulations’ subsection in the next chapter of this thesis (see Section 6.3.2). Please refer to this later section to observe the heating effects cause by the intensity fields presented above.

5.4: Chapter Conclusion

To conclude, in this fifth chapter the theory used to create a suitable simulation model capable of calculating acoustic pressure and intensity fields based on Huygen's principle, has been defined.

The relevant equations used in the custom written MATLAB code were introduced and briefly explained. Using this simulation model numerous parameters affecting the output of the transducer have been investigated. These have included initial tests to find a suitable and useable grid size for the simulations to be computed, a characterisation of the expected pressure fields, tests for performance optimisation and finally the expected acoustic intensities that the designed transducer will be capable of producing. These tests have included simulating the activation of both half and all of the total number of elements of the designed array. Steering of the focal point has also been considered and simulated.

Chapter 6:

Bio-Heat Transfer Simulations

6.1: Chapter Introduction

In this chapter the theory and model used in the simulation of the target tissue temperature rise, resulting from the acoustic intensity fields simulated previously will be explained. The results from the performed simulations will then be presented, using the intensity fields theoretically created by the selected transducer geometry (performed in MATLAB, see Chapter 5). By this method the resulting temperature distribution in the simulated target tissue volume will be calculated and discussed.

A 'Thermal Dose' model [4] will be introduced to allow the accurate comparison of differing heating regimes, caused by different simulation parameters being used as inputs. This model will greatly facilitate comparisons between different transducer parameters as well as steering of the focus and other factors that require investigation before a safe and effective design can be finalised. The simulation results presented here were computed using the COMSOL Multiphysics simulation package.

6.2: Simulation Theory

Building on the theory presented in the previous chapter (see Chapter 5) the mechanism for the rise in tissue temperature will be briefly described here.

It has already been shown that the acoustic intensity field for the proposed transducer can be calculated. The heat deposition within a tissue exposed to such an intensity field can be calculated by computing the BHTE, which for Cartesian coordinates can be written as follows [2] [87] [88].

$$\rho C_t \frac{\partial T}{\partial t} = K\left(\frac{\partial^2 T}{\partial x^2} + \frac{\partial^2 T}{\partial y^2} + \frac{\partial^2 T}{\partial z^2}\right) - wC_b(T - T_a) + q_{met} \qquad \textbf{\{6.1\}}$$

Where 'C_t' is the specific heat of the tissue, 'K' is the thermal conductivity, 'T' is the temperature, 'w' is the blood perfusion rate, 'C_t' is the specific heat of the blood, 'T_a' is the arterial blood temperature, 'q_{met}' is the metabolic heat and all other symbols are as stated previously.

Here we assume the total heat deposited is equal to the absorption (or attenuation) of the acoustic energy within the tissue in question. This gives us the relationship [89].

$$q(x, y, z) = 2\alpha I(x, y, z) \qquad \textbf{\{6.2\}}$$

We can then use this to replace the metabolic heat term 'q_{met}' in the BHTE as the heat produced by metabolism is negligible compared to that produced by the absorption of the incident acoustic energy. Thus the BHTE becomes

$$\rho C_t \frac{\partial T}{\partial t} = K\left(\frac{\partial^2 T}{\partial x^2} + \frac{\partial^2 T}{\partial y^2} + \frac{\partial^2 T}{\partial z^2}\right) - wC_b(T - T_a) + q(x, y, z) \qquad \textbf{\{6.1a\}}$$

The COMSOL Multiphysics software package was used to solve the above equation, using the resultant acoustic intensity distribution for all points obtained from the

custom-written MATLAB code mentioned previously. With a suitable mesh size (determined by the frequency of the acoustic waves involved and the maximum available computational power) the time-dependent temperature rise was obtained. In addition a model for calculating the 'Thermal Dose' (TD) was employed (using COMSOL) according to the equation presented below.

$$(t_{43} =) \quad TD = \int_{t_0}^{t_f} R^{(43-T(t))}\, dt \qquad \{6.3\}$$

Where 'R' equals 0.25 for 37°C < T < 43°C or 0.5 for T ≥ 43°C and 't_0' & 't_f' are the initial and final times respectively [4].

The above provides a datum to measure the effect of differing heating regimes, thus allowing them to be quantifiably compared. For reference, the plot below (see Figure 61) shows a visual representation of the above relationship. Please note however that the temperature-time combinations shown by the plot assume the temperature has been held constant for the entire time period. This will not be the case for the heating effects caused by HIFU sonications as the (tissue) temperature will be time-dependent, increasing as more energy is deposited by incoming sonications.

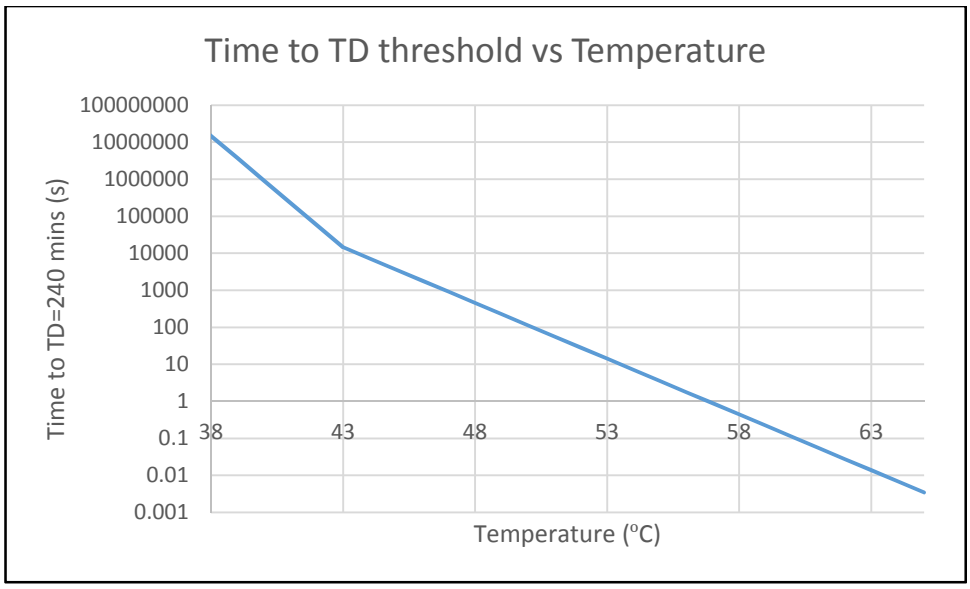

Figure 61 - Plot showing relationship of Time to Temperature in 'Thermal Dose' (TD) model (cell necrosis predicted above line shown)

As a general rule of thumb, once tissue temperature reaches 65 °C the tissue can said to be necrosed. This can be seen by comparing the time-dependent temperature rise with the TD value. The TD (or ' t_{43}') value is measured in 'equivalent minutes', equivalent to tissue held at 43 °C. It is generally accepted that tissue is destroyed once the dose reaches 240 of these 'equivalent minutes'. This value will be used as the threshold in determining the feasibility of tissue ablation in the simulations following (see Section 6.3).

6.3: COMSOL Simulations

As stated in the 'Theory' section, presented earlier, the COMSOL Multiphysics software package was used to simulate the expected time-dependent temperature rise and equivalent thermal dose given the intensity fields obtained from the pressure field simulations performed using MATLAB. As COMSOL is processor and RAM intensive, models of interest were simulated using a relatively coarse mesh. Once areas of interest were identified the simulations were re-performed, using a mesh size matching the mesh size used in the MATLAB pressure field simulations, thus allowing more accurate results to be observed. This was particularly important for the contour plots of equivalent thermal dose and was achieved by reducing the total simulation area and focusing on a smaller area, containing the regions of interest. This allowed solutions to be obtained without the PC being used running out of resources or errors being caused in the simulation results. A number of these simulations performed overnight as the timescales involved in converging on a solution were suitably large.

Many simulations have been performed while learning to use COMSOL and during the fine-tuning of the model such that it produced reliable, repeatable results. The number of simulations performed easily exceeds seventy individual tests and as such only the simulations pertinent to the narrative of this thesis will be included, with references being made to those omitted as deemed appropriate.

As the minimum element width and spacing has been set according to manufacturing constraints subsequent simulations will involve intensity fields produced by a transducer array with element width 0.43 mm and inter-element spacing of 0.1 mm. Additionally the phase resolution will be set to 0.044 rads (2 ns time delay equivalent) as described in the previous section of this thesis.

The parameters used in these simulations have been listed earlier (see Table 5) and so will not be listed here again. A time step size of 0.01 s was used in all COMSOL simulations.

6.3.1: TAP vs. Exposure Time Simulations

In the course of discussions with manufacturer Imasonic it has become necessary to define the exposure conditions for treatment sonications using the designed device. As the transducer will heat up while active it has been suggested (and accepted) that two thermocouples will be fixed to the back of the transducer, allowing operation to be halted if a certain maximum temperature is reached that would cause irreparable damage to the transducer. Furthermore to allow Imasonic to produce a detailed technical specification of permitted exposure regimes, a number of simulations have been performed. These simulations were performed for the cases of TAP output ranging from 1 W to 5 W in steps of 1 W, with an attenuation coefficient of 7.5 Np m^{-1} MHz^{-1}. Using COMSOL the time at which the equivalent thermal dose is greater than 240 mins [4] was recorded, thus allowing an approximation of the *maximum* necessary sonication periods required to ablate the target tissue. These results have been tabulated, for the case of all elements being active (see Table 17 & Table 18) and for half elements being active (see Table 19 & Table 20). Additionally the temperature distribution plots are presented for the time at which the thermal dose exceeds the threshold value of 240 equivalent minutes (accurate to *at least* 0.1 seconds, 'HiDef' simulations additionally are accurate to 0.01s) for each TAP value (1 W to 5 W). These plots will also include the 'extreme' focus (x=25 mm for *half* elements and x=45 mm for *all* elements) as well as the geometrically centred focus (x=0) to allow the effects of both the minimum and maximum steering angles to be observed at all TAP values. The results of these simulations will be tabulated (see Table 17 to Table 20) following the relevant plots (see Figure 62 to Figure 81 & Figure 84 to Figure 102) and will include at least 1 and 2 second values for all cases (in addition to the time at which a thermal dosage of 240 equivalent minutes is exceeded) to allow some comparison between different TAP values at similar points in the simulated treatment time. The first two plots (see Figure 62 and Figure 63) have been enlarged to allow labels to be seen more clearly.

6.3.1.1: All Elements

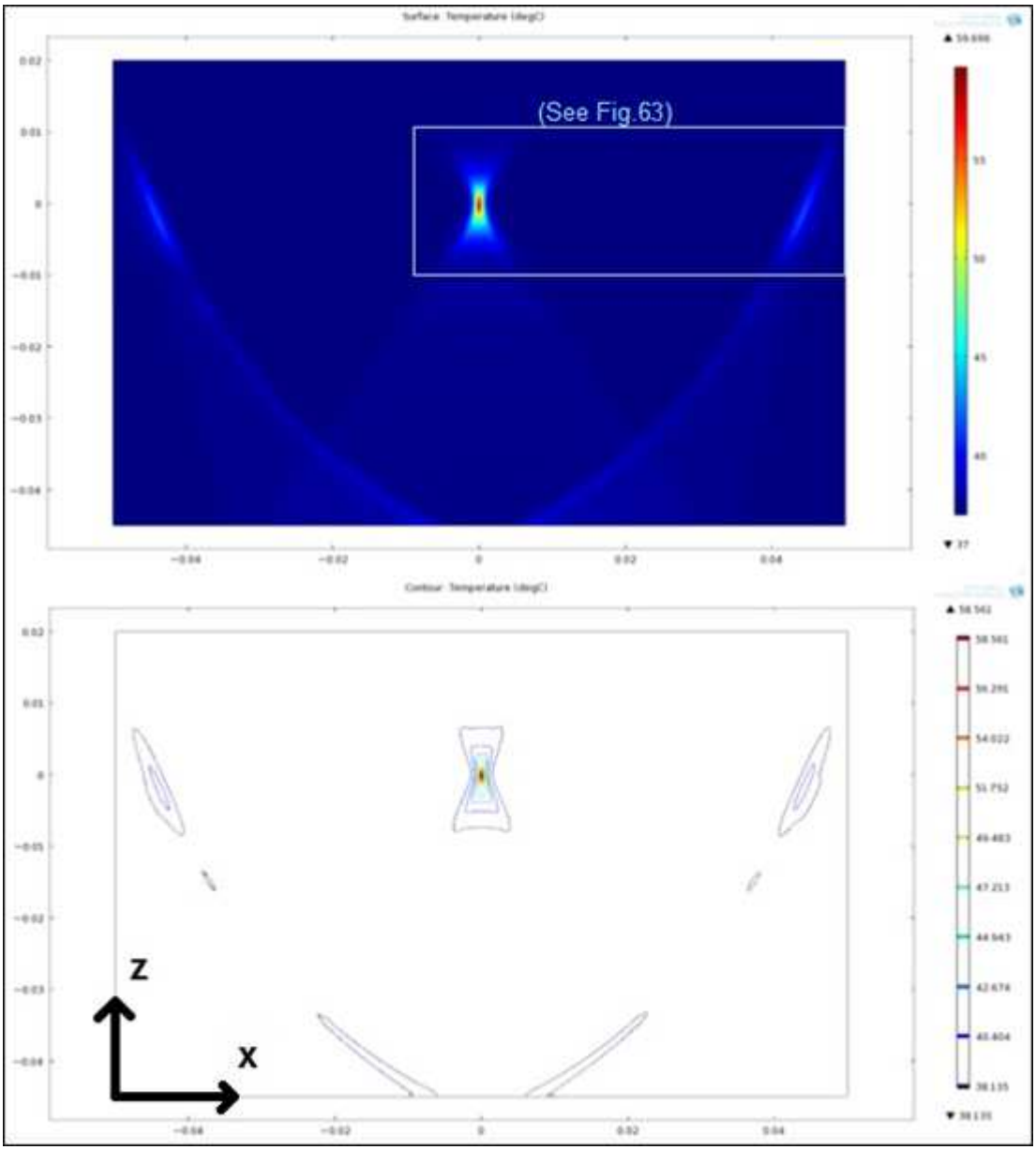

Figure 62 - ***Surface and contour Temperature plots (°C) for TAP = 1 W cm^{-2} after 1.8 seconds - focus at x=0, ALL elements activated***

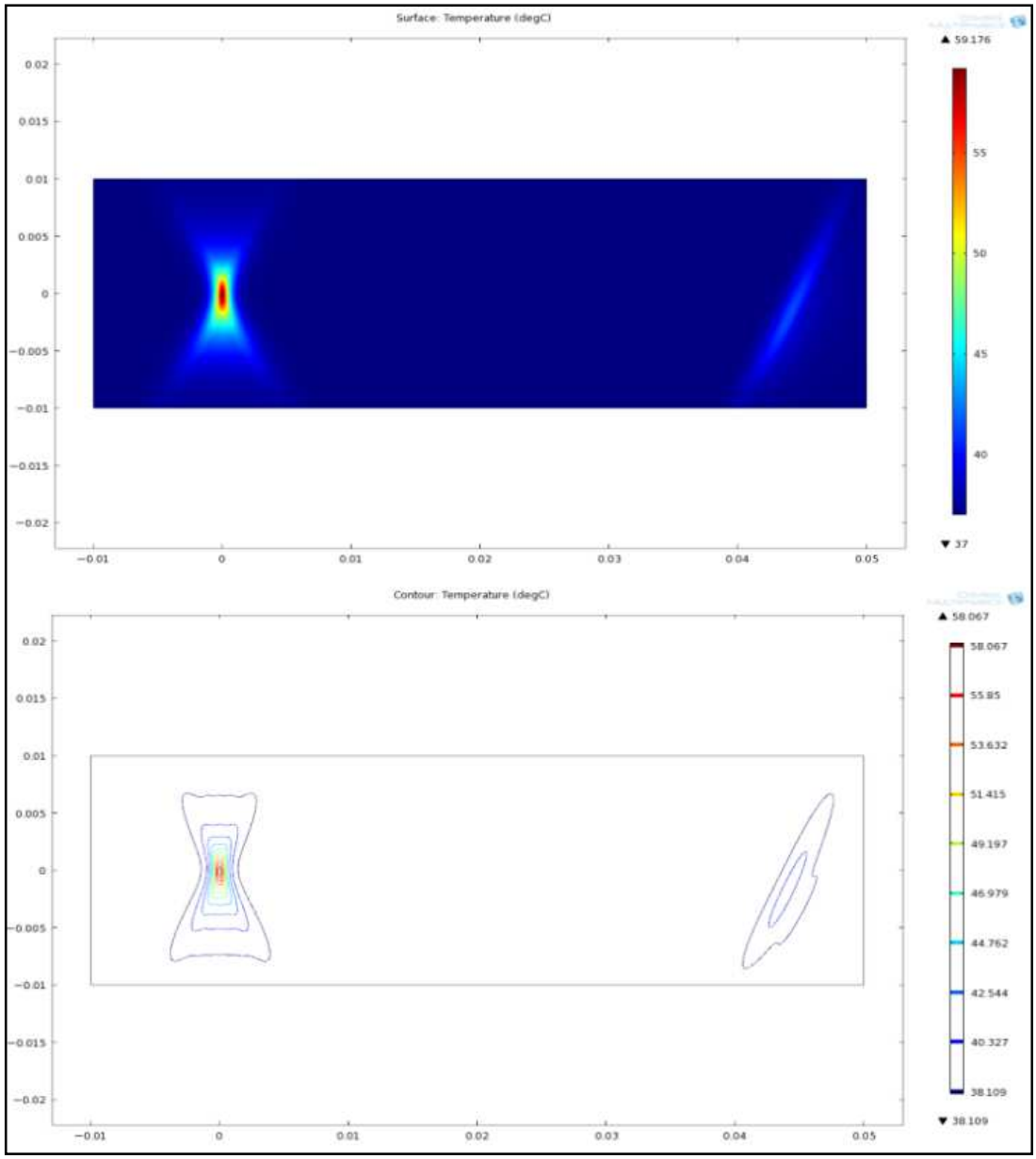

Figure 63 - ***Surface and contour Temperature plots (°C) for TAP = 1 W cm^{-2} after 1.75 seconds - focus at x=0, ALL elements activated (HiDef)***

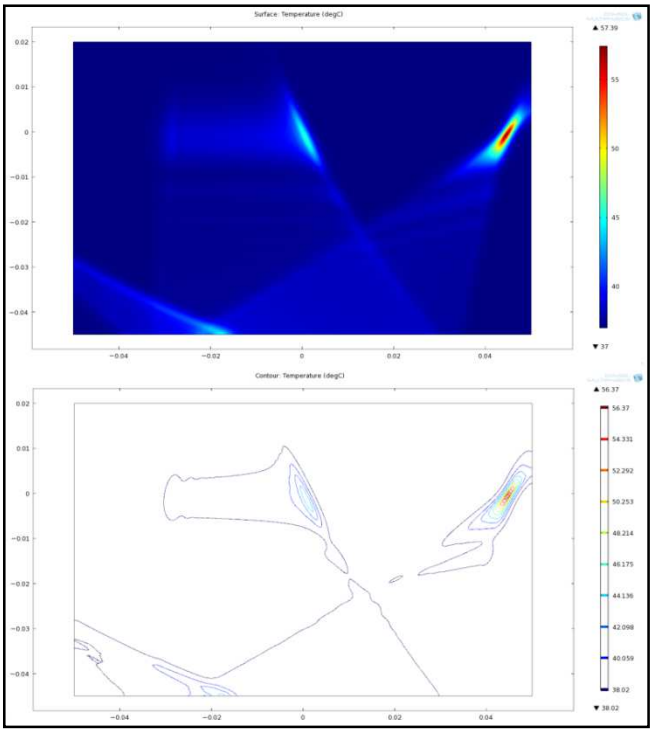

Figure 64 - ***Surface and contour Temperature plots (°C) for TAP = 1 W cm^{-2} after 4.8 seconds - focus at x=45, ALL elements activated***

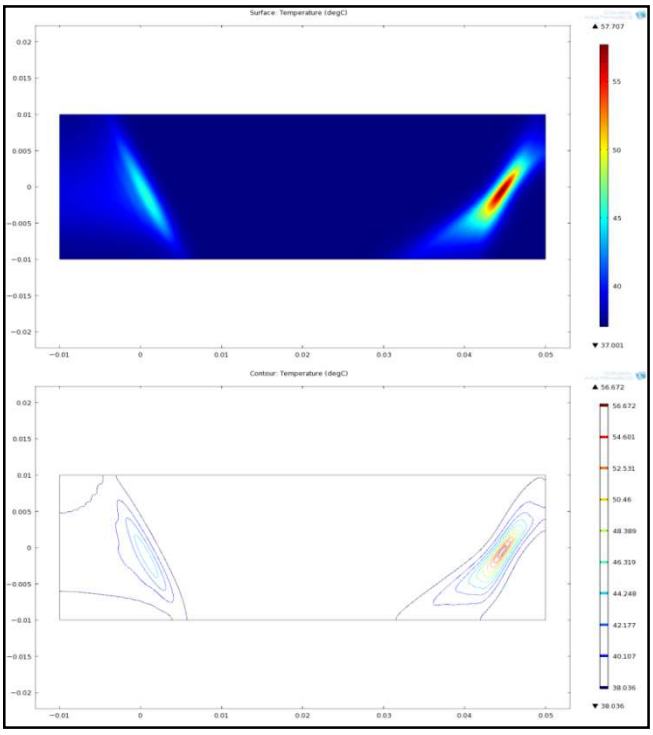

Figure 65 - ***Surface and contour Temperature plots (°C) for TAP = 1 W cm^{-2} after 4.77 seconds - focus at x=45, ALL elements activated (HiDef)***

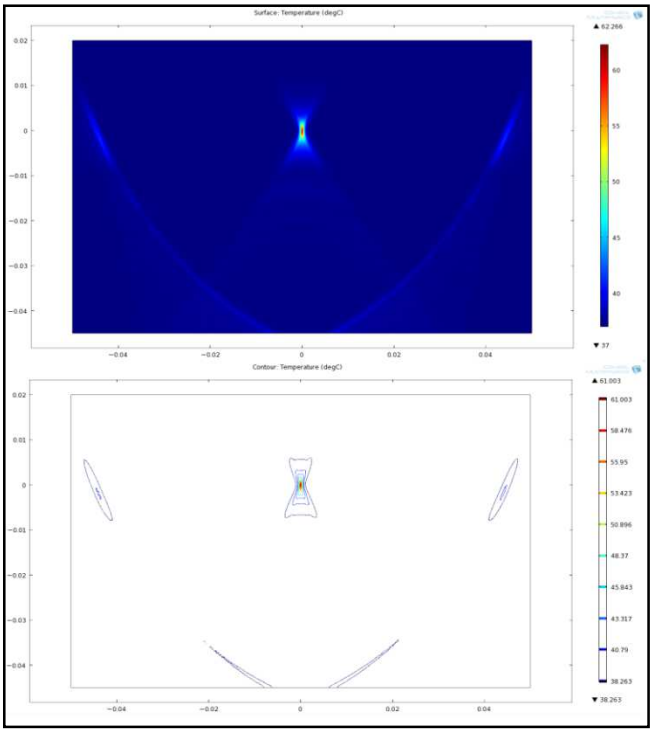

Figure 66 - ***Surface and contour Temperature plots (°C) for TAP = 2 W cm^{-2} after 0.7 seconds - focus at x=0, ALL elements activated***

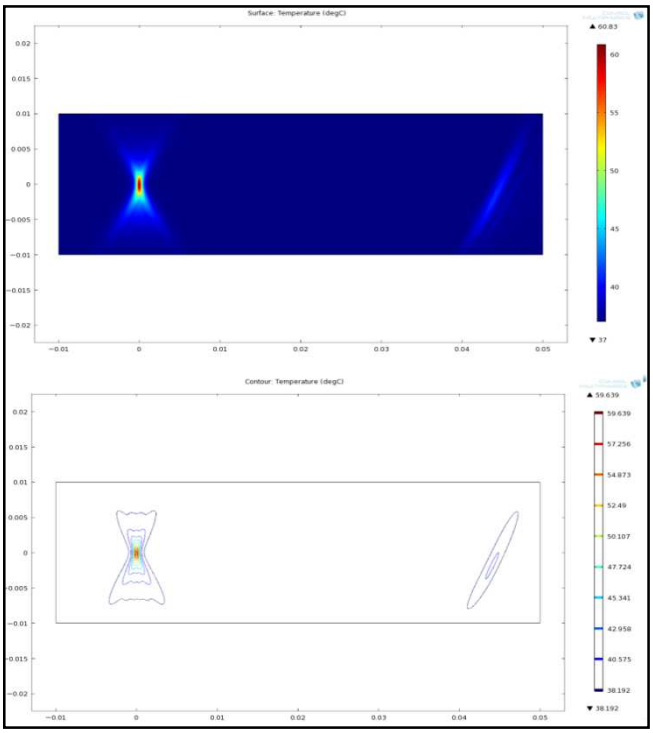

Figure 67 - ***Surface and contour Temperature plots (°C) for TAP = 2 W cm^{-2} after 0.65 seconds - focus at x=0, ALL elements activated (HiDef)***

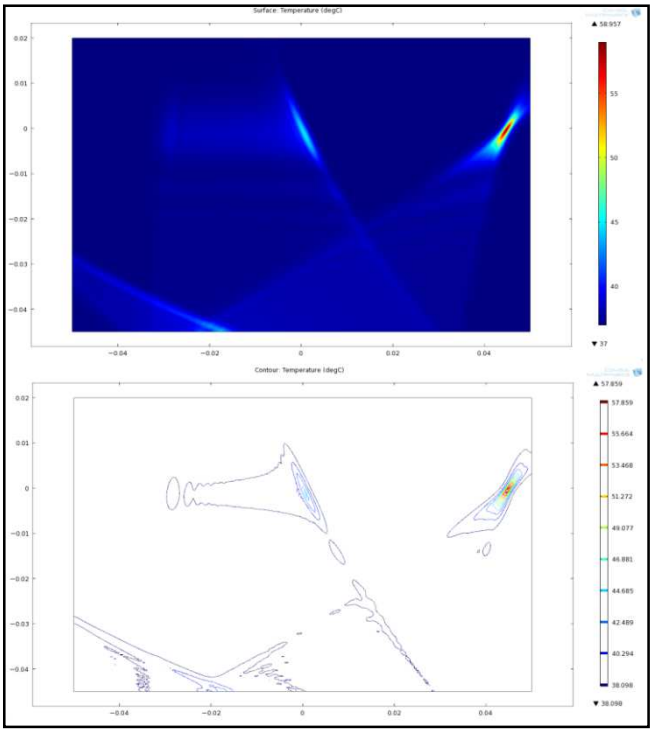

Figure 68 - ***Surface and contour Temperature plots (°C) for TAP = 2 W cm^{-2} after 1.8 seconds - focus at x=45, ALL elements activated***

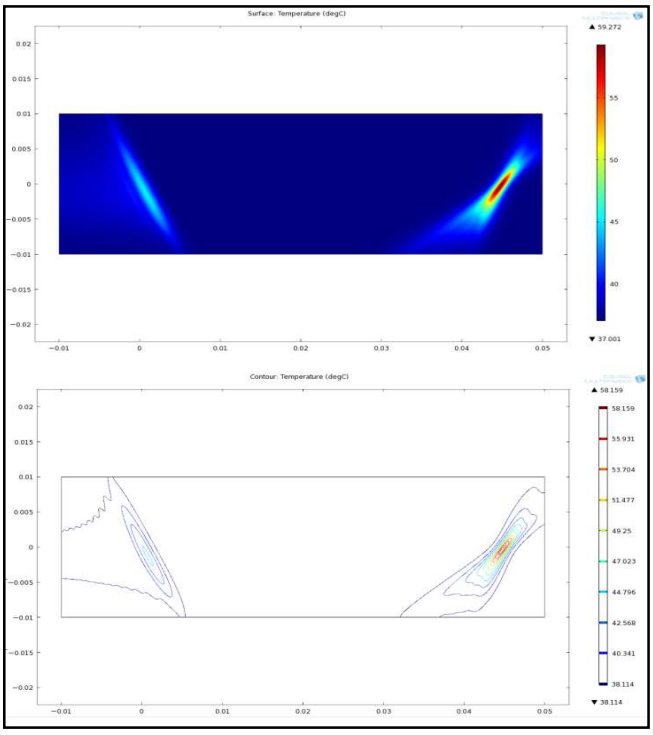

Figure 69 - ***Surface and contour Temperature plots (°C) for TAP = 2 W cm^{-2} after 1.76 seconds - focus at x=45, ALL elements activated (HiDef)***

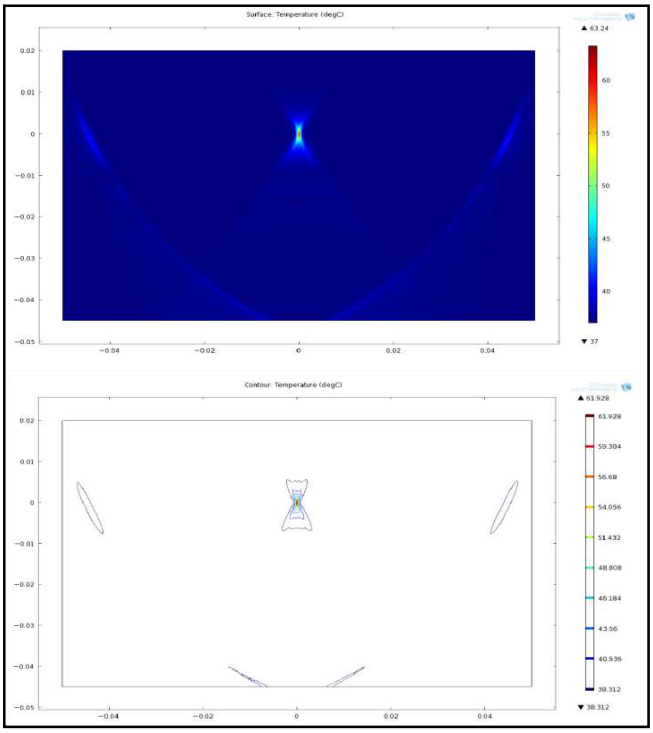

Figure 70 - ***Surface and contour Temperature plots (°C) for TAP = 3 W cm^{-2} after 0.4 seconds - focus at x=0, ALL elements activated***

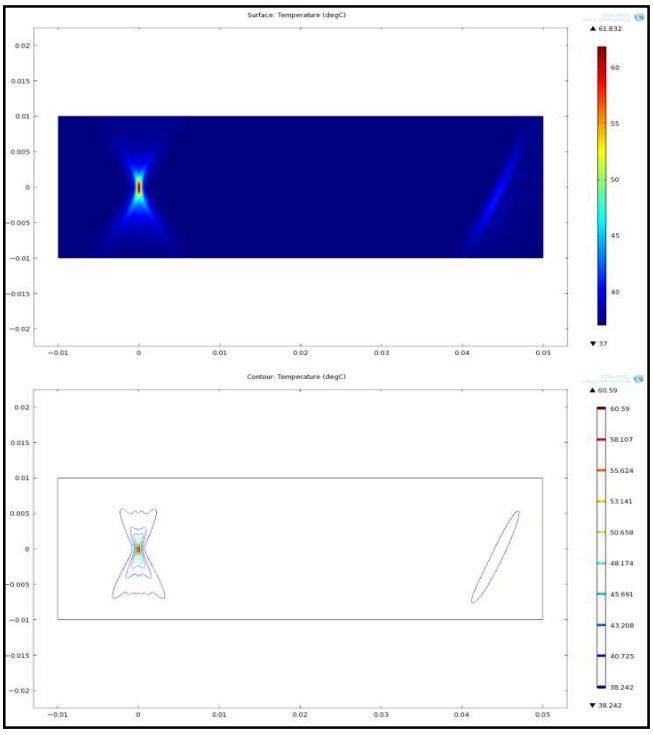

Figure 71 - ***Surface and contour Temperature plots (°C) for TAP = 3 W cm^{-2} after 0.38 seconds - focus at x=0, ALL elements activated (HiDef)***

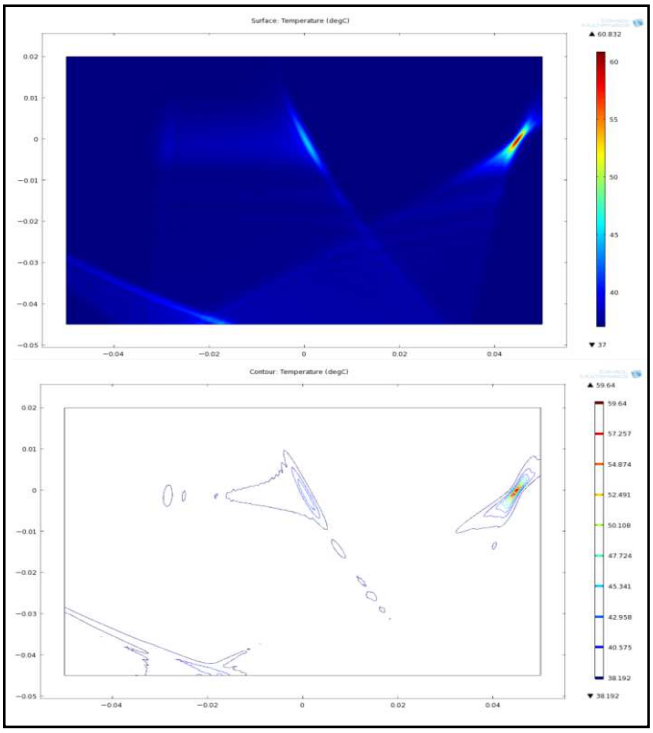

Figure 72 - ***Surface and contour Temperature plots (°C) for TAP = 3 W cm^{-2} after 1.1 seconds - focus at x=45, ALL elements activated***

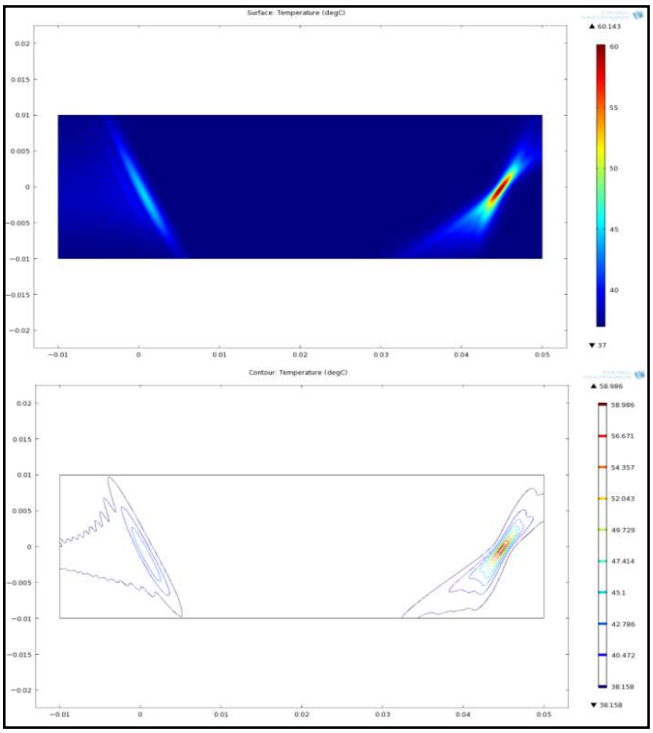

Figure 73 - ***Surface and contour Temperature plots (°C) for TAP = 3 W cm^{-2} after 1.01 seconds - focus at x=45, ALL elements activated (HiDef)***

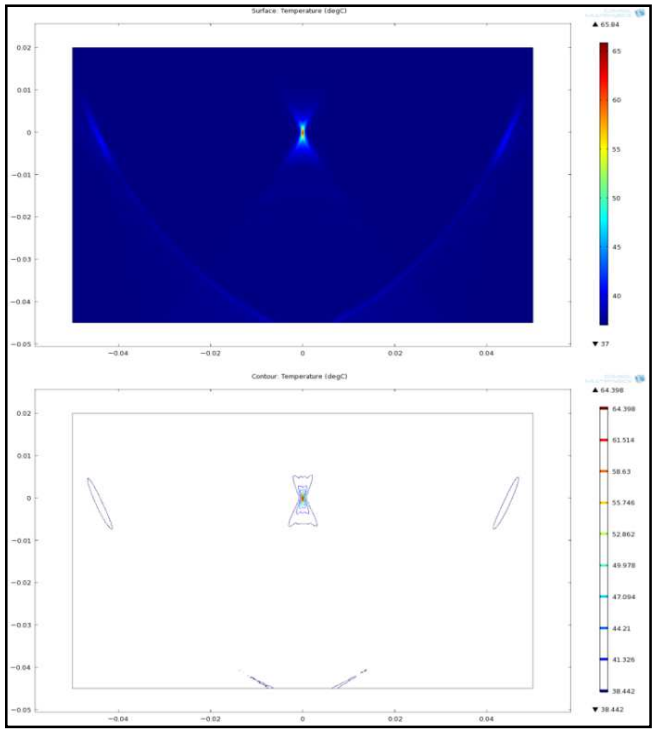

Figure 74 - ***Surface and contour Temperature plots (°C) for TAP = 4 W cm^{-2} after 0.3 seconds - focus at x=0, ALL elements activated***

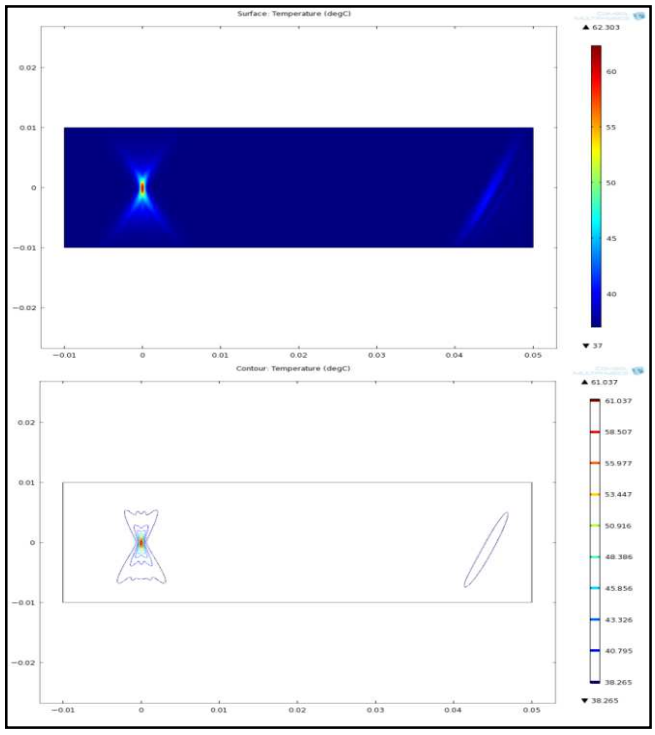

Figure 75 - ***Surface and contour Temperature plots (°C) for TAP = 4 W cm^{-2} after 0.26 seconds - focus at x=0, ALL elements activated (HiDef)***

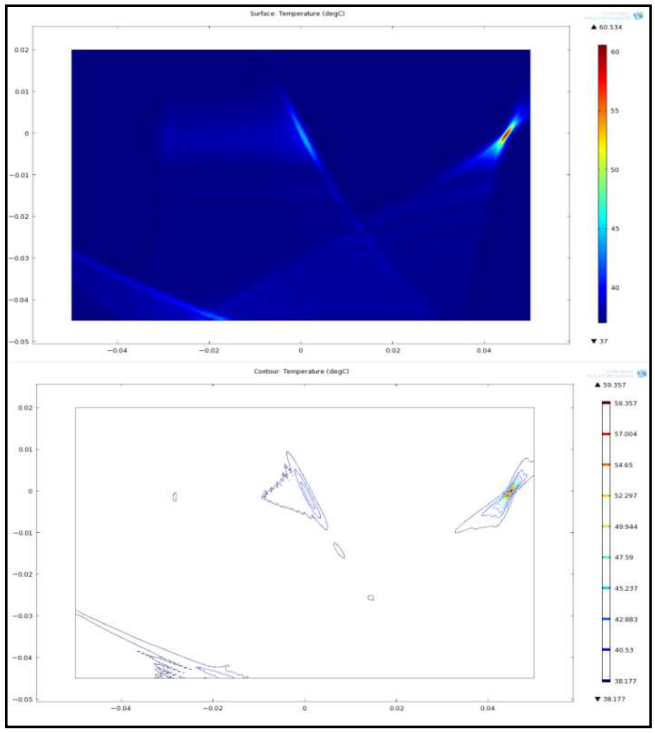

Figure 76 - ***Surface and contour Temperature plots (°C) for TAP = 4 W cm^{-2} after 0.7 seconds - focus at x=45, ALL elements activated***

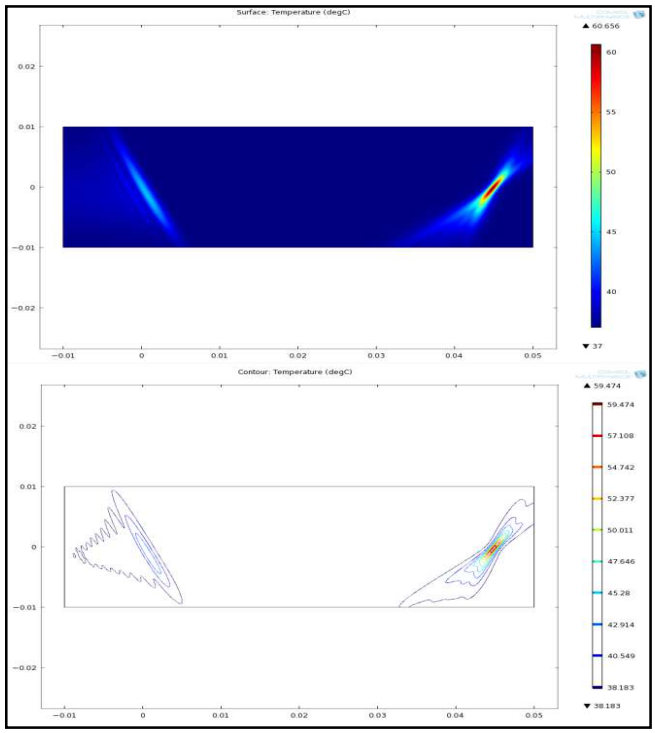

Figure 77 - ***Surface and contour Temperature plots (°C) for TAP = 4 W cm^{-2} after 0.69 seconds - focus at x=45, ALL elements activated (HiDef)***

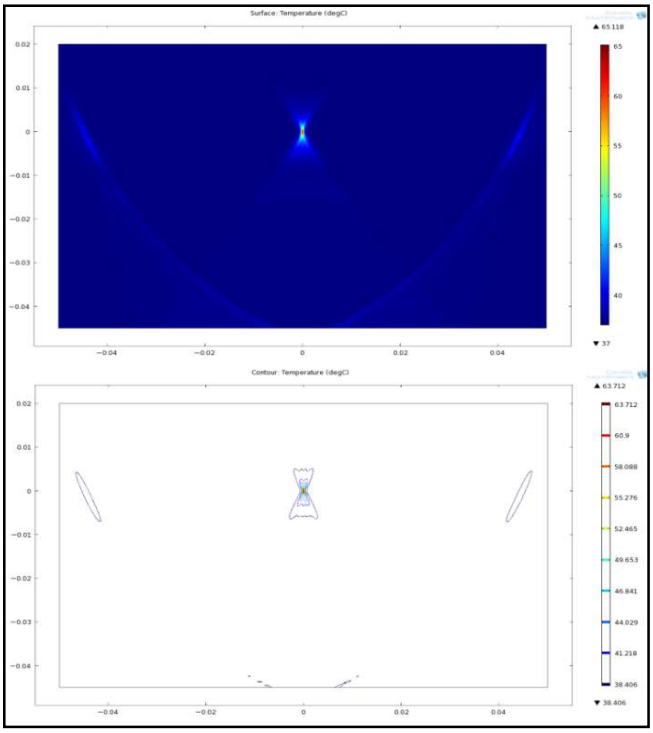

Figure 78 - ***Surface and contour Temperature plots (°C) for TAP = 5 W cm^{-2} after 0.21 seconds - focus at x=0, ALL elements activated***

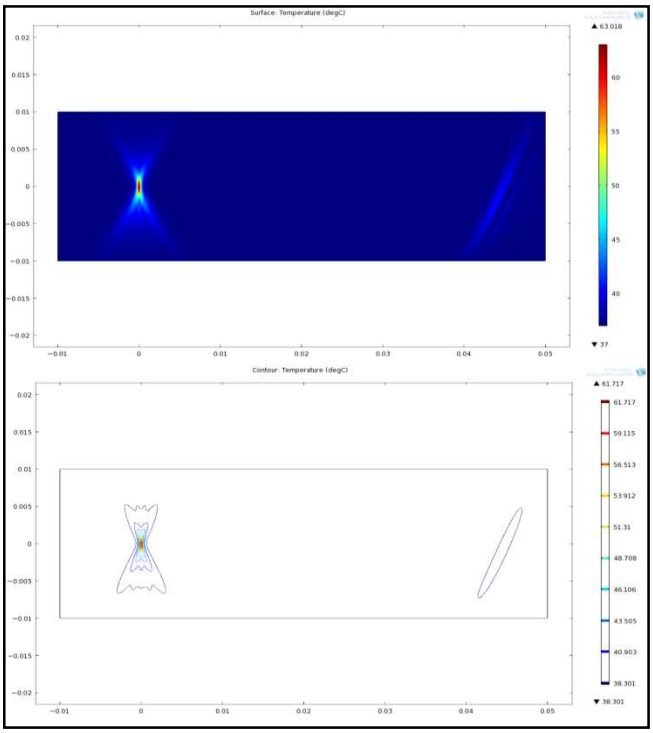

Figure 79 - ***Surface and contour Temperature plots (°C) for TAP = 5 W cm^{-2} after 0.2 seconds - focus at x=0, ALL elements activated (HiDef)***

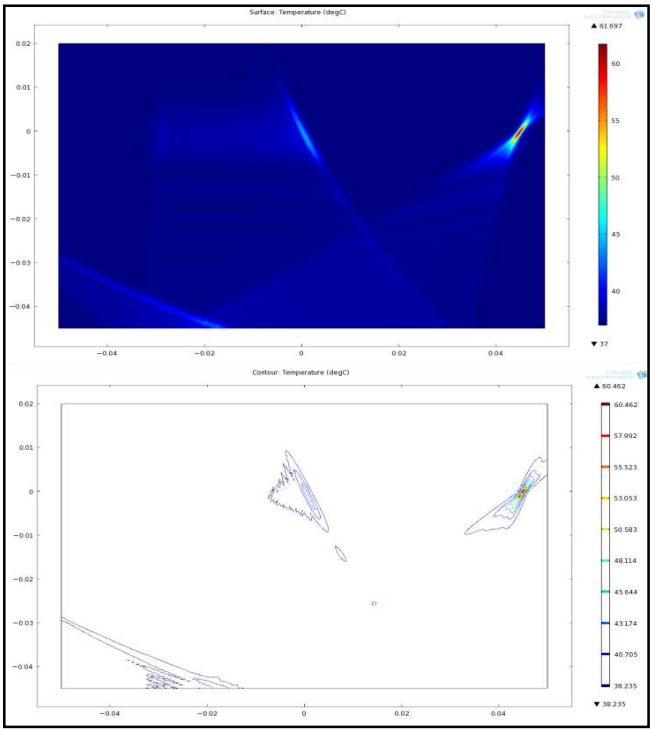

Figure 80 - ***Surface and contour Temperature plots (°C) for TAP = 5 W cm^{-2} after 0.55 seconds - focus at x=45, ALL elements activated***

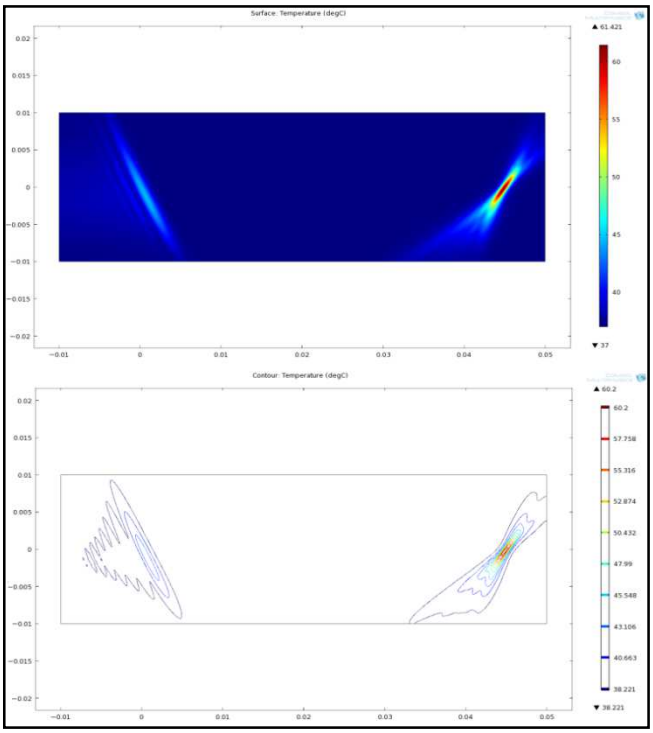

Figure 81 - ***Surface and contour Temperature plots (°C) for TAP = 5 W cm^{-2} after 0.53 seconds - focus at x=45, ALL elements activated (HiDef)***

Focus x=0:

Table 17 - ***Exposure time vs. TAP, results for the case of ALL elements being active, with a focus of x=0 mm*** **(Figure 62** ***to*** **Figure 79,** ***see legend(s) for relevant plots)***

TAP ($W\ cm^{-2}$)	Time (s)	Focal temp (°C)	Focal TD (mins)	Lobe temp (°C)	Lobe TD (mins)
1	1	51.89	2.33	39.35	<0.0001
	1.75	58.07	248.66	40.33	0.0006
	2	59.83	935.12	40.61	0.0012
2	0.65	59.64	270.13	40.58	0.0001
	1	66.82	60279	41.71	0.0015
	2	82.64	$7.82x10^{9}$	44.21	0.0713
3	0.38	60.59	313.15	38.24	<0.0001
	1	81.70	$1.86x10^{9}$	44.06	0.0153
	2	105.45	$8.47x10^{16}$	47.81	1.3905
4	0.26	61.04	305.36	38.27	<0.0001
	1	96.59	$7.08x10^{13}$	46.41	0.0872
	2	128.27	$1.09x10^{24}$	51.41	33.2131
5	0.2	61.72	333.25	40.42	<0.0001
	1	111.48	$3.13x10^{18}$	50.95	0.6957
	2	143.57	$1.9586x10^{30}$	61.09	847.4314

Focus x=45:

Table 18 - ***Exposure time vs. TAP, results for the case of ALL elements being active, with an 'extreme' focus of x=45 mm*** **(Figure 64** ***to*** **Figure 81,** ***see legend(s) for relevant plots)***

TAP (W cm^{-2})	Time (s)	Focal temp (°C)	Focal TD (mins)	Lobe temp (°C)	Lobe TD (mins)
1	1	44.42	0.02	38.95	<0.0001
	2	48.47	0.76	41.22	0.0011
	3	51.84	6.43	42.47	0.0107
	4	54.70	54.75	44.22	0.0473
	4.77	56.67	243.15	45.46	0.1086
2	1	51.51	1.659	42.83	0.0012
	1.76	58.16	247.17	44.80	0.0284
	2	59.97	942.22	45.46	0.0515
3	1	58.84	235.76	43.77	0.0189
	1.01	58.99	262.45	44.00	0.0194
	2	71.45	2.73×10^{6}	49.69	1.0978
4	0.69	59.47	246.37	42.91	0.0064
	1	66.08	31406	44.65	0.0527
	2	82.92	8.48×10^{9}	53.92	15.0070
5	0.53	60.20	286.31	43.11	0.0045
	1	73.33	5.02×10^{6}	46.56	0.2572
	2	94.40	2.98×10^{13}	58.15	2.04×10^{9}

Generally with *all* elements being activated it can be observed that a focus of x=0 mm (see Table 17 & Figure 82) allows the threshold thermal dose to be reached much more rapidly than in the case of an 'extreme' focus at x=45 mm (see Table 18 & Figure 82) even at low powers (approximately 2 seconds at TAP 1 W cm^{-2} and less than 1 second at 2 W cm^{-2} and above). Also the grating lobes are much reduced when focusing on the geometric centre at x=0 mm. Hence the treatment plan, once formulated, will have to take into account this discrepancy and adjust exposure times accordingly such that all of the focal points within the target volume will receive the same thermal dose, taking into account the beam steering angle.

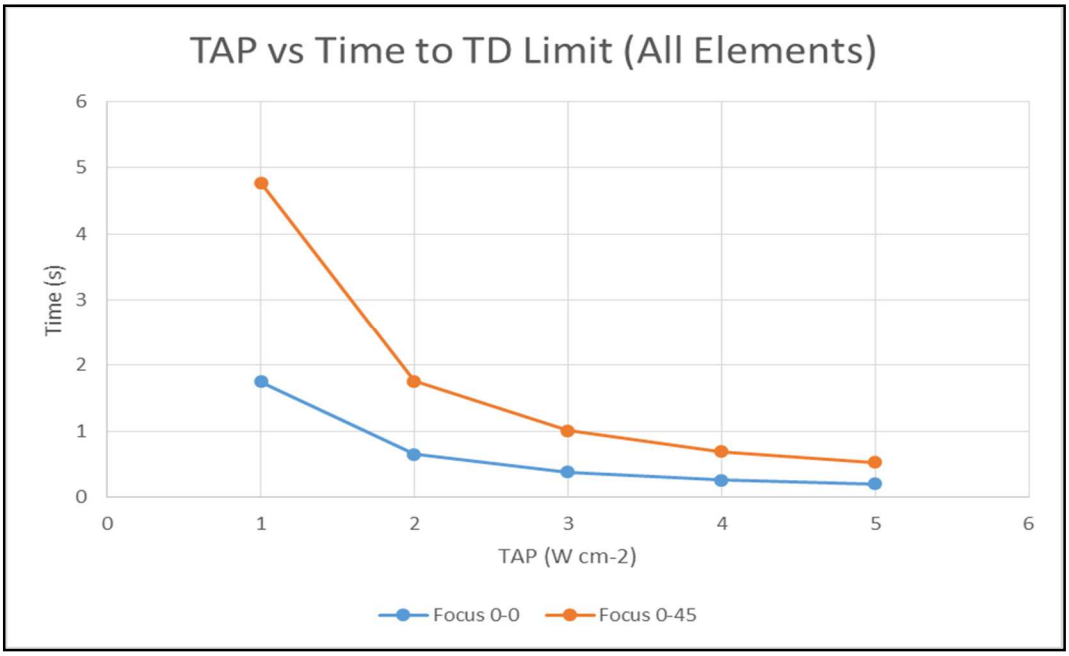

Figure 82 - ***Graph of TAP against time taken to reach the TD threshold limit at the focal point (ALL elements activated)***

In all cases presented the maximum thermal dose in *non-focal* areas was observed to be less than 0.11 equivalent minutes (See Figure 83, Table 17 & Table 18) with a maximum lobe temperature of less than 45 °C at the time at which the *focal* thermal dose threshold of 240 equivalent minutes was exceeded. Please note the corresponding graph for the 'natural' focus (x=0 mm) has been omitted as values were low enough to be considered insignificant.

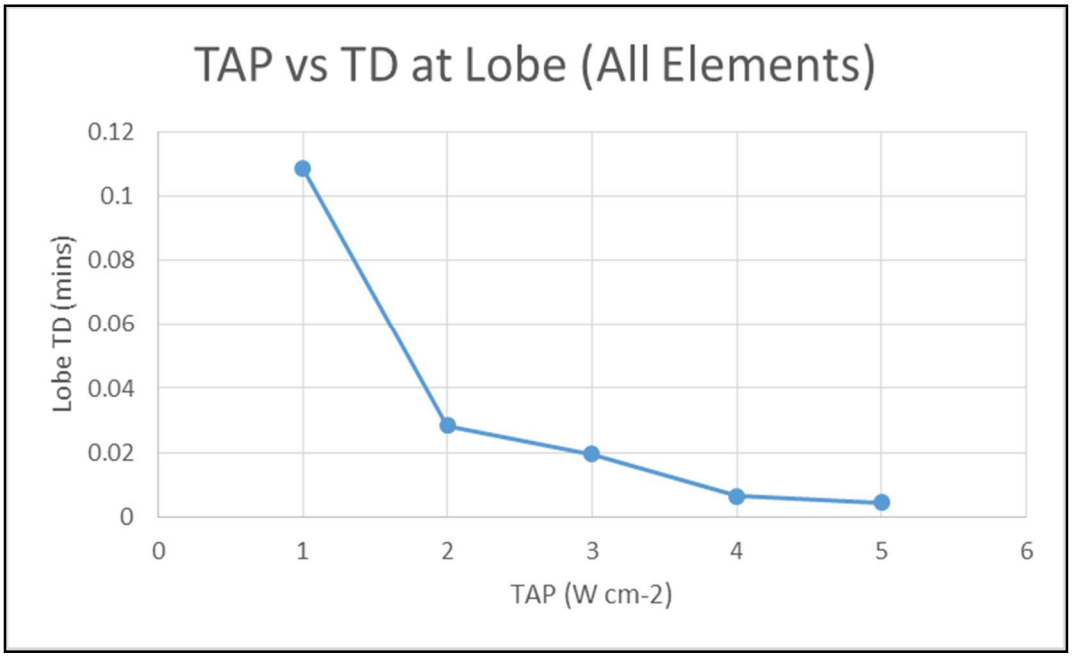

Figure 83 - ***TAP against TD at the grating lobe for the case of the extreme focus at x=45 mm (ALL elements activated)***

In the case of the 'extreme' focus of x=45 mm it can be seen there is a sharp rise in the equivalent thermal dose in certain cases, as can be seen when looking at the 1 and 2 second TD values for 3, 4 and 5 W/cm^2 (TAP). This is not a major concern as the sonications will be halted before these times, as the thermal dose at the focus will have already been reached. However this effect will be more important for the case of *half* elements being activated as expected exposure times would be longer and therefore it is more probable that non-focal TD levels may rise. This will be relevant when defining *maximum* exposure times. The results above, for *all* elements have been included to allow a meaningful comparison to the case of *half* elements and also to give an impression of how the transducer performance differs when *all* elements are activated and targeted on a single focal point.

6.3.1.2: Half Elements

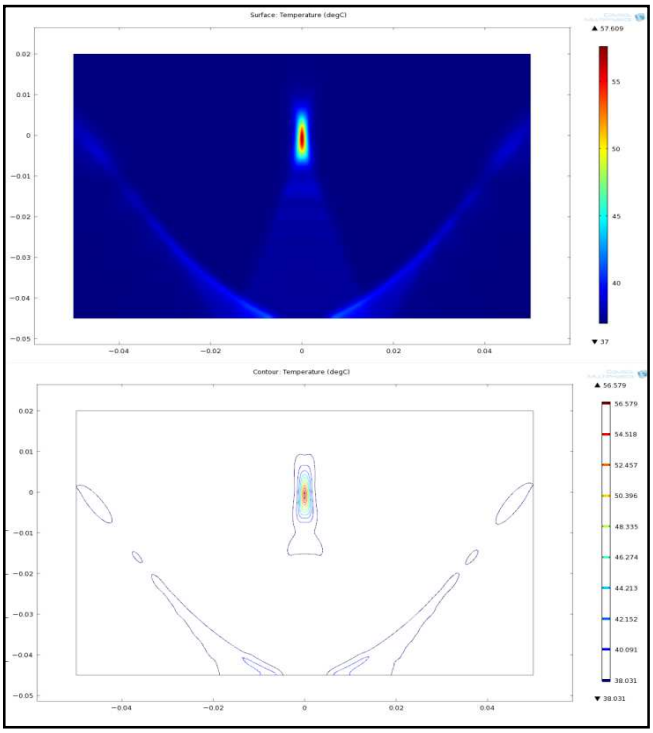

Figure 84 - ***Surface and contour Temperature plots (°C) for TAP = 1 W cm^{-2} after 4.7 seconds - focus at x=0, HALF elements activated***

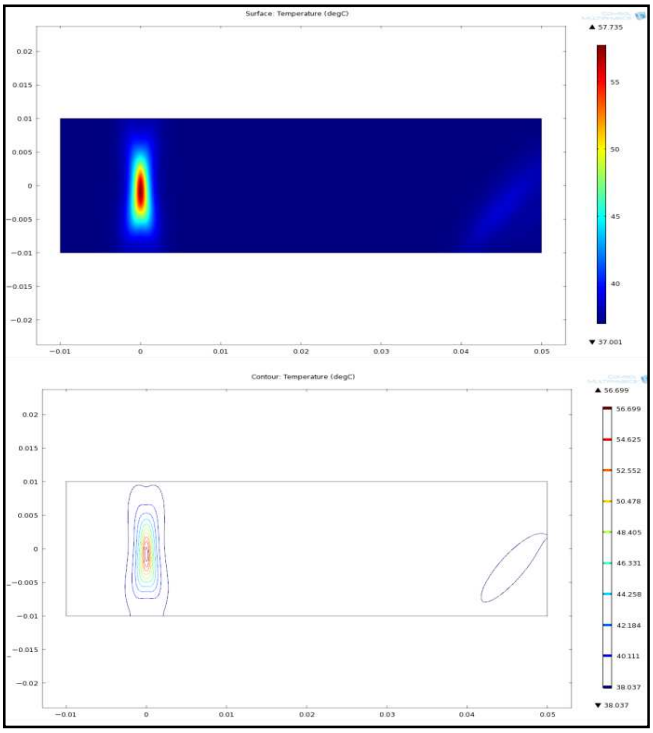

Figure 85 - ***Surface and contour Temperature plots (°C) for TAP = 1 W cm^{-2} after 4.77 seconds - focus at x=0, HALF elements activated (HiDef)***

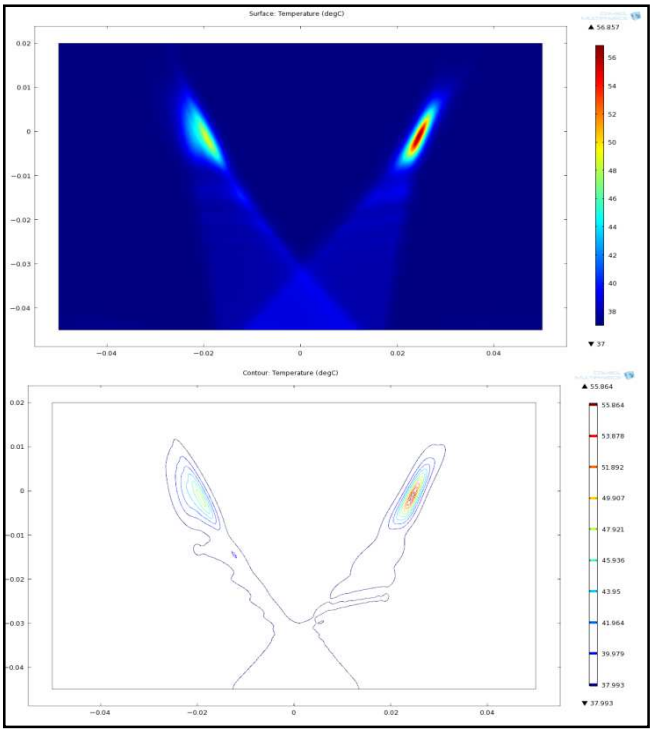

Figure 86 - ***Surface and contour Temperature plots (°C) for TAP = 1 W cm^{-2} after 7.1 seconds - focus at x=25, HALF elements activated***

[Note – The 'HiDef' simulation here failed due to hardware limitations of the PC used]

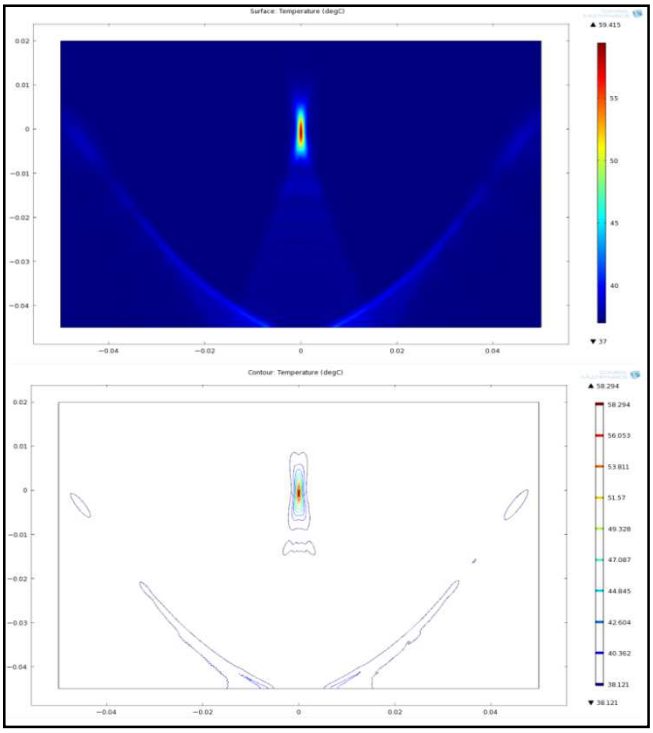

Figure 87 - ***Surface and contour Temperature plots (°C) for TAP = 2 W cm^{-2} after 1.8 seconds - focus at x=0, HALF elements activated***

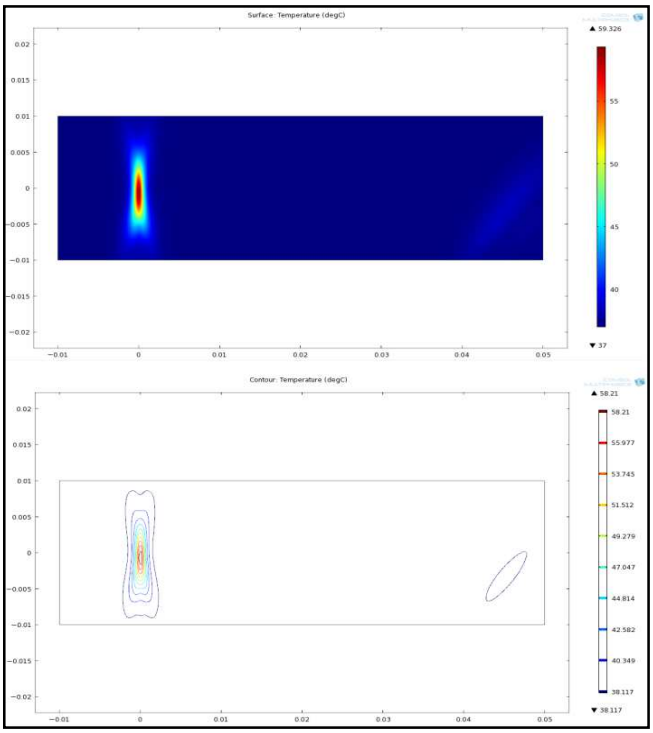

Figure 88 - ***Surface and contour Temperature plots (°C) for TAP = 2 W cm^{-2} after 1.8 seconds - focus at x=0, HALF elements activated (HiDef)***

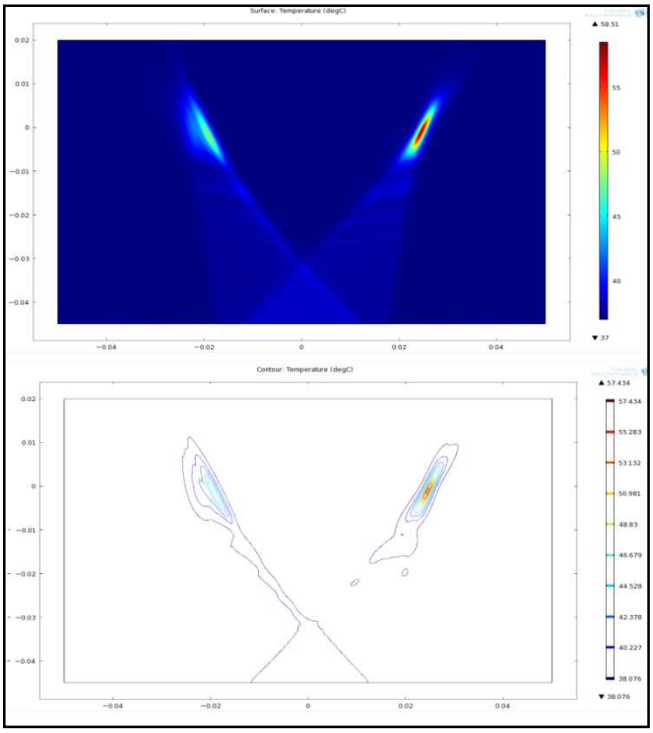

Figure 89 - ***Surface and contour Temperature plots (°C) for TAP = 2 W cm^{-2} after 2.7 seconds - focus at x=25, HALF elements activated***

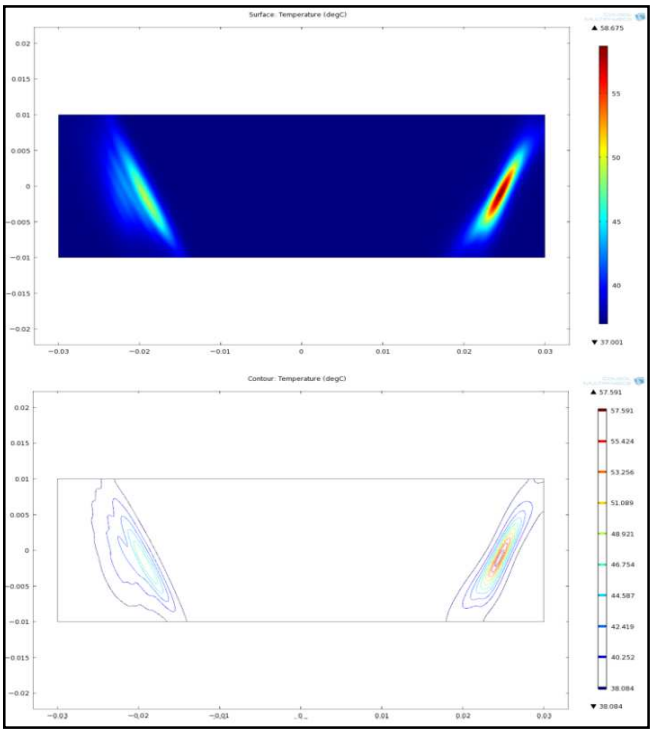

Figure 90 - ***Surface and contour Temperature plots (°C) for TAP = 2 W cm^{-2} after 2.73 seconds - focus at x=25, HALF elements activated (HiDef)***

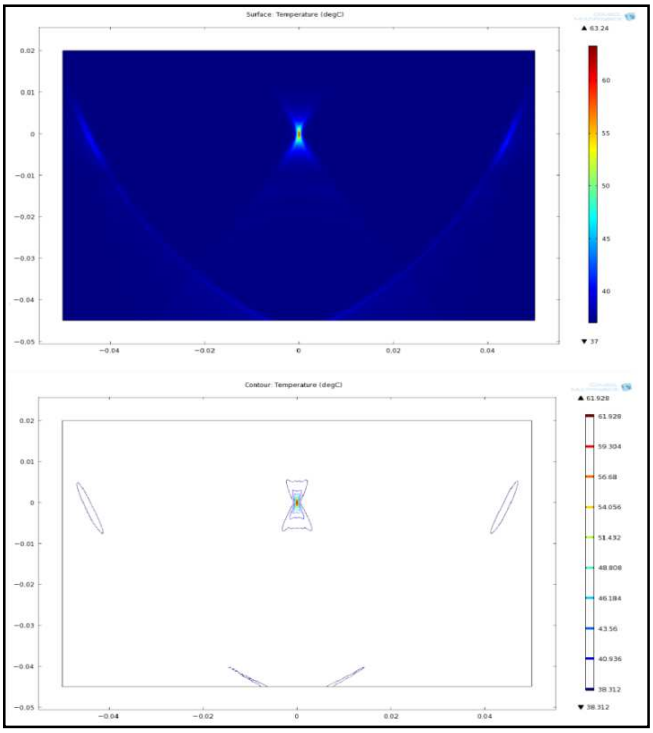

Figure 91 - ***Surface and contour Temperature plots (°C) for TAP = 3 W cm^{-2} after 1.1 seconds - focus at x=0, HALF elements activated***

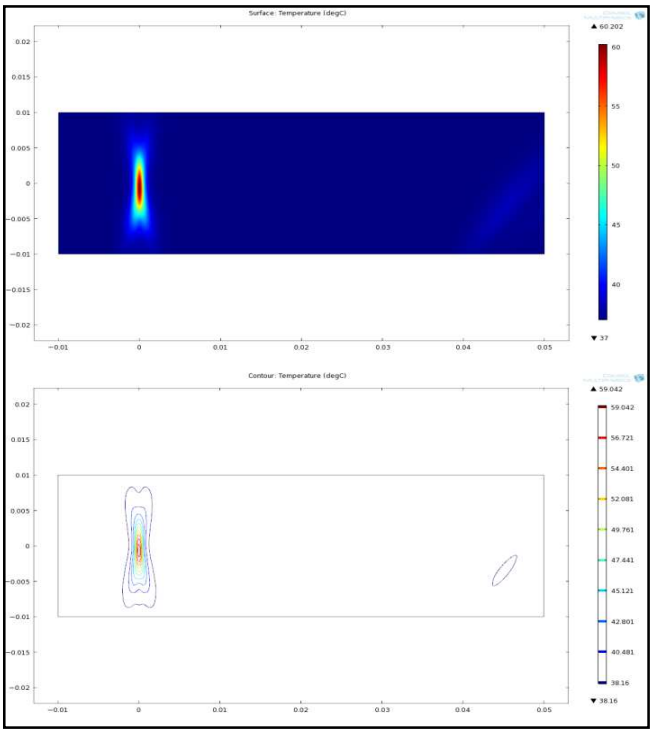

Figure 92 - ***Surface and contour Temperature plots (°C) for TAP = 3 W cm^{-2} after 1.05 seconds - focus at x=0, HALF elements activated (HiDef)***

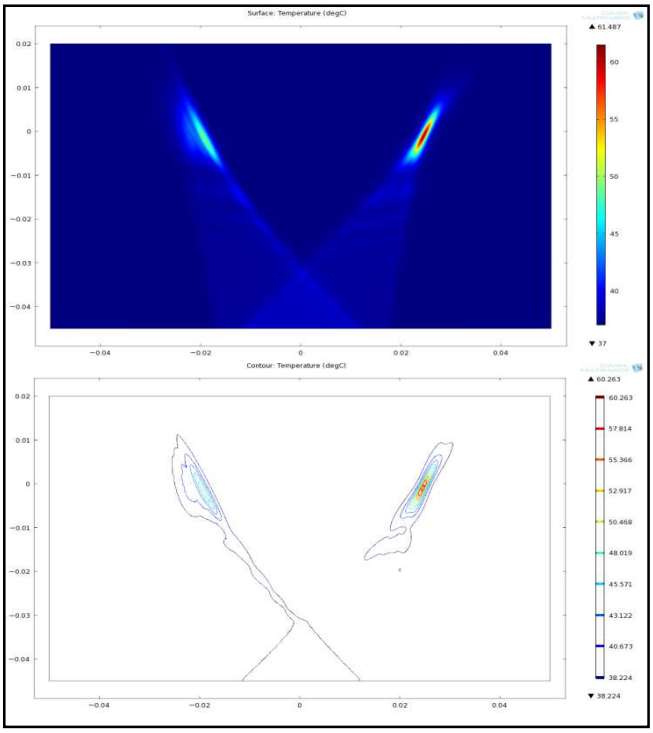

Figure 93 - ***Surface and contour Temperature plots (°C) for TAP = 3 W cm^{-2} after 1.6 seconds - focus at x=25, HALF elements activated***

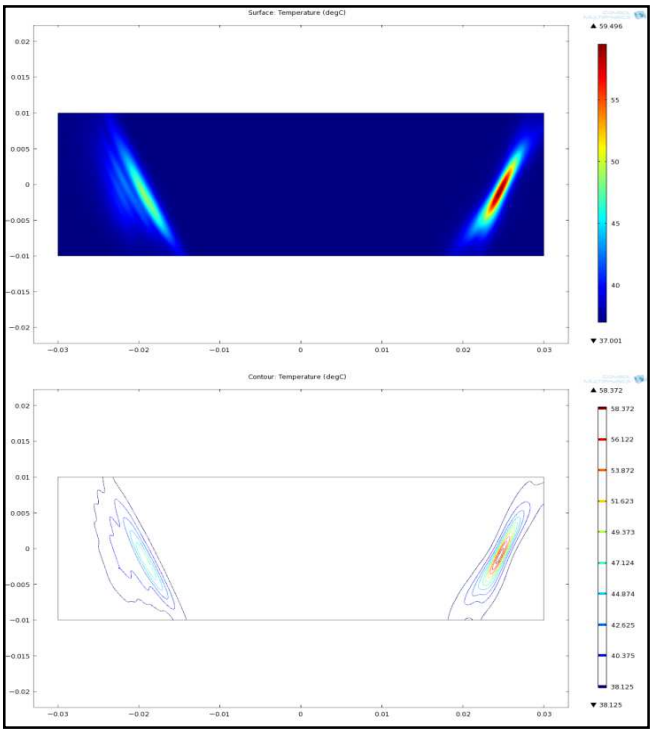

Figure 94 - ***Surface and contour Temperature plots (°C) for TAP = 3 W cm^{-2} after 1.59 seconds - focus at x=25, HALF elements activated (HiDef)***

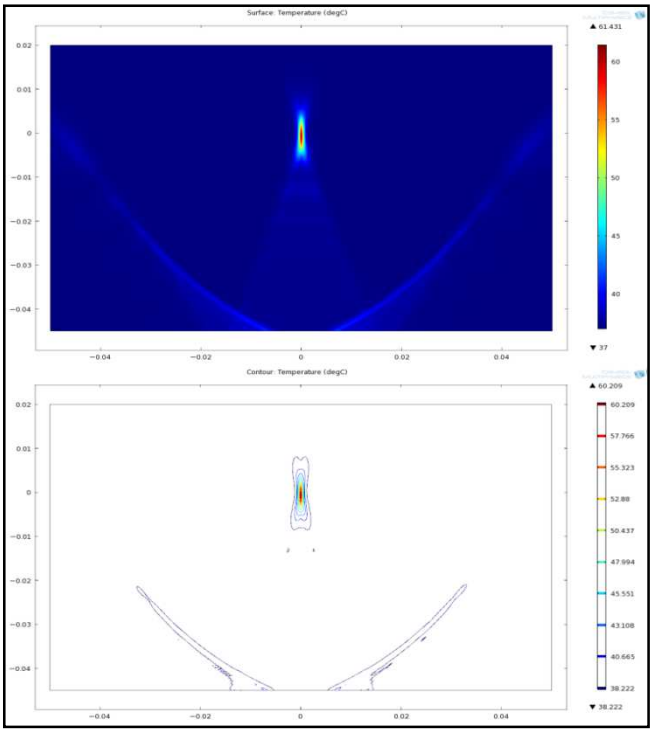

Figure 95 - ***Surface and contour Temperature plots (°C) for TAP = 4 W cm^{-2} after 0.75 seconds - focus at x=0, HALF elements activated***

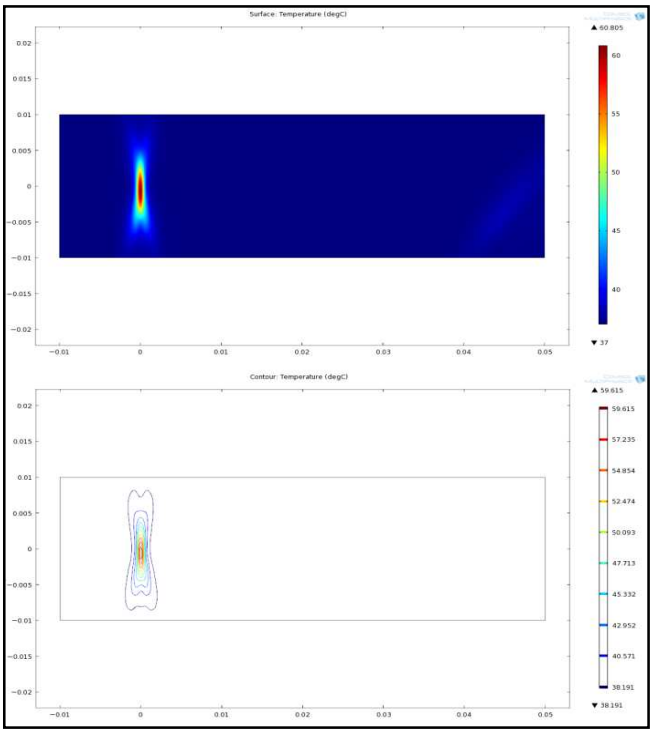

Figure 96 - ***Surface and contour Temperature plots (°C) for TAP = 4 W cm^{-2} after 0.73 seconds - focus at x=0, HALF elements activated (HiDef)***

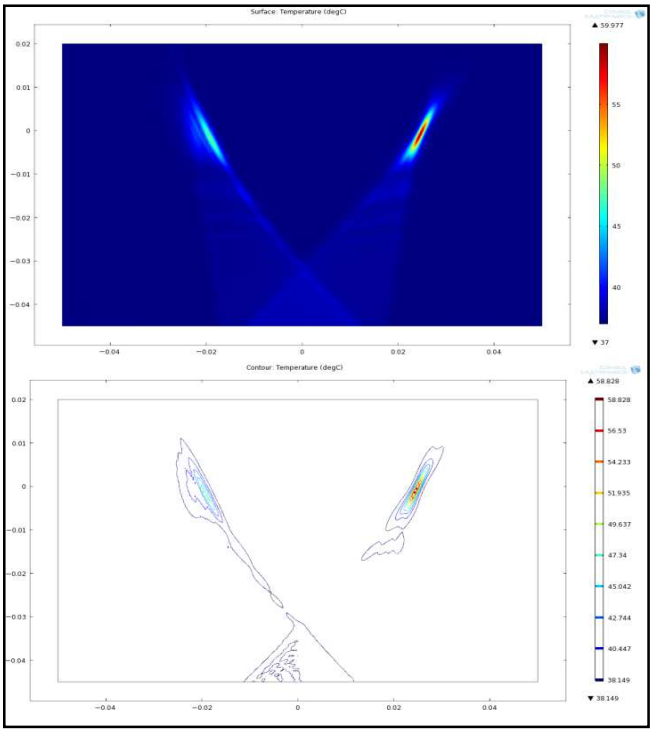

Figure 97 - ***Surface and contour Temperature plots (°C) for TAP = 4 W cm^{-2} after 1.1 seconds - focus at x=25, HALF elements activated***

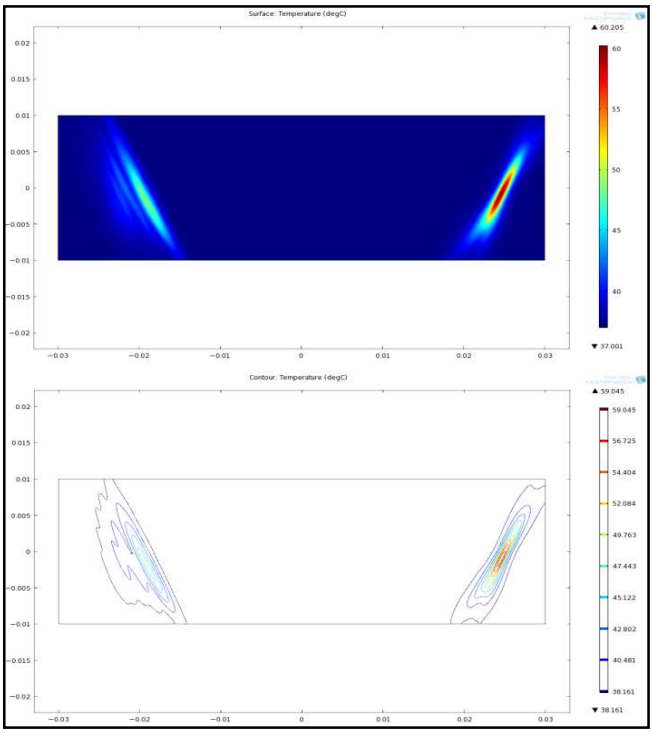

Figure 98 - ***Surface and contour Temperature plots (°C) for TAP = 4 W cm^{-2} after 1.11 seconds - focus at x=25, HALF elements activated (HiDef)***

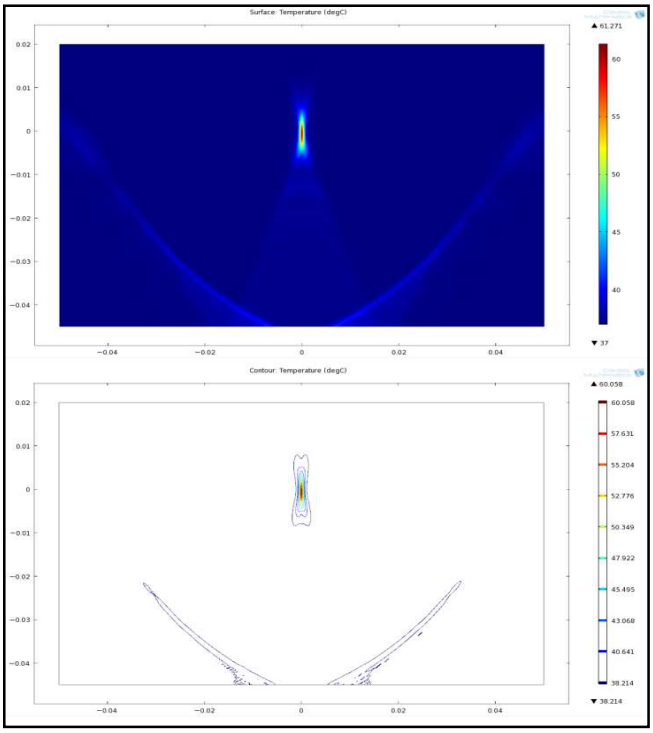

Figure 99 - ***Surface and contour Temperature plots (°C) for TAP = 5 W cm^{-2} after 0.55 seconds - focus at x=0, HALF elements activated***

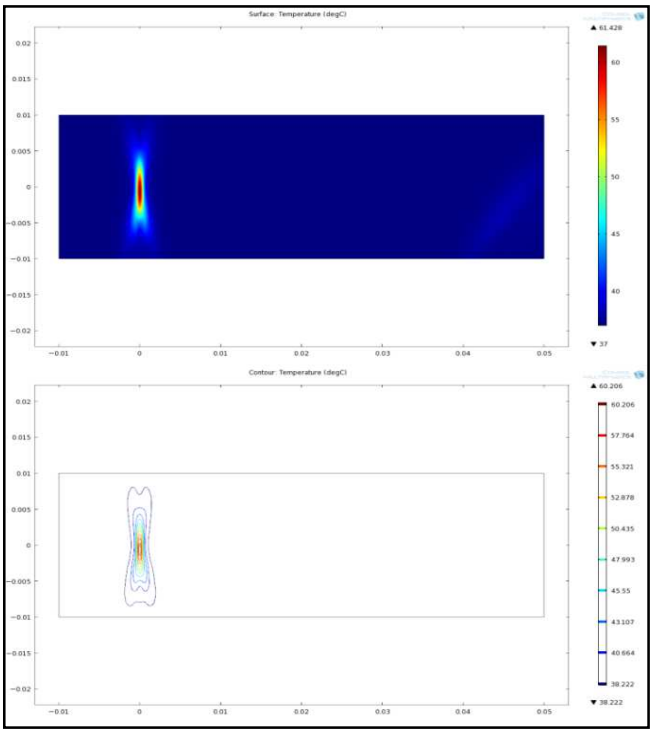

Figure 100 - ***Surface and contour Temperature plots (°C) for TAP = 5 W cm^{-2} after 0.56 seconds - focus at x=0, HALF elements activated***

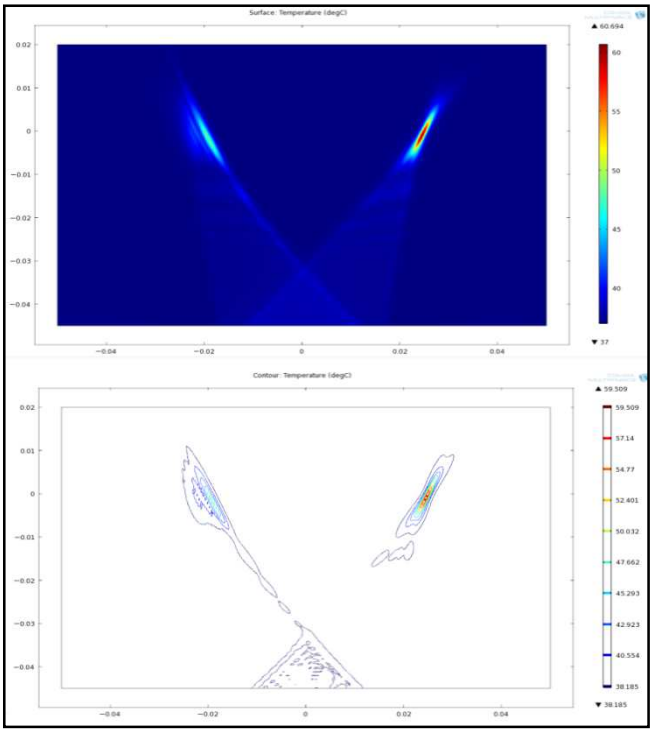

Figure 101 - ***Surface and contour Temperature plots (°C) for TAP = 5 W cm^{-2} after 0.85 seconds - focus at x=25, HALF elements activated***

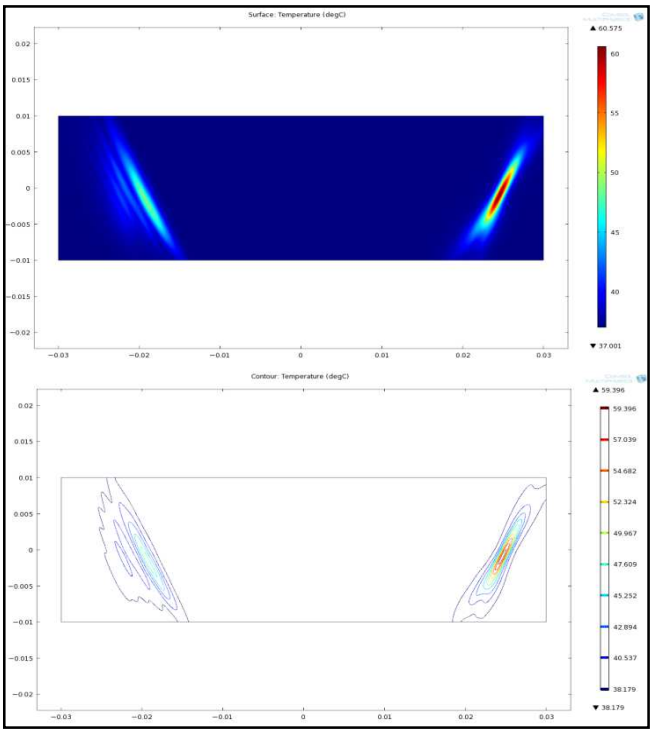

Figure 102 - ***Surface and contour Temperature plots (°C) for TAP = 5 W cm^{-2} after 0.84 seconds - focus at x=25, HALF elements activated (HiDef)***

Focus x=0:

Table 19 - ***Exposure time vs. TAP, results for the case of HALF elements being active, with a focus of x=0 mm (*****Figure 84, Figure 85 & Figure 87** ***to*** **Figure 100,** ***see legend(s) for relevant plots)***

TAP (W cm^{-2})	Time (s)	Focal temp (°C)	Focal TD (mins)	Lobe temp (°C)	Lobe TD (mins)
1	1	44.23	0.01	37.38	<0.0001
	2	48.36	0.40	37.60	<0.0001
	3	51.79	6.13	37.78	<0.0001
	4	54.70	53.81	37.93	<0.0001
	4.77	56.70	243.46	38.07	<0.0001
2	1	51.11	1.20	37.74	<0.0001
	1.8	58.21	246.59	38.12	<0.0001
	2	59.74	770.45	38.20	<0.0001
3	1	58.30	150.87	38.12	<0.0001
	1.05	59.04	254.76	38.16	<0.0001
	2	71.12	2.17×10^{6}	38.80	<0.0001
4	0.73	59.62	263.67	38.19	<0.0001
	1	65.36	19431	38.49	<0.0001
	2	82.49	6.15×10^{9}	39.40	0.0002
5	0.56	60.21	306.73	38.22	<0.0001
	1	72.45	2.67×10^{6}	38.87	<0.0001
	2	93.86	1.93×10^{13}	39.99	0.0003

Focus x=25:

Table 20 - ***Exposure time vs. TAP, results for the case of HALF elements being active, with an 'extreme' focus of x=25 mm (*****Figure 86 & Figure 89 to Figure 102,*** ***see legend(s) for relevant plots)***

TAP (W/cm^{-2})	Time (s)	Focal temp (°C)	TD (mins)	Lobe temp (°C)	TD (mins)
1	2	45.52	0.10	41.03	0.0020
	4	50.29	3.80	44.69	0.0485
	6	54.034	60.33	46.87	0.4706
	7	55.70	213.11	47.83	1.2004
	7.1	55.86	242.01	47.92	1.3494
2	1	47.20	0.07	41.83	0.0030
	2	53.70	12.00	44.91	0.0714
	2.73	57.59	241.62	46.75	0.4355
3	1	52.30	2.60	44.25	0.0227
	1.59	58.37	245.93	48.11	0.3203
	2	62.05	3833.40	50.28	1.4466
4	1	57.42	79.68	46.68	0.1072
	1.11	59.05	259.79	47.44	0.2173
	2	70.40	$1.23x10^{6}$	52.82	23.1510
5	0.84	59.40	247.24	47.61	0.1672
	1	62.51	2474.60	49.08	0.5986
	2	78.73	$4.22x10^{8}$	56.77	471.1324

As with the case in which all elements are excited (see Section 6.3.1.1) simulations were performed to allow a more accurate thermal dose pattern to be observed, In this case only *half* the total elements were excited. The tables presented (see Table 19 & Table 20) show the results of these tests, performed to further define the time at which each power level causes the thermal dose to exceed the threshold of 240 equivalent minutes. As with the case of all elements being excited, the central focus at x=0 mm allows the target thermal dose to be achieved more quickly and with lower lobe temperatures than the 'extreme focus at x=25 mm (see Figure 103). Additionally it can

again be seen grating lobe levels are reduced when the focus is central, at x=0 mm (see Table 19 & Table 20).

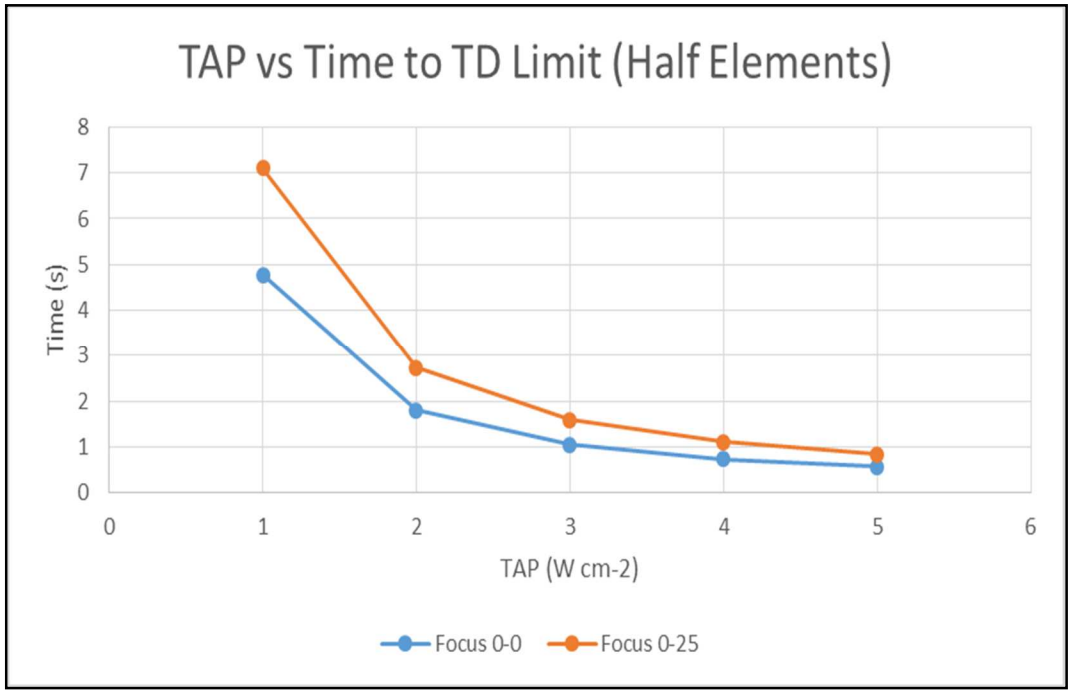

Figure 103 - ***Graph of TAP against time taken to reach the TD threshold limit at the focal point (HALF elements activated)***

In all cases the thermal dose in *non-focal* areas was observed to be less than 1.35 equivalent minutes (see Figure 104, Table 19 & Table 20) with a corresponding maximum lobe temperature of 47.9 °C at the time at which the *focal* thermal dose threshold of 240 equivalent minutes was exceeded. As previously the corresponding graph for the 'natural' focus (x=0 mm) has been omitted as values were low enough to be considered insignificant.

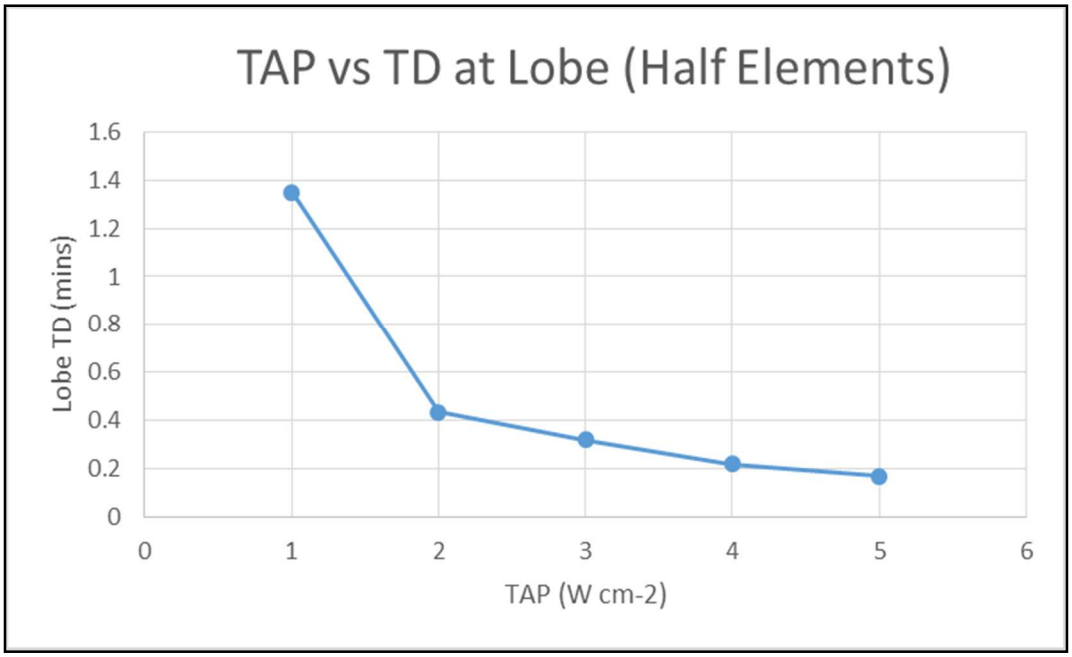

Figure 104 - ***TAP against TD at the grating lobe for the case of the extreme focus at x=25 mm (HALF elements activated)***

From the results of both cases (all and half elements being activated) it can be said that even though TD values were marginally higher, using half the elements of the array would be feasible and would allow the focal thermal dose threshold to be exceeded while avoiding permanent damage to the surrounding tissue. Even though the TD deposited at the non-focal grating lobe decreases with increasing TAP (see Figure 104) the values are low enough that the actual TAP used seems significant only in determining the total sonication time, with higher values allowing shorter sonication periods to be used. The exposure time in this regard will be investigated in the following section (see Section 6.3.1.3). Having said this it would be preferable to use a TAP of 2 W cm-1 or higher to reduce the lobe TD by a factor of three (see Figure 104 & Table 20)

6.3.1.3: TAP vs. Exposure Time Specification

From the simulation results presented previously (see Section 6.3.1.2) the following information has been officially added to the technical specification for the transducer to be manufactured by Imasonic (see Table 21). These times are based on the maximum times necessary when activating only *half* the total elements and focusing at the 'extreme' focus (x=25 mm for *half* elements) hence they represent the *absolute maximum* necessary sonication/exposure times of any case.

It should be noted here that actual exposure times will likely be much smaller (for example when activating all elements or focusing at a distance of less than 45 mm from the centre of the transducer) which will have no adverse effects on the transducer as the ON time will be reduced, while the OFF time will remain as shown (see Table 21) to allow extra cooling time, therefore decreasing the probability of damage to the device.

Table 21 - ***Table showing allowable continuous transducer activation time periods, as suggested by manufacturer IMASONIC***

TAP at transducer (W cm^{-2})	ON time (s)	OFF time (s)
1	7.3	2
2	2.9	2
3	1.7	2
4	1.2	5
5	0.9	5

The above OFF times (see Table 21) should not interfere with any treatment plan used as during the scanning phase (between HIFU sonications) the plate in which the HIFU and possible diagnostic transducers are held has to rotate to scan the target volume. This process will take approximately 5 seconds and so could interleave with the HIFU treatment times for each sonication period, as shown above.

6.3.2: Steering Simulations

In the following simulations the effect of steering angle on exposure time (to reach 240 equivalent minutes thermal dosage) will be investigated. A mid-range TAP value of 3 W cm^{-2} will be used, and the focus will be varied from x=0 mm to x=45 mm (for *all* elements, see Figure 105 to Figure 122) and x=0 mm to x=25 mm (for *half* elements, see Figure 125 to Figure 138) in steps of 10 mm, and once at the edge of the length of the transducer array. As previously, plots will be given for the point at which thermal dose at the focus exceeds 240 equivalent minutes.

6.3.2.1: All Elements

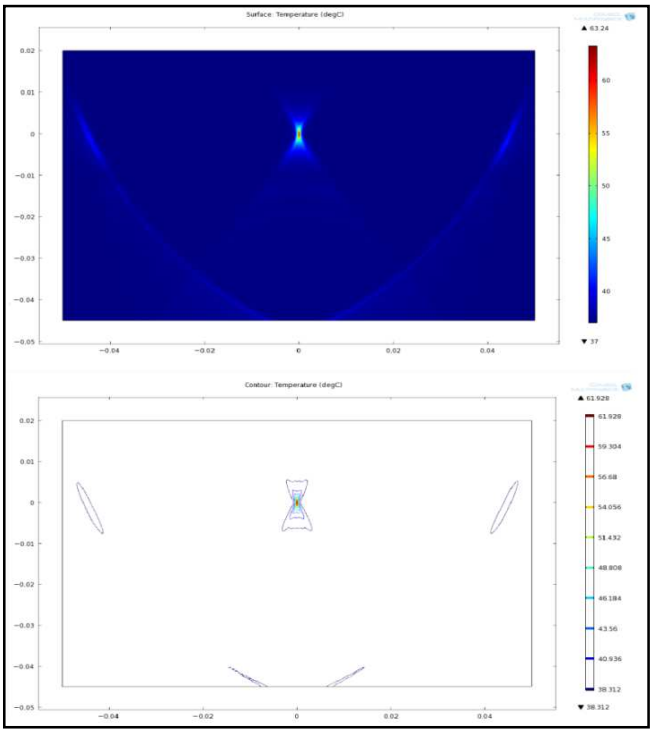

Figure 105 - ***Surface and contour Temperature plots (°C) for TAP = 3 W cm^{-2} after 0.4 seconds - focus at x=0, ALL elements activated***

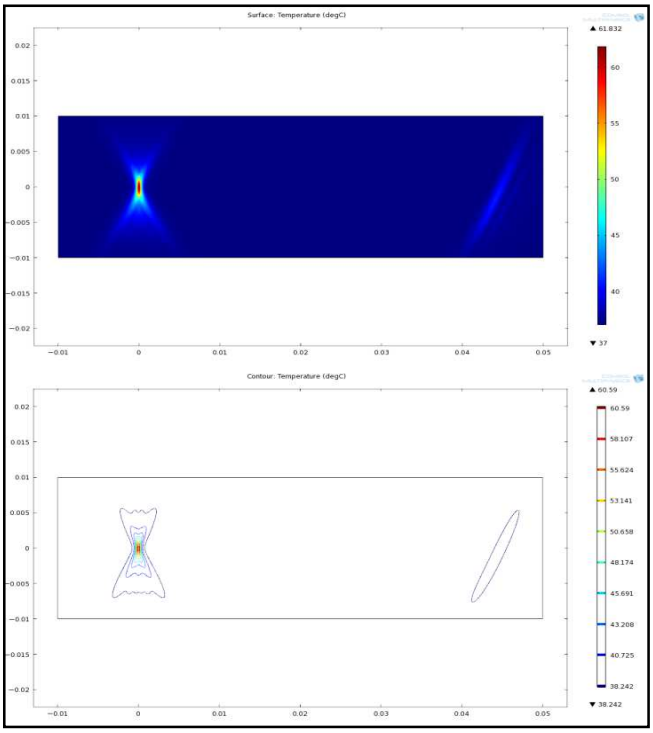

Figure 106 - ***Surface and contour Temperature plots (°C) for TAP = 3 W cm^{-2} after 0.38 seconds - focus at x=0, ALL elements activated (HiDef)***

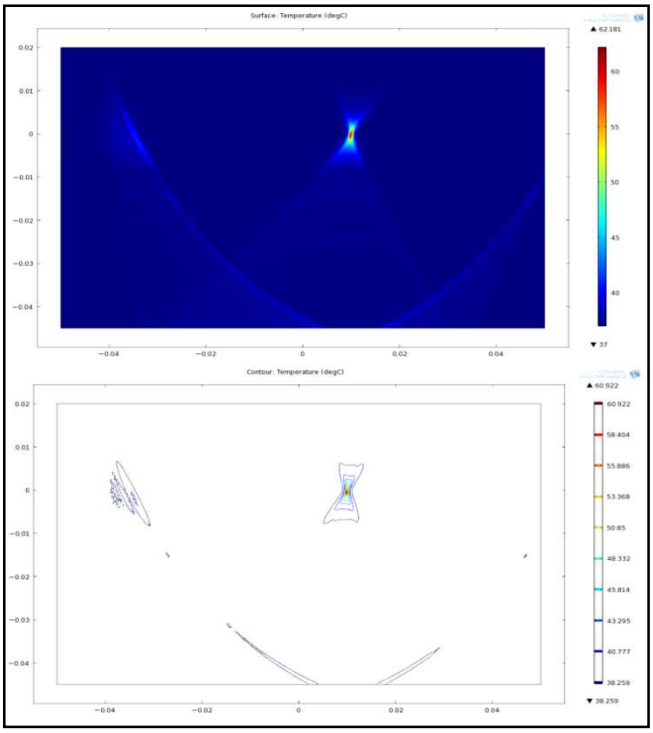

Figure 107 - ***Surface and contour Temperature plots (°C) for TAP = 3 W cm^{-2} after 0.5 seconds - focus at x=10, ALL elements activated***

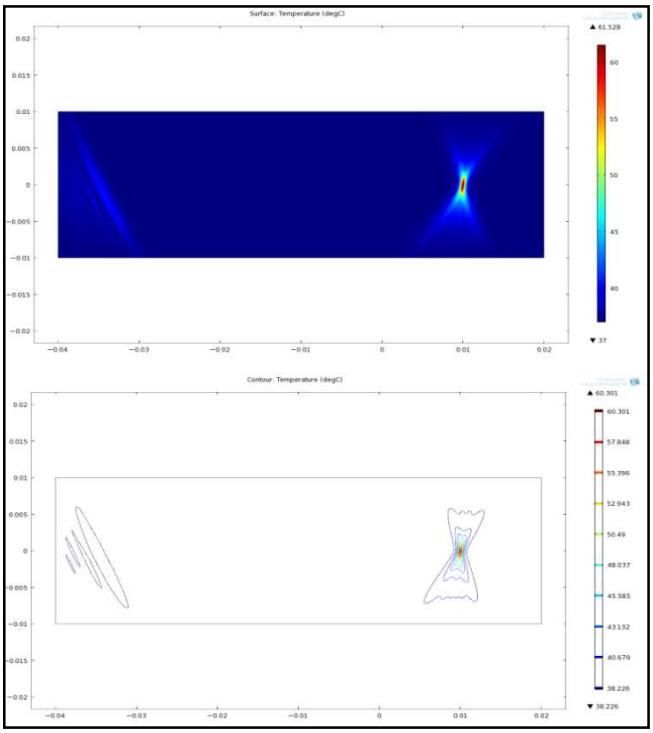

Figure 108 - ***Surface and contour Temperature plots (°C) for TAP = 3 W cm^{-2} after 0.39 seconds - focus at x=10, ALL elements activated (HiDef)***

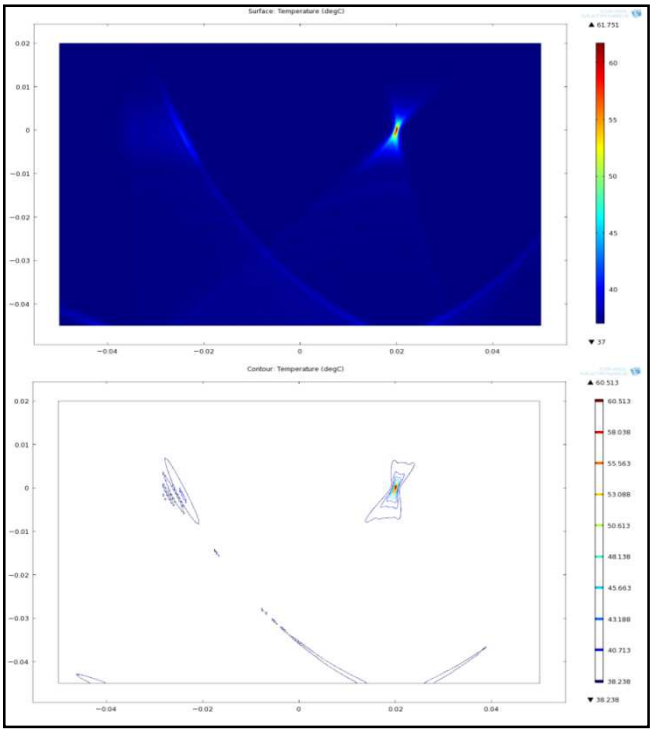

Figure 109 - ***Surface and contour Temperature plots (°C) for TAP = 3 W cm^{-2} after 0.5 seconds - focus at x=20, ALL elements activated***

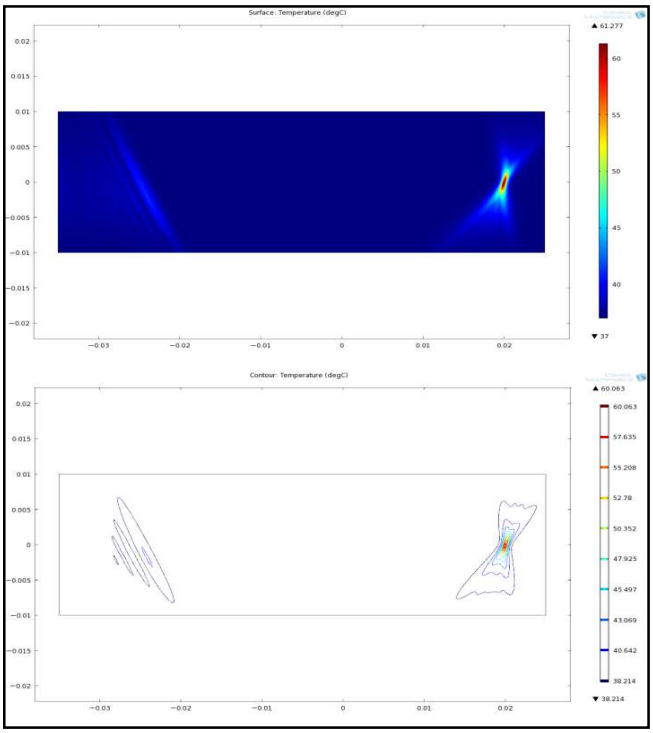

Figure 110 - ***Surface and contour Temperature plots (°C) for TAP = 3 W cm^{-2} after 0.46 seconds - focus at x=20, ALL elements activated (HiDef)***

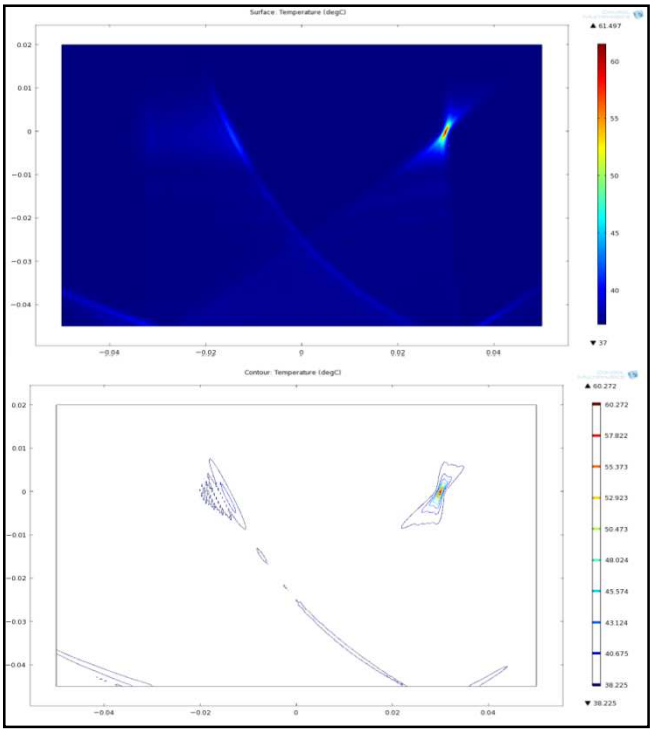

Figure 111 - ***Surface and contour Temperature plots (°C) for TAP = 3 W cm^{-2} after 0.6 seconds - focus at x=30, ALL elements activated***

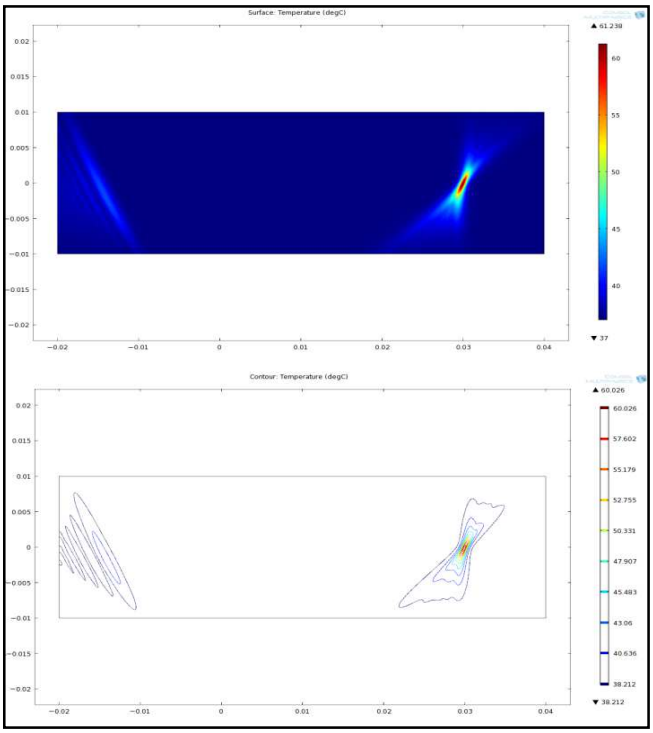

Figure 112 - ***Surface and contour Temperature plots (°C) for TAP = 3 W cm^{-2} after 0.59 seconds - focus at x=30, ALL elements activated (HiDef)***

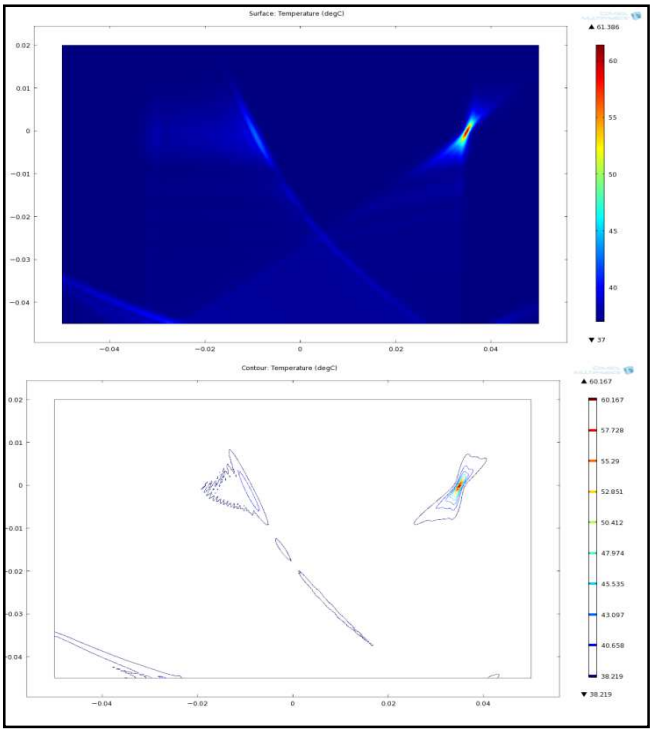

Figure 113 - ***Surface and contour Temperature plots (°C) for TAP = 3 W cm^{-2} after 0.75 seconds - focus at x=35, ALL elements activated***

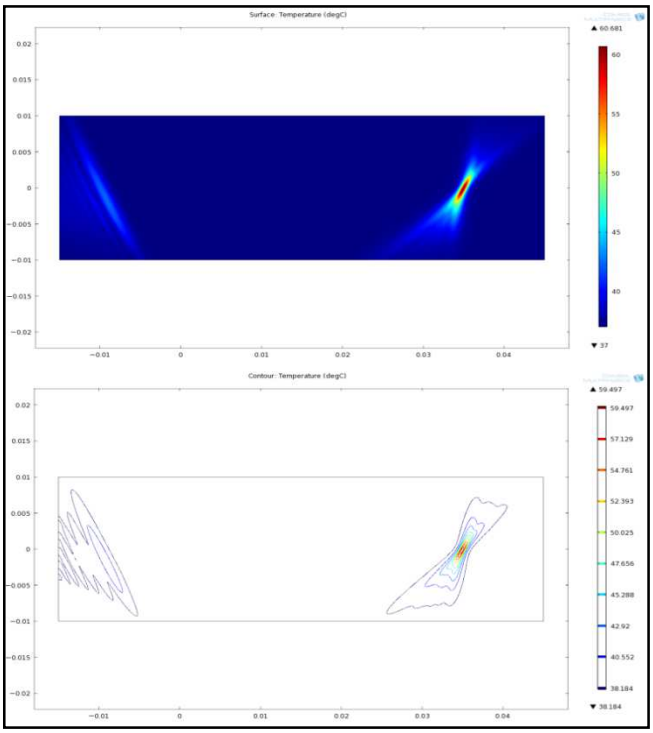

Figure 114 - ***Surface and contour Temperature plots (°C) for TAP = 3 W cm^{-2} after 0.68 seconds - focus at x=35, ALL elements activated (HiDef)***

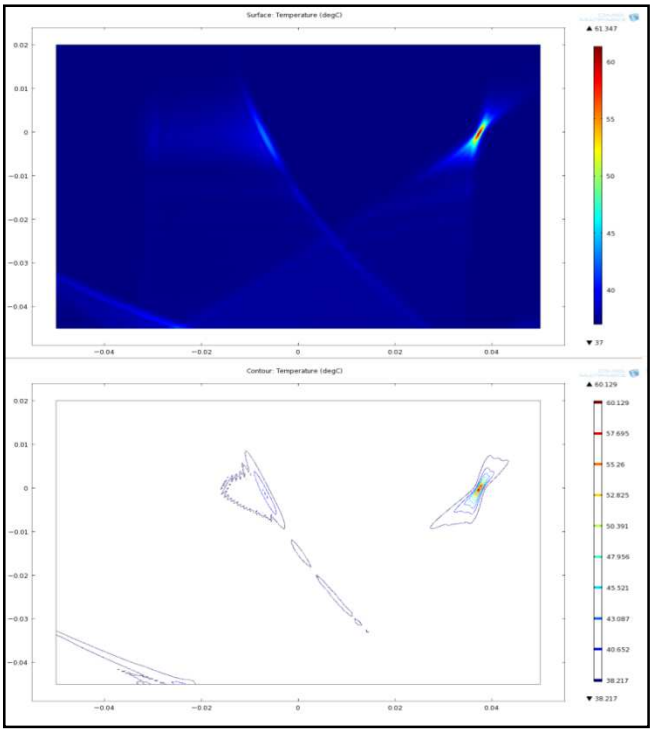

Figure 115 - ***Surface and contour Temperature plots (°C) for TAP = 3 W cm^{-2} after 0.8 seconds - focus at x=37.5, ALL elements activated***

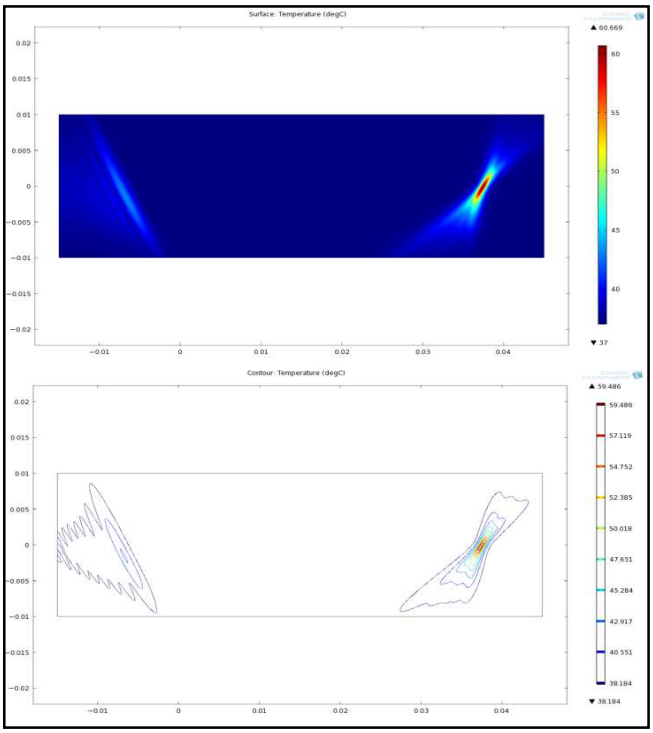

Figure 116 - ***Surface and contour Temperature plots (°C) for TAP = 3 W cm^{-2} after 0.75 seconds - focus at x=37.5, ALL elements activated***

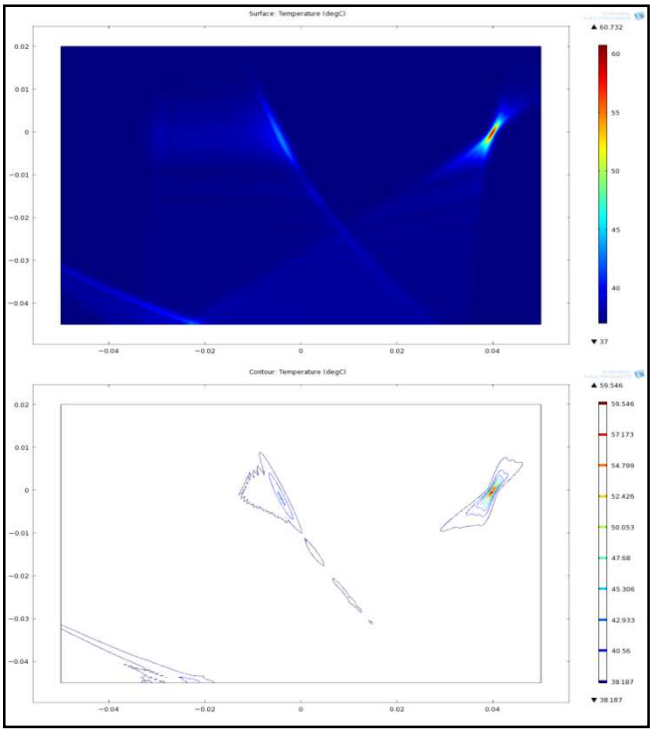

Figure 117 - ***Surface and contour Temperature plots (°C) for TAP = 3 W cm^{-2} after 0.85 seconds - focus at x=40, ALL elements activated***

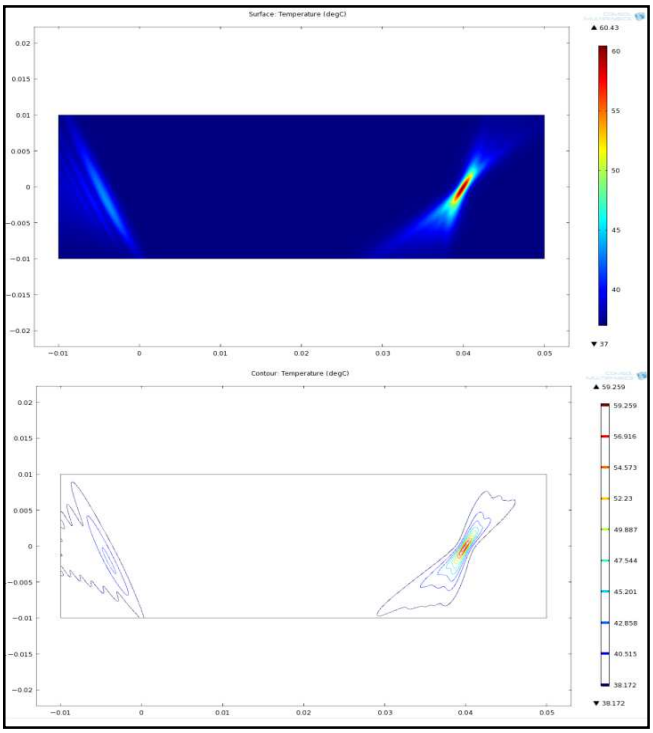

Figure 118 - ***Surface and contour Temperature plots (°C) for TAP = 3 W cm^{-2} after 0.82 seconds - focus at x=40, ALL elements activated (HiDef)***

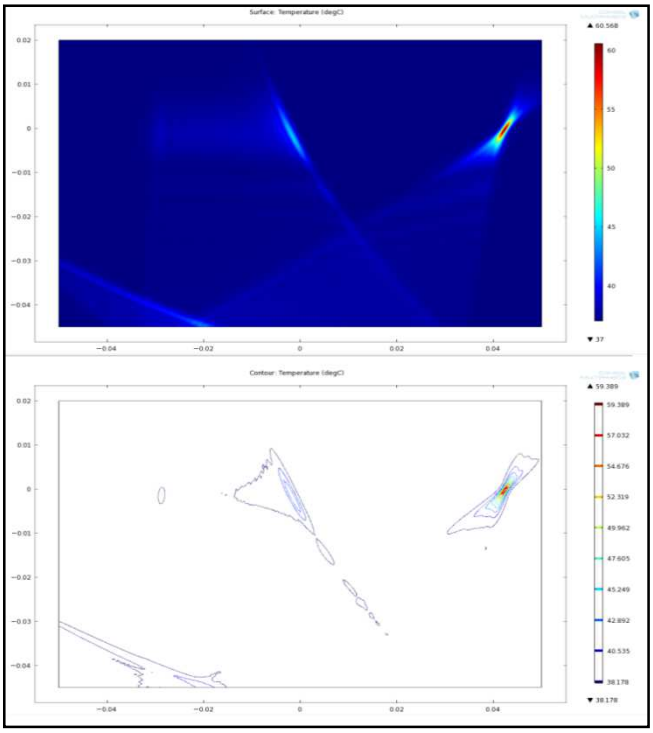

Figure 119 - ***Surface and contour Temperature plots (°C) for TAP = 3 W cm^{-2} after 1.0 seconds - focus at x=42.5, ALL elements activated***

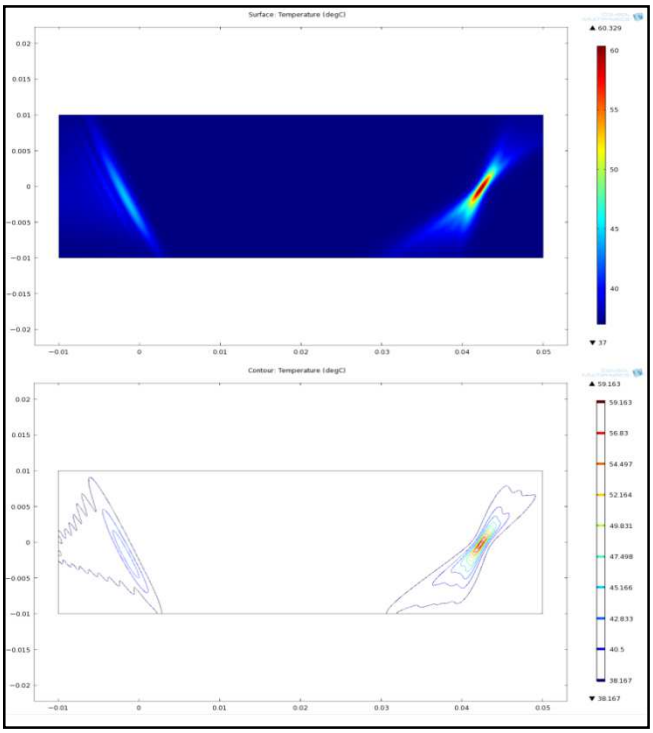

Figure 120 - ***Surface and contour Temperature plots (°C) for TAP = 3 W cm^{-2} after 0.9 seconds - focus at x=42.5, ALL elements activated (HiDef)***

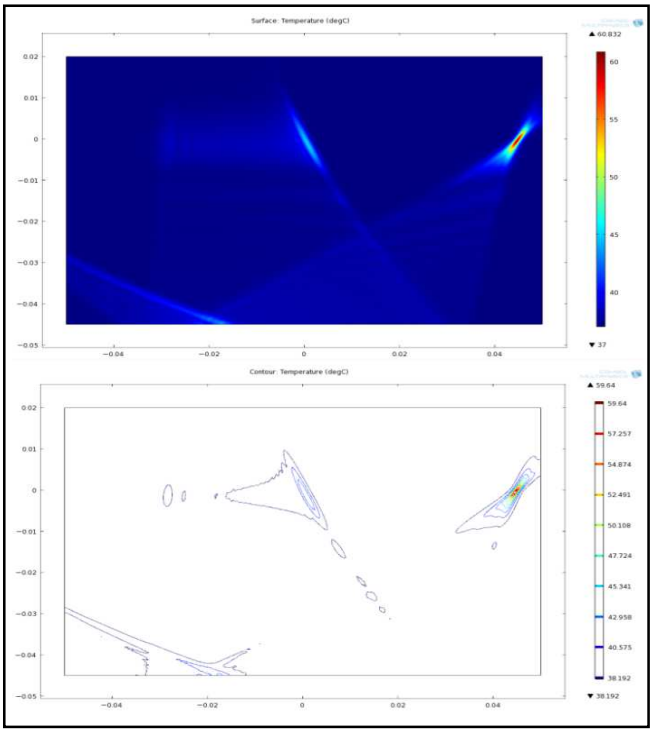

Figure 121 - ***Surface and contour Temperature plots (°C) for TAP = 3 W cm^{-2} after 1.1 seconds - focus at x=45, ALL elements activated***

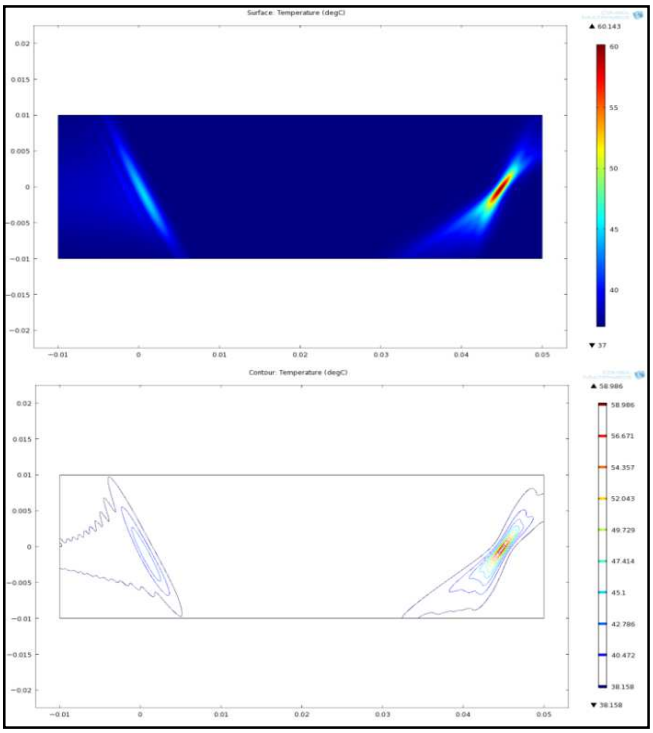

Figure 122 - ***Surface and contour Temperature plots (°C) for TAP = 3 W cm^{-2} after 1.01 seconds - focus at x=45, ALL elements activated (HiDef)***

Table 22 - ***Effect of steering the focal point (ALL elements) on the resulting thermal dose (TD) (*****Figure 105** ***to*** **Figure 122*****)***

Focus at (mm)	Time (s)	Focal temp (°C)	Focal TD (mins)	Lobe temp (°C)	Lobe TD (mins)
0	0.38	60.59	313.15	38.24	<0.0001
	1	81.70	$1.86x10^{9}$	44.06	0.01528
	2	105.45	$8.47x10^{16}$	47.81	1.3905
10	0.39	60.30	266.36	38.23	<0.0001
	1	80.44	$7.69x10^{8}$	39.29	0.01964
	2	103.54	$2.31x10^{16}$	47.51	1.0566
20	0.45	60.06	250.74	40.64	<0.0001
	1	76.16	$4.09x10^{7}$	43.18	0.0181
	2	97.22	$2.39x10^{14}$	46.51	0.9547
30	0.59	60.03	311.52	40.64	<0.0001
	1	69.75	$4.23x10^{5}$	42.17	0.0082
	2	87.79	$2.80x10^{11}$	45.02	0.9161
35	0.68	59.50	247.09	40.55	0.0020
	1	66.15	35955	41.60	0.0155
	2	82.40	$6.20x10^{9}$	48.95	0.8151
37.5	0.75	59.49	270.04	42.92	0.0047
	1	64.29	9419.22	44.18	0.0180
	2	79.63	$9.04x10^{8}$	46.36	0.9186
40	0.87	59.26	247.68	42.86	0.0076
	1	62.46	2832.80	43.70	0.0142
	2	76.92	$1.34x10^{8}$	47.51	0.7432
42.5	0.91	59.16	252.62	42.83	0.0167
	1	60.63	762.79	43.22	0.0254
	2	74.16	$1.88x10^{7}$	50.69	1.3529
45	1	58.84	235.76	43.77	0.0189
	1.01	58.99	262.45	44.00	0.0194
	2	71.45	$2.73x10^{6}$	49.69	1.0978

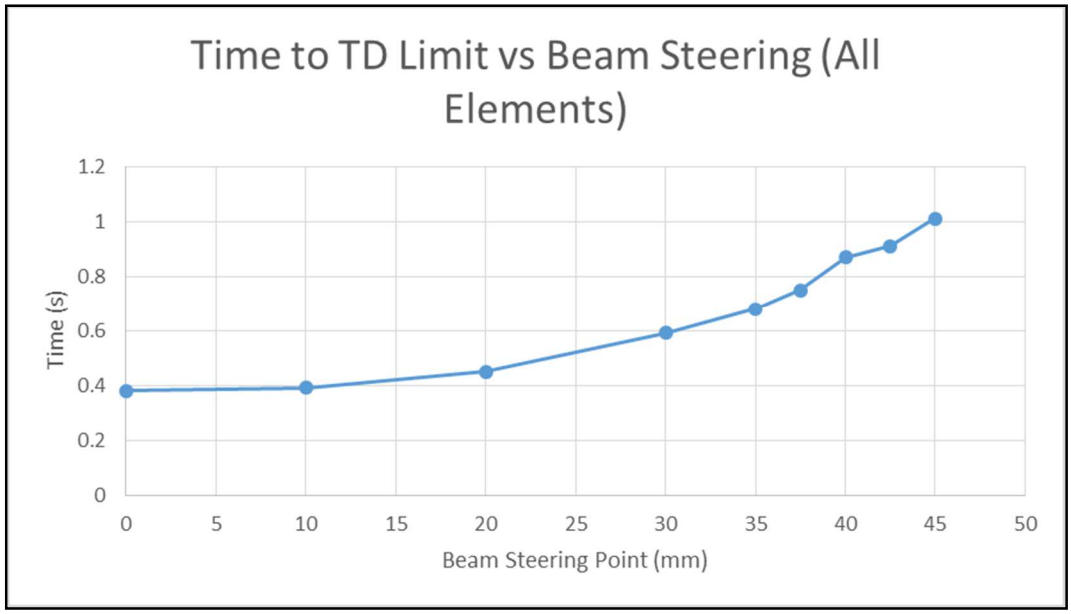

Figure 123 - ***Graph of time to focal TD threshold against beam steering point (ALL elements activated)***

From these results (see Table 22 & Figure 123) it can be seen that the threshold thermal dose of 240 mins was reached in under one second in all cases except from the extreme focus at x=45, for which the threshold was exceed at 1.01 seconds. The maximum temperature outside of the focus was under 43 °C in all simulations and was the lowest at the 'natural' focus of x=0 mm where the temperature rose just over 1.2 °C above normal human body temperature. In all cases thermal dose outside the focus did not exceed 0.02 equivalent minutes (see Figure 124).

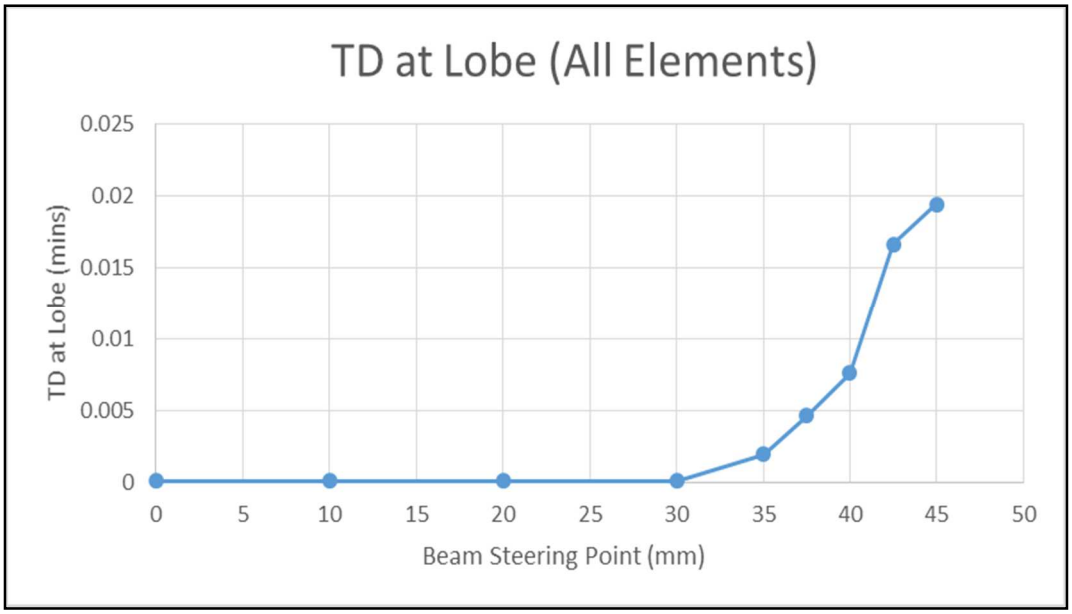

Figure 124 - ***Graph of TD developed at the non-focal lobe against the beam steering point (ALL elements activated)***

From these results we can draw the conclusion that ablation would be feasible at all points simulated using a TAP of 3 W, with all of the transducer elements being excited to create the desired focus. Also all times to a TD of 240 mins were less than 1.7 s, the limit of allowable continuous transducer activation period for 3 W TAP at the transducer (see Table 21). In the following section (see Section 6.3.2.2) these simulations will be performed using half the elements of the array.

6.3.2.2: Half Elements

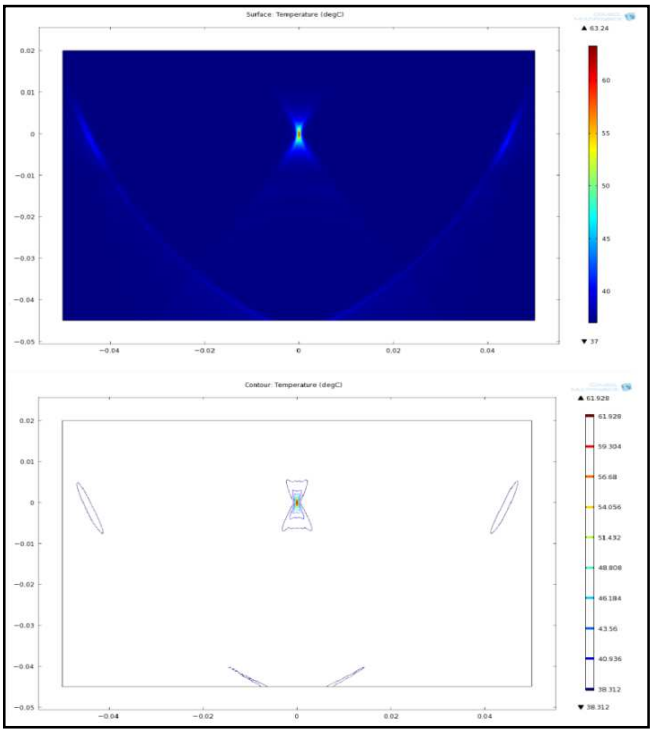

Figure 125 - ***Surface and contour Temperature plots (°C) for TAP = 3 W cm^{-2} after 1.1 seconds - focus at x=0, HALF elements activated***

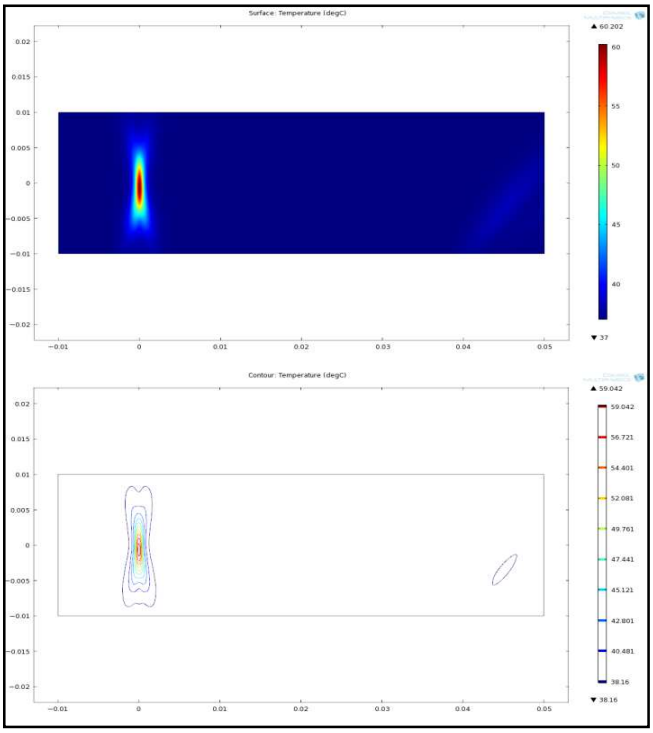

Figure 126 - ***Surface and contour Temperature plots (°C) for TAP = 3 W cm^{-2} after 1.05 seconds - focus at x=0, HALF elements activated (HiDef)***

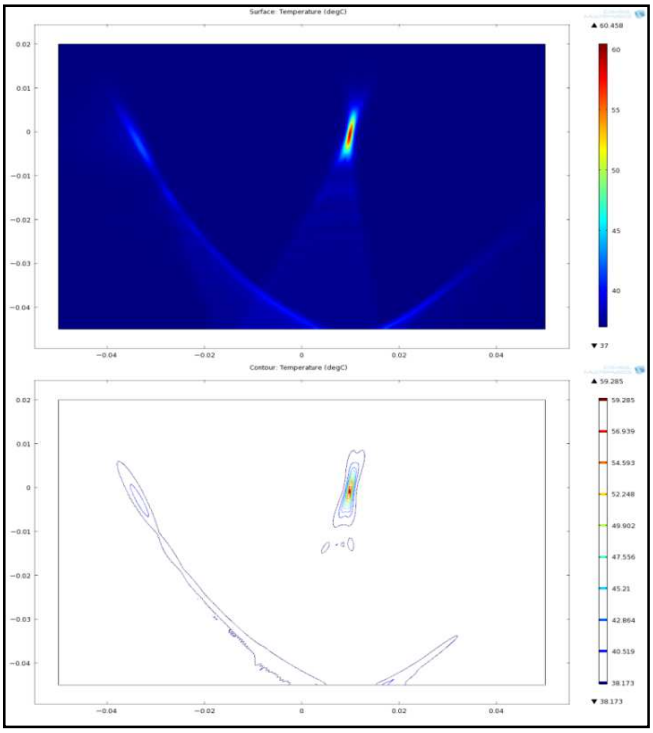

Figure 127 - ***Surface and contour Temperature plots (°C) for TAP = 3 W cm^{-2} after 1.15 seconds - focus at x=10, HALF elements activated***

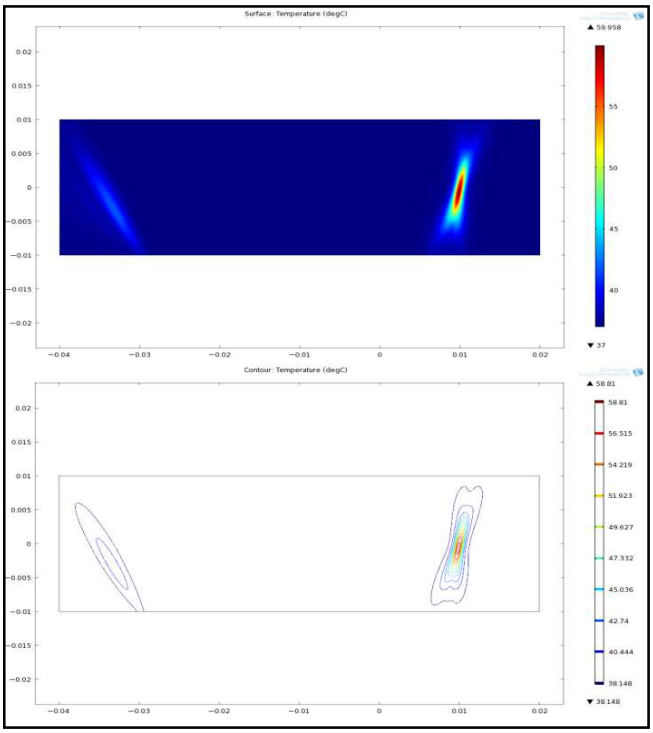

Figure 128 - ***Surface and contour Temperature plots (°C) for TAP = 3 W cm^{-2} after 1.11 seconds - focus at x=10, HALF elements activated (HiDef)***

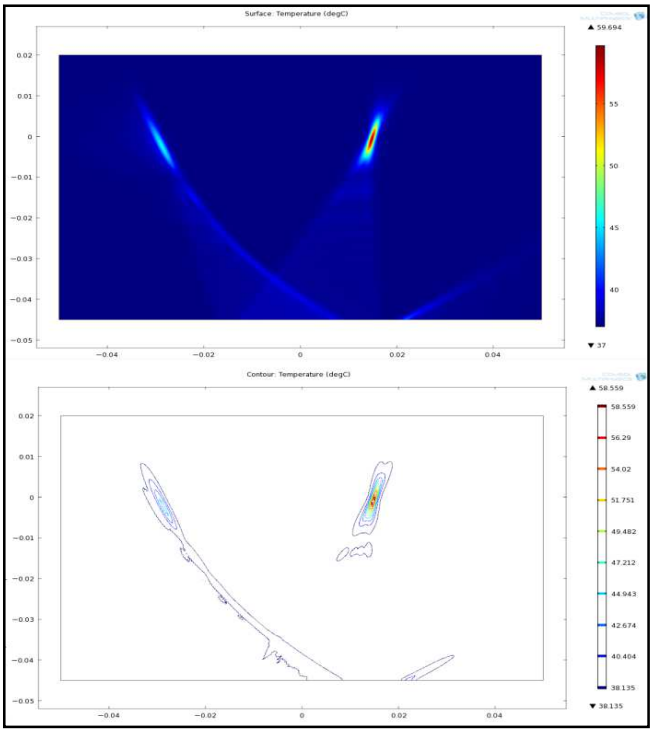

Figure 129 - ***Surface and contour Temperature plots (°C) for TAP = 3 W cm^{-2} after 1.24 seconds - focus at x=15, HALF elements activated***

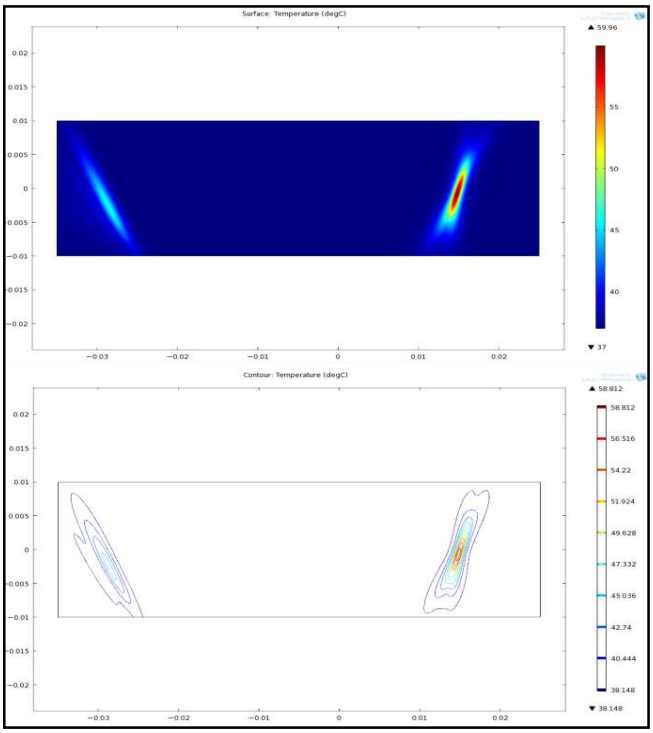

Figure 130 - ***Surface and contour Temperature plots (°C) for TAP = 3 W cm^{-2} after 1.22 seconds - focus at x=15, HALF elements activated (HiDef)***

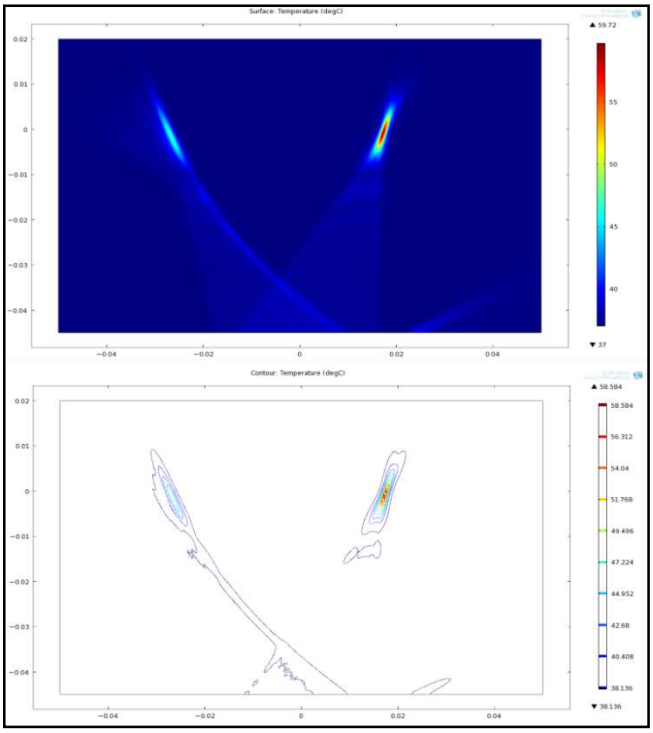

Figure 131 - ***Surface and contour Temperature plots (°C) for TAP = 3 W cm^{-2} after 1.3 seconds - focus at x=17.5, HALF elements activated***

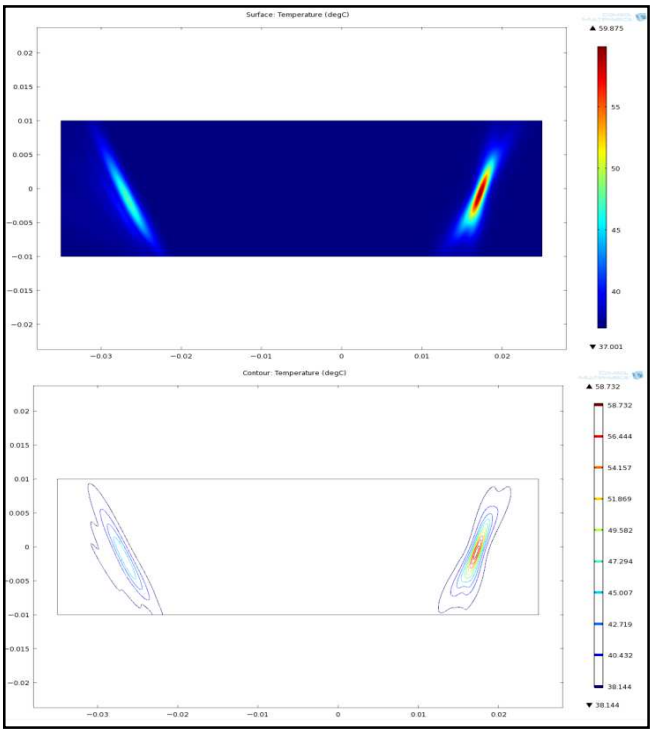

Figure 132 - ***Surface and contour Temperature plots (°C) for TAP = 3 W cm^{-2} after 1.29 seconds - focus at x=17.5, HALF elements activated (HiDef)***

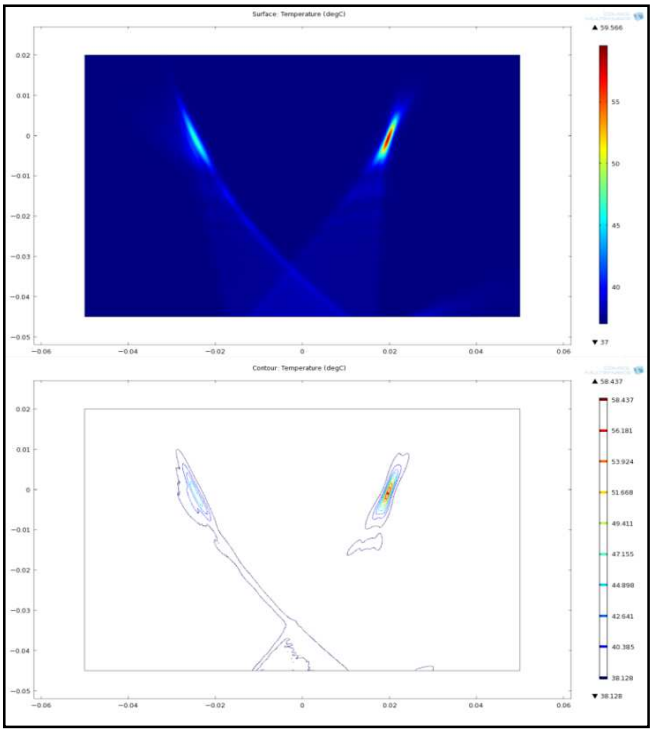

Figure 133 - ***Surface and contour Temperature plots (°C) for TAP = 3 W cm^{-2} after 1.35 seconds - focus at x=20, HALF elements activated***

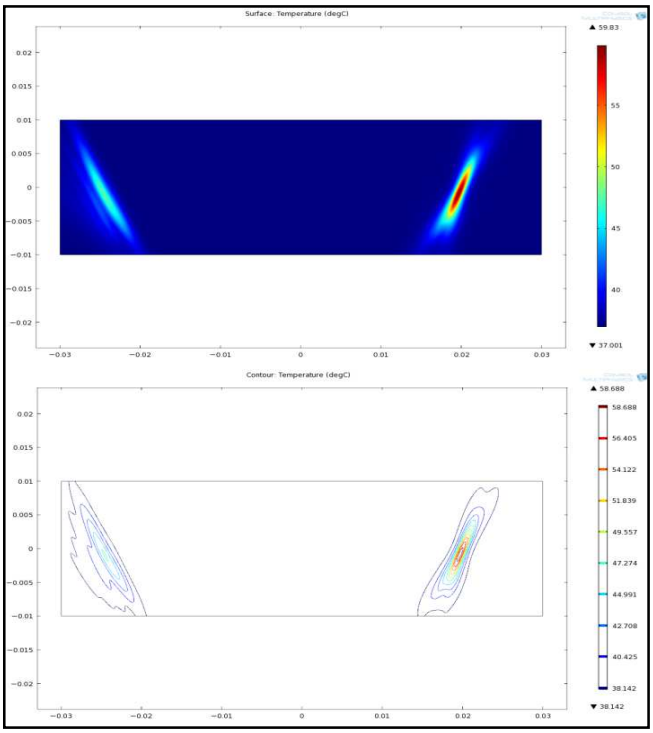

Figure 134 - ***Surface and contour Temperature plots (°C) for TAP = 3 W cm^{-2} after 1.38 seconds - focus at x=20, HALF elements activated (HiDef)***

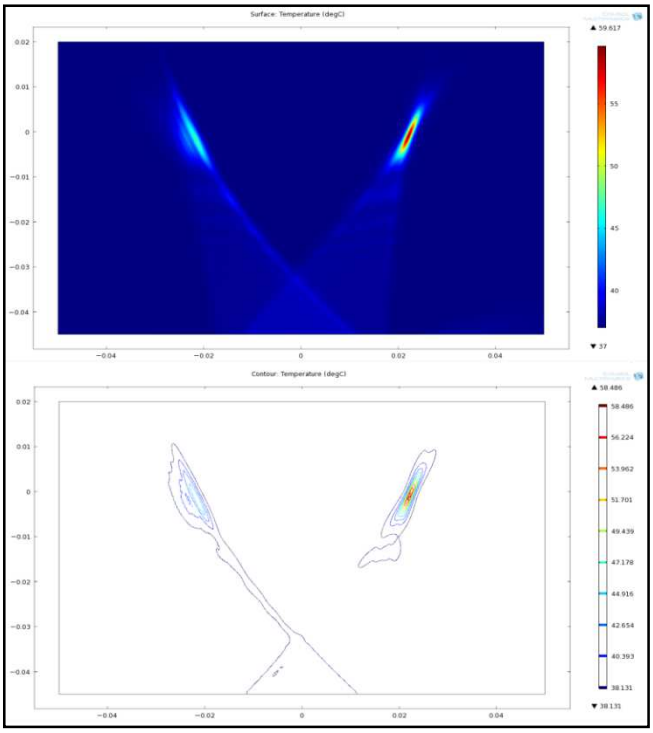

Figure 135 - ***Surface and contour Temperature plots (°C) for TAP = 3 W cm^{-2} after 1.5 seconds - focus at x=22.5, HALF elements activated***

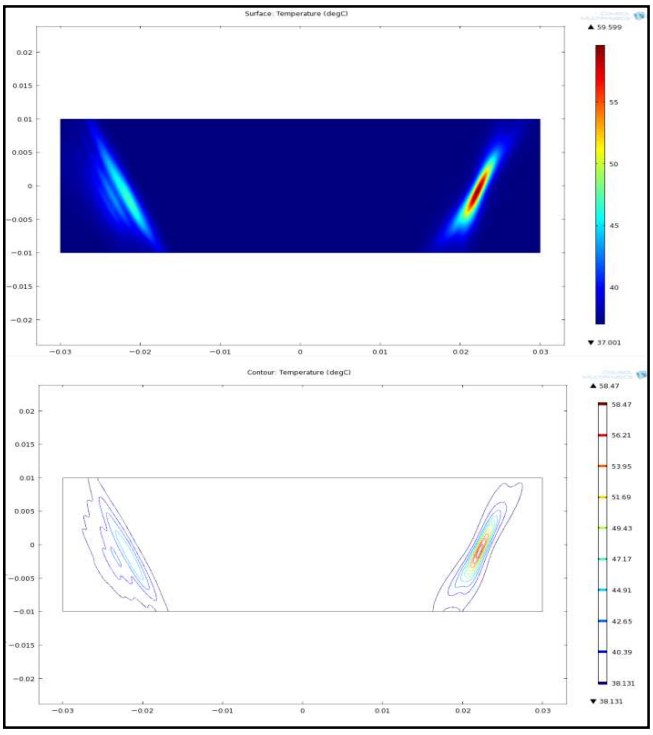

Figure 136 - ***Surface and contour Temperature plots (°C) for TAP = 3 W cm^{-2} after 1.47 seconds - focus at x=22.5, HALF elements activated (HiDef)***

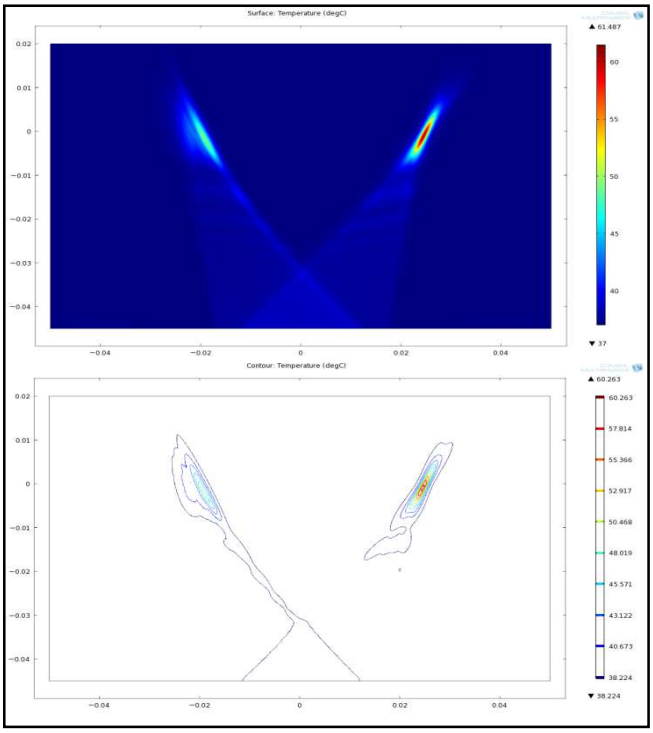

Figure 137 - ***Surface and contour Temperature plots (°C) for TAP = 3 W cm^{-2} after 1.6 seconds - focus at x=25, HALF elements activated***

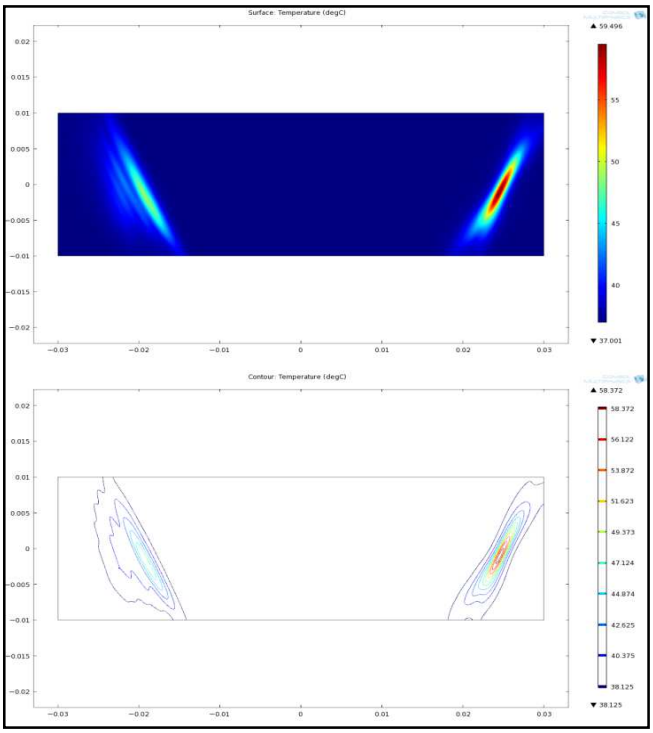

Figure 138 - ***Surface and contour Temperature plots (°C) for TAP = 3 W cm^{-2} after 1.59 seconds - focus at x=25, HALF elements activated (HiDef)***

Table 23 - ***Effect of steering the focal point (HALF elements) on the resulting thermal dose (TD) (Figure 125 to Figure 138)***

Focus at (mm)	Time (s)	Focal temp (°C)	Focal TD (mins)	Lobe temp (°C)	Lobe TD (mins)
0	1	58.30	150.87	38.12	<0.0001
	1.05	59.04	254.76	38.16	<0.0001
	2	71.12	2.17×10^6	38.80	<0.0001
10	1	57.27	87.41	40.23	<0.001
	1.15	58.82	244.33	40.44	0.0012
	2	69.54	6.15×10^5	42.14	0.0230
15	1	56.33	32.47	42.83	0.0149
	1.23	58.62	247.59	43.82	0.0461
	2	68.38	1.2212×10^5	47.27	0.7708
17.5	1	55.15	18.65	43.69	0.0311
	1.29	58.73	253.27	45.01	0.1046
	2	66.34	71552	50.90	1.6132
20	1	54.25	10.02	43.36	0.2458
	1.38	58.69	259.54	47.27	0.1276
	2	64.98	28318	50.25	1.4240
22.5	1	53.30	5.63	43.04	0.0149
	1.47	58.47	248.52	44.91	0.1163
	2	63.54	10452	49.57	0.7470
25	1	52.30	2.60	44.25	0.02270
	1.59	58.37	245.93	48.11	0.3203
	2	62.05	3833.41	50.28	1.4466

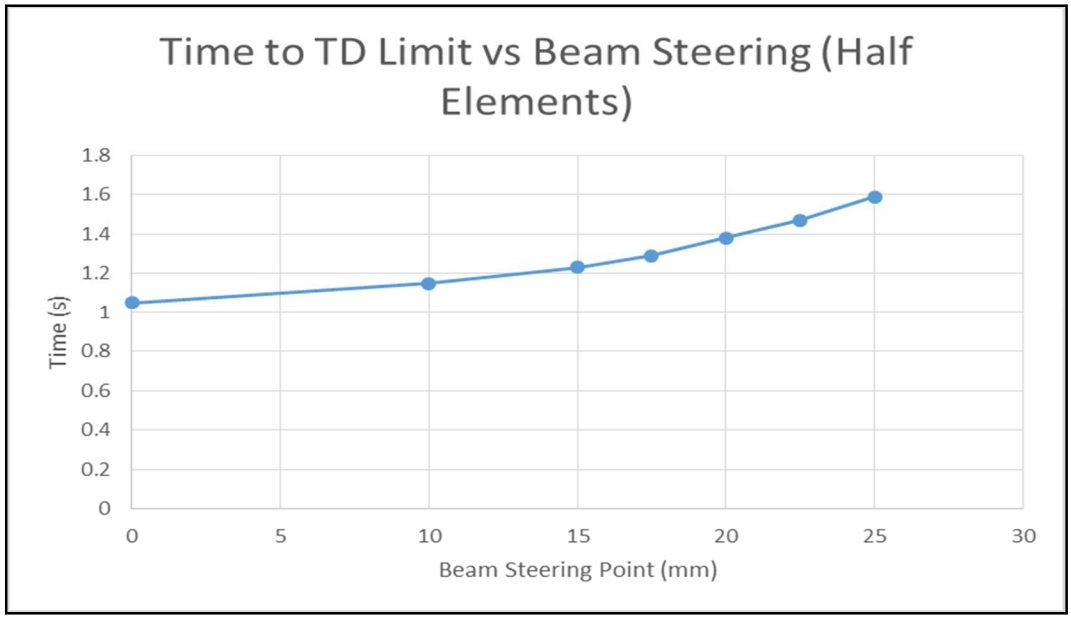

Figure 139 - ***Graph of time to focal TD threshold against beam steering point (HALF elements activated)***

From the results of these simulations (see Table 23 & Figure 139) it can be observed that the thermal dose threshold was exceeded between 1 and 1.6 seconds for all cases, within the limit set by manufacturers Imasonic (see Table 21).. The further away from the geometric centre the beam was steered the longer time was required to exceed the focal TD threshold. The maximum temperature outside of the focus was under 48.2 °C in all simulations and was the lowest when directed at the 'natural' focus of x=0 mm where the simulated temperature at the lobe rose just over 1.1 °C above normal human body temperature. In all cases thermal dose outside the focus did not exceed 0.35 equivalent minutes (see Figure 140).

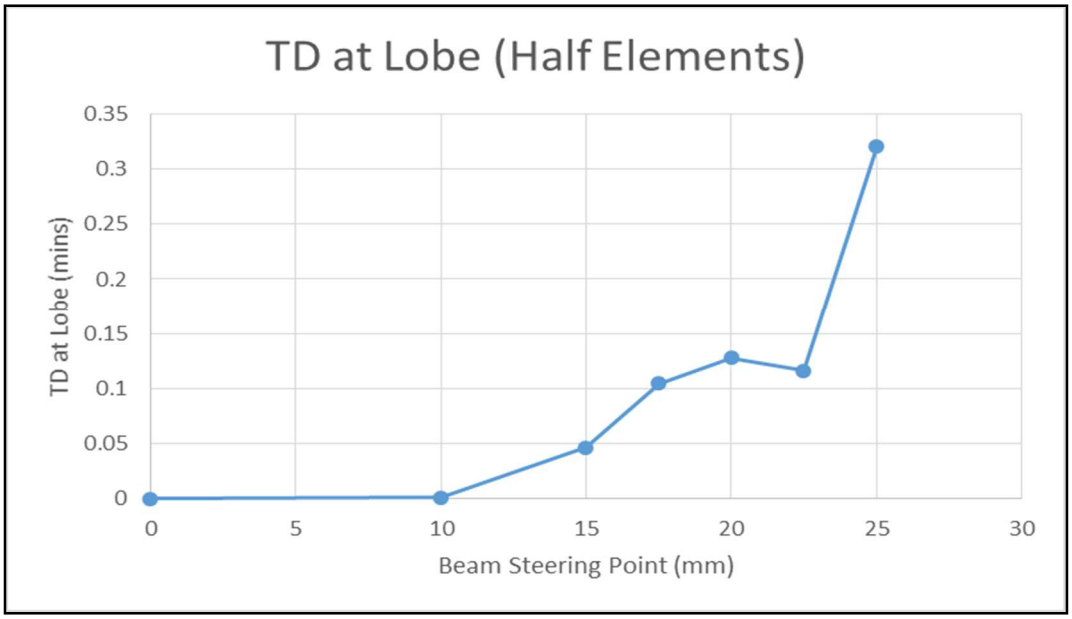

Figure 140 - ***Graph of TD developed at the non-focal lobe against the beam steering point (HALF elements activated)***

From these results we can again draw the conclusion that ablation would be feasible at all points simulated using a TAP of 3 W, with just half of the transducer elements being excited to create the desired focus. An interesting point of note here is the anomalous result of the TD at the grating lobe when the beam is steered to x=22.5 mm (see Figure 140). Here the TD decreased, rather than increased as in the case of all elements (see Figure 124). The simulation data for this point was checked and retested a number of times with the same result. However, whether this was due to a limitation in the simulation mesh size, or due to a property of the interaction of the acoustic waves themselves, it can be said that the TD levels at non-focal points are well within safe levels and as such this outlying point cannot be said to affect the efficacy of the transducer design or treatment plan.

6.4: Chapter Conclusion

To conclude, in this chapter the theory used to simulate the time-dependent tissue temperature rise using acoustic intensity fields obtained earlier, has been defined. Using this theory the BHTE was computed using suitable software with the effects of acoustic power input and exposure time being thoroughly investigated, with a thermal dose model being used to compare the surgical affectivity of differing heating regimes.

Steering of the focal point has also been considered and simulated. The result of these simulations have shown that enough energy was delivered at the focus to ablate tissue whilst not causing permanent damage in non-focal areas. Overall this has resulted in a novel design that is both compatible with the existing EIM device and theoretically capable of ablating tissue within the defined volume, as described in the problem definition specified previously (see Section 4.2). Results have been discussed with emphasis on the ability of the designed transducer to perform as a surgical instrument.

Chapter 7:

Conclusions & Future Work

7.1: Chapter Introduction

In this brief final chapter conclusions from the work described in previous chapters will be drawn. These conclusions will be based on the achievement of the goals set out in the original project proposal (see Appendix B) which has been included as a supplement to this thesis.

Additionally suggestions for the direction of future work will be outlined. These will include topics that would have been considered had time constraints allowed and other useful avenues of research, such as research into adaptation of the designed device for cancers that affect tissues other than the breast.

7.2: Project Conclusions

To summarise, the work described in this thesis has shown that the incorporation of a surgical HIFU device into the existing EIM system developed at the University of Sussex is indeed feasible, thus fulfilling the research aim (see Section 1.6.1: Aims).

It has been shown that modification of the existing electrode plate would allow sufficient space to fit a suitably powerful HIFU transducer, capable of targeted tissue ablation within a known volume, namely that of human breast tissue. The research objectives have therefore also been satisfied in that the research questions posed have been effectively answered (see Section 1.6.2: Objectives & Appendix B: Original Project Proposal). Referring to the first two questions, the feasibility study has indeed shown that HIFU can be used as a surgical tool in combination with EIM to provide diagnosis and targeted treatment. It has also been shown *how* a suitably powerful HIFU transducer can be incorporated into the existing EIM system, designed by the BMEng group at the University of Sussex, allowing the region of interest to be effectively targeted by the designed device via mechanical movement of the EIM electrode plate and electronic steering of the focal point using a phased array. This study has included the factors that must be considered when designing such a device, with simulations used to investigate the effect of these factors and of the surgical of the HIFU device as a whole.

The benefits of HIFU over existing comparable treatments was one of the driving forces of the investigations described in this thesis. Ablation using radiofrequency has the drawback of requiring direct contact with the treatment area, thus cannot be termed truly non-invasive. Although technological advances may allow progressively smaller electrodes to be used, this techniques would still require insertion of some type of device into the patients' body. The same is true for laser, microwave and cryoablation. Even though these techniques may be performed laparoscopically or percutaneously, an incision, regardless of the size, would still be required for the treatment of breast cancer in current surgical environments. Moreover radiation based ablation techniques such as brachytherapy and hadron therapy however safe could have negative psychological implications to patients due to the negative public opinion

of radiation. Given a choice it is likely patients would favour ‘acoustic therapy’ over a technique based on radiation. For these reasons the development of HIFU treatments seems to provide true progress, minimising treatment time and greatly improving patient comfort during the treatment process. Furthermore incorporating HIFU as a treatment device into a system capable of performing a non-invasive diagnosis of breast cancer seems to be a progressive step in creating an ‘all-in-one’ device for breast cancer treatment. The main body of work described in previous chapters has focused on this goal.

Using current fabrication methods HIFU transducers generally have many features in common with one another, such as using a piezoelectric element and incorporating a matching layer to minimise the losses arising when acoustic waves propagate through more than one medium with differing acoustic impedances. Using an element thickness of half a wavelength and a matching layer with a thickness equal to a quarter wavelength in the piezoelectric material is optimal to minimise these losses. The designed transducer follows this principle.

Focusing of the HIFU beam was one of the most important factors to consider in the HIFU transducer design. To allow maximum coverage in the scanned volume of the EIM system, using a spherical type array was deemed impractical due to the difficulty in moving the device to surgically advantageous positions relative to the treatment region. Using an annular truncated array, as commonly used in transrectal devices for the treatment of prostate cancer was also not implemented due to the absence of a need to vary the focal depth using control of annular phased elements. This requirement was met by the mechanical movement of the electrode plate in the EIM system. Using a lens or lenses to focus the beam was an option, however using a lens causes a loss in the power output of the transducer and therefore decreases the intensity of the focal point. As the space available, and therefore the maximum power output of the transducer, was limited, a lens was deemed unsuitable and was not included as part of the design. In place of a lens the transducer elements themselves were designed with a linear concave geometry, causing propagated ultrasound to focus naturally along one axis, or rather along a line. Using the phasing of individual

elements allows this line to be focused into a point and using the vertical translation of the electrode plate allows the target focal depth to be varied. This is the technique employed by the transducer described in this thesis.

With a transducer geometry and operation of focus decided, the remaining characteristics of the transducer were considered. Assuming a maximum focal depth of 4 cm it was shown that the optimal operating frequency of the transducer would be approximately 3.5 MHz. Simulations were performed using these values and were carried out to fully explore the feasibility of the project and to optimise design parameters to meet the necessary criteria of surgical ablation.

Using a custom-written MATLAB code based on Huygen's principle investigations showed the most efficient spacing of sub-elements was equal to one-sixth of a wavelength in the piezoelectric material. As the attenuation coefficient of breast tissue in different patients will vary, the effect of altering the value was investigated, resulting in 7.5 Np m^{-1} MHz^{-1} being used for the majority of simulations performed. Compared to similar studies this would allow the focal intensity to be underestimated, allowing a suitable 'safety factor' and ensuring ablation at the focus would be possible. Element width and kerf were initially optimised to reduce or prevent grating lobes but were later modified following discussions with transducer manufacturer Imasonic. Eventually these two parameters were selected as a compromise between manufacturing limitations and optimal values found from simulation. Following further simulations, this resulted in an element width and kerf of 0.43 mm and 0.1 mm respectively to be used.

The expected focal intensities and magnitude of grating lobes were investigated and used as inputs in the Pennes Bio-Heat Transfer Equation computed using the COMSOL Multiphysics software package. Using a thermal dose model, simulations showed that it would indeed be feasible to ablate tissue in a reasonable timeframe using the acoustic power value limitations advised on by the transducer manufacturers, in accordance with the proprietary piezoelectric materials available. Simulations involving steering the focus were then carried out and proved steering to be feasible in terms of

focused tissue heating, with heating of surrounding tissue outside the focal area falling within acceptable limits, leading to no permanent cell damage.

To conclude, not only has feasibility been proven but a design has been developed, up to the stage of plausible manufacture. This design is based on the numerous simulations performed to allow the optimisation of a small but powerful device, capable of steering a suitably focused point along the major axis of the device. Combined with the mechanical, stepper motor controlled height and rotation of the EIM electrode plate, this transducer would allow ablation of tissue at any surgically useful point in the scanned volume. This focus has been proven capable of depositing enough energy, in the form of heat from attenuated acoustic waves, such that targeted tissue will be ablated via coagulative necrosis at the cellular level. Once necrosed, these cells would be naturally absorbed by cellular phagocytosis, resulting over time in the disappearance of the palpable lump that would likely be present immediately following treatment. While the presence of this lump may be a psychological factor involved in prospective patients' decision to undergo HIFU surgery, it is an inconvenience that would allow invasive surgery to be completely avoided. This is one of, if not the major benefit of undergoing a non-invasive surgical procedure such as FUS. It should also be noted that anaesthesia is rarely necessary during HIFU procedures as mentioned in a number of the publications reviewed, furthering the move away from the necessity of major surgical operations for the treatment breast cancer. Some patients may favour conventional surgery, such as a mastectomy, over HIFU treatment due to the persistence of the resulting palpable lump but nonetheless the option of avoiding this type of surgery altogether will almost certainly lead a large number prospective patients to choose the non-invasive HIFU option. The exact proportions of patients making this choice may vary from country to country and culture to culture, and it remains to be seen where this balance may lie. Further investigations and interviews with prospective patients would help to illuminate the general consensus on this matter, as would consultations with practicing oncologists prior to the mainstream introduction of this type of treatment.

7.3: Future Work

For various reasons a number of investigated research areas had to be omitted from this thesis. In this section these areas and some additional topics not covered in the body of this thesis will be described, with suggestions made for useful further developments.

7.3.1: Prototype Manufacture & Test

The next logical step for the work described in this thesis would be the manufacture of a prototype device. Primarily this would allow simulation findings to be verified *in vitro*, thus allowing adjustment of the model to reflect 'real world' results if and where necessary. Originally it was intended the project would reach this prototype stage but due to unfortunate external pressures and suspension of funding this could not be achieved.

In anticipation of prototype fabrication a specialised manufacturer was contacted resulting in the modification of certain simulation parameters reflecting the limitations of manufacture and manufacturing technology. It is possible however that as the technology for creating suitable materials and devices that these limitation may be lifted or at least relaxed allowing for a reappraisal of the feasibility study performed, paving the way for development of a more advanced device.

Once a prototype has been manufactured and laboratory tested progress toward medical trials could begin. It seems fair to assume that, given suitable approval, the device described could eventually be used in clinical trials. Following this path to successful completion it is hoped that the designed device, or a development henceforth could be usefully adopted into the treatment of breast cancer patients. At the least the use of the device or similar could become a viable option to patients facing conventional treatment and invasive surgery.

7.3.2: Driving Electronics & Circuitry

To operate the designed HIFU transducer a system capable of driving current to the elements of the array must be developed. This in itself warrants a separate research project similar in magnitude to that described in this thesis. An overview of the requirements of such a system is given below in addition to a block diagram showing a basic system layout (see Figure 141, [90]).

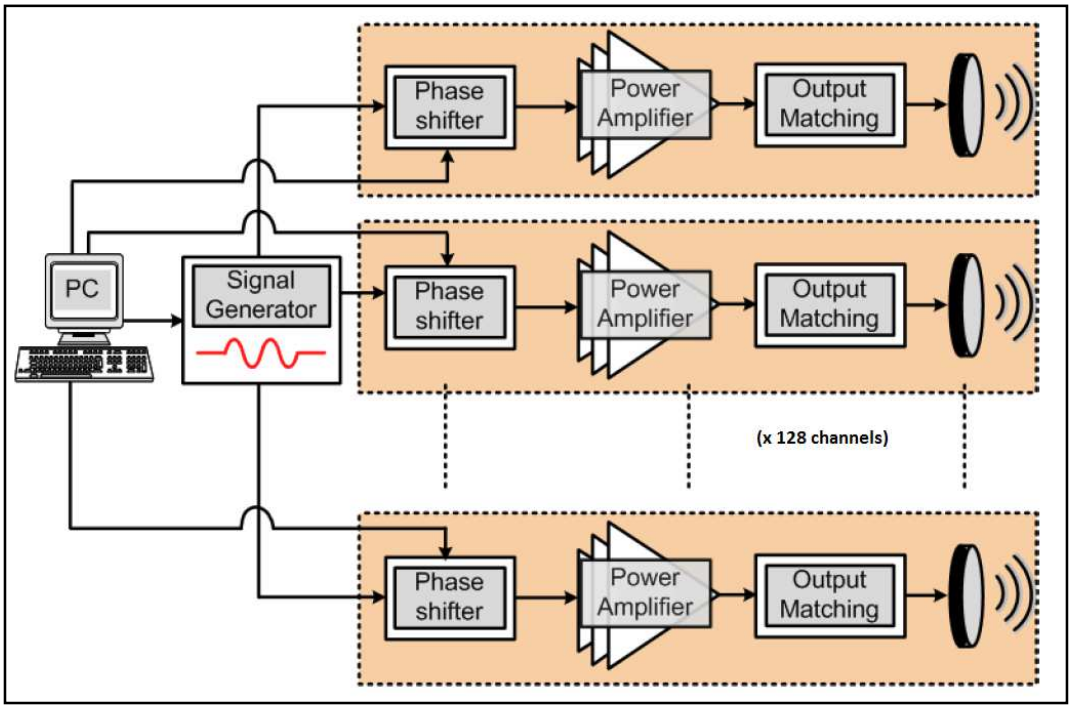

Figure 141 - ***General layout of HIFU array driving circuitry***

- 128 Channels
- Sine wave input
- Variable power: Electrical power of 0.27 W to 1 W per channel (advantageous if this *could* go higher / with small a resolution as possible (3W TAP = 0.5522 W per element at 59 % efficiency))
- Delay line(s) for phase shift between 0 and 2π (approx. 0 to 286 ns at 3.5 MHz) for each channel, resolution of 2 ns (lower if possible)

The development of driving circuitry may originally have been included as part of this thesis, but as project funding was withdrawn the work required to continue was omitted in favour of the main narrative, the design of the HIFU transducer and

simulation of surgical efficacy. It is highly recommended that this design work and fabrication of a completed design be undertaken as the 'next step' following on from the work presented in this thesis. This, along with the manufacture of the designed transducer, would allow trials to begin, at which stage results could be compared to simulations and the simulation model validated or adapted using the test data.

7.3.3: Two Media Simulations

As mentioned in a previously, the simulations performed involved the propagation of ultrasound through a single, homogenous media. This allowed the parameters involved in the design of the selected transducer to be characterised and optimised. However, once integrated into the existing EIM system and put to use, more than one media would be present, most notably the saline bath within the scanned volume into which a patient's breast would be placed prior to scanning or treatment taking place. Although saline in-between the transducer and the tissue to be treated would affect the resulting ultrasound beam properties, this should be kept to a minimum, as by design the breast being scanned may be compressed by the electrode plate of the EIM system, pushing the saline out to the sides of the breast, to locations where treatment should not be necessary. To what extent this occurs would vary patient to patient. Nevertheless it would be advantageous to model this second media and investigate the effect this would have on acoustic intensity and focal steering that would affect the resulting heat deposition within the tissue in question. This would allow for a more accurate treatment regime to be planned and as such would increase the overall usefulness of the simulation work presented in terms of use for treatment planning and targeting.

Furthermore the tissue was modelled as homogenous, having a constant acoustic impedance throughout the simulated volume. In reality breast tissue is far from homogenous. Fatty tissues, muscle and blood vessels have different acoustic impedance and would affect the propagation of ultrasound and would therefore alter the path to the focus in different ways. Additionally blood vessels may cause a small amount of heat to be carried away from the focus, especially with longer sonications, and as a result less energy would be deposited than reported in the simulations

described earlier, although it is generally agreed that, as mentioned previously, for short exposure times this effect can be ignored. To ensure this is indeed the case further investigation is warranted

To make accurate estimations more difficult there is also the problem that individual patient's breast tissue will differ from one another, making precise, non-generic simulations difficult. Using a method such as diagnostic ultrasound it may be possible to develop a model that would take into account the composition of a patient's breast prior to treatment, by identifying the volume and type of each tissue present to create personalised treatment plans. This would be a useful topic to consider in surgical planning and future development of the device.

7.3.4: Dual Mode Transducers

An interesting topic worthy of consideration is the use of 'dual-mode' transducers, examples of which have been described in the literature review presented earlier (see Section 2.3.1). This type of transducer could be used to supplement the diagnostic part of the EIM scanning procedure, in addition providing accurate location information on the cancerous tissue within the scanned volume.

This dual mode could operate in various ways, such as interleaving diagnostic sonications with those intended for the ablation of cancerous tissue. Progress could be monitored during treatment, offering advantages in terms of in-treatment supervision and feedback.

Alternatively, with the development of signal processing it may be possible to both monitor and treat the target tissue *simultaneously.* This may allow treatment to be monitored in real-time. As ultrasound devices are far more accessible in terms of cost, this offers the possibility of a machine capable of real-time treatment feedback, for the fraction of the cost involved with MR machines and imaging. To develop similar monitoring capabilities using ultrasound alone would vastly increase the practicality of device adoption and could well tip the balance in favour of comparatively inexpensive yet highly effective surgical EIM-HIFU devices, thus making valuable progress towards a widely accepted all-in-one device for the treatment of breast cancer.

It is also worth noting here that there is a current project researching the possibility of combining a diagnostic ultrasound with the EIM system at the University of Sussex. This project combines diagnostic ultrasound with EIM and has been named Combined Electrical Impedance Mammography with Ultrasound (CEIMUS). This work is out of the scope of the current research, but nevertheless offers an interesting avenue of research that could help further develop a truly all in one device, capable of detection, diagnosis and treatment of breast cancer.

7.3.5 Application to Other Cancer Types

Treatment of breast cancer has been the main focus of this thesis. While the device was designed to treat breast cancer alone, this does not deny the possibility of treatment of other types of cancer. Most notably the treatment of testicular cancer may be possible, with a few adaptions of the EIM device. HIFU has been successfully used to treat many different cancers as has been described in the literature review. The challenge here would be to develop an EIM system capable of scanning volumes of tissue other than the breast, from which point a suitable HIFU transducer could well be designed to complement the detection and diagnosis with a treatment modality that requires little or no anaesthesia. The treatment of other types of cancer, along with the other suggestions described in this final thesis section, could easily form the basis of a new and novel research project. It is the hope of the author that such a project be taken on and the ideas and approaches described herein be developed to the point that breast cancer surgery may truly become an outpatient procedure.

Bibliography

[1] (Software). *MATLAB*. 2011 [cited 2011 12th February]; Available from: http://uk.mathworks.com/.

[2] Pennes, H.H., *Analysis of Tissue and Arterial Blood Temperatures in the Resting Human Forearm*, Journ. Appl Physiol, 1948, **1**(2): pp 93-122.

[3] (Software). *COMSOL Multiphysics*. 2011 [cited 2011 12th February]; Available from: http://www.comsol.com/.

[4] Haar, G.t., *Acoustic Surgery*. Vol. 54. 2001: AIP. pp 29-34.

[5] Ni, Y., et al., *A review of the general aspects of radiofrequency ablation,* Abdom Imaging, 2005. **30** (4): pp 381-400.

[6] Haigron, P., et al., *Image-guided therapy: evolution and breakthrough* IEEE Eng Med Biol Mag, 2010. **29**(1): pp 100-4.

[7] Harries, S.A., et al., *Interstitial laser photocoagulation as a treatment for breast cancer.* Br J Surg, 1994. **81**(11): pp 1617-9.

[8] Simon, C.J., D.E. Dupuy, and W.W. Mayo-Smith, *Microwave ablation: principles and applications.* Radiographics, 2005. **25**(1): pp S69-83.

[9] Kennedy, J.E., *High-intensity focused ultrasound in the treatment of solid tumours.* Nat Rev Cancer, 2005. **5**(4): pp 321-7.

[10] Kennedy, J.E., G.R. Ter Haar, and D. Cranston, *High intensity focused ultrasound: surgery of the future?* Br J Radiol, 2003. **76**(909): pp 590-9.

[11] Goldberg, B.B., *Medical diagnostic ultrasound : a retrospective on its 40th anniversary*, 1988.

[12] (Web). *Urologync - HIFU*. 2010 [cited 2010 26th January]; Available from: http://www.urologync.com/services/services-for-men/hifu.html.

[13] (Web). *EDAP*. 2010 [cited 2010 11th January]; Available from: http://www.edap-tms.com/

[14] (Web). *Insightec*. 2010 [cited 2010 11th January]; Available from: http://www.insightec.com/.

[15] (Web). *Sumo Corp.* 2010 [cited 2010 11th January]; Available from: http://www.sumo.com.hk/

[16] Wu, F., et al., *A randomised clinical trial of high-intensity focused ultrasound ablation for the treatment of patients with localised breast cancer.* Br J Cancer, 2003. **89**(12): pp 2227-33.

[17] Zhu, H., et al., *Extracorporeal high-intensity focused ultrasound treatment for breast cancer.* Chinese Journal of Clinical Oncology, 2004. **1**(5): pp 377-380.

[18] Wu, F., et al., *Extracorporeal high intensity focused ultrasound ablation in the treatment of 1038 patients with solid carcinomas in China: an overview.* Ultrason Sonochem, 2004. **11**(3-4): pp 149-54.

[19] Wu, F., et al., *Extracorporeal high intensity focused ultrasound treatment for patients with breast cancer.* Breast Cancer Res Treat, 2005. **92**(1): pp 51-60.

[20] Wu, F., et al., *Wide local ablation of localized breast cancer using high intensity focused ultrasound.* J Surg Oncol, 2007. **96**(2): pp 130-6.

[21] Patel, P.R., et al., *In vitro and in vivo evaluations of increased effective beam width for heat deposition using a split focus high intensity ultrasound (HIFU) transducer.* Int J Hyperthermia, 2008. **24**(7): pp 537-49.

[22] Ji, X., et al., *High-intensity focused ultrasound with large scale spherical phased array for the ablation of deep tumors.* J Zhejiang Univ Sci B, 2009. **10**(9): pp 639-47.
[23] ter Haar, G., D. Sinnett, and I. Rivens, *High intensity focused ultrasound--a surgical technique for the treatment of discrete liver tumours.* Phys Med Biol, 1989. **34**(11): pp 1743-50.
[24] Chapelon, J.Y., et al. *The feasibility of tissue ablation using high intensity electronically focused ultrasound*. Ultrasonics Symposium Proc., IEEE 1993.
[25] Arditi, M., F.S. Foster, and J.W. Hunt, *Transient fields of concave annular arrays.* Ultrason Imaging, 1981. **3**(1): pp 37-61.
[26] Faure, P., et al., *On the pressure field of a transducer in the form of a curved stripp* Vol. 95. 1994: ASA. pp 628-637.
[27] Bushberg, J.T., *The essential physics of medical imaging*. 2nd ed. 2002, Philadelphia: Lippincott Williams & Wilkins. xvi, pp 933.
[28] Hanafy, A. and C.I. Zanelli. *Quantitative real-time pulsed Schlieren imaging of ultrasonic waves*. Ultrasonics Symposium Proc*.,* IEEE. 1991.
[29] Zanelli, C.I., et al. *Beamforming for therapy with high intensity focused ultrasound (HIFU) using quantitative schlieren*. Ultrasonics Symposium Proc, IEEE 1993
[30] Zanelli, C.I., C.W. Hennige, and N.T. Sanghvi. *Design and characterization of a 10 cm annular array transducer for high intensity focused ultrasound (HIFU) applications*. Ultrasonics Symposium Proc, IEEE. 1994.
[31] Hendee, W.R. and E.R. Ritenour, *Medical imaging physics*. 4th ed. ed. 2002: New York ; Wiley-Liss. xix, pp 512.
[32] Curiel, L., et al. *1.5D multi-elements phased array applied to high intensity focused ultrasound*. Ultrasonics Symposium Proc. IEEE. 1999.
[33] Chapelon, J.Y., et al., *New piezoelectric transducers for therapeutic ultrasound.* Ultrasound Med Biol, 2000. **26**(1): pp 153-9.
[34] Qi, W. and W. Cao, *Finite element study on 1-D array transducer design.* IEEE Trans Ultrason Ferroelectr Freq Control, 2000. **47**(4): pp 949-55.
[35] (Web). *ANSYS*. 2011 [cited 2011 6th June]; Available from: http://www.ansys.com/
[36] Friedrich, W., H. Kaarmann, and R. Lerch. *Finite element modeling of acoustic radiation from piezoelectric phased array antennas*. Ultrasonics Symposium Proc., IEEE 1990.
[37] Seip, R., et al. *Comparison of split-beam transducer geometries and excitation configurations for transrectal prostate HIFU treatments*. Ultrasonics Symposium, IEEE. 2001.
[38] ter Haar, G.R., *High intensity focused ultrasound for the treatment of tumors.* Echocardiography, 2001. **18**(4): pp 317-22.
[39] Chen, L., et al., *Histological changes in rat liver tumours treated with high-intensity focused ultrasound.* Ultrasound Med Biol, 1993. **19**(1): pp 67-74.
[40] Hill, C.R., *Optimum acoustic frequency for focused ultrasound surgery.* Ultrasound Med Biol, 1994. **20**(3): pp 271-7.
[41] ter Haar, G., *High Intensity Ultrasound.* Surgical Innovation, 2001. **8**(1): pp 77-89.

[42] Sharafi, H. and H. Soltanian-Zadeh, *New 2D ultrasound phased-array design for hyperthermia cancer therapy.* SPIE Proc, 2001. **4325**: pp 473-482.

[43] Ebbini, E.S., et al. *Self-guided ultrasound phased arrays for noninvasive surgery*. Ultrasonics Symposium Proc. IEEE 1999.

[44] Seip, R., et al., *High-Intensity Focused Ultrasound (HIFU) Phased Arrays: Recent Developments in Transrectal Transducers and Driving Electronics Design.* ISTU Proc., 2003.

[45] Saleh, K.Y. and N.B. Smith, *Two-dimensional ultrasound phased array design for tissue ablation for treatment of benign prostatic hyperplasia.* Int J Hyperthermia, 2004. **20**(1): pp 7-31.

[46] Hutchinson, E.B. and K. Hynynen. *Evaluation of an aperiodic phased array for prostate thermal therapies*. Ultrasonics Symposium Proc., IEEE 1995.

[47] Rivens, I., et al., *A Phased Strip Array HIFU Transducer.* AIP Conference Proc., 2006. **829**(1): pp 425-429.

[48] Held, R.T., et al., *Annular phased-array high-intensity focused ultrasound device for image-guided therapy of uterine fibroids.* IEEE Trans Ultrason Ferroelectr Freq Control, 2006. **53**(2): pp 335-48.

[49] Melodelima, D., et al., *Toric HIFU transducer for large thermal ablation.* Conf Proc IEEE Eng Med Biol Soc, 2007 pp 230-3.

[50] Ma, Y., et al., *A New Clinical HIFU System (Teleson II).* AIP Conference Proc., 2007. **911**(1): pp 87-91.

[51] Glynn, H.R., et al., *Bubbles and HIFU: the good, the bad and the ugly.* ISTU Proc., 2002: pp 120-131.

[52] Zhou, C.W., et al., *Non-thermal ablation of rabbit liver VX2 tumor by pulsed high intensity focused ultrasound with ultrasound contrast agent: Pathological characteristics.* World J Gastroenterol, 2008. **14**(43): pp 6743-7.

[53] Roberts, W.W., et al., *Pulsed cavitational ultrasound: a noninvasive technology for controlled tissue ablation (histotripsy) in the rabbit kidney.* J Urol, 2006. **175**(2): pp 734-8.

[54] Hall, T.L., et al., *Temporal Trends in the Histology of the Rabbit Kidney after Cavitational Tissue Ablation.* AIP Conference Proc., 2007. **911**(1): pp 191-197.

[55] Liu, C.M., et al., *Duty cycle affect on in vitro bovine liver treated with pulsed high intensity focused ultrasound.* Zhongguo Chaoseng Yixue Zazhi 2007. **23**: pp 567-570.

[56] Gin-Shin, C., et al. *Development of 1.5D cylindrical HIFU phased array*. In Ultrasonics Symposium, IEEE, IUS 2008 .

[57] (Web). *Field II Simulation Program, Technical University of Denmark*. 2011 [cited 2011 1st June]; Available from: http://server.electro.dtu.dk/personal/jaj/field/

[58] Hancock, H., et al., *Evaluation of pulsed high intensity focused ultrasound exposures on metastasis in a murine model.* Clin Exp Metastasis, 2009. **26**(7): pp 729-38.

[59] Jeong, J.S., J.H. Chang, and K.K. Shung, *Ultrasound transducer and system for real-time simultaneous therapy and diagnosis for noninvasive surgery of prostate tissue.* IEEE Trans Ultrason Ferroelectr Freq Control, 2009. **56**(9): pp 1913-22.

[60] Pernot, M., et al., *High power phased array prototype for clinical high intensity focused ultrasound : applications to transcostal and transcranial therapy.* Conf Proc IEEE Eng Med Biol Soc, 2007. **2007**: pp 234-7.

[61] Ebbini, E.S. and C.A. Cain, *A spherical-section ultrasound phased array applicator for deep localized hyperthermia.* IEEE Trans Biomed Eng, 1991. **38**(7): pp 634-43.

[62] Hutchins, D.A., *Continuous-wave pressure fields of ultrasonic transducers.* Journal of The Acoustical Society of America, 1986. **80**(1).

[63] Spadoni, A. and C. Daraio, *Generation and control of sound bullets with a nonlinear acoustic lens.* Proc Natl Acad Sci U S A, 2010. **107**(16): pp 7230-4.

[64] Spoo, J., et al. *MRI controlled HIFU treatment of breast tissue*. Ultrasonics Symposium Proc., IEEE 1999.

[65] Huber, P.E., et al., *A new noninvasive approach in breast cancer therapy using magnetic resonance imaging-guided focused ultrasound surgery.* Cancer Res, 2001. **61**(23): pp 8441-7.

[66] Murat, F.-J., L. Poissonier, and A. Galet, *Recurrent prostate cancer after radiotherapy – salvage treatment by high intensity focused ultrasound.* European Nephrology, 2006. **1**: pp 67-69.

[67] Wu, J. and W.L.M. Nyborg, *Emerging therapeutic ultrasound*. 2006, Hackensack, N.J.: World Scientific. xvi, 346 pp

[68] Schmitz, A.C., et al., *Image-guided focused ultrasound ablation of breast cancer: current status, challenges, and future directions.* Eur Radiol, 2008. **18**(7): pp 1431-41.

[69] Xie, B., et al., *Experimental ablation of the pancreas with high intensity focused ultrasound (HIFU) in a porcine model.* Int J Med Sci, 2010. **8**(1): pp 9-15.

[70] (Web). *Haifu*. 2010 [cited 2010 11th January]; Available from: http://www.haifumedical.com/Products/.

[71] (Web). *Blatek Inc*. 2010 [cited 2010 11th January]; Available from: http://www.blatek.com/med_HIFU.aspx/.

[72] Guillaume, B., et al., *Dual Mode Transducer for Ultrasound Monitored Thermal Therapy.* AIP Conference Proc., 2006. **829**(1): pp 390-394.

[73] (Web). *Bercli (images)*. 2010 [cited 2010 7th Novemeber]; Available from: http://www.bercli.net/

[74] (Software). *ProEngineer*. 2011 [cited 2014 8th June]; Available from: http://www.ptc.com/product/creo/proengineer/.

[75] (Web). *Ultrasound images*. 2010 [cited 2010 7th Novemeber]; Available from: http://www.ob-ultrasound.net/

[76] (Web). *Focus Surgery (image)*. 2010 [cited 2010 17th Novemeber]; Available from: http://www.focus-surgery.com/Documents/SB500_PRESENTATION_UIA2002.pdf/

[77] Tan, J.S., et al., *Ultrasound phased arrays for prostate treatment.* J Acoust Soc Am, 2001. **109**(6): pp 3055-64.

[78] (Software). *Autodesk Inventor*. 2011 [cited 2014 8th June]; Available from: http://www.autodesk.com/products/inventor/overview.

[79] (Web). *Piezo Technologies*. 2011 [cited 2011 1st March]; Available from: http://www.piezotechnologies.com/hifu-transducers.htm/

[80] (Web). *Morgan Electroceramics*. 2010 [cited 2010 20th December]; Available from: http://www.morganelectroceramics.com/download.php?7a46627a6f4d7734303733682f2f514c35682f6c7643724c2b596f673351754f6758323939526d5a436d32662b673d3d/

[81] Rantanen, N.W., *Diagnostic ultrasound*. 1986, Philadelphia ; London: Saunders. 24cm.

[82] Silverman, R.H., et al., *Improved visualization of high-intensity focused ultrasound lesions.* Ultrasound in Medicine & Biology, 2006. **32**(11): pp 1743-1751.

[83] Kim, Y.S., et al., *High-intensity focused ultrasound therapy: an overview for radiologists.* Korean J Radiol, 2008. **9**(4): pp 291-302.

[84] (Web). *Engineering Toolbox*. 2010 [cited 2010 12th December]; Available from: http://www.engineeringtoolbox.com/sound-speed-water-d_598.htm/.

[85] Cheeke, J.D.N., *Fundamentals and applications of ultrasonic waves*. CRC series in pure and applied physics. 2002, Boca Raton: CRC Press. pp 462.

[86] Meng Tong, T., C. Chang Min, and S. Chauhan. *High intensity ultrasound phased array for surgical applications*. Biomedical and Pharmaceutical Engineering, ICBPE 2006. International Conference on. 2006.

[87] Arkin, H. Xu, L. X & Holmes, K.R., *Recent developments in modeling heat transfer in blood perfused tissues*, IEEE Trans on Biomedical Eng., 1994, **41**(2): pp 97,107.

[88] Wissler, E.H., *Pennes' 1948 paper revisited*, Journ Appl Physiol, 1998, **85(**35-41).

[89] Thomenius K. *Thermal dosimetry model for diagnostic ultrasound.* Proc. IEEE Ultrasound Symposium Proc., 1990: pp 1399–1408.

[90] El-Desouki, MM, Hynynen, K. *Driving Circuitry for Focused Ultrasound Noninvasive Surgery and Drug Delivery Applications*. Sensors. 2011; **11**(1): pp 539-556.

Appendix A: MATLAB Simulation Code

In this appendix a sample of the custom-written MATLAB code is given, for reference. It should be noted that the code was adapted & modified for the various simulations presented in this thesis and as such underwent many changes as the project evolved. The sample below simulates a 'mini-array' comprising only sixteen elements and so compared to the simulations shown previously, that simulated a minimum of 64 elements, would produce a much less powerful and less defined focus. It has been included as a characteristic example.

Additional parameters used in sample include the following:

- 'Kerf' (Gap between elements) = 0.05 mm
- Element Width = 0.32 mm
- No. elements simulated = 16
- Focus at 1 mm (positive x-direction)

[CODE BEGINS]

```
r=0.05;
c=1500;
freq=3500000;
lambda=c/freq;

kerf=0.00005;
elemwidth=0.00032;
numelem=16;
elempitch=elemwidth+kerf;
%numelem=fix((0.07/(elempitch))/2);

 A=((r*sin(((28.955*2*pi))/360))*elemwidth)*numelem;
 S=((r*sin(((28.955*2*pi))/360))*elemwidth);

maxacousticpower=3;
W=A*10000*maxacousticpower;

k=(2*pi)/lambda;
att=5*(freq/1000000);
rho=998;
n=lambda/5;

alphaT=(28.96*2*pi)/360;

circ=r*alphaT;
minsize=(lambda/2);
nmin=circ/minsize;
intn=ceil(nmin);
alphastep=alphaT/intn;

subS=S/intn;
constant=(sqrt(((2*W*rho)/(c*A))))*(freq)*subS;
```

```
startalpha=(-14.48)*(2*pi)/(360);
endalpha=(14.48)*(2*pi)/(360);

alpha=[startalpha:alphastep:endalpha];

% origin at focus (x=a,y=b) - ie directly 'in front of'/above centre
of (centre) element
a=0;
b=0;

focusx=0.001;
focusy=0.01;
focusz=0;

elemxc=0;
elemyc=0;
elemzc=-0.05;

% decimal places to round phi (rads) to
dp=(1/0.044);

subelemx=a+(r*sin(alpha));
        % 'subelemx' is the x co-ords of the sub-elements
        % & 'a'&'b' are the co-ords of the centre of the arc
subelemz=b+(-r*cos(alpha));

[Y,Z]=meshgrid(-0.05:n:0.05,-0.045:n:0.02);    % 'n' is grid 'step'
size
% distance for each sub element to every point in the x,z grid
% how big is the array
[r,c]=size(Y);
Y1d=reshape(Y,r*c,1);
Z1d=reshape(Z,r*c,1);



%Element 1
% loop through each subelemx
elemxc1=0;
elemyc1=0;
elemzc1=-0.05;

phi1=round((((sqrt(((elemxc1-focusx)^2)+((elemyc1-
focusy)^2)+((elemzc1-focusz)^2)))-(sqrt(((elemxc-focusx)^2+((elemyc-
focusy)^2)+((elemzc-focusz)^2)))))*((2*pi)/lambda))*dp)/dp
ephi1=exp(1i*phi1);
for sCnt1=1:length(subelemx);
    dist1(:,sCnt1)=sqrt(((subelemx(sCnt1)).^2) +((Z1d-
subelemz(sCnt1)).^2)+((Y1d-elemyc1).^2));
end
% aY1d and Z1d are the points within the grid
    attd1 = exp(-att.*dist1);
    ejkd1 = exp(-1i.*k.*dist1);
    Texp1 = (ephi1.*attd1.*ejkd1);
    Texpd1 = (Texp1./dist1);
    ATTexpd1 = sum(Texpd1,2);

pmatrix1=reshape(ATTexpd1,(size((Y),1)),(size((Y),2)));
pmatrix1s=pmatrix1;
```

```
clear pmatrix1
clear dist1
clear attd1
clear ejkd1
clear Texp1
clear Texpd1
clear ATTexpd1
clear sCnt1
clear phi1
clear ephi1
clear elemyc1
clear elemxc1
clear elemzc1


%Element 2%

elemxc2=0;
elemyc2=1*elempitch;
elemzc2=-0.05;

phi2=round((((sqrt(((elemxc2-focusx)^2)+((elemyc2-
focusy)^2)+((elemzc2-focusz)^2)))-(sqrt(((elemxc-focusx)^2+((elemyc-
focusy)^2)+((elemzc-focusz)^2)))))*((2*pi)/lambda))*dp)/dp
ephi2=exp(1i*phi2);
for sCnt2=1:length(subelemx)
    dist2(:,sCnt2)=sqrt(((subelemx(sCnt2)).^2) +((Z1d-
subelemz(sCnt2)).^2)+((Y1d-elemyc2).^2));
end
    attd2 = exp(-att.*dist2);
    ejkd2 = exp(-1i.*k.*dist2);
    Texp2 = (ephi2.*attd2.*ejkd2);
    Texpd2 = (Texp2./dist2);
    ATTexpd2 = sum(Texpd2,2);

pmatrix2=reshape(ATTexpd2,(size((Y),1)),(size((Y),2)));
pmatrix2s=pmatrix1s+pmatrix2;

clear pmatrix1s
clear pmatrix2
clear dist2
clear attd2
clear ejkd2
clear Texp2
clear Texpd2
clear ATTexpd2
clear sCnt2
clear phi2
clear ephi2
clear elemyc2
clear elemxc2
clear elemzc2


% %Element 3%

elemxc3=0;
elemyc3=-1*elempitch;
elemzc3=-0.05;
```

```
phi3=round((((sqrt(((elemxc3-focusx)^2)+((elemyc3-
focusy)^2)+((elemzc3-focusz)^2)))-(sqrt(((elemxc-focusx)^2+((elemyc-
focusy)^2)+((elemzc-focusz)^2)))))*((2*pi)/lambda))*dp)/dp
ephi3=exp(1i*phi3);
for sCnt3=1:length(subelemx)
    dist3(:,sCnt3)=sqrt( ((subelemx(sCnt3)).^2) +((Z1d-
subelemz(sCnt3)).^2)+((Y1d-elemyc3).^2) );
end
    attd3 = exp(-att.*dist3);
    ejkd3 = exp(-1i.*k.*dist3);
    Texp3 = (ephi3.*attd3.*ejkd3);
    Texpd3 = (Texp3./dist3);
    ATTexpd3 = sum(Texpd3,2);

pmatrix3=reshape(ATTexpd3,(size((Y),1)),(size((Y),2)));
pmatrix3s=pmatrix2s+pmatrix3;

clear pmatrix2s
clear pmatrix3
clear dist3
clear attd3
clear ejkd3
clear Texp3
clear Texpd3
clear ATTexpd3
clear sCnt3
clear phi3
clear ephi3
clear elemyc3
clear elemxc3
clear elemzc3


% %Element 4%

elemxc4=0;
elemyc4=2*elempitch;
elemzc4=-0.05;

phi4=round((((sqrt(((elemxc4-focusx)^2)+((elemyc4-
focusy)^2)+((elemzc4-focusz)^2)))-(sqrt(((elemxc-focusx)^2+((elemyc-
focusy)^2)+((elemzc-focusz)^2)))))*((2*pi)/lambda))*dp)/dp
ephi4=exp(1i*phi4);
for sCnt4=1:length(subelemx)
    dist4(:,sCnt4)=sqrt( ((subelemx(sCnt4)).^2) +((Z1d-
subelemz(sCnt4)).^2)+((Y1d-elemyc4).^2) );
end
    attd4 = exp(-att.*dist4);
    ejkd4 = exp(-1i.*k.*dist4);
    Texp4 = (ephi4.*attd4.*ejkd4);
    Texpd4 = (Texp4./dist4);
    ATTexpd4 = sum(Texpd4,2);

pmatrix4=reshape(ATTexpd4,(size((Y),1)),(size((Y),2)));
pmatrix4s=pmatrix3s+pmatrix4;

clear pmatrix3s
clear pmatrix4
clear dist4
```

```
clear attd4
clear ejkd4
clear Texp4
clear Texpd4
clear ATTexpd4
clear sCnt4
clear phi4
clear ephi4
clear elemyc4
clear elemxc4
clear elemzc4


% %Element 5%

elemxc5=0;
elemyc5=-2*elempitch;
elemzc5=-0.05;

phi5=round((((sqrt(((elemxc5-focusx)^2)+((elemyc5-
focusy)^2)+((elemzc5-focusz)^2)))-(sqrt(((elemxc-focusx)^2+((elemyc-
focusy)^2)+((elemzc-focusz)^2)))))*((2*pi)/lambda))*dp)/dp
ephi5=exp(1i*phi5);
for sCnt5=1:length(subelemx)
    dist5(:,sCnt5)=sqrt( ((subelemx(sCnt5)).^2) +((Z1d-
subelemz(sCnt5)).^2)+((Y1d-elemyc5).^2) );
end
    attd5 = exp(-att.*dist5);
    ejkd5 = exp(-1i.*k.*dist5);
    Texp5 = (ephi5.*attd5.*ejkd5);
    Texpd5 = (Texp5./dist5);
    ATTexpd5 = sum(Texpd5,2);

pmatrix5=reshape(ATTexpd5,(size((Y),1)),(size((Y),2)));
pmatrix5s=pmatrix4s+pmatrix5;

clear pmatrix4s
clear pmatrix5
clear dist5
clear attd5
clear ejkd5
clear Texp5
clear Texpd5
clear ATTexpd5
clear sCnt5
clear phi5
clear ephi5
clear elemyc5
clear elemxc5
clear elemzc5


% %Element 6%

elemxc6=0;
elemyc6=3*elempitch;
elemzc6=-0.05;
```

```
phi6=round((((sqrt(((elemxc6-focusx)^2)+((elemyc6-
focusy)^2)+((elemzc6-focusz)^2)))-(sqrt(((elemxc-focusx)^2+((elemyc-
focusy)^2)+((elemzc-focusz)^2)))))*((2*pi)/lambda))*dp)/dp
ephi6=exp(1i*phi6);
for sCnt6=1:length(subelemx)
    dist6(:,sCnt6)=sqrt( ((subelemx(sCnt6)).^2) +((Z1d-
subelemz(sCnt6)).^2)+((Y1d-elemyc6).^2) );
end
    attd6 = exp(-att.*dist6);
    ejkd6 = exp(-1i.*k.*dist6);
    Texp6 = (ephi6.*attd6.*ejkd6);
    Texpd6 = (Texp6./dist6);
    ATTexpd6 = sum(Texpd6,2);

pmatrix6=reshape(ATTexpd6,(size((Y),1)),(size((Y),2)));
pmatrix6s=pmatrix5s+pmatrix6;

clear pmatrix5s
clear pmatrix6
clear dist6
clear attd6
clear ejkd6
clear Texp6
clear Texpd6
clear ATTexpd6
clear sCnt6
clear phi6
clear ephi6
clear elemyc6
clear elemxc6
clear elemzc6


% %Element 7%

elemxc7=0;
elemyc7=-3*elempitch;
elemzc7=-0.05;

phi7=round((((sqrt(((elemxc7-focusx)^2)+((elemyc7-
focusy)^2)+((elemzc7-focusz)^2)))-(sqrt(((elemxc-focusx)^2+((elemyc-
focusy)^2)+((elemzc-focusz)^2)))))*((2*pi)/lambda))*dp)/dp
ephi7=exp(1i*phi7);
for sCnt7=1:length(subelemx)
    dist7(:,sCnt7)=sqrt( ((subelemx(sCnt7)).^2) +((Z1d-
subelemz(sCnt7)).^2)+((Y1d-elemyc7).^2) );
end
    attd7 = exp(-att.*dist7);
    ejkd7 = exp(-1i.*k.*dist7);
    Texp7 = (ephi7.*attd7.*ejkd7);
    Texpd7 = (Texp7./dist7);
    ATTexpd7 = sum(Texpd7,2);

pmatrix7=reshape(ATTexpd7,(size((Y),1)),(size((Y),2)));
pmatrix7s=pmatrix6s+pmatrix7;

clear pmatrix6s
clear pmatrix7
clear dist7
clear attd7
```

```
clear ejkd7
clear Texp7
clear Texpd7
clear ATTexpd7
clear sCnt7
clear phi7
clear ephi7
clear elemyc7
clear elemxc7
clear elemzc7


% %Element 8%

elemxc8=0;
elemyc8=4*elempitch;
elemzc8=-0.05;

phi8=round((((sqrt(((elemxc8-focusx)^2)+((elemyc8-
focusy)^2)+((elemzc8-focusz)^2)))-(sqrt(((elemxc-focusx)^2+((elemyc-
focusy)^2)+((elemzc-focusz)^2)))))*((2*pi)/lambda))*dp)/dp
ephi8=exp(1i*phi8);
for sCnt8=1:length(subelemx)
    dist8(:,sCnt8)=sqrt( ((subelemx(sCnt8)).^2) +((Z1d-
subelemz(sCnt8)).^2)+((Y1d-elemyc8).^2) );
end
    attd8 = exp(-att.*dist8);
    ejkd8 = exp(-1i.*k.*dist8);
    Texp8 = (ephi8.*attd8.*ejkd8);
    Texpd8 = (Texp8./dist8);
    ATTexpd8 = sum(Texpd8,2);

pmatrix8=reshape(ATTexpd8,(size((Y),1)),(size((Y),2)));
pmatrix8s=pmatrix7s+pmatrix8;

clear pmatrix7s
clear pmatrix8
clear dist8
clear attd8
clear ejkd8
clear Texp8
clear Texpd8
clear ATTexpd8
clear sCnt8
clear phi8
clear ephi8
clear elemyc8
clear elemxc8
clear elemzc8


% %Element 9%

elemxc9=0;
elemyc9=-4*elempitch;
elemzc9=-0.05;
```

```
phi9=round((((sqrt(((elemxc9-focusx)^2)+((elemyc9-
focusy)^2)+((elemzc9-focusz)^2)))-(sqrt(((elemxc-focusx)^2+((elemyc-
focusy)^2)+((elemzc-focusz)^2)))))*((2*pi)/lambda))*dp)/dp
ephi9=exp(1i*phi9);
for sCnt9=1:length(subelemx)
    dist9(:,sCnt9)=sqrt( ((subelemx(sCnt9)).^2) +((Z1d-
subelemz(sCnt9)).^2)+((Y1d-elemyc9).^2) );
end
    attd9 = exp(-att.*dist9);
    ejkd9 = exp(-1i.*k.*dist9);
    Texp9 = (ephi9.*attd9.*ejkd9);
    Texpd9 = (Texp9./dist9);
    ATTexpd9 = sum(Texpd9,2);

pmatrix9=reshape(ATTexpd9,(size((Y),1)),(size((Y),2)));
pmatrix9s=pmatrix8s+pmatrix9;

clear pmatrix8s
clear pmatrix9
clear dist9
clear attd9
clear ejkd9
clear Texp9
clear Texpd9
clear ATTexpd9
clear sCnt9
clear phi9
clear ephi9
clear elemyc9
clear elemxc9
clear elemzc9


% %Element 10%

elemxc10=0;
elemyc10=5*elempitch;
elemzc10=-0.05;

phi10=round((((sqrt(((elemxc10-focusx)^2)+((elemyc10-
focusy)^2)+((elemzc10-focusz)^2)))-(sqrt(((elemxc-focusx)^2+((elemyc-
focusy)^2)+((elemzc-focusz)^2)))))*((2*pi)/lambda))*dp)/dp
ephi10=exp(1i*phi10);
for sCnt10=1:length(subelemx)
    dist10(:,sCnt10)=sqrt( ((subelemx(sCnt10)).^2) +((Z1d-
subelemz(sCnt10)).^2)+((Y1d-elemyc10).^2) );
end
    attd10 = exp(-att.*dist10);
    ejkd10 = exp(-1i.*k.*dist10);
    Texp10 = (ephi10.*attd10.*ejkd10);
    Texpd10 = (Texp10./dist10);
    ATTexpd10 = sum(Texpd10,2);

pmatrix10=reshape(ATTexpd10,(size((Y),1)),(size((Y),2)));
pmatrix10s=pmatrix9s+pmatrix10;

clear pmatrix9s
clear pmatrix10
clear dist10
clear attd10
```

```
clear ejkd10
clear Texp10
clear Texpd10
clear ATTexpd10
clear sCnt10
clear phi10
clear ephi10
clear elemyc10
clear elemxc10
clear elemzc10


% %Element 11%

elemxc11=0;
elemyc11=-5*elempitch;
elemzc11=-0.05;

 phi11=round((((sqrt(((elemxc11-focusx)^2)+((elemyc11-
focusy)^2)+((elemzc11-focusz)^2)))-(sqrt(((elemxc-focusx)^2+((elemyc-
focusy)^2)+((elemzc-focusz)^2)))))*((2*pi)/lambda))*dp)/dp
ephi11=exp(1i*phi11);
for sCnt11=1:length(subelemx)
    dist11(:,sCnt11)=sqrt( ((subelemx(sCnt11)).^2) +((Z1d-
subelemz(sCnt11)).^2)+((Y1d-elemyc11).^2) );
end
    attd11 = exp(-att.*dist11);
    ejkd11 = exp(-1i.*k.*dist11);
    Texp11 = (ephi11.*attd11.*ejkd11);
    Texpd11 = (Texp11./dist11);
    ATTexpd11 = sum(Texpd11,2);

pmatrix11=reshape(ATTexpd11,(size((Y),1)),(size((Y),2)));
pmatrix11s=pmatrix10s+pmatrix11;

clear pmatrix10s
clear pmatrix11
clear dist11
clear attd11
clear ejkd11
clear Texp11
clear Texpd11
clear ATTexpd11
clear sCnt11
clear phi11
clear ephi11
clear elemyc11
clear elemxc11
clear elemzc11


% %Element 12%

elemxc12=0;
elemyc12=6*elempitch;
elemzc12=-0.05;
phi12=round((((sqrt(((elemxc12-focusx)^2)+((elemyc12-
focusy)^2)+((elemzc12-focusz)^2)))-(sqrt(((elemxc-focusx)^2+((elemyc-
focusy)^2)+((elemzc-focusz)^2)))))*((2*pi)/lambda))*dp)/dp
ephi12=exp(1i*phi12);
```

```
for sCnt12=1:length(subelemx)
    dist12(:,sCnt12)=sqrt( ((subelemx(sCnt12)).^2) +((Z1d-
subelemz(sCnt12)).^2)+((Y1d-elemyc12).^2) );
end
    attd12 = exp(-att.*dist12);
    ejkd12 = exp(-1i.*k.*dist12);
    Texp12 = (ephi12.*attd12.*ejkd12);
    Texpd12 = (Texp12./dist12);
    ATTexpd12 = sum(Texpd12,2);

pmatrix12=reshape(ATTexpd12,(size((Y),1)),(size((Y),2)));
pmatrix12s=pmatrix11s+pmatrix12;

clear pmatrix11s
clear pmatrix12
clear dist12
clear attd12
clear ejkd12
clear Texp12
clear Texpd12
clear ATTexpd12
clear sCnt12
clear phi12
clear ephi12
clear elemyc12
clear elemxc12
clear elemzc12


% %Element 13%

elemxc13=0;
elemyc13=-6*elempitch;
elemzc13=-0.05;

phi13=round((((sqrt(((elemxc13-focusx)^2)+((elemyc13-
focusy)^2)+((elemzc13-focusz)^2)))-(sqrt(((elemxc-focusx)^2+((elemyc-
focusy)^2)+((elemzc-focusz)^2)))))*((2*pi)/lambda))*dp)/dp
ephi13=exp(1i*phi13);
for sCnt13=1:length(subelemx)
    dist13(:,sCnt13)=sqrt( ((subelemx(sCnt13)).^2) +((Z1d-
subelemz(sCnt13)).^2)+((Y1d-elemyc13).^2) );
end
    attd13 = exp(-att.*dist13);
    ejkd13 = exp(-1i.*k.*dist13);
    Texp13 = (ephi13.*attd13.*ejkd13);
    Texpd13 = (Texp13./dist13);
    ATTexpd13 = sum(Texpd13,2);

pmatrix13=reshape(ATTexpd13,(size((Y),1)),(size((Y),2)));
pmatrix13s=pmatrix12s+pmatrix13;

clear pmatrix12s
clear pmatrix13
clear dist13
clear attd13
clear ejkd13
clear Texp13
clear Texpd13
clear ATTexpd13
```

```
clear sCnt13
clear phi13
clear ephi13
clear elemyc13
clear elemxc13
clear elemzc13


% %Element 14%

elemxc14=0;
elemyc14=7*elempitch;
elemzc14=-0.05;

phi14=round((((sqrt(((elemxc14-focusx)^2)+((elemyc14-
focusy)^2)+((elemzc14-focusz)^2)))-(sqrt(((elemxc-focusx)^2+((elemyc-
focusy)^2)+((elemzc-focusz)^2)))))*((2*pi)/lambda))*dp)/dp
ephi14=exp(1i*phi14);
for sCnt14=1:length(subelemx)
    dist14(:,sCnt14)=sqrt( ((subelemx(sCnt14)).^2) +((Z1d-
subelemz(sCnt14)).^2)+((Y1d-elemyc14).^2) );
end
    attd14 = exp(-att.*dist14);
    ejkd14 = exp(-1i.*k.*dist14);
    Texp14 = (ephi14.*attd14.*ejkd14);
    Texpd14 = (Texp14./dist14);
    ATTexpd14 = sum(Texpd14,2);

pmatrix14=reshape(ATTexpd14,(size((Y),1)),(size((Y),2)));
pmatrix14s=pmatrix13s+pmatrix14;

clear pmatrix13s
clear pmatrix14
clear dist14
clear attd14
clear ejkd14
clear Texp14
clear Texpd14
clear ATTexpd14
clear sCnt14
clear phi14
clear ephi14
clear elemyc14
clear elemxc14
clear elemzc14


% %Element 15%

elemxc15=0;
elemyc15=-7*elempitch;
elemzc15=-0.05;

phi15=round((((sqrt(((elemxc15-focusx)^2)+((elemyc15-
focusy)^2)+((elemzc15-focusz)^2)))-(sqrt(((elemxc-focusx)^2+((elemyc-
focusy)^2)+((elemzc-focusz)^2)))))*((2*pi)/lambda))*dp)/dp
ephi15=exp(1i*phi15);
for sCnt15=1:length(subelemx)
    dist15(:,sCnt15)=sqrt( ((subelemx(sCnt15)).^2) +((Z1d-
subelemz(sCnt15)).^2)+((Y1d-elemyc15).^2) );
```

```
end
    attd15 = exp(-att.*dist15);
    ejkd15 = exp(-1i.*k.*dist15);
    Texp15 = (ephi15.*attd15.*ejkd15);
    Texpd15 = (Texp15./dist15);
    ATTexpd15 = sum(Texpd15,2);

pmatrix15=reshape(ATTexpd15,(size((Y),1)),(size((Y),2)));
pmatrix15s=pmatrix14s+pmatrix15;

clear pmatrix14s
clear pmatrix15
clear dist15
clear attd15
clear ejkd15
clear Texp15
clear Texpd15
clear ATTexpd15
clear sCnt15
clear phi15
clear ephi15
clear elemyc15
clear elemxc15
clear elemzc15


% %Element 16%

elemxc16=0;
elemyc16=8*elempitch;
elemzc16=-0.05;

phi16=round((((sqrt(((elemxc16-focusx)^2)+((elemyc16-
focusy)^2)+((elemzc16-focusz)^2)))-(sqrt(((elemxc-focusx)^2+((elemyc-
focusy)^2)+((elemzc-focusz)^2)))))*((2*pi)/lambda))*dp)/dp
ephi16=exp(1i*phi16);
for sCnt16=1:length(subelemx)
    dist16(:,sCnt16)=sqrt( ((subelemx(sCnt16)).^2) +((Z1d-
subelemz(sCnt16)).^2)+((Y1d-elemyc16).^2) );
end
    attd16 = exp(-att.*dist16);
    ejkd16 = exp(-1i.*k.*dist16);
    Texp16 = (ephi16.*attd16.*ejkd16);
    Texpd16 = (Texp16./dist16);
    ATTexpd16 = sum(Texpd16,2);

pmatrix16=reshape(ATTexpd16,(size((Y),1)),(size((Y),2)));
pmatrix16s=pmatrix15s+pmatrix16;

clear pmatrix15s
clear pmatrix16
clear dist16
clear attd16
clear ejkd16
clear Texp16
clear Texpd16
clear ATTexpd16
clear sCnt16
clear phi16
clear ephi16
```

```
clear elemyc16
clear elemxc16
clear elemzc16

clear Y1d
clear Z1d

figure(1);
 [C,h] = contour(Y,Z,abs((pmatrix16s)*constant),10);
 clabel(C,h)

figure(2);
 mesh(Y,Z,abs((pmatrix16s)*constant))

pmatrixabs=(abs(pmatrix16s))*constant;
Imatrixabs=((pmatrixabs).^2)/(2*rho*c);

figure(3);
 [C,h] = contour(Y,Z,Imatrixabs,10);
 clabel(C,h)

figure(4);
 mesh(Y,Z,Imatrixabs);

normI=Imatrixabs./(max(max(Imatrixabs)));
v1=0.1:0.1:1.0;

figure(5);
 [C,h] = contour(Y,Z,normI,v1);
 clabel(C,h)

lognormI=10*log10(normI);
v2=[-3,-6,-9,-12,-15,-18,-21];

figure(6);
 [C,h] = contour(Y,Z,lognormI,v2);
 clabel(C,h)

v3=[-21:-1];

figure(7);
 [C,h] = contour(Y,Z,lognormI,v3);
 clabel(C,h)

Q=2*att*Imatrixabs; % For Export
```

[CODE ENDS]

Appendix B: Original Project Proposal

Development of a medical imaging-based technology for cancer treatment

The research project proposed is the integration of a therapeutic high intensity focused ultrasound (HIFU) transducer array into an existing electrical impedance modelling (EIM) non-invasive medical imaging device. The resulting system therefore will allow dual modalities of diagnosis and treatment to be available using a single device.

Background & Rationale

HIFU involves bringing ultrasonic waves into a tight focus at a targeted spot within the body. As ultrasonic waves are attenuated in tissue, the loss in power is converted into heat. This allows ablation of internal structures caused by coagulative necrosis of the tissue when heated to temperatures in excess of 65 degrees Celsius. A major advantage of using HIFU is that the overlying skin and tissue remains unharmed, as ablation will only occur at the focal spot or point. This fact has led to the use of HIFU being referred to as a 'trackless scalpel'.

In recent years the use of HIFU for the treatment of various ailments has been given much attention. Although the concepts and theory of using HIFU as a surgical tool have existed for decades it is only recently that the supporting technology has evolved sufficiently to effectively use such a device. In the last few years the use of HIFU to treat prostate cancer has been given particular attention and is now an approved treatment methodology in countries around the world including, but not limited to China, where it is understood that the largest number of clinical trials have taken place.

Breast cancer, amongst others, has the potential to be efficiently treated using a HIFU device. This is because the breast is easily accessible from outside the body and also contains no pockets of air that would negatively affect the propagation of ultrasound through tissue (such as are present in the lungs).

The use of EIM for early detection of breast cancer has been under investigation by numerous groups worldwide, but to the authors knowledge none of these groups have incorporated a suitable treatment methodology to allow diagnosis and treatment to be performed using the same device. The bio-medical engineering (BMEng) group, currently based at the University of Sussex, are working towards this goal. Therefore it can be seen that the research proposed here would have a greatly beneficial effect on obtaining this goal and progressing towards a system allowing early detection and destruction of breast cancer

Research Questions

The questions this research project aims to answer are numerous. To simplify, these questions can be broadly split into the following.

- Can EIM be used in conjunction with HIFU to provide both diagnosis and targeted treatment?

- What factors must be considered when designing and manufacturing a HIFU transducer? (Including, but in no way limited to the phasing of array elements, allowing electronic steering)
- How can a HIFU transducer be integrated into the existing EIM system designed by the BMEng group at the University of Sussex?
- How can the resulting device be made viable for treatment of human patients?

Methods

Much of the methodology for the proposed research can be inferred from the questions above. More specifically research will begin with an extensive literature review of current groups working in the field of HIFU and tumour ablation and of existing texts on the theory of ultrasonics and interaction with tissue. Following this suitable transducer designs will be created and a simulation methodology will be employed to model the pressure fields and resulting heat deposition caused by the propagation of ultrasound into tissue. Once satisfactory simulation has been completed a prototype will be manufactured using the created designs in conjunction with advice from the preferred manufacturers. The prototype, once manufactured, will then undergo extensive testing largely using phantoms that represent human tissue. The prototype will then be evaluated and modified as necessary, with improvement being made as and when they are required. Eventually the finished HIFU/EIM device will be tested in medical trials, following sufficient approval from the relevant bodies.

Ethical Considerations

As the existing EIM system has been created largely using external funding confidentiality is an issue here. All parties consulted during this research project should be asked to sign non-disclosure agreements (NDAs) prior to any sensitive information being divulged. In addition to this how the HIFU treatment will be tested should be considered, especially in terms of acceptability to patients when considering all available treatment options.

Timescales

The timescales involved in a project such as has been proposed here are largely dependent on existing deadlines and on-going work presently being carried out by the BMEng group at the University of Sussex. That being said, the first working prototype HIFU transducer will aim to be manufactured and initially tested within 4 weeks of the start of July 2011.